

ANALYTICA CHIMICA ACTA

An international journal devoted to all branches of analytical chemistry

EDITORS

HARRY L. PARDUE (West Lafayette, IN, U.S.A.)

ALAN TOWNSEND (Hull, Great Britain)

J.T. CLERC (Berne, Switzerland)

WILLEM E. VAN DER LINDEN (Enschede, The Netherlands)

PAUL J. WORSFOLD (Plymouth, Great Britain)

Editorial Advisers

F.C. Adams, Antwerp
J.F. Alder, Manchester
C.M.G. van den Berg, Liverpool
A.M. Bond, Bundoora, Vic.
S.D. Brown, Newark, DE
J. Buffle, Geneva
P.R. Coulet, Lyon
S.R. Crouch, East Lansing, MI
R. Dams, Ghent
L. de Galan, Vlaardingen
M.L. Gross, Lincoln, NE
W. Heineman, Cincinnati, OH
G.M. Hieftje, Bloomington, IN
T. Imasaka, Fukuoka
D. Jagner, Gothenburg
G. Johansson, Lund
D.C. Johnson, Ames, IA
I. Karube, Tokyo
A.M.G. Macdonald, Birmingham
D.L. Massart, Brussels
P.C. Meier, Schaffhausen

M.E. Meyerhoff, Ann Arbor, MI
J.N. Miller, Loughborough
H.A. Mottola, Stillwater, OK
M.E. Munk, Tempe, AZ
M. Otto, Freiberg
D. Pérez-Bendito, Córdoba
C.F. Poole, Detroit, MI
E. Pungor, Budapest
J. Ruzicka, Seattle, WA
A. Sanz-Medel, Oviedo
S. Sasaki, Toyohashi
T. Sawada, Tokyo
K. Schügerl, Hannover
M. Thompson, Toronto
G. Tölg, Dortmund
Y. Umezawa, Tokyo
E. Wang, Changchun
H.V. Wenger, Eindhoven
C.S. Wolfbeis, Graz
Yu.A. Zolotov, Moscow
J. Zupan, Ljubljana

ANALYTICA CHIMICA ACTA

Scope. *Analytica Chimica Acta* publishes original papers, preliminary communications and reviews dealing with every aspect of modern analytical chemistry. Reviews are normally written by invitation of the editors, who welcome suggestions for subjects. Preliminary communications of important urgent work can be printed within four months of submission, if the authors are prepared to forego proofs.

Submission of Papers

Americas

Prof. Harry L. Pardue
Department of Chemistry
1393 BRWN Bldg, Purdue University
West Lafayette, IN 47907-1393
USA
Tel: (+ 1-317) 494 5320
Fax: (+ 1-317) 496 1200

Computer Techniques

Prof. J.T. Clerc
Universität Bern
Pharmazeutisches Institut
Baltzerstrasse 5, CH-3012 Bern
Switzerland
Tel: (+ 41-31) 654171
Fax: (+ 41-31) 654198

Other Papers

Prof. Alan Townshend
Department of Chemistry
The University
Hull HU6 7RX
Great Britain

Tel: (+ 44-482) 465027
Fax: (+ 44-482) 466410

Prof. Willem E. van der Linden
Laboratory for Chemical Analysis
Department of Chemical Technology
Twente University of Technology
P.O. Box 217, 7500 AE Enschede
The Netherlands
Tel: (+ 31-53) 892629
Fax: (+ 31-53) 356024

Prof. Paul Worsfold
Dept. of Environmental Sciences
University of Plymouth
Plymouth PL4 8AA
Great Britain

Tel: (+ 44-752) 233006
Fax: (+ 44-752) 233009

Submission of an article is understood to imply that the article is original and unpublished and is not being considered for publication elsewhere. *Anal. Chim. Acta* accepts papers in English only. There are no page charges. Manuscripts should conform in layout and style to the papers published in this issue. See inside back cover for "Information for Authors".

Publication. *Analytica Chimica Acta* appears in 14 volumes in 1993. The subscription price for 1993 (Vols. 267-280) is Dfl. 4214.00 plus Dfl. 462.00 (p.p.h.) (total approx. US\$ 2816.75). *Vibrational Spectroscopy* appears in 2 volumes in 1993. The subscription price for *Vibrational Spectroscopy* (Vols. 4 and 5) is Dfl. 700.00 plus Dfl. 66.00 (p.p.h.) (total approx. US\$ 461.50). The price of a combined subscription (*Anal. Chim. Acta* and *Vib. Spectrosc.*) is Dfl. 4592.00 plus Dfl. 528.00 (p.p.h.) (total approx. US\$ 3084.25). All earlier volumes (Vols. 1-266) except Vols. 23 and 28 are available at Dfl. 259.50 (US\$ 156.25), plus Dfl. 18.00 (US\$ 10.75) p.p.h., per volume. The Dutch guilder price is definitive. The U.S. dollar price is subject to exchange-rate fluctuations and is given only as a guide. Subscriptions are accepted on a prepaid basis only, unless different terms have been previously agreed upon.

Our p.p.h. (postage, packing and handling) charge includes surface delivery of all issues, except to subscribers in the U.S.A., Canada, Australia, New Zealand, China, India, Israel, South Africa, Malaysia, Thailand, Singapore, South Korea, Taiwan, Pakistan, Hong Kong, Brazil, Argentina and Mexico, who receive all issues by air delivery (S.A.L.-Surface Air Lifted) at no extra cost. For Japan, air delivery requires 25% additional charge of the normal postage and handling charge; for all other countries airmail and S.A.L. charges are available upon request.

Subscription orders. Subscription orders can be entered only by calendar year and should be sent to: Elsevier Science Publishers B.V., Journals Department, P.O. Box 211, 1000 AE Amsterdam, The Netherlands. Tel: (+ 31-20) 5803 642, Telex: 18582, Telefax: (+ 31-20) 5803598, to which requests for sample copies can also be sent. Claims for issues not received should be made within three months of publication of the issues. If not they cannot be honoured free of charge. Readers in the U.S.A. and Canada can contact the following address: Elsevier Science Publishing Co. Inc., Journal Information Center, 655 Avenue of the Americas, New York, NY 10010, U.S.A. Tel: (+ 1-212) 6333750, Telefax: (+ 1-212) 6333990, for further information, or a free sample copy of this or any other Elsevier Science Publishers journal.

Advertisements. Advertisement rates are available from the publisher on request.

Detailed "Instructions to Authors" for *Analytica Chimica Acta* was published in Volume 256, No. 2, pp. 373-376. Free reprints of the "Instructions to Authors" of *Analytica Chimica Acta* and *Vibrational Spectroscopy* are available from the Editors or from: Elsevier Science Publishers B.V., P.O. Box 330, 1000 AH Amsterdam, The Netherlands. Telefax: (+ 31-20) 5862845.

US mailing notice - *Analytica Chimica Acta* (ISSN 0003-2670) is published biweekly by Elsevier Science Publishers (Molenwerf 1, Postbus 211, 1000 AE Amsterdam). Annual subscription price in the USA US\$ 2816.75 (subject to change), including air speed delivery. Application to mail at second class postage rate is pending at Jamaica, NY 11431. *USA Postmasters:* Send address changes to Anal. Chim. Acta, Publications Expediting, Inc., 200 Meacham Av., Elmont, NY 11003. Airfreight and mailing in the USA by Publication Expediting.

ANALYTICA CHIMICA ACTA

An international journal devoted to all branches of analytical chemistry

(Full texts are incorporated in CJELSEVIER, a file in the Chemical Journals Online database available on STN International; Abstracted, indexed in: Aluminum Abstracts; Anal. Abstr.; Biol. Abstr.; BIOSIS; Chem. Abstr.; Curr. Contents Phys. Chem. Earth Sci.; Engineered Materials Abstracts; Excerpta Medica; Index Med.; Life Sci.; Mass Spectrom. Bull.; Material Business Alerts; Metals Abstracts; Sci. Citation Index)

VOL. 269 NO. 1

CONTENTS

NOVEMBER 2, 1992

Flow Analysis

- Coupled flow-injection analysis-flame atomic absorption spectrometry for the quantitative determination of aluminium in beverages and waters incorporating on-line cation exchange
H.J. Salacinski (London, UK), P.G. Riby (Beltsville, MD, USA) and S.J. Haswell (Hull, UK) 1
- Comparison of three propulsion systems for application in flow-injection zone penetration dilution and sorbent extraction preconcentration for flame atomic absorption spectrometry
Z.-L. Fang, M. Sperling and B. Welz (Überlingen, Germany) 9
- Enhanced automatic flow-injection determination of the total polyphenol index of wines using Folin-Ciocalteu reagent
M. Celeste, C. Tomás, A. Cladera, J.M. Estela and V. Cerdà (Palma de Mallorca, Spain) 21
- Automated continuous-flow titration
J. Bartroli and L. Alerm (Barcelona, Spain) 29
- Characteristics and readout correlation of flow-injection analysis for penicillin
X.-M. Li (Kowloon, Hong Kong), M.-X. Chen, F.-C. Ruan (Guangzhou, China) and W.-Y. Ng (Kowloon, Hong Kong) .. 35
- Amperometric techniques in flow-injection analysis: determination of magnesium in sera and natural waters
A.J. Downard, J.B. Hart, H.K.J. Powell and S. Xu (Christchurch, New Zealand) 41

Electroanalytical Chemistry and Sensors

- Pressure insensitive solid state reference electrode for in-situ voltammetric measurements in lake water
R. Jermann, M.-L. Tercier and J. Buffle (Geneva, Switzerland) 49
- Blocking of chemically modified graphite electrodes by surfactants
M. Skoog, K. Kronkvist and G. Johansson (Lund, Sweden) 59
- Plasticized poly(vinyl chloride) as a permselective barrier membrane for high-selectivity amperometric sensors and biosensors
I.M. Christie, P.H. Treloar and P. Vadgama (Salford, UK) 65
- Silicon-based chlorine sensor with on-wafer deposited chemically anchored diffusion membrane. Part I. Basic sensor concept
A. Van den Berg, M. Koudelka-Hep, B.H. Van der Schoot, N.F. De Rooij (Neuchâtel, Switzerland), E. Verney-Norberg (Ecully, France) and A. Grisel (Neuchâtel, Switzerland) 75
- Development of an optical-chemical sensor for the detection of ammonium ions
W. Sellien, R. Czolk, J. Reichert and H.J. Ache (Karlsruhe, Germany) 83

Chromatography

- Noise analysis of the reflected power signal from a microwave-induced plasma gas chromatographic detector
R.M. Alvarez Bolainez and C.B. Boss (Raleigh, NC, USA) 89

Chemiluminescence

- Light emission from bilirubin using the peroxyoxalate chemiluminescence reaction
N. Wu, W.J. Horvath and C.W. Huie (Binghamton, NY, USA) 99

(Continued overleaf)

15 NOV 25 1992

Contents (continued)

Flow injection and liquid chromatographic postcolumn detection of amino acids by mimetic peroxidase-catalysed chemiluminescence reaction Y.-X. Ci, J.-K. Tie, Q.-W. Wang and W.-B. Chang (Beijing, China)	109
<i>Spectrometry</i>	
Multi-element analysis of biological tissues by inductively coupled plasma mass spectrometry: healthy Sprague Dawley rats Y. Gélinas, M. Youla, R. Béliveau, J.-P. Schmit (Montréal, Canada) and J. Ferraris (Dakar, Senegal)	115
Laser-induced plasma atomic emission spectrometry in liquid aerosols K.C. Ng, N.L. Ayala, J.B. Simeonsson and J.D. Winefordner (Gainesville, FL, USA)	123
Development of a laser-excited atomic fluorescence spectrometer and a method for the direct determination of lead in Great Lakes waters V. Cheam, J. Lechner, I. Sekerka, R. Desrosiers, J. Nriagu and G. Lawson (Burlington, Canada)	129
Usefulness of stopped-flow mixing methodology for the determination of fluorescent and absorbing species. Spectrofluorimetric determination of imipramine in serum L. De la Peña, A. Gómez-Hens and D. Pérez-Bendito (Córdoba, Spain)	137
Versatile stopped-flow apparatus with adjustable pistons P.-O. Freskgård, N. Bergenhem and U. Carlsson (Linköping, Sweden)	143
<i>Chemometrics</i>	
Regression analysis of piezoelectric titration data to estimate system parameters W.-Z. Wei, L.-H. Nie and S.-Z. Yao (Changsha, China)	149
<i>Thermometric Methods</i>	
Thermoanalytical studies of water on aluminum oxides with different porosities P. Staszczuk (Lublin, Poland), M. Jaroniec and R.K. Gilpin (Kent, OH, USA)	157

ANALYTICA CHIMICA ACTA
VOL. 269 (1992)

ANALYTICA CHIMICA ACTA

*An international journal devoted to all branches of analytical chemistry
Revue internationale consacrée à tous les domaines de la chimie analytique
Internationale Zeitschrift für alle Gebiete der analytischen Chemie*

EDITORS

HARRY L. PARDUE (West Lafayette, IN, U.S.A.)

ALAN TOWNSHEND (Hull, Great Britain)

J.T. CLERC (Berne, Switzerland)

WILLEM E. VAN DER LINDEN (Enschede, The Netherlands)

PAUL J. WORSFOLD (Plymouth, Great Britain)

Editorial Advisers

F.C. Adams, Antwerp
J.F. Alder, Manchester
C.M.G. van den Berg, Liverpool
A.M. Bond, Bundoora, Vic.
S.D. Brown, Newark, DE
J. Buffle, Geneva
P.R. Coulet, Lyon
S.R. Crouch, East Lansing, MI
R. Dams, Ghent
L. de Galan, Vlaardingen
M.L. Gross, Lincoln, NE
W. Heineman, Cincinnati, OH
G.M. Hieftje, Bloomington, IN
T. Imasaka, Fukuoka
D. Jagner, Gothenburg
G. Johansson, Lund
D.C. Johnson, Ames, IA
I. Karube, Tokyo
A.M.G. Macdonald, Birmingham
D.L. Massart, Brussels
P.C. Meier, Schaffhausen

M.E. Meyerhoff, Ann Arbor, MI
J.N. Miller, Loughborough
H.A. Mottola, Stillwater, OK
M.E. Munk, Tempe, AZ
M. Otto, Freiberg
D. Pérez-Bendito, Córdoba
C.F. Poole, Detroit, MI
E. Pungor, Budapest
J. Ruzicka, Seattle, WA
A. Sanz-Medel, Oviedo
S. Sasaki, Toyohashi
T. Sawada, Tokyo
K. Schügerl, Hannover
M. Thompson, Toronto
G. Tölg, Dortmund
Y. Umezawa, Tokyo
E. Wang, Changchun
H.W. Werner, Eindhoven
O.S. Wolfbeis, Graz
Yu.A. Zolotov, Moscow
J. Zupan, Ljubljana



Anal. Chim. Acta, Vol. 269 (1992)

ELSEVIER, Amsterdam–London–New York–Tokyo

No part of this publication may be reproduced, stored in a retrieval system or transmitted in any form or by any means, electronic, mechanical, photocopying, recording or otherwise, without the prior written permission of the publisher, Elsevier Science Publishers B.V., Copyright and Permissions Dept., P.O. Box 521, 1000 AM Amsterdam, The Netherlands.

Upon acceptance of an article by the journal, the author(s) will be asked to transfer copyright of the article to the publisher. The transfer will ensure the widest possible dissemination of information.

Special regulations for readers in the U.S.A.—This journal has been registered with the Copyright Clearance Center, Inc. Consent is given for copying of articles for personal or internal use, or for the personal use of specific clients. This consent is given on the condition that the copier pays through the Center the per-copy fee for copying beyond that permitted by Sections 107 or 108 of the U.S. Copyright Law. The per-copy fee is stated in the code-line at the bottom of the first page of each article. The appropriate fee, together with a copy of the first page of the article, should be forwarded to the Copyright Clearance Center, Inc., 27 Congress Street, Salem, MA 01970, U.S.A. If no code-line appears, broad consent to copy has not been given and permission to copy must be obtained directly from the author(s). All articles published prior to 1980 may be copied for a per-copy fee of US \$2.25, also payable through the Center. This consent does not extend to other kinds of copying, such as for general distribution, resale, advertising and promotion purposes, or for creating new collective works. Special written permission must be obtained from the publisher for such copying.

No responsibility is assumed by the publisher for any injury and/or damage to persons or property as a matter of products liability, negligence or otherwise, or from any use or operation of any methods, products, instructions or ideas contained in the material herein.

Although all advertising material is expected to conform to ethical (medical) standards, inclusion in this publication does not constitute a guarantee or endorsement of the quality or value of such product or of the claims made of it by its manufacturer.

This issue is printed on acid-free paper.

PRINTED IN THE NETHERLANDS

Coupled flow-injection analysis–flame atomic absorption spectrometry for the quantitative determination of aluminium in beverages and waters incorporating on-line cation exchange

Henryk J. Salacinski

*The Advanced Centre for Biochemical Engineering, Department of Chemical and Biochemical Engineering, Torrington Place,
University College London, London WC1 7JE (UK)*

Philip G. Riby

US Department of Agriculture, Beltsville Human Nutrition Research Center, BLDG 161, BARC-EAST, Beltsville, MD 20705 (USA)

Stephen J. Haswell

School of Chemistry, The University of Hull, Hull HU6 7RX (UK)

(Received 30th March 1992; revised manuscript received 1st June 1992)

Abstract

A method for determining the aluminium levels in local water, tea leaf digest, tea and coffee infusions by means of on-line cation exchange flow-injection–flame atomic absorption spectrometry (FIA–FAAS) is described. Quantitative results can be carried out down to 75 ng ml^{-1} of Al using sample volumes in the range 6.0–24.0 ml. The method using a conventional FAAS system was found to be rapid, simple and relatively inexpensive offering good selectivity and typical R.S.D.s of 1–2% ($n = 10$) with a relative error of about 2%.

Keywords: Atomic absorption spectrometry; Flow injection; Ion chromatography; Aluminium determination; Cation exchange; Flame atomic absorption spectrometry; Waters

It is now known that tea and coffee infusions contain high levels of aluminium [1,2] and it has been suggested that consumption of such beverages contributes extensively to the daily dietary intake of aluminium [3]. Numerous techniques have been reported for the quantification of aluminium in a range of matrix types at both trace and ultratrace levels. These have included; electrothermal atomisation atomic absorption spec-

troscopy [4–6]; fluorimetry [7]; spectrophotometry [8,9]; liquid phosphorimetry [10]; chromatography [11,12] flow injection methods [13–17] and inductively coupled plasma spectrometry–atomic emission spectrometry (ICP–AES) [18].

Many of these methods however, require expensive and often elaborate instrumentation and are prone to various interferences or calibration problems [19]. Therefore, it would be highly advantageous to have an accurate, economical and rapid method for the determination of Al in beverages. The flow-injection analysis (FIA) approach to aluminium analysis using an on-line

Correspondence to: S.J. Haswell, School of Chemistry, The University of Hull, Hull HU6 7RX (UK).

column to preconcentrate and matrix modify has made flame atomic absorption spectrometry (FAAS) an attractive technique for sub- $\mu\text{g ml}^{-1}$ detection [20–25]. Whilst the previous work almost exclusively describes the use of Chelex and Amberlite resins in on-line columns, this paper focuses on the development of an FIA method based on an on-line cation exchange resin, for the determination of aluminium at the sub- $\mu\text{g ml}^{-1}$ level in local water, tea leaf digests, and tea and coffee infusions with direct FAAS quantification. The use of cation exchange resin was investigated in this study as it was considered to offer a kinetically faster and thermodynamically more stable extraction of the aluminium ions over the previously described solid phase extraction techniques.

EXPERIMENTAL

Reagents and materials

High-purity water was obtained by using reverse osmosis (Milli-R04; Millipore, Harrow) followed by adsorption, de-ionisation and ultrafiltration (Millipore Milli-Q system). All reagents were of analytical reagent grade and high purity distilled/de-ionized water was used unless stated otherwise. A stock 1000 $\mu\text{g ml}^{-1}$ solution of aluminium nitrate (Spectrosol) was obtained from BDH (Poole) and used to prepare standards made up in 5% v/v nitric acid (BDH).

In the FI manifold high purity distilled/de-ionized water was used as the carrier stream with 4 M HCl (250 μl) being used as the eluent for aluminium from the SCX column. All glassware was scrupulously cleaned and soaked in 10% v/v nitric acid prior to rinsing with high-purity distilled/de-ionized water.

Instrumentation

A Thermo Electron 357 atomic absorption spectrometer equipped with an aluminium hollow cathode lamp operated at 4 mA was used with an optimized nitrous oxide–acetylene flame. The selected wavelength for aluminium was 309.3 nm with a spectral bandpass of 1 nm. The flow-injection (FI) manifold, constructed in-house, is shown schematically in Fig. 1. The peristaltic pump was

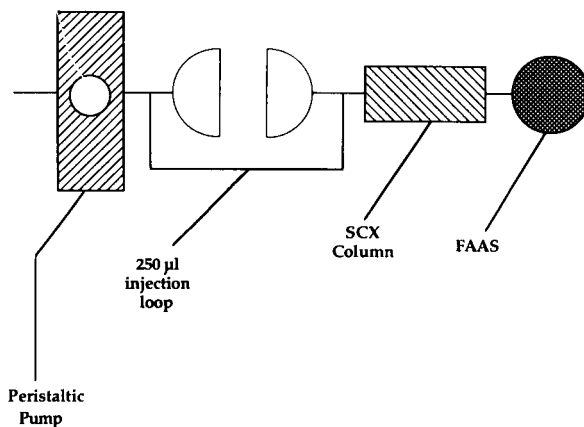


Fig. 1. Schematic diagram of the on-line flow analysis system.

a four-way Gilson Minipuls 3 (Anachem, Luton) fitted with appropriate flow and connecting tubing (0.8 mm i.d., PTFE supplied by Anachem) and the rotary injection valve (Anachem) was fitted with a 250- μl injection loop. The SCX column was prepared from 500 mg commercially available preparative column (Bond Elut, Jones Chromatography, Mid Glamorgan). These columns are supplied with a solvent reservoir above the SCX material. This reservoir was removed (10 mm above the exchange material) to allow inter-connecting tubes to be slotted inside and so reduce the dead volume. The end fitting was constructed of various internal diameter PTFE tubes of 15-mm length which slot into each other to form a single orifice to allow the carrier to enter the column. The cut column has an i.d. of 8 mm into which an 8 mm o.d., 6 mm i.d. tube was fitted. A 6 mm o.d., 5 mm i.d. tube was slotted into this fitting followed by a 5 mm o.d., 3 mm i.d. tube. Finally, a tube of 3 mm o.d. and 0.8 mm i.d. was fitted to allow connection into the flow system. The end fitting was then coated in epoxy resin (Araldite) to make it liquid tight [26]. Absorbance signals were recorded on a Linseis LS-52 chart recorder operating in the 50 mV FSD range. Following optimization for aluminium of the FAAS the FIA system was coupled up with the flow rate (approximately 6 ml min^{-1}) adjusted to match the nebulizer uptake rate. Throughout this work the FIA manifold remained connected to the nebulizer of the FAAS.

Measurement procedure

(i) *Beverage tea sample preparation.* For the tea leaf digest, (500 mg) aliquots of dry tea leaves were accurately weighed out (dried prior to experimental usage to a constant weight at 85°C) and decomposed in a mixture of HNO₃ (4 ml) and HClO₄ (1 ml) in a micro-Kjeldahl flask.

After heating during approximately 45 min, (i.e. when no more brown/black oxides of nitrogen were evolved), the digest was cooled carefully in an ice bath, and diluted to a volume of 10.0 ml with 5% v/v nitric acid.

For the tea leaf infusions, 2.0 g aliquots of neat tea leaves were submerged carefully in 40 ml of high-purity water at a temperature of 100 ± 5°C for 3 min. Then, after a period of cooling the infusion was gently filtered (Whatman No. 541 filter paper) into previously cleaned centrifuge tubes, the total volume of filtrate being acidified with 3 ml of concentrated HNO₃. The sample was then centrifuged in order to separate the precipitated organic material. Following centrifugation, the acidified clear infusion was diluted to a total volume of 50 ml with 5% v/v nitric acid.

(ii) *Beverage coffee sample preparation.* For the ground coffee bean infusions, initially 20.0 g of neat roasted coffee beans were freshly fine ground (Hamilton Beach Seven, a seven-speed blender), every time measurements were required. Then, 2.0 g aliquots of neat ground coffee beans were submerged carefully in 40 ml of high purity water at a temperature of 100 ± 5°C for 3 min. After a period of cooling, the infusion was gently filtered into previously cleaned centrifuge tubes, the total volume of filtrate being acidified with 3 ml of concentrated HNO₃. The sample was then centrifuged in order to separate the precipitated organic material. Following centrifugation the acidified clear infusion was diluted to a total volume of 50 ml with 5% v/v nitric acid.

(iii) *Local water samples.* The local water samples: tap and reservoir waters, prior to analysis, were filtered through a filter-paper with pore size of 0.45 μm (Millipore) and collected in a polyethylene container that had been cleaned carefully with nitric acid [27]. A small amount of concentrated nitric acid 0.25 ml l⁻¹ was added to preserve the sample.

RESULTS AND DISCUSSION

Optimization of flow-injection variables

The atomic absorption instrument was optimized for the maximum absorbance signal prior to each period of operation in accordance with the manufacturers advice. As an integral part of this set-up procedure the nebulizer flow-rate was adjusted to give an optimum absorbance signal for aluminium in the 4–6 ml min⁻¹ range (Fig. 2). Once this value had been set it was a simple matter to adjust the peristaltic pump to give an equivalent delivery rate from the FI manifold. As part of the optimization procedure a study was

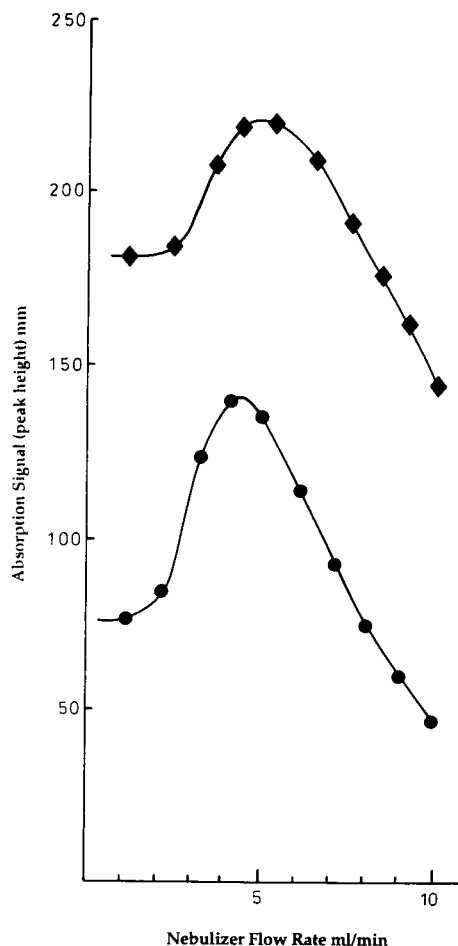


Fig. 2. Signal response for aluminium with variation in nebulizer flow-rate. ● = 5 μg ml⁻¹ Al solution; ◆ = 12.5 μg ml⁻¹ Al solution.

carried out on the influence that sample flow-rates may have on the deposition and elution of aluminium from the exchange resin used. The deposition flow-rate for the aluminium on the cation exchange resin was varied between 1 and 12 ml min⁻¹ whilst the elution flow-rate was held constant at 6 ml min⁻¹ (Fig. 3). The results indicated that the column affinity for aluminium was similar for deposition flow-rates in the range 4-7 ml min⁻¹. At flow-rates above and below the range the signal can be seen to decrease and this is due in part to nebulizer effects (Fig. 2). In addition at higher flow-rates there will be some degree of kinetic hindrance with respect to the aluminium ion exchange mechanism. In comparison, the elution flow-rate for the deposited aluminium by 4 M HCl (250 μl) was found to be a little more critical with an optimum range 4-5 ml min⁻¹ which is directly related to the elution acid volume 250 μl selected (Fig. 4). The volume of 250

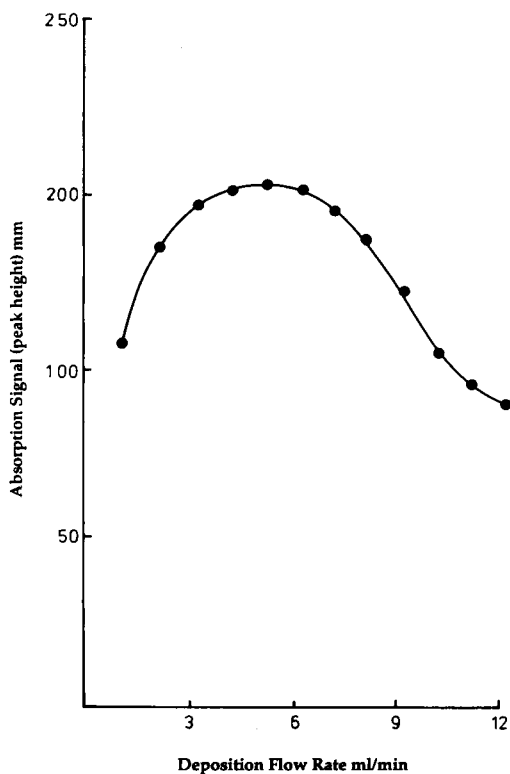


Fig. 3. Deposition flow-rates as a function of signal response for a 12.5 μg ml⁻¹ solution of aluminium.

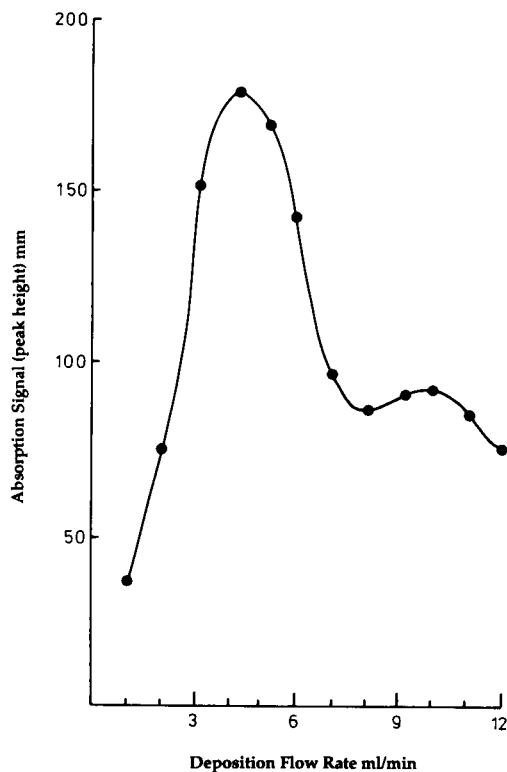


Fig. 4. Elution flow-rates as a function of signal response for a 6.25 μg ml⁻¹ solution of aluminium.

μl was chosen to give maximum sensitivity for the transient FAAS signal with the minimum dilution effect. The results for the sample flow-rate experiments indicated that 5 ml min⁻¹ would offer the best conditions for both the deposition and elution of aluminium. However at 5 ml min⁻¹ it was found that column regeneration with the 4 M HCl (the highest acid concentration advised for the column material) was more suited to a slightly higher flow-rate and a compromise flow-rate of 6 ml min⁻¹ was found to be practically more suitable for the analysis of real samples.

Various experiments were next carried out to establish the column loadings, calibration and precision of the proposed methodology. Column loading capacity was estimated by injecting (2 ml) increasingly higher concentrations of aluminium solution onto the column until a break-through point (i.e. no retention of aluminium) was observed as a signal by the FAAS. During these

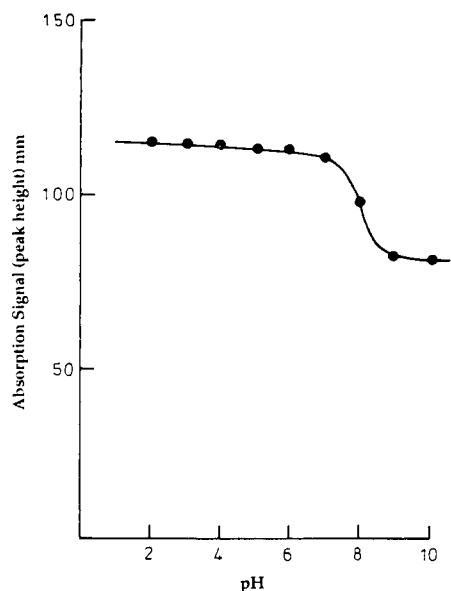


Fig. 5. Effect of sample pH on the absorption signal for a 6.25 $\mu\text{g ml}^{-1}$ solution of aluminium.

deposition elution experiments the column was regenerated between each sample injection. Sample break-through was seen to occur when a 950 $\mu\text{g ml}^{-1}$ solution was used and this corresponded to an approximate column loading capacity for aluminium of 1.8 ng. This capacity was considered to be adequate for the preconcentration requirements of the column. During method optimization some consideration was also given to the pH in which the cation exchange process for aluminium takes place. The aquo chemistry of group 3B elements such as aluminium tend to produce strongly hydrolysed species and in acid solutions aluminium is present as the $[\text{Al}(\text{H}_2\text{O})_6]^{3+}$ ion. However as the level of acidity decreases polymeric hydrolysed species such as the hydrated $[\text{Al}_2(\text{OH})_2]^{4+}$ and $[\text{Al}_7(\text{OH})_{10}]^{5+}$ may be formed. As the preconcentration step relies on all the aluminium in the sample to be as the tripositive aquo ions a study on the effect of the sample pH was carried out. The pH of a 12.5

TABLE 1

Aluminium levels in tea leaf digests, tea and coffee infusions, and in local water samples determined by on-line cation exchange preconcentration FIA-FAAS

Sample	Loading pre-concentration factor (s^{-1})	Aluminium ($\mu\text{g ml}^{-1}$)	Relative standard deviation (%)
<i>Tea leaf digest</i>			
Commercial blend ("Tea leaves") ^{a,c}	240	552 ± 38	6.1
Darjeeling ^{a,c}	240	299 ± 8	2.9
Sri Lankan ^{a,c}	240	482 ± 8	3.6
<i>Tea infusions</i>			
Commercial blend ("Tea bag") ^{a,c}	240	12.60 ± 0.8	3.5
Darjeeling ("Tea bag") ^{a,c}	240	4.4 ± 0.6	2.0
<i>Coffee infusions</i>			
Commercial Columbian/Brazilian blend ("Coffee beans") ^{b,c}	60	7.3 ± 1	1.8
<i>Local waters</i>			
London tap water ^{c,c}	960	20.0 ± 0.2	0.5
Mid-Sussex Reservoir tap water ^{d,c}	240	35.0 ± 0.6	0.4
	480	39.8 ± 0.6	0.5
	960	45.0 ± 0.8	0.98

^a Mean and standard deviations based on six determinations. ^b Mean and standard deviations based on two determinations.

^c Mean and standard deviations based on sixteen determinations. ^d Mean and standard deviations based on fifteen determinations.

^e Recovery tests were performed by adding known amounts of aluminium. Recovery = $100 \pm 2\%$.

$\mu\text{g ml}^{-1}$ Al standard was adjusted in the range 2–10 using concentrated HCl and NaOH. Figure 5 shows a plot of the signal for the exchanged aluminium eluted versus pH. As expected the results indicate a decrease in signal intensity as the pH increases in alkalinity corresponding to a shift away from the presence of Al^{3+} concentrations. This shift was however not as large as expected and this was thought to be due to (a) the low concentrations of aluminium used not thermodynamically attaining the species expected and (b) a buffering effect associated with the cation exchange resin which was essentially in the H^+ form. In this work all samples were adjusted to have a $\text{pH} < 4$ to avoid differences in aluminium species between samples. Precision of the deposition time was carried out using a $12.5 \mu\text{g ml}^{-1}$ solution ($\text{pH} 4$) of aluminium nitrate deposited for 1 min, 10 replicate determinations gave an R.S.D. of 1.12% with $100 \pm 2\%$ recovery. The technique of timed depositions for aluminium from aluminium solutions was used in this work to (a) gain maximum flexibility in the preconcentration of different samples and (b) to simplify the calibration procedure. The calibration evaluation was carried out using a $0.2 \mu\text{g ml}^{-1}$ solution ($\text{pH} 4$) of aluminium nitrate deposited on the column for times varying from 1–5 min. This produced a curve with the equation $y = 0.052x + 0.044$ correlation coefficient of 0.9742 and a lower limit of detection of 75 ng ml^{-1} , offering good linearity over the required range of measurements for a wide variety of matrices.

In order to establish the process of sample preconcentration more fully a range of solutions of differing aluminium concentration (0.07 – $6.25 \mu\text{g ml}^{-1}$) were studied and these results are shown in Fig. 6. From the results it can be seen that a high enough mass of aluminium can be deposited in the SCX column even for the lowest standard to allow an accurate response to be obtained in ca. < 60 s. In addition a reasonably wide linear range over which aluminium could be concentrated was found to exist.

In Table 1 are summarized the results obtained for a range of tea and coffee infusions in deionized distilled water, tea leaf digest and local

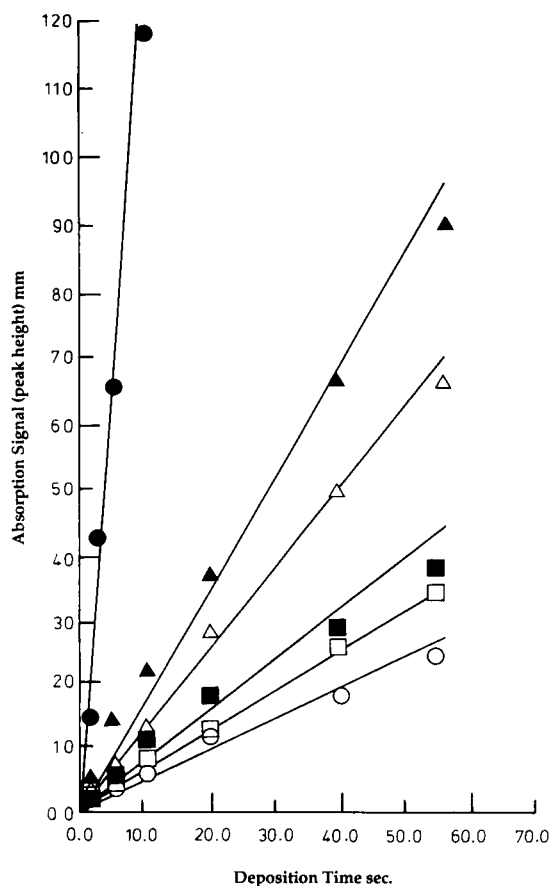


Fig. 6. Plot of signal response vs. deposition time for a range of aluminium solutions. Key: ● = 6.25; ▲ = 1.0; △ = 0.5; ■ = 0.25, □ = 0.15; ○ = $0.07 \mu\text{g ml}^{-1}$.

tap water samples. The table shows the preconcentration factor as a function of time or load of sample which corresponds to approximately 6.0–96.0 ml of sample. The quantification given in appropriate units for the tea and coffee samples are found to be in the same range as those previously reported [1–3,28–30].

Conclusions

It has been shown that the use of FIA–FAAS offers a rapid, economical, and relatively simple determination for aluminium at the ng ml^{-1} level in matrices such as tea and coffee infusions and tea leaf digests.

The advantages of the FIA–FAAS method are: relatively small sample volumes are required

(6–20 ml) for the preconcentration procedure and a reasonably wide dynamic range can be used. In addition few potential interferences exist with the methodology developed when operating at a pH < 4. Further, there exists a great potential for easy and rapid speciation studies, to be carried out in slightly acidified, as well as unmodified tea infusions.

REFERENCES

- 1 A.M. Coriat and R.D. Gillard, *Nature* (London), 321 (1986) 570.
- 2 S.J. Fairweather-Tait, G.R. Moore and S.E. Jemil Fatemi, *Nature* (London), 330 (1987) 213.
- 3 K.R. Kich, M.A.B. Pougnet, S. De Villiers and F. Montegudo, *Nature* (London), 333 (1988) 123.
- 4 E.M. Skelly and F.T. DiStefano, *Appl. Spectrosc.*, 42 (7), (1988) 1302.
- 5 H.J. Gitelman, *Aluminium and Health. A Critical Review*, Marcel Dekker, New York, 1988.
- 6 J. Smeyers-Verbeke and D. Verbeeden, *Anal. Chem.*, 60 (1988) 380.
- 7 A. Munoz de la Pena, F. Salinas, M.E. Sanchez and J.A. Murillo, *Analyst*, 113 (1988) 1435.
- 8 K. Ohzeki, T. Uno, I. Nukatsuka and R. Ishida, *Analyst*, 113 (1988) 1545.
- 9 M.T.M. Zaki and A.M. El-Didamony, *Analyst*, 113 (1988) 577.
- 10 M.R. Fernandez de la Campa, M.E. Diaz Garcia and A. Sanz-Medel, *Anal. Chim. Acta*, 212 (1988) 235.
- 11 P. Jones, L. Ebdon and T. Williams, *Analyst*, 113 (1988) 641.
- 12 S.E. Meek and D.J. Pietrzyk, *Anal. Chem.*, 60 (1988) 1397.
- 13 B. Bouzid and A.M.G. MacDonald, *Anal. Chim. Acta*, 207 (1988) 337.
- 14 P. Hernandez, L. Hernandez and J.Z. Losada, *Fresenius' Z. Anal. Chem.*, 325 (1986) 300.
- 15 P.W. Alexander, R.J. Finlayson, L.E. Smythe and A. Thalib, *Analyst*, 107 (1982) 1335.
- 16 S. Olsen, L.C.R. Pessenda, J. Ruzicka and E.H. Hansen, *Analyst*, 108 (1983) 905.
- 17 C.M. McLeod, *J. Anal. At. Spectrom.*, 2 (1987) 549.
- 18 A. Sanz-Medel, R.M. Rodriguez, R. Gonzalez Alonso, A. Noval Vallina and J.B. Cannata, *J. Anal. At. Spectrom.*, 2 (1987) 177.
- 19 J.F. Tyson, C.E. Adeemuro and S.R. Beysouth, *J. Anal. At. Spectrom.*, 4 (1989) 191.
- 20 M. Pesarento, A. Profumo, C. Riolo and T. Soldi, *Analyst*, 114 (1989) 632.
- 21 M.R. Pereiro Garcia, M.E. Diaz Garcia and A. Sanz-Medel, *J. Anal. At. Spectrom.*, 2 (1987) 2 699.
- 22 S.C. Pai, P.Y. Whung and R.L. Lai, *Anal. Chim. Acta*, 211 (1988) 257.
- 23 S.C. Pai, *Anal. Chim. Acta*, 211 (1988) 271.
- 24 L. Bakobza and G. Cote, *Polyhedron*, 4 (1985) 1499.
- 25 M.R. Pereiro Garcia, A. Lopez Garcia, M.F. Diaz Garcia and A. Sanz-Medel, *J. Anal. At. Spectrom.*, 5 (1990) 15.
- 26 P.G. Riby, S.J. Haswell and R. Grzeskowiak, *J. Anal. At. Spectrom.*, 4 (1989) 181.
- 27 *Standard Methods for Examination of Water and Wastewater*, Fifteenth Edition, American Public Health Association–American Water Works Association and Water Pollution Control Federation, Washington, DC, 1980.
- 28 R.T. Ellis, *Biologist*, 30 (1983) 247.
- 29 O. Talibudeen and S. Sivasubramanian, *J. Sci. Food Agric.*, 22 (1971) 325.
- 30 W.D. Kachny, *New Engl. J. Med.*, 290 (1977) 1389.

Comparison of three propulsion systems for application in flow-injection zone penetration dilution and sorbent extraction preconcentration for flame atomic absorption spectrometry

Zhao-Lun Fang¹, Michael Sperling and Bernhard Welz

Department of Applied Research, Bodenseewerk Perkin-Elmer GmbH, D(W)-7770 Überlingen (Germany)

(Received 13th April 1992)

Abstract

Better precision can be achieved in flow-injection on-line dilution for flame atomic absorption spectrometry by zone penetration using knotted reactor sample loops and transport conduits than with straight conduits. About a 2% R.S.D. was obtained for a dilution factor of 20 using the valley between two peaks with a peristaltic and a reciprocating piston pump. A sinusoidal syringe pump gave an inferior precision of 8% R.S.D. under the same conditions owing to a lack of proper interfacing between such pumps and the atomic absorption spectrometer. On-line sorbent extraction column preconcentration was shown to be feasible using sinusoidal and reciprocating pump systems, which obviated the need for solvent-proof pump tubes. However, both systems had to be supplemented by peristaltic pumps. Air segmentation between sample and eluent was found to be effective in preventing dispersion at the interface when sample loading and elution were performed in one piston stroke of the sinusoidal pump. The concentration efficiency (15–18 min⁻¹) and short-term precision (ca. 2% R.S.D.) of both preconcentration systems were generally comparable to those of previously reported systems for sorbent extraction preconcentration with time-based sampling, but the long-term precision of the piston and syringe pump systems (4–5% R.S.D.) was better than that of the time-based peristaltic pump system (10–20% R.S.D.).

Keywords: Atomic absorption spectrometry; Flow injection; Preconcentration; Sorbent extraction; Zone penetration dilution

Flow injection (FI) is a technique for automated solution handling that is based on the reproducible timing of events during the determinations [1]. Therefore, the precision of the delivery rate of carrier, samples and reagents, which is determined by the propulsion system, is very important for achieving optimum analytical performance.

The requirements for an ideal propulsion system for FI may be summarized as follows: reproducible flow-rates on a short-term (hours) and on a long-term (days) basis; multi-channel capability, providing at least four parallel pumping channels, to ensure versatility; pulse-free fluid delivery; resistance to aggressive reagents and solvents; flow-rates readily adjustable; and low initial investment and running costs.

A large variety of different devices and approaches have been used to meet these requirements, including peristaltic pumps, pressurized reservoirs, piston pumps for liquid chromatography, suction from a nebulizer and, most recently,

Correspondence to: B. Welz, Department of Applied Research, Bodenseewerk Perkin-Elmer GmbH, D(W)-7770 Überlingen (Germany).

¹ On leave from the Institute of Applied Ecology, Academia Sinica, Shenyang, China.

a specially designed sinusoidal piston pump [2]. Unfortunately, hitherto, none of the available approaches could meet all the requirements listed above. However, it may be possible to approach ideal conditions in specific applications where some of the requirements are not critical, or by a combination of different propulsion systems.

A relatively large number of FI on-line dilution systems for flame atomic absorption spectrometry (FAAS), based on different principles, have been reported [3]. One of the most versatile and routinely applicable techniques for on-line dilution seems to be the zone penetration or sequential injections approach [4]. Three or even five different dilution levels of the analyte may be obtained with this technique in one injection without resorting to complicated gradient evaluations. However, the technique appears not to have been evaluated critically since its introduction by Zagatto et al. [4] in 1985, particularly in terms of precision, which is an important criterion for a dilution system. This feature is obviously strongly dependent on the performance of the propulsion system, and it appeared worthwhile to make a more critical evaluation of the precision of this versatile on-line dilution technique.

On-line preconcentration with sorbent extraction now appears to be well established for FAAS [5] and graphite furnace (GF) AAS [6]. However, long term drift was observed in routine application with the time-based sampling approach using peristaltic pumps, probably owing to drift in flow-rates. Although in most instances this may not pose a serious problem, as frequent calibration can be easily performed in FI-AAS, further improvement in this direction is nevertheless desirable. In this work, an attempt was made to evaluate three different propulsion systems in two representative FI-FAAS applications. The systems studied were a peristaltic pump, a reciprocating piston pump and a sinusoidal syringe pump. The FI systems used for the study were a zone penetration dilution system and an on-line sorbent extraction preconcentration system. The systems had to be redesigned to accommodate all three propulsion systems with minor modifications, so that comparison was more meaningful.

A volume-based system was developed for on-line preconcentration, with some sacrifice in sample throughput, to improve the performance with respect to long-term drift for the comparison of the different pump systems. Another reason for adopting a volume-based sampling approach was that this was the only possibility for performing on-line column preconcentration using the sinusoidal pump.

EXPERIMENTAL

Instrumentation

A Perkin-Elmer Model 2100 atomic absorption spectrometer equipped with a deuterium arc background corrector was used in the FI mode with a flow spoiler impact system in the spray chamber. Calcium and lead hollow-cathode lamps, both operated at 7 mA, were used with the wavelengths set at 422.7 and 283.3 nm, respectively. The acetylene and air flow-rates for the flame were chosen as recommended by the manufacturer for the zone penetration dilution studies, but the flame conditions were slightly leaner than recommended for the on-line sorbent extraction in order to compensate for the effect of the methanol introduced during column elution. The nebulizer was adjusted to the lowest uptake rate giving the optimum response in the conventional mode of sample introduction, which was 6 ml min⁻¹.

A Perkin-Elmer Model FIAS-200 FI system was connected to the FAAS instrument, and the two programmable peristaltic pumps of the system, equipped with Tygon pump tubes, were used in this study.

A Sanuki (Tokyo) Model DMX-2000 dual-piston reciprocating pump was used with the two channels connected with a T-piece.

An Alitea (Medina, WA) Model S2-V dual-syringe sinusoidal flow pump was used in combination with a modified Bifok/Tecator Model V-100 injector valve, with eight channels each on the rotor and the stator. The valve was actuated by a laboratory-made motor-driven unit cased in a metal housing with the valve on top of the housing. The flow-rate and phase intervals of the

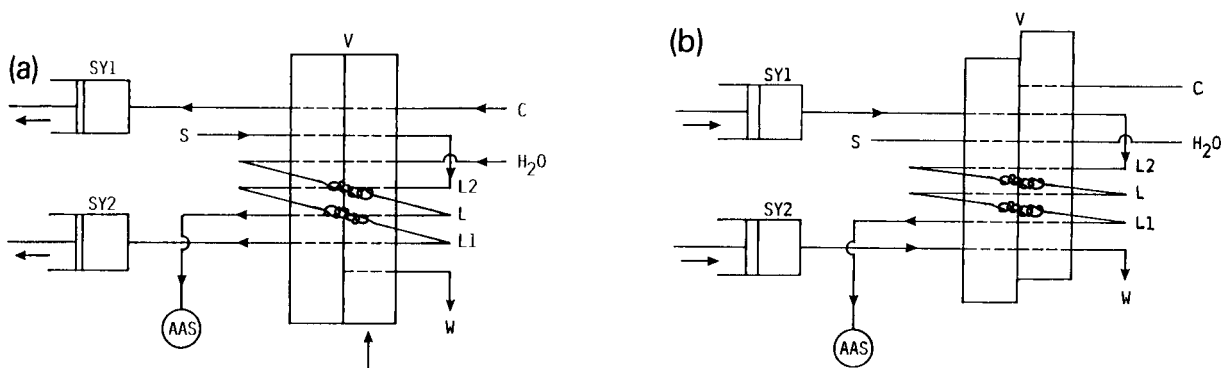


Fig. 1. FI manifold for zone penetration dilution using a sinusoidal syringe pump. SY1, SY2 = syringes 1 and 2; C = carrier solution; S = sample solution; L1, L2 = sample loops; L = intermediate loop; V = eight port valve; W = waste; AAS = flame AAS detector. (a) Loading sequence; (b) injection sequence.

pump and the sequence of operation of the valve were controlled by a computer program written for this study. In order to synchronize the program with the data acquisition sequence of the spectrometer, the read cycle was initiated by the pump program rather than by the spectrometer.

The time-resolved analyte absorbance signals were displayed on the high-resolution graphic screen and were printed by a Model EX-85 printer (Epson, Japan). Time constants of 0.5 and 0.2 s were used for the studies on dilution and sorbent extraction preconcentration, respectively. The peak-height absorbance for the preconcentration application and that for the tallest peak in the dilution application were obtained directly from the instrument readout, which was set in the

peak-height mode. The absorbance of the lower peak and the valley were taken from the signal printout. Expansion factors were adjusted for each measurement so that peak-height and -valley absorbance reached at least 50% full scale (full-scale = 50 mm), to decrease errors in the evaluation.

In the studies on zone penetration dilution, knotted reactor (KR) sample loops and transport conduits were made by tying overlying knots of 6 mm diameter in 0.5 mm i.d., 1.5 mm o.d. Micro-Line tubing (Thermoplastic Scientifics, Stirling, NY). The intermediate loop was made from 0.75 mm i.d. Micro-Line tubing and had a volume of 150 μ l. Two different connection lines from the injector to the nebulizer were compared in these

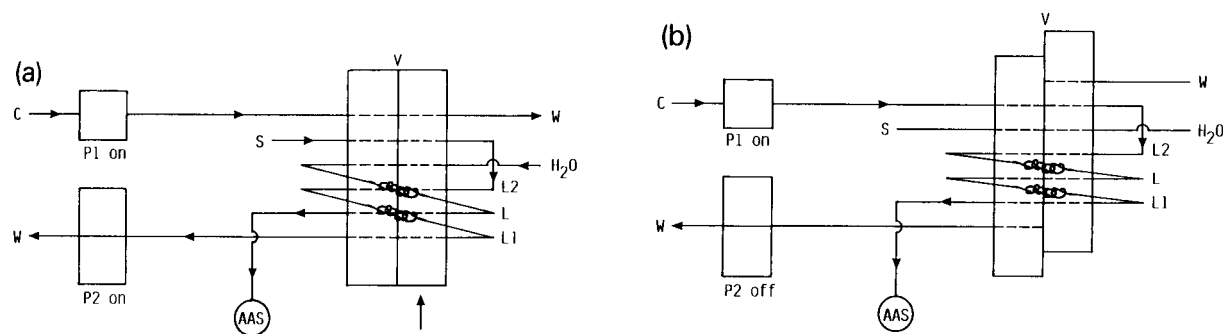


Fig. 2. FI manifold for zone penetration dilution using a reciprocating piston pump. P1 = piston pump; P2 = peristaltic pump; other components as in Fig. 1.

studies. The first was a KR made of a 100-cm length of tubing with the above-described dimensions and the second was a 20-cm length of straight 0.35 mm i.d. PTFE tubing.

A Perkin-Elmer conical micro-column, pre-packed with octadecyl-bonded silica sorbent (RP-C 18), was used in the preconcentration studies, with column dimensions as described previously [5]. The sample loop used in this study was made from 1.5 mm i.d. PTFE tubing. The connection line from the injector to the nebulizer was a 20-cm length of 0.35 i.d. PTFE tubing.

Reagents and standard solutions

All reagents were of analytical-reagent grade and deionized water was used throughout. Sodium diethyldithiocarbamate (DDTC) (Merck, Darmstadt) solution (0.05%) was prepared by dissolving the reagent in water. This solution was prepared freshly every day.

Standard solutions of calcium and lead were obtained by diluting 1000 mg l⁻¹ stock solutions prepared from Titrisol standard concentrates (Merck).

All carrier solutions and solvents which were introduced into the spray chamber were degassed before use.

Procedures

The FI manifold shown in Fig. 1 was used for zone penetration dilution studies with the sinusoidal pump system and that in Fig. 2 was used with the peristaltic pump and reciprocating pump

system. When a piston pump was used to propel the carrier, the sample was loaded with a peristaltic pump. Calcium was used as a model analyte for the studies on dilution at a concentration of 40 mg l⁻¹.

Dilution studies using a sinusoidal syringe pump

The operation of the FI manifold is summarized in Table 1. The piston stroke of the sinusoidal pump was set to operate from a starting point of 30°, with a flow-rate setting of 70. This corresponded to a starting point of ca. 1.2 ml and an end-point of 2.0 ml on the plastic syringe in a 10 s stroke, giving an average flow-rate of about 4.8 ml min⁻¹. The pump was programmed for the piston to move in the backward direction (sucking) during the sample loading stage for 10 s, and 11 s in the forward direction (injection) in order to ensure that the piston was on the same starting point after each cycle. Although the 30° starting (and ending) point were determined by the setting for actuation of the microswitch in the pump, any small deviation from returning to this point might accumulate to larger errors after a number of cycles. A prolongation of the return sequence could prevent this from happening. The valve was programmed to turn to the loading position 1 s before the actuation of the syringe in order to avoid sucking against a blocked valve while it was turning, which might produce gas segments in the sample and carrier streams.

A large KR sample loop of 100 μl (L1) and a small straight sample loop (L2) of 20 μl con-

TABLE 1

Operation of the FI manifold for zone penetration dilution using a sinusoidal syringe pump

Sequence	Fig.	Duration (s)	Pump		Valve position	Function
			Average flow-rate (ml min ⁻¹)	Direction		
1	–	1	Off		Loading	Turn valve to loading position before starting the pump
2	1a	10	4.8	Sucking	Loading	SY1: load carrier SY2: load sample into loops
3	1b	11	4.8	Injection	Injection	SY1: sample into flame SY2: excess sample to waste Read: 1-s delay

TABLE 2

Operation of the FI manifold for zone penetration dilution using a reciprocating piston pump and a peristaltic pump or using two peristaltic pumps

Sequence	Fig.	Duration (s)	Flow-rate (ml min ⁻¹)		Valve position	Function
			Pump 1 ^a	Pump 2 ^a		
1	2a	10	4.2	3.0	Loading	P1: carrier to waste P2: load sample into loops
2	2b	10	4.2	Off	Injection	P1: sample into flame

^a Pump 1 = piston pump or peristaltic pump; pump 2 = peristaltic pump.

nected to the rotor of the injector valve (V) were sequentially filled in series with the sample in the loading sequence (Fig. 1a), the surplus sample being drawn into the sampling syringe (SY1). Simultaneously, the carrier syringe (SY2) was filled with the water carrier, while water was also aspirated into the nebulizer–burner system of the spectrometer through an intermediate loop (L) by the suction of the nebulizer.

At the end of the loading sequence the valve was turned to the injection position (Fig. 1b), while the moving direction of the syringe piston was simultaneously reversed, and a reading sequence of 10 s was initiated after a delay of 1 s. The two sample zones were carried to the detector by a carrier stream provided by the carrier syringe (SY2), separated by a zone of water contained in the intermediate loop (150 μ l). The two sample zones overlapped each other to an extent controlled by the length and volume of the inter-

mediate loop as well as the downstream dispersion producing a valley in the recorded absorbance signal when aspirated into the nebulizer–burner system of the detector. Simultaneously, the sample solution in SY1 was discharged to waste. Care was taken at this stage that the surface levels of sample and water for filling the intermediate loop were approximately equal in order to prevent cross-contamination between water and sample by siphoning. A separately controlled additional pump or valve could easily obviate this special precaution, but would have resulted in a more complicated system.

Dilution studies using a reciprocating piston pump

The operation of the FI manifold is summarized in Table 2. In this mode, the carrier need not be filled into a syringe as in the previous mode. The carrier stream was pumped through

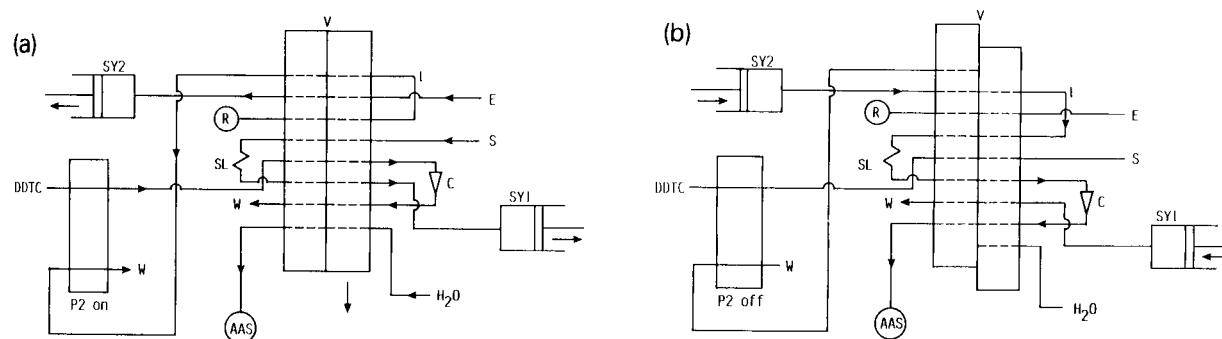


Fig. 3. FI manifold for on-line sorbent extraction preconcentration using a combined sinusoidal and peristaltic pump system. SY1, SY2 = syringes 1 and 2; P2 = peristaltic pump; L = loop (3 cm long \times 0.5 mm i.d.); E = eluent; R = air reservoir, 5-ml volume; S = sample; SL = sample loop, 1.3-ml volume; C = conical column; W = waste; V = eight port valve; AAS = flame AAS detector. (a) Loading sequence; (b) elution sequence.

the piston pump continuously at a flow-rate of 4.2 ml min⁻¹. The carrier was directed to waste during the sample loading stage. The sample was loaded using a continuously operating peristaltic pump with a flow-rate of 3.0 ml min⁻¹. The same injector valve, sample loops and intermediate loop as in the previous mode were used, with the loading, injection and reading sequences controlled by the same computer program as used for the sinusoidal pump, with the exception that 10 s were used for each of the sequences and that the injection and reading sequence were initiated simultaneously.

Dilution studies using a peristaltic pump

The FI manifold and pump connections in this mode were almost the same as those for the reciprocating pump, except that the water stream for filling the intermediate loop was also controlled by the peristaltic pump for sample loading, and was stopped during the injection. The operation of the FI manifold was the same as in the set-up with the reciprocating pump and is also summarized in Table 2.

On-line sorbent extraction preconcentration using a combined sinusoidal and peristaltic pump system

Lead at a concentration of 200 µg l⁻¹ was used as a model element in the sorbent extraction

preconcentration studies. The manifold for this application is shown in Fig. 3 and its operation is summarized in Table 3. The sinusoidal pump was programmed to work within a 30–120° arc stroke, corresponding to an average flow-rate of about 6 ml min⁻¹, with the starting point set at 30°. The loading and preconcentration periods were 20 s each, but the valve was programmed to be actuated 1 s earlier and the return time of the syringe 1 s later, for reasons mentioned in the dilution applications section.

In sequence a, the loading sequence, water was aspirated into the burner system by the suction of the nebulizer. The sampling syringe (SY1) of the sinusoidal pump was used to load the sample into the sample loop, SL (volume 1.3 ml), while the eluent syringe (SY2) was loading methanol. About 12 s were required to fill the sample loop, and 8 s were used to expel the eluent of the previous run. In this sequence the peristaltic pump of the FIAS-200 was used to propel the DDTC reagent through the column at 0.4 ml min⁻¹ for 10 s to precondition the column, and to evacuate the methanol contained within the short loop L (3 cm long), to produce an air segment, after which the pump was stopped for the remainder of the analytical cycle. At this stage L was connected to a reservoir of air, R, made from a 5-ml plastic disposable syringe, with the piston pulled to the fully outward position. At

TABLE 3

Operation of the FI manifold for on-line sorbent extraction preconcentration using a combined sinusoidal (SIN) and peristaltic (PER) pump system and volume-based sample loading

Sequence	Fig.	Duration (s)	Flow-rate (ml min ⁻¹)		Flow direction	Valve position	Function
			PER	SIN			
1	3a	1	Off	Off	–	Loading	Turn valve to loading position before starting the pumps
2	3a	20 10	0.4	6	Sucking	Loading	SY1: load sample into loops SY2: load eluent (methanol) PER: load DDTC on to column, fill air into loop L
3	3b	12	Off	6	Injection	Injection	SY1: excess sample to waste
4	3b	8	Off	6	Injection	Injection	SY2: load sample on to column SY1: excess sample to waste SY2: elute sample into flame READ: activate

^a Valve rotated 1 s prior to sequence 3.

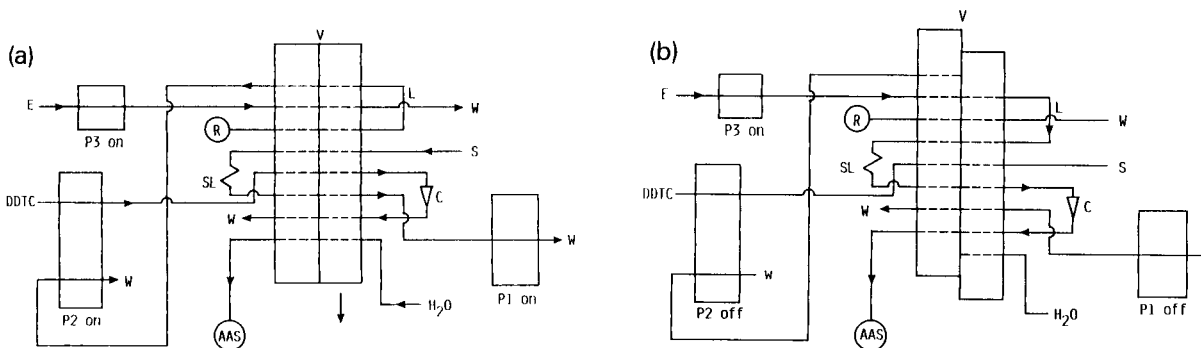


Fig. 4. FI manifold for on-line sorbent extraction preconcentration using a combined reciprocating and peristaltic pump system. P1, P2 = peristaltic pumps; P3 = reciprocating piston pump; other components as in Fig. 3.

the end of sequence a, the valve was turned to the preconcentration position, synchronized with the reversal of the flow direction of the sinusoidal pump.

In sequence b, SY2 was used to load the sample stored in the sample loop SL on to the sorbent column while the content in SY1 was expelled to waste. The sample was pushed forward through the sorption column, C, by the methanol eluent, with the sample and eluent zones separated by a small segment of air created in loop L in the previous sequence. The complexation and sorption of the analyte complex occurred almost simultaneously on the RP-C 18 sorbent column, which was preloaded with DDTc in the preceding sequence. The sorption of the analyte, lasting about 12 s, was immediately fol-

lowed by its elution, which was completed in 8 s. The read cycle was initiated in this sequence after a 10-s delay.

On-line sorbent extraction preconcentration using a combined reciprocating and peristaltic pump system

In these studies the FI manifold and sequences of operation were almost the same as for the previous application, except that one of the peristaltic pumps on the FIAS-200 was used to load the sample into the sample loop by suction at a flow-rate of 6.0 ml min^{-1} (pump setting 100) during sequence 1 (Fig. 4a), and the reciprocating pump was connected to the inlet of the eluent on the injector valve and used to propel methanol continuously during the two sequences. The oper-

TABLE 4

Operation of the FI manifold for on-line sorbent extraction preconcentration using a combined reciprocating (REC) and peristaltic (PER) pump system and volume-based sample loading

Sequence	Fig.	Duration (s)	Flow-rate (ml min^{-1})			Valve position	Function
			PER 1	PER 2	REC (P3)		
1	4a	20	6	0.4	6	Loading	PER 1: load sample into SL PER 2: Load DDTc on to column and load air into L REC: eluent to waste
2	4b	12	Off	Off	6	Injection	Load sample on to column
3	4b	8	Off	Off	6	Injection	Elute sample into flame READ: activate

ation of the FI manifold is described in detail in Table 4. The methanol propelled in the loading sequence might be collected and used again.

RESULTS AND DISCUSSION

Performance of the FI zone penetration dilution systems

The type of signals that were obtained with the FI zone penetration dilution system, using a 40 mg l^{-1} Ca standard solution, two sample loops of 100 and $20 \mu\text{l}$, and an intermediate loop of $150 \mu\text{l}$, are shown in Fig. 5 for the peristaltic pump system. Details of the FI manifold were shown in Fig. 2 and the sequence of operation was described under Experimental. Ten signals were superimposed in Fig. 5 in order to give an impression of the repeatability of the procedure. The signals were printed on three different absorbance scales in order to optimize readability at the three dilution levels, at the top of the two peaks and in the valley.

The same dispersion coefficients, D , of 1.02 and 4.7 were obtained for the two peaks for all three propulsion systems. Different values for D of 20, 18 and 17 were obtained, however, for the valley using the sinusoidal, peristaltic and reciprocating pump, respectively. The three different dilutions may be acquired in one injection at a sampling frequency of $150\text{--}180 \text{ h}^{-1}$ for all three systems. The calibration graphs for calcium at the three dilution levels are shown in Fig. 6 for the sinusoidal pump system.

The precision of measurement at the different dilution levels of a 40 mg l^{-1} Ca standard solu-

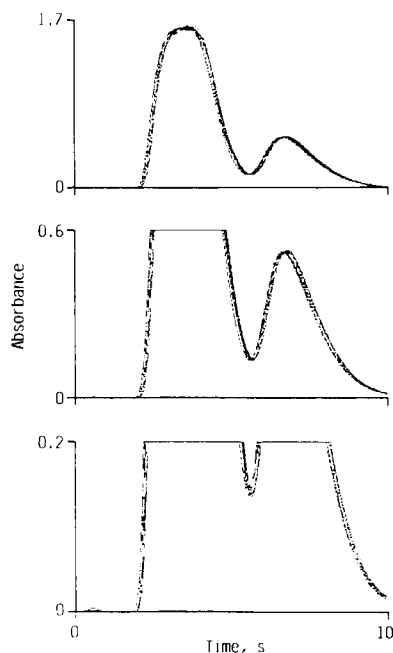


Fig. 5. FI zone penetration dilution using a peristaltic pump system. Standard solution containing 40 mg l^{-1} Ca; sample loops of 100 and $20 \mu\text{l}$ with an intermediate loop of $150 \mu\text{l}$. Ten determinations superimposed; three different absorbance scales.

tion, with straight and KR transport conduits between the valve and the nebulizer, are given in Table 5. The results showed a general improvement in precision when using KR transport conduits, apparently owing to better radial mixing of the sample zones and the carrier.

The differences in the precision of the higher and medium peaks for the three propulsion systems were generally not significant. However,

TABLE 5

Relative standard deviations ($n = 10$) for different propulsion systems in on-line dilution by zone penetration and two different conduits from the valve to the nebulizer^a

Propulsion system	Relative standard deviation (%)					
	100-cm knotted reactor conduit			20-cm straight conduit		
	High peak	Low peak	Valley	High peak	Low peak	Valley
Peristaltic pump	0.64	0.64	2.2	0.95	1.6	4.0
Reciprocating pump	0.79	0.73	2.1	1.1	1.6	5.7
Sinusoidal pump	0.83	1.0	8.0	1.2	1.9	11

^a Standard solution 40 mg l^{-1} Ca. For details see text.

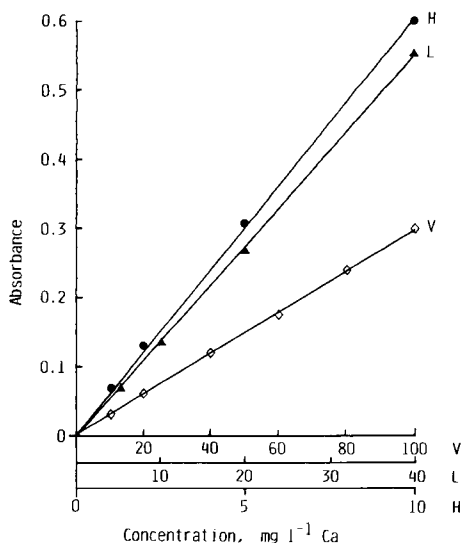


Fig. 6. Calibration graphs for calcium at the three dilution levels using FI zone penetration dilution. H = high peak; L = low peak; V = valley.

these data reflect the peak evaluations of single sample zone injections rather than penetration zones, considering the limited degree of zone overlapping in this study. There is little doubt that the precision of the measurements in the valley, where the two zones were sure to overlap, would provide a more stringent evaluation of the flow stabilities. The good precision obtained for the peristaltic pump (see Fig. 5) was unexpected, considering the larger pulsation of such systems. As the carrier flow of 4.2 ml min^{-1} was achieved at a pump rotation speed of 120 min^{-1} , this was suspected to be the reason for the limited influence from pulsation. However, this was not found to be the case. When the rotation speed was decreased to 30 min^{-1} using a wider bore pump tube, producing the same flow-rate, the results were consistent with those of the higher rotation speed. We assume that this was a result of the damping effect and the strong radial mixing capabilities of the long KR sample loops. With such a system the pulsation from the pump appeared to be damped to an extent that not even the reproducibility of the interface of two fast-changing gradients was affected. The good precision of about 2% R.S.D. obtained at a dilution factor of about 20 shows favourably the applicability of the

zone penetration dilution approach using peristaltic pump systems.

Although the precisions achieved for the reciprocating pump were similar to those for the peristaltic pump, the system was less versatile as only one pump channel was available and a peristaltic pump had to be used in addition for sample loading. Another drawback of the reciprocating pump was the precautions that should be taken when working against suction, as in the FAAS system. Piston pumps for LC are designed to work against high back-pressures. The check valves of such pumps might be displaced under suction and the pump could be deactivated, the resulting flow-rate being controlled by suction rather than by the pump. Such conditions may develop under flow starvation conditions where the carrier flow-rates for sample introduction are lower than the nebulizer uptake, as in this work. In this study, with the FI system interfaced between the pump and the nebulizer of the FAAS instrument, the pump was deactivated at a flow-rate of about 3 ml min^{-1} . At lower pump rates the flow rate was determined by the nebulizer suction. Therefore, one has to be careful not to work with flow-rates lower than those critical values, which have to be evaluated separately for each specific application.

The inferior precision for the sinusoidal pump was also unexpected, considering the excellent precision obtained with this system in spectrometric applications. This phenomenon may also be explained by the special features of the FAAS nebulizing system and the specific working mode of the sinusoidal pump. An unavoidable feature of the sinusoidal pump inherent in its design is that it has to undergo a phase during flow reversal where the flow is virtually stopped. This phase appeared to be much longer than the switching of the injector valve, which may also cause temporary blockage of the flow. In spectrometric applications it is of no consequence, or even advisable that the flow be stopped during turning of the valve, in order to avoid pulsation. This temporary stoppage of flow may, however, create detrimental effects on the stability of a flow which is under sustained suction as in FAAS applications. The normal flow pattern appeared to be disturbed

TABLE 6

Figures of merit for the performance of on-line sorbent extraction preconcentration of $200 \mu\text{g l}^{-1}$ Pb using three different propulsion systems and volume-based or time-based sample loading ^a

Parameter	Propulsion and sample loading system		
	Sinusoidal volume-based	Reciprocating volume-based	Peristaltic time-based
Enrichment factor (EF)	10.5	10.5	9
Enhancement factor ^b	23	23	20
Sample volume loaded (ml)	1.3	1.3	1.1
Sampling frequency (h^{-1})	85	90	120
Concentration efficiency (EF min^{-1})	15	16	18
Precision (R.S.D., %):			
Short-term ($n = 11$)	2.5	2.1	1.6
Long-term (3 days)	4.8	4.2	10–20

^a For details see text. ^b including the effect of the organic solvent.

during the flow reversal due to the suction, the effect becoming apparent in such delicate situations as the zone penetration dilution investigated in this study. This assumption was supported by the fact that the precision for the sinusoidal pump was improved by a factor of 2 when the nebulizer uptake was decreased to zero, although the signal decreased to half of that at normal uptake rates. On the other hand, stopping the pump purposely for a longer period of 2 s during the turning of the valve resulted in a further decrease in the precision to 14% R.S.D., verifying this assumption additionally.

Design of the volume-based on-line sorbent extraction preconcentration system for sinusoidal and reciprocating pumps

It appeared obvious that volume-based sample loading was the only practical solution when piston and syringe pumps were used to load the sample on a packed column, as pumping sample solutions through such pumps might require very long wash-out times between samples. While this inevitably added a sequence for sample loop filling, an attempt was made to compensate for its effect on sample throughput by using a higher loading flow-rate, which was readily achievable with piston and syringe pumps.

In order to simplify the system, loading of the sample on the column and elution were achieved sequentially in one valve phase. In fact, the sam-

ple was introduced into the column by the eluent flow, which in turn was propelled by the pumps. It was therefore essential that the sample and eluent zones were well separated by a small air bubble to prevent their mutual dispersion. Preliminary studies without air segmentation produced only about 50% of the sensitivity achieved later with the present design.

Another feature of the system design was the preconditioning of the column with DDTC instead of merging the sample stream with the reagent before introduction into the column. This approach was used by Ruzicka and Arndal [7] in their pioneering work on FI sorbent extraction preconcentration. It was not used in our previous systems because it was thought that such a pre-treatment phase would decrease the sample throughput. In the present system, however, this was easily accomplished in parallel with the sample loop filling without affecting the throughput.

Performance of the on-line sorbent extraction preconcentration system

The figures of merit for the performance of the volume-based sorbent extraction preconcentration system in the determination of lead using two different propulsion systems are shown in Table 6. The sensitivity enhancement and enrichment factors were identical for the syringe and the piston pump systems, and were higher than those obtained in a previously described time-

based system with peristaltic pumps [5]. This was due to a slightly larger sample volume of 1.3 ml used in this study. The sample throughput for the volume-based approach was substantially lower, as expected, owing to the extra sequence of loading the sample into a loop prior to preconcentration. However, this was almost compensated for because the syringe and the piston pump systems made it possible to use higher sample flow-rates of about 6 instead of 3.3 ml min⁻¹, which was almost the highest reliable flow-rate applicable with peristaltic pumps, when pumping through a micro RP-C18 column. This higher flow-rate made it possible that larger sample volumes could be pumped through the column in a shorter time. Therefore, the resulting concentration efficiency values were only marginally inferior for the volume-based approach.

The precision for short-term operation (ca. 7 min) was slightly better for the time-based peristaltic pump system than for the volume-based piston and syringe pump systems. The reasons for this rather unexpected behaviour might be the same as discussed for the zone penetration dilution systems. The precision data for long-term operation (about 3 days, 3–5 h per day), however, showed better reproducibilities for the volume-based approaches using piston or syringe pumps. This appeared to be mainly the result of the better precision of the sample volume processed on the column in the volume-based approach. This may be connected at least in part, with the better flow stability of the piston and syringe pumps, the pumping conditions of which are much more easily reproduced from day to day than those of the peristaltic pumps, when pumping through packed columns.

Conclusion

The results of the studies favour the general use of peristaltic pumps for FI-FAAS applica-

tions. For zone penetration dilution the precision of the peristaltic pump system was equal to or better than that of the piston and syringe pump systems so that the significantly lower cost and the easier handling of the peristaltic pumps can take full effect.

In FI on-line sorbent extraction column preconcentration, the superiority of the volume-based piston and syringe pump systems could show itself only in an improved long-term stability. This shortcoming of the time-based approach using peristaltic pumps will not, however, in most instances pose a serious problem, as frequent recalibration can be easily performed in FI-FAAS. A combination of a peristaltic with a piston or syringe pump, however, will no doubt further enhance the versatility of the preconcentration system. Another important advantage of using piston or syringe pumps in such applications is the convenience in delivering organic solvents.

The authors are grateful to B. Huber for creating the software and constructing the control system for the sinusoidal pump.

REFERENCES

- 1 J. Ruzicka and E.H. Hansen, *Flow-Injection Analysis*, Wiley, New York, 2nd edn., 1988.
- 2 J. Ruzicka, G.D. Marshall and G.D. Christian, *Anal. Chem.*, 62 (1990) 1861.
- 3 Z.-L. Fang, J.L. Burguera (Ed.), *Flow-Injection Atomic Spectroscopy*, Dekker, New York, 1989, Chap. 4.
- 4 E.A.G. Zagatto, M.F. Gine, E.A.N. Fernandes, B.F. Reis and F.J. Krug, *Anal. Chim. Acta*, 173 (1985) 289.
- 5 Z.-L. Fang, T.-Z. Guo and B. Welz, *Talanta*, 38 (1991) 613.
- 6 Z.-L. Fang, M. Sperling and B. Welz, *J. Anal. At. Spectrom.*, 5 (1990) 639.
- 7 J. Ruzicka and A. Arndal, *Anal. Chim. Acta*, 216 (1989) 243.

Enhanced automatic flow-injection determination of the total polyphenol index of wines using Folin–Ciocalteu reagent

Mercedes Celeste, Consuelo Tomás, Andreu Cladera, José Manuel Estela and Victor Cerdà

Department of Chemistry, University of the Balearic Islands, E-07071 Palma de Mallorca (Spain)

(Received 12th March 1992; revised manuscript received 3rd June 1992)

Abstract

A new automated flow-injection method for the determination of the total polyphenol index in wines based on the Folin–Ciocalteu reaction in 0.5 mol l^{-1} NaOH is proposed. The method allows different types of wine to be analysed automatically at a rate of 60 h^{-1} by using gallic or tannic acid as standard. By applying the proposed method to real samples of white, rosé and red wines, their total polyphenol indices were determined with a higher reproducibility (R.S.D. = 0.8%) than that afforded by earlier methods, whatever the dilution used. The method is highly tolerant towards the most common interferences that occur with its batch counterpart (viz. SO_2 , reducing sugars and ascorbic acid) and is subject to a smaller synergistic effect from SO_2 , reducing sugars and *o*-hydroxypolyphenols.

Keywords: Flow injection; UV–Visible spectrophotometry; Polyphenol index; Wines

The determination of total polyphenols is commonplace in the agricultural and food industries [1]. Wine contains a variety of phenol compounds, commonly referred to as “tannins”, which cannot be determined singly, so they are measured collectively as the so-called “total polyphenol index”. The determination of this index requires the absorbance of the unknown sample to be referred to a calibration graph obtained previously with a standard polyphenol, usually tannic or gallic acid. Hence, the result obtained is an average of the different analytical responses from the phenol compounds present in the sample. The total polyphenol index of wines varies markedly with their origin. Nevertheless, concentrations of $1500 \mu\text{g l}^{-1}$ of gallic acid in red wines, roughly half that amount in rosé wines and one

tenth in white wines, can be considered to be normal.

Spectrophotometric methods have so far been the most commonly used to determine the total polyphenol index on account of their simplicity and convenience, notwithstanding their slowness and liability to interference from some substances that commonly occur in wines. These shortcomings led to the original batch methods being adapted for use in continuous-flow systems [e.g. flow-injection analysis (FIA)] in order to improve their applicability. To the best of our knowledge, there are only two references to the use of FIA systems for the determination of the total polyphenol index based on the Jerumanis and Folin–Ciocalteu redox reactions. One of the methods was not checked for potential interferences; in addition, its performance was heavily dependent on the experimental conditions and its reproducibility varied greatly depending on the particular standard compound used [2]. The other

Correspondence to: V. Cerdà, Department of Chemistry, University of the Balearic Islands, E-07071 Palma de Mallorca (Spain).

method [3] was checked for interferences, to which it was found to be highly tolerant. However, it gave rise to double peaks at low standard concentrations and failed to provide adequate reproducibility with real samples.

In order to increase the applicability and automatability of methods based on the Folin–Ciocalteu reaction and in continuation of work on the automation of analytical methods, this study of the automated determination of the total polyphenol index of wines was carried out.

EXPERIMENTAL

Apparatus and software^a

The automatic system used included a personal computer for controlling injections and acquiring and processing data. Samples were automatically driven to the injection position by means of a Gilson Sample Changer 222 autosampler, the motion of which was governed by the computer. Instrumental control and data acquisition and processing were achieved with the program DARRAY [4], which was previously developed in this laboratory.

Figure 1d depicts the FI manifolds used. It consisted of a Gilson Minipuls 3 eight-way peristaltic pump, a Rheodyne Model 50 injection valve that was controlled by the computer via a laboratory-made mechanical actuator and a Hewlett-Packard Model 8452A diode-array spectrophotometer furnished with a flow cell of 18 μl void volume and 10 mm path length. Absorbance values were measured at 760 nm. All tubing and injection loops were of PTFE and 0.5 mm i.d.

Reagents

Analytical-reagent grade chemicals were used unless indicated otherwise.

Solutions containing 250 mg l^{-1} of gallic acid (Fluka assay grade for LC, purity > 98%) or tannic acid (Fluka, used for enzyme immobilization

and protein adsorption, or Sigma) in distilled water were used as standards.

Folin–Ciocalteu reagent (FCR) (Fluka) was used at 1:10 dilutions in distilled water.

Sodium hydroxide solution (0.5 M) and sodium carbonate solution (30 g l^{-1}) were also used.

Reference method

The Ribereau–Gayon method [5,6] was used for reference purposes.

Procedure

The manifold in Fig. 1d was used to circulate streams of distilled water (carrier), reagent 1 (1:10 FCR) and reagent 2 (0.5 mol l^{-1} NaOH) at flow-rates of 0.7, 1.0 and 1.0 ml min^{-1} , respectively. The length of L2 was 1 m. Once the system had equilibrated and the spectrophotometer had been zeroed ($\lambda = 760$ nm), a calibration graph was obtained using tannic acid (12.5–150 mg l^{-1}) or gallic acid (5–100 mg l^{-1}) standards that were injected in 107- μl volumes. Then, unknown wine samples were analysed similarly after appropriate dilution in distilled water. The dilutions used were 1:2–1:10 for white, 1:5–1:25 for rosé and 1:10–1:50 for red wine. The sample throughput was 60 h^{-1} .

RESULTS AND DISCUSSION

FIA variables

The recommended conditions for the standard and FIA methods for the determination of the total polyphenol index [2] were used in order to optimize the experimental design. The four FIA configurations shown in Fig. 1 were tested using 10 g l^{-1} Na_2CO_3 solution as reagent 2 and a 1:100 dilution of FCR as reagent 1. The FIA manifold shown in Fig. 1a has been described previously [2]. Each configuration was tested by injecting tannic acid at concentrations of 5, 10, 25, 50, 75, 100 and 125 mg l^{-1} .

The configurations in Fig. 1a and b provided double peaks at standard concentrations below 75 and 25 mg l^{-1} , respectively. Such double peaks could not be eliminated by including further reactors, altering their lengths or changing the vol-

^a The software used in this work can be obtained on request from SCTWARE, Banco de Programas, Departamento de Química, Universidad de las Islas Baleares, E-07071 Palma de Mallorca, Spain.

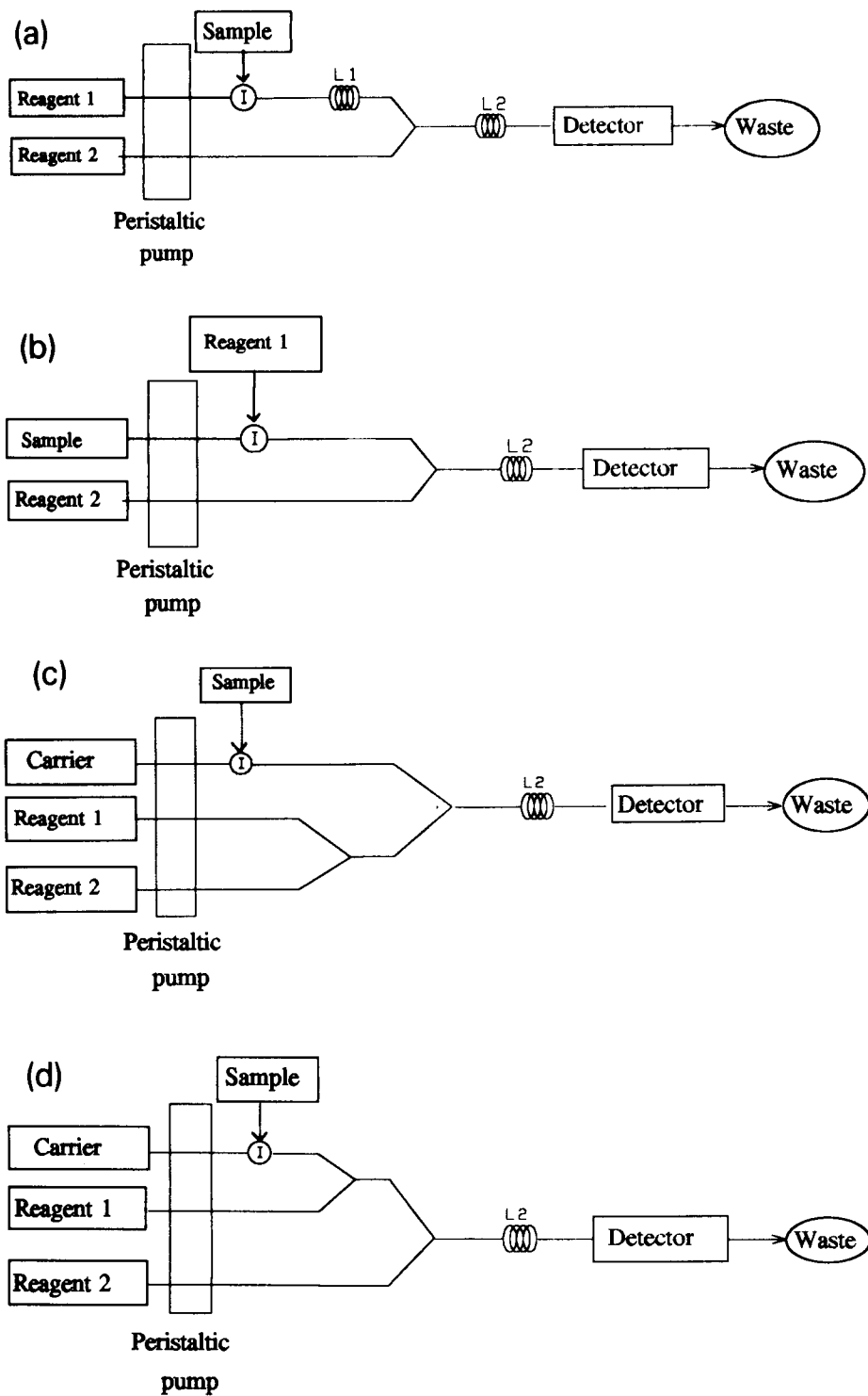


Fig. 1. FI manifolds used. Reagent 1 = FCR (1 : 100, 1 ml min⁻¹); reagent 2 = Na₂CO₃ (10 g l⁻¹, 1 ml min⁻¹); carrier = distilled water (0.7 ml min⁻¹); injection volume = 107 μl; L1 = 30 cm; L2 = 2 m.

umes injected. Therefore, both manifolds were discarded and those shown in Fig. 1c and d were examined. Both provided sharp peaks throughout the application range, but the latter yielded a smoother baseline, so it was chosen for subsequent experiments.

Using the manifold in Fig. 1d the influence of reactor lengths between 0 and 6 m and injection volumes from 50 to 194 μl on the analytical signal was studied. It was found that a reactor length of 1–2 m provided the maximum sensitivity, so 1 m was adopted in order to maximize the sampling rate. The optimum injection volume was found to be 107 μl as higher volumes did not result in significantly larger signals (peak height).

Chemical variables

The optimization of the chemical variables was performed by means of the univariate method. First the influence of Folin–Ciocalteu dilutions (reagent 1) between 2:100 and 20:100 on the height of the FIA peaks obtained by injecting 107 μl of two standards of tannic acid (10 and 25 mg l^{-1}) and using a 30 g l^{-1} Na_2CO_3 solution as reagent 2 was studied. Under these conditions, dilutions between 8:100 and 20:100 resulted in the release of gas (probably CO_2 arising from the neutralization of the Na_2CO_3 by the acidic medium of the FCR solution), which hindered spectrophotometric monitoring of the process. On the other hand, the height of the signal was not influenced by FCR dilutions between 2:100 and 4:100. A dilution of 2:100 was chosen for subsequent experiments.

No influence of the Na_2CO_3 concentration on the peak height was observed over the range studied (9–78 g l^{-1}). A concentration of 30 g l^{-1} was chosen.

The equations for the calibration graphs obtained under the above optimum conditions by using gallic and tannic acid concentrations of 5–100 and 12.5–150 mg l^{-1} , respectively, ($n = 6$) are shown in Table 1 in the form peak height (absorbance) = $A + B[\text{standard} (\text{mg l}^{-1})]$. As regards reproducibility and precision, the standard deviations were 2.6 and 2.9 mg l^{-1} for a 25 mg l^{-1} tannic acid standard from Fluka and Sigma,

TABLE 1

Equations (see text) of the calibration graphs obtained by using the proposed FIA manifold, 30 g l^{-1} Na_2CO_3 and 4:100 FCR

Standard	<i>A</i>	<i>B</i>	<i>r</i>	RMS ^a
Tannic acid (Fluka)	0.36×10^{-2}	4.39×10^{-3}	0.99994	0.0024
Tannic acid (Sigma)	0.43×10^{-3}	5.2×10^{-3}	0.99971	0.0032
Gallic acid (Fluka)	0.25×10^{-1}	9.02×10^{-3}	0.99986	0.0022

^a RMS = mean of fit residuals.

respectively, and 2.5 mg l^{-1} for a 25 mg l^{-1} gallic acid standard from Fluka.

Application to the analysis of wines

The above method, based on the use of 30 g l^{-1} Na_2CO_3 and 2:100 FCR, was used to analyse six different wine samples (two each white, rosé and red) that were previously diluted. Their total polyphenol indices were expressed in mg l^{-1} of the standard compound used. Each type of wine was measured at three different dilutions, viz., 1:10, 1:5 and 1:2 for the white wines, 1:25, 1:10 and 1:5 for the rosé wines and 1:50, 1:20 and 1:10 for the red wines. The results obtained showed that the polyphenol indices referred to the undiluted samples depend on the dilution used (the higher the dilution, the higher was the index obtained). Also, further dilution of the samples was required in order to obtain more consistent results. However, some samples (e.g., the white wines) could not be diluted further owing to their low polyphenol contents. The dependence of the polyphenol index on the dilution can be ascribed to wines behaving differently from standards towards the Folin–Ciocalteu reagent. Probably the FCR/polyphenol ratio needed to ensure that the analytical signal is independent of the FCR concentration was different for standards and samples.

Table 2 shows the results and standard deviations obtained for different wine samples. The high standard deviations can be attributed to the above effect.

TABLE 2

Results obtained in the analysis of wines by the proposed FIA method using $30 \text{ g l}^{-1} \text{ Na}_2\text{CO}_3$ and 4:100 FCR (means \pm S.D., $n = 6$)

Type of wine	Tannic acid (Fluka) (mg l^{-1})	Tannic acid (Sigma) (mg l^{-1})	Gallic acid (Fluka) (mg l^{-1})
White	206 ± 20	174 ± 23	114 ± 21
Rosé	560 ± 98	471 ± 97	298 ± 69
Red	1359 ± 64	1159 ± 64	746 ± 93

Revision of the chemical conditions

It was thought that solving the above problem would require an increase in the FCR concentration. However, this would entail modifying the reaction medium in order to avoid bubble formation in the reaction coils and hence spurious readouts. Therefore, Na_2CO_3 was replaced with a base that releases no CO_2 on neutralization. Whereas one of the two bases assayed, viz., $\text{Na}_2\text{B}_4\text{O}_7$, provided no substantial improvement in terms of sensitivity, the other, NaOH , resulted in increased peak heights at a concentration of 0.5 mol l^{-1} and was therefore chosen for subsequent experiments. Using this new medium the effects of FCR dilutions between 2:100 and 20:100 on the signals yielded by different gallic and tannic acid standards and wine samples were studied. Whereas the signals yielded by the gallic acid standards remained unchanged for FCR dilutions in the range 4:100–20:100, the wine samples required dilutions between 10:100 and 20:100. Therefore, $0.5 \text{ mol l}^{-1} \text{ NaOH}$ and an FCR dilution of 10:100 were chosen as reagents 2 and 1, respectively, in the new set of experimental conditions.

Table 3 shows the equations for the calibration graphs ($5\text{--}100 \text{ mg l}^{-1}$ of gallic acid and $12.5\text{--}150$

mg l^{-1} of tannic acid) in the form peak height (absorbance) = $A + B[\text{standard}(\text{mg l}^{-1})]$ obtained with the new conditions for the different standard compounds used. The standard deviation for a 25 mg l^{-1} gallic acid standard analysed with the modified method was 0.2 mg l^{-1} (R.S.D. = 0.8%, $n = 6$), compared with 2.5 mg l^{-1} ($n = 6$) obtained with the unmodified method ($30 \text{ g l}^{-1} \text{ Na}_2\text{CO}_3$ and a 4:100 FCR dilution) with the same standard. In summary, the linear determination range of the modified method was similar to that of the original method, but its precision was substantially higher. The modified method provides a much more acceptable linear range and precision than some reported FIA methods, e.g., linear range 0–40 mg l^{-1} of gallic acid, R.S.D. = 1.77% for 200 mg l^{-1} of oenological tannin [3]; linear range not specified, R.S.D. = 1.79% for 124 mg l^{-1} of gallic acid [2].

Table 4 gives the results obtained for different wine samples that were subjected to dilutions of 1:10, 1:5 and 1:2 for white wine, 1:25, 1:20 and 1:5 for rosé wine and 1:50, 1:20 and 1:10 for red wine. Figure 2 shows the corresponding FIA recording. As can be seen, the peak heights for the different injections are concordant with the dilution effected, except for the two last peaks for the red wine, which are slightly outside the linear range. More reproducible polyphenol indices are obtained as a result of the sample dilution not affecting the final result.

Study of interferences

Sulphur dioxide, reducing sugars and ascorbic acid are known to interfere in the determination of tannins by the Folin–Ciocalteu method [2,3]. In addition, the co-occurrence of the first two can result in synergistic effects. The interferences of these compounds are particularly obvious with

TABLE 3

Equations (see text) of the calibration graphs obtained by using the proposed FIA manifold, $0.5 \text{ mol l}^{-1} \text{ NaOH}$ and 10:100 FCR

Standard	A	B	r	RMS ^a
Tannic acid (Fluka)	-0.82×10^{-2}	8.09×10^{-3}	0.99991	0.0059
Tannic acid (Sigma)	-0.17×10^{-1}	9.51×10^{-3}	0.99996	0.0044
Gallic acid (Fluka)	0.40×10^{-2}	1.16×10^{-2}	0.99997	0.0029

^a RMS = mean of fit residuals.

TABLE 4

Results obtained in the analysis of wines by the proposed FIA method using 0.5 mol l^{-1} NaOH and 10:100 FCR (means \pm S.D., $n = 6$)

Type of wine	Tannic acid (Fluka) (mg l^{-1})	Tannic acid (Sigma) (mg l^{-1})	Gallic acid (Fluka) (mg l^{-1})
White	228 ± 2.3	199 ± 5	153 ± 3
Rosé	596 ± 6	518 ± 15	399 ± 8.5
Red	1702 ± 16	1474 ± 37	1138 ± 1.4

white wines on account of their low tannin contents. Consequently, the effects of these substances on the determination of the total polyphenol index in white wine samples by the proposed method were studied.

Sulphur dioxide. As the usual free SO_2 contents of the different types of wine range from 10 to 50 mg l^{-1} , and their overall contents in this compound vary between 50 and 200 mg l^{-1} [3], and bearing in mind that the maximum dilution one could use with white wines in order to accommodate their contents within the linear range of the proposed method was 1:10, the potential interfering effect of SO_2 in the determination of the total polyphenol index was investigated by adding increasing amounts of sodium hydrogen-sulphite to a sample of white wine to give SO_2 concentrations between 0 and 400 mg l^{-1} . Table

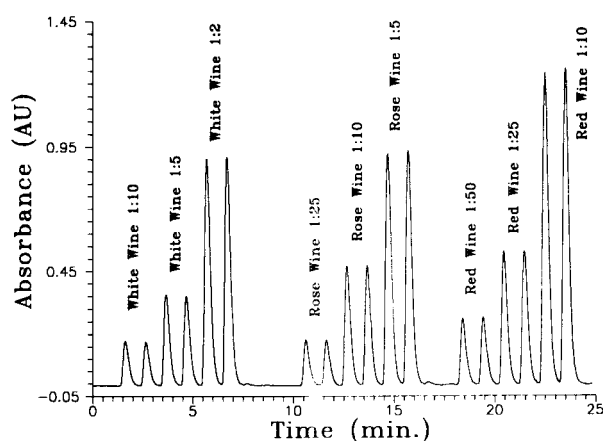


Fig. 2. FIA recording obtained in the analysis of different dilutions of three types of wine samples by the proposed method.

TABLE 5

Results obtained by applying the proposed and reference methods to a white wine sample spiked with various amounts of SO_2

SO_2 added (mg l^{-1})	FIA method		Reference method	
	TPI ^a	Interference (%)	TPI ^a	Interference (%)
0	136	–	178	–
100	143	5.2	232	30.3
200	148	8.8	–	–
400	155	14.0	396	122.5

^a Total polyphenol index (mg l^{-1} gallic acid).

5 gives the results provided by the proposed FIA method and the reference method. With the former, analyses were carried out on 1:10 diluted, SO_2 -spiked samples, whereas the latter was applied to 1:100 diluted samples. According to the results, the FIA method is more tolerant to the presence of SO_2 even though the dilution used was lower. This can be ascribed to the fact that the proposed FIA method is essentially a fixed-time kinetic method whereas the reference batch method is an equilibrium method (readings are made 1 h after the reaction is started); consequently, any effect from SO_2 may not have come into play by the time measurements are made in the FIA method.

Reducing sugars. Table 6 lists the results obtained by analysing a white wine sample that had been spiked with different amounts of glucose using the proposed and reference methods. The samples were diluted 1:10 and 1:100 in distilled water for the FIA and the batch method, respectively. As with SO_2 , reducing sugars interfere less markedly in the FIA method than they do in the reference method, which can be interpreted in the same way as above.

Ascorbic acid. Table 7 shows the results obtained for the determination of the total polyphenol index of white wine to which increasing concentrations of ascorbic acid up to the maximum tolerated concentration according to Spanish legislation (100 mg l^{-1}) had been added. The wine sample was diluted as in the previous cases prior

TABLE 6

Results obtained by applying the proposed and reference methods to a white wine sample spiked with various amounts of glucose

Glucose added (g l ⁻¹)	FIA method		Reference method	
	TPI ^a	Inter- ference (%)	TPI ^a	Inter- ference (%)
0	136	–	178	–
5	138	1.5	187	5.1
20	145	6.6	–	–
40	148	8.8	203	14.0

^a Total polyphenol index (mg l⁻¹ gallic acid).

to analysis. As can be seen, the interference of ascorbic acid is more serious than those of SO₂ and glucose, but it is still less for the proposed FIA method than for the reference method. This can be explained as in the previous instances.

Synergistic effect. The interfering effect of SO₂ with the batch method is markedly affected by the presence of *o*-dihydroxyphenols and reducing sugars as a result of a synergistic effect between the three species [7,8]. In order to determine the potential influence of such an effect on the proposed FIA method it was applied to a series of solutions containing the interferents, both alone and in mixtures. The results obtained are given in Table 8. As can be seen, whereas SO₂ and glucose provided no signal by themselves, they did enhance the signal of gallic acid. When the two species are present together, the global effect is

TABLE 7

Results obtained by applying the proposed and reference methods to a white wine sample spiked with various amounts of ascorbic acid

Ascorbic acid added (mg l ⁻¹)	FIA method		Reference method	
	TPI ^a	Inter- ference (%)	TPI ^a	Inter- ference (%)
0	136	–	178	–
50	153	12.5	–	–
100	169	23.3	269	51.1

^a Total polyphenol index (mg l⁻¹ gallic acid).

TABLE 8

Synergistic effect of the interferents studied

Sample ^a	Gallic acid (mg l ⁻¹) ^b	Sample ^a	Gallic acid (mg l ⁻¹) ^b
GLU	0	GA+SDO	517
SDO	0	GA+AA	515
AA	25	GA+GLU+SDO	544
GA	500	GA+GLU+AA	536
GLU+SDO+		GA+GLU+	
AA	30	SDO+AA	566
GA+GLU	508		

^a GA = 500 mg l⁻¹ gallic acid; GLU = 40 g l⁻¹ glucose; SDO = 400 mg l⁻¹ SO₂; AA = 100 mg l⁻¹ ascorbic acid.

^b Results obtained by using 1:20 dilutions of the stated samples.

greater than the sum of their individual contributions. On the other hand, the effect of ascorbic acid was additive and seemingly independent of the other species investigated.

In any case, the effects are scarcely significant compared with those reported for the batch method [7,8].

Conclusions

By using an optimized flow-injection manifold and the most suitable values for the chemical variables involved in the determination of the total polyphenol index of wines, an FIA method was developed that proved to be more reliable than the previously described methods for this determination. The total polyphenol index obtained is independent of the wine dilution used and the analytical features of the method (reproducibility, applicability range) are scarcely affected by the standard compound used (gallic or tannic acid), in clear contrast to other reported FIA methods [2]. In addition, the proposed method is hardly affected by the usual interferents in the batch determination: it tolerates up to 400 mg l⁻¹ of SO₂, 50 mg l⁻¹ of ascorbic acid and 40 g l⁻¹ of glucose with errors less than 10%.

The authors express their gratitude to the DGICYT (the Spanish Council for Research in Science and Technology) for financial support granted for the realization of this work as part of Project PB 90-0359.

REFERENCES

- 1 S.S. Deshpande, M. Cheryan and D.K. Salunkhe, *Crit. Rev. Food Sci. Nutr.*, 24 (1986) 401.
- 2 J. Buitrago, R. Cela and J.A. Pérez-Bustamante, *Afinidad*, 43 (1986) 530.
- 3 M. Peris-Tortajada, M. Pérez Cerrada and A. Maquieira, *Quím. Anal.*, 8 (1989) 211.
- 4 A. Cladera, E. Gómez, J.M. Estela and V. Cerdà, *Analyst*, 116 (1991) 913.
- 5 P. Ribereau-Gayon, E. Peynaud and P. Sudrau, *Traité D'Enologie. Sciences et Technique du Vin. Vol. 1. Analyse et Contrôle des Vins*, Bordas, Paris, 1976.
- 6 P. Ribereau-Gayon, *Chim. Anal. (Paris)*, 52 (1970) 627.
- 7 C. Miconi, *L'Enotecnico*, March (1982) 11.
- 8 M. Moutounet, *Connaiss. Vigne Vin*, 15 (1981) 287.

Automated continuous-flow titration

Jordi Bartroli and Llorenç Alerm

Unitat de Química Analítica, Departament de Química, Facultat de Ciències, Universitat Autònoma de Barcelona, 08193 Bellaterra, Barcelona (Spain)

(Received 30th January 1992; revised manuscript received 19th May 1992)

Abstract

An automated continuous titration method is described in which the use of a piston burette as a variable-volume injection device in a flow system allows a continuous-flow titration of a sample solution to be performed similarly to classical batch titrimetric procedures. It is found that by plotting the peak height for each injection versus the titrant volume injected, a titration curve very similar to a batch titrimetric curve can be obtained, and an equivalence volume can be precisely determined. A linear relationship between the logarithm of the equivalence volume and the logarithm of the carrier concentration has been observed over a wide concentration range. The use of reagent is kept to a minimum because titrations are performed by adding only microlitres of reagent. The time required for the titration is comparable to the time consumed by a process titration system.

Keywords: Flow injection; Titrimetry

Ideally, a flow-injection system is constructed in such a manner that the sample solution is injected into the carrier solution stream by means of an instant pulse of precisely defined volume and short duration, so that the movement of the carrier solution remains virtually undisturbed. Two ways of sample injection have been used in flow-injection systems: syringe injection and rotary or slide valve injection. The former can approximately simulate a pulse injection, which may be advantageous from a theoretical point of view. Although the latter device generally does not yield a pulse injection, known sample volumes can be inserted into a flowing carrier stream with greater reproducibility. At the same time, it can be easily automated, which is the reason why valves are more often chosen for flow-injection applications. In spite of these advantages, injection

systems that use a manual syringe and a flap valve are still of interest as they are easily built and can be part of an inexpensive set-up. The main disadvantage is that they rely heavily on experimental skill and that it is more difficult to add small volumes reproducibly [1].

The introduction of the piston burette gave a great impulse to the automation of titrations, especially after the appearance of the stepping motor. A commercial microprocessor can control the stepping motor-driven piston burette with great precision and reproducibility [2]. Piston burettes can offer a good alternative for the introduction of sample or reagent in a flow system. The widespread use of on-line titrators in process analysis ensures the ruggedness of burettes used as injection devices in automated continuous-flow analysis.

In classical titrimetric procedures, titrant is added to a closed stationary system (the titration vessel), the titrant volume being used to calculate the original analyte concentration in the test solu-

Correspondence to: J. Bartroli, Unitat de Química Analítica, Departament de Química, Facultat de Ciències, Universitat Autònoma de Barcelona, 08193 Bellaterra, Barcelona (Spain).

tion. Alternatively, continuous-flow titration systems have been developed based on the introduction of a controlled but variable amount of titrant by means of a concentration gradient. At present, the titration of a continuously streaming solution can be achieved only by using an appropriate method of reagent supply together with changes in the flow-rate or concentration of the titrant solution [3].

Procedures for flow-injection titrations by means of the injection of equal volumes of a solution with increasing concentration have also been described [1,4]. When the standard concentration increases, the peak width increases. The peak width is related to a time span (Δt) measured between two elements of fluid having identical dispersion coefficients, one being placed on the leading edge and the other on the trailing edge of the dispersed sample zone. By injecting standards of different concentration (C_{0i}), different peak widths can be recorded. The relationship between $\log C_{0i}$ and Δt appears to be linear. A calibration graph can be obtained by plotting Δt versus concentration.

In this work an automated continuous titration concept was applied to an acid–base reaction, but it is equally applicable to other types of titration

(redox, precipitation, etc.). The use of a piston burette as a variable-volume injection device in a flow system allows a continuous-flow titration of a sample solution to be performed in a similar manner to classical batch titrimetric procedures.

EXPERIMENTAL

Instrumentation

An inexpensive commercial titrator (Crison MicroTT-2050) was used to inject a titrant solution (sodium hydroxide with a known concentration) into the carrier stream (acetic acid with variable concentration). The detector was a flat-surface pH combined electrode (Ingold P/N 10 453 3003). In order to adapt the electrode to this flow system, a Perspex cell designed for flat electrodes was used (Fig 1).

The flow assembly (Fig. 2) consists of a single-line manifold with a peristaltic pump (Gilson Minipuls 3) that propels the carrier stream solution of acetic acid through a narrow PTFE tube. The titrant solution is injected done by means of a piston burette controlled by a microprocessor, and connected to the carrier tube by means of a T-piece. Downstream there is a reactor coil, in which the titrant disperses and reacts with the carrier, giving rise to pH variations that are sensed by a flow-through detector. The recorded signal is a flow-injection peak, from which peak-height measurements are made rather than peak width, as in flow-injection pseudo-titrations.

Reagents

Analytical-reagent grade chemicals and distilled water were used. The titrant solution was sodium hydroxide (Panreac 131687) and the carrier solution was acetic acid (Panreac 131008). In both solutions an ionic strength of 0.05 M was achieved by adding potassium nitrate (Panreac 131524). The sodium hydroxide solutions were standardized with potassium hydrogenphthalate (Panreac 241481).

Procedure

An acetic acid solution in to which increasing volumes of the titrant agent (sodium hydroxide)

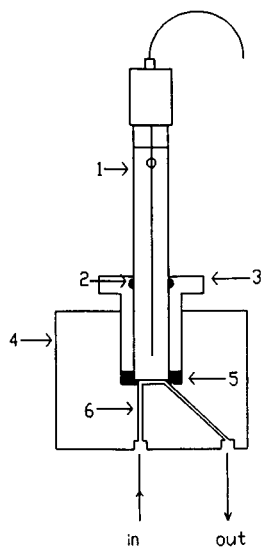


Fig. 1. Combination pH electrode cell. 1 = Glass electrode with flat membrane; 2 = O-ring; 3 = Perspex screw; 4 = Perspex body; 5 = silicone-rubber seal; 6 = flow channel.

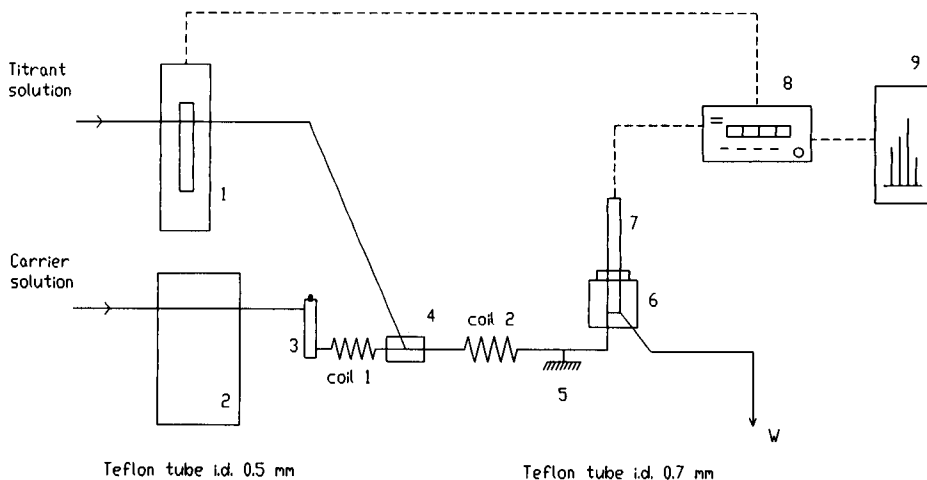


Fig. 2. Schematic diagram of the flow-injection titration system. 1 = Piston burette; 2 = peristaltic pump; 3 = pulse suppressor cell; 4 = T-piece; 5 = grounding electrode; 6 = combination pH electrode cell; 7 = combination pH electrode; 8 = microprocessor; 9 = recorder. Coil 1, 255 cm \times 0.5 mm i.d.; coil 2, 200 cm \times 0.7 mm i.d. Flow-rate, 3.63 ml min⁻¹. Syringe volume, 2.5 ml.

have been injected flows through the flow system. The potential read-out by the pH electrode is continuously recorded. By adding titrant volumes to the single line of the continuous solution stream to be analysed, the peaks corresponding to each injection are found. Logically, the peak height is related to the titrant volume injected. When the peak height (H_{peak} , mV) is plotted against the volume injected (V_{inj} , μl), a dynamic titration curve can be obtained and also an equivalence point (V_{eq} , μl). This volume is determined by means of the usual titrimetric discontinuous procedures (Fig. 3).

Once the hydrodynamic conditions of the flow system have been fixed, the equivalence volume obtained allows a relationship to be found between the acetic acid carrier and the sodium hydroxide titrant concentrations.

RESULTS AND DISCUSSION

A strip-chart recording obtained with this titration system is shown in Fig. 3. The titrant volumes injected are a function of the acetic acid and sodium hydroxide concentrations. It is found that plotting the peak height for each injection versus the titrant volume injected, a titration curve very similar to a classical batch titrimetric curve is

obtained (Fig. 3). At the same time, the equivalence volume is precisely determined. Further, in this instance, the equivalence volume obtained is only tens or, at most, hundreds of microlitres. Perfectly reproducible equivalence volumes between 10 and 200 μl of injected titrant have been obtained.

The procedure that has been followed, after optimizing the hydrodynamic conditions for a maximum response, consists of different acetic acid carrier measurements with the same sodium hydroxide as titrant. By doing so, it is possible to obtain calibrations where the equivalence volume (V_{eq} , μl) versus acetic acid concentration (M) is plotted, keeping the flow system manifold unaltered and using the same titrant solution concentration. No linear relationship between these two variables was found. However, if $\log V_{\text{eq}}$ is plotted versus $\log[\text{CH}_3\text{COOH}]$, a calibration line is obtained (Fig. 4) that shows small deflections for large values of the equivalence volume (if titrant volumes that exceed the 200 μl are injected, the hydrodynamic conditions and the dispersion coefficient are possibly affected). Similar results are obtained on changing the sodium hydroxide concentration, so that acetic acid carriers with concentrations in the range $0.1\text{--}6 \times 10^{-5}$ M can be titrated with sodium hydroxide titrant with concentrations ranging from 0.1 to 0.001 M.

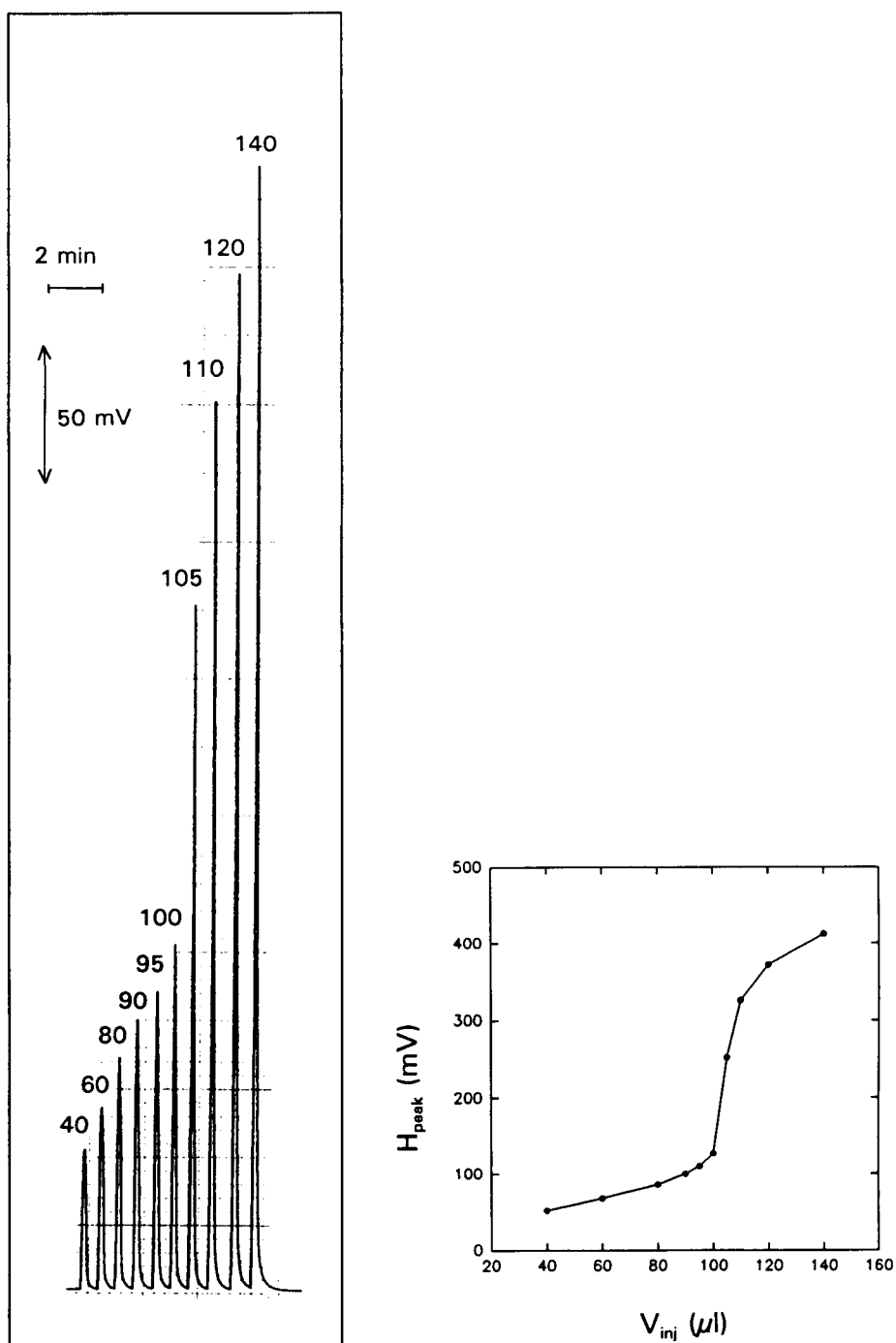


Fig. 3. Strip-chart recording for flow-injection titration. Injection volumes in μl . Representation of experimental points for the evaluation of equivalence volume. Carrier stream: $[\text{CH}_3\text{COOH}] = 0.0326 \pm 0.0001$ M. Tirant solution: $[\text{NaOH}] = 0.0993 \pm 0.0001$ M.

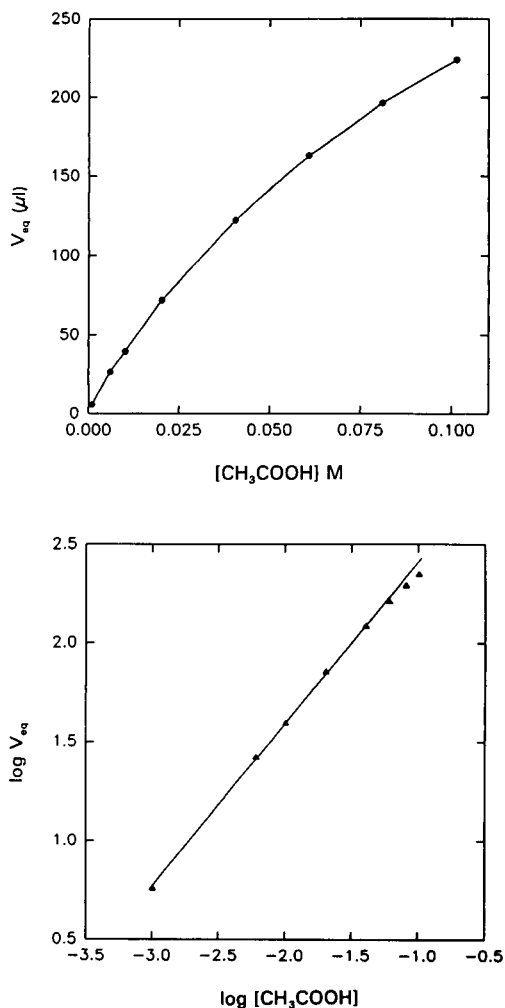


Fig. 4. Calibration with carrier concentration $[\text{CH}_3\text{COOH}]$ between 0.1 and 0.001 M and titrant solution $[\text{NaOH}] = 0.100$ M.

Obviously, the mathematical expression used to describe the batch titrations, $V_a C_a = V_b C_b$ (at the equivalence point), cannot be applied to this flow-injection titration system. The existence of a linear relationship between $\log V_{eq}$ and $\log [\text{CH}_3\text{COOH}]$ allows interpolation of equivalence volume values on the calibration graph. From this, the following expressions were found:

$$\log V_{eq} = b + m \log [\text{CH}_3\text{COOH}]$$

$$V_{eq} = K [\text{CH}_3\text{COOH}]^m$$

where K contains the dispersion factor and a

factor related to the titrant concentration, m is the slope of the calibration line and b is its intercept. The experimental values found for the slope and the intercept are as follows: for $[\text{CH}_3\text{COOH}]$ between 0.1 and 0.001 M and $[\text{NaOH}] = 0.1$ M, $m = 0.821 \pm 0.030$, $b = 3.231 \pm$

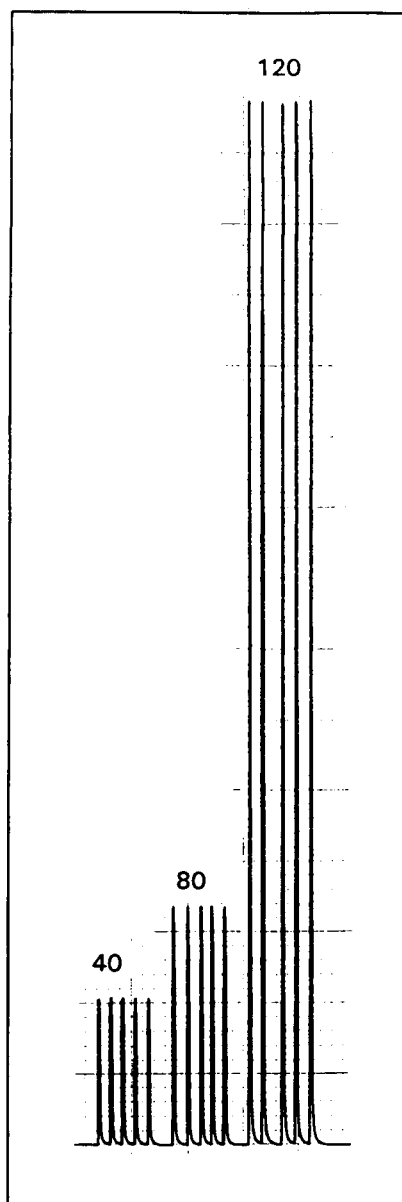


Fig. 5. Strip-chart recording of the reproducibility evaluation. Injection volumes in μl . Carrier stream: $[\text{CH}_3\text{COOH}] = 0.0326 \pm 0.0001$ M. Titrant solution: $[\text{NaOH}] = 0.0993 \pm 0.0001$ M.

0.060, $r^2 = 0.9993$; for $[\text{CH}_3\text{COOH}]$ between 0.01 and 0.0001 M and $[\text{NaOH}] = 0.01$ M, $m = 0.725 \pm 0.029$, $b = 3.841 \pm 0.087$, $r^2 = 0.9995$; and for $[\text{CH}_3\text{COOH}]$ between 0.001 and 6×10^{-5} M and $[\text{NaOH}] = 0.001$ M, $m = 0.772 \pm 0.051$, $b = 4.89 \pm 0.19$, $r^2 = 0.9995$. Although the slope and the intercepts found for the three calibration lines are slightly different, most importantly, they show the same linear behaviour when representing $\log V_{\text{eq}}$ versus $\log[\text{CH}_3\text{COOH}]$ at a constant concentration of the titrant solution while keeping the flow-injection system undisturbed.

An important aspect of the present method is the time required to determine the equivalence point. Figure 5 shows the good reproducibility of the different injections, which makes it unnecessary to repeat the injection of each volume during the titration. The equivalence volume can be determined in less than 7 min by means of a complete titration as shown in Fig. 3. This time can be reduced further to ca. 3 min using end-point titrations or Gran's method in determining the equivalence volume.

However, the time required for analysis depends on the detector response time. In some assays realized with flow-through pH-ISFET detectors [5] the analysis time can be reduced considerably. Although the glass electrode with a flat membrane has a slower response, it was used because it is commercially available.

Conclusions

The viability of using a piston burette as an injection device in a flow system has been demonstrated. Its usefulness lies in the precision and reproducibility when injecting small volumes of reagent into the carrier channel by means of short-duration pulsations. Moreover, the piston burette can be easily controlled by a computer with an attenuated dispensing program, supervised by the electrode signal. Simultaneously, this program creates a file of data pairs $[V_{\text{inj}}, E_{\text{peak}}(\text{maximum})]$, from which the equivalence volume of the titration can be calculated. The flow titration system can be totally automated, thus becoming a competitive substitute for the process titration system.

The wide working range allows for the determination of very low concentrations of acetic acid. The use of reagent is kept to a minimum as titrations are performed by adding only microlitres of reagent. The time required for the complete titration varies between 5 and 10 min, depending on the magnitude of the equivalence volume found. This time is considerable reduced by the application of the same methods as used in the automatic process control.

The ideal situation for this new methodology should allow an expression such as the following to be found:

$$[\text{NaOH}]V_{\text{eq}} = f(\text{disp})[\text{CH}_3\text{COOH}]$$

where the dispersion function, $f(\text{disp})$, should depend only on the flow system manifold conditions. At present, research is under way to obtain a calibration surface relating all three variables (equivalence volume, carrier concentration and titrant concentration). The main aim of this research is to evaluate the influence of the flow system on dispersion phenomena. If a theoretical expression for the dispersion function can be found, the equivalence volume obtained by flow-injection titration would be an absolute measure, in the same way as the equivalence volume determined by batch titration is. This objective requires further studies using dispersion patterns in the flow system.

The authors thank Dr. F. Valdés-Perezgasga for revision of the manuscript and assistance with the instrumentation.

REFERENCES

- 1 B. Karlberg and G.E. Pacey, *Flow Injection Analysis. A Practical Guide*, Elsevier, Amsterdam 1989, pp. 41, 124.
- 2 E.A.M.F. Dahmen, *Electroanalysis. Theory and Application in Aqueous and Non-Aqueous Media, and in Automated Chemical Control (Techniques and Instrumentation in Analytical Chemistry, Vol. 7)*, Elsevier, Amsterdam, 1986, pp. 322–335.
- 3 E. Pungor and I. Buzás, *Modern Trends in Analytical Chemistry*, Akadémiai Kiadó, Budapest, 1984, p. 285.
- 4 J. Ruzicka and E.H. Hansen, *Flow Injection Analysis*, Wiley-Interscience, New York, 2nd edn., 1988, pp. 54, 229.
- 5 J. Alonso, S. Alegret, J. Bartroli, X. Domènech, Y. Duval and N. Jaffrezic, *Anal. Chim. Acta*, 222 (1989) 373.

Characteristics and readout correlation of flow-injection analysis for penicillin

Xiang-Ming Li

Department of Applied Biology and Chemical Technology, Hong Kong Polytechnic, Kowloon (Hong Kong)

Man-Xiang Chen

Department of Applied Physics, South China University of Technology, Guangzhou (China)

Fu-Chang Ruan

Research Institute of Chemical Engineering, South China University of Technology, Guangzhou (China)

Wing-Yan Ng

Department of Applied Biology and Chemical Technology Hong Kong Polytechnic, Kowloon (Hong Kong)

(Received 21st April 1992; revised manuscript received 1st June 1992)

Abstract

A flow-injection analysis (FIA) system based on the enzymatic reactor with immobilized penicillinase on silica gel is developed for the measurement of penicillin. The basic principle of the system is to convert penicillin in the injected sample into penicilloic acid through the enzymatic reactor and to detect the penicilloic acid with a pH sensor in a flow cell following the reactor. A model based on theoretical analysis is developed to correlate the output signal of the pH sensor with the sample concentrations, which shows superior linearity compared to that correlating the peak height of the pH sensor output with the sample concentrations. The life time of the enzymatic reactor is about 600 h. The reactor can be easily replaced after the enzyme activity has declined to a level where the penicillin in the passing carrier stream cannot reach hydrolysis equilibrium. The signal output of the pH sensor is processed on-line by an interfaced microcomputer using an algorithm of the model.

Keywords: Flow injection; Penicillin; Readout correlation

Flow-injection analysis (FIA) is based on the injection of a liquid sample into a carrier stream that flows through a testing cell continuously. The analysis of the sample is conducted by using the sensor in the flow cell. Because of its flexibility in handling samples and suitability for automation, more and more FIA systems are being

utilized in laboratories and industrial processes recently [1–6].

Penicillin is one of the major antibiotics produced in the world. In order to replace the time-consuming testing method based on titration [7], various biosensors have been developed for the measurement of penicillin. Most of these biosensors are made with an electrochemical, or optical pH sensor with immobilized penicillinase on their sensing surface [8–11]. The enzymatic hydrolysis of penicillin to penicilloic acid [12] reduces the

Correspondence to: X.-M. Li, Department of Applied Biology and Chemical Technology, Hong Kong Polytechnic, Hung Hom, Kowloon (Hong Kong).

pH at the sensor surface. The changes of pH detected are correlated with the penicillin concentrations. Because of the limited life-time of the immobilized enzyme, it should be replaced after a number of assays. If the enzyme electrode is not made to be disposable, the reimmobilization of enzyme on the electrode can be difficult for many users. In addition, the linear response ranges of these electrodes depend on the buffer capacity [8]. Trial-and-error is required for finding the appropriate dilution factor in the pre-treatment of the samples with unknown penicillin concentrations. These shortcomings of the immobilized enzyme electrodes are obstacles to their practical application. The FIA system with separate enzyme micro-reactor and detector makes the replacement of the enzyme far easier than for an immobilized enzyme electrode. Changes of dilution factor in a FIA system can be accomplished readily by changing the flow-rate and the sample volume. Various FIA systems had been developed for penicillin measurement [13–15].

The FIA system we developed for penicillin measurement is shown in Fig. 1. The silica gel beads with immobilized penicillinase are packed in the enzymatic reactor. The enzyme hydrolyses the amide bond in the β -lactam ring of penicillin in the injected sample with formation of the penicilloic acid. The residence time of the sample in the enzymatic reactor is kept long enough to ensure that the penicillin reaches hydrolysis equilibrium. The concentrations of the penicilloic acid are then measured by a pH glass electrode in a flow cell connected downstream from the micro-reactor. The signal output of the pH electrode is converted to a hydrogen ion concentration in the

computer for further processing. The data processing method is outlined in the next section.

THEORETICAL ANALYSIS

The correlation of the FIA readouts with the concentrations of penicillin is always a problem. One simple way to correlate the FIA readouts is to use the changes of voltage output of the pH electrode, which is directly proportional to the logarithm of the maximum change in hydrogen ion activity [13,14]. However the linear range is rather narrow. At buffer concentrations greater than 0.4 mM, a linear relationship between the voltage output and concentration was obtained for penicillin concentrations below 0.5 mM [13]. Using the same correlation method, calibration curves were found to be linear up to 5 mM [14]. A very sophisticated linear pH buffer was used by Olsson as the carrier solution which enables the change of pH in the detector to become linear versus the penicillin concentration below 20 mM [15]. It should be noticed that the preparation of the buffer required trial-and-error with repeated titration and regression. We have used a different approach to correlate the FIA readouts with the sample concentrations based on theoretical analysis which gives a linear response range up to 100 mM of penicillin concentration.

At hydrolysis equilibrium

$$[\text{PA}^-][\text{H}^+]/([\text{PEN}]_c - [\text{PA}^-]) = K_e \quad (1)$$

where $[\text{PA}^-]$ is the concentration of hydrolysed penicilloic acid, $[\text{H}^+]$ is the concentration of hydrogen ion, $[\text{PEN}]_c$ is the concentration of penicillin in carrier solution before hydrolysis, and K_e is the hydrolysis equilibrium constant. On the basis of Eqn. 1 the concentration of penicillin in the carrier stream before hydrolysis can be written as

$$[\text{PEN}]_c = [\text{H}^+]^2/K_e + [\text{H}^+] \quad (2)$$

when $[\text{PA}^-] = [\text{H}^+]$ is assumed. The concentration of penicillin in the injected sample should be

$$[\text{PEN}]_s = K_c(V_c/V_s) \int_{t_0}^{t_1} \left\{ ([\text{H}^+]^2/K_e + [\text{H}^+]) - ([\text{H}^+]_b^2/K_e + [\text{H}^+]_b) \right\} dt \quad (3)$$

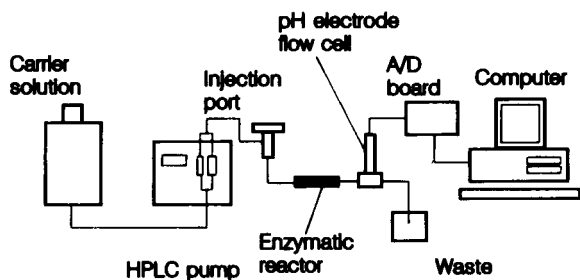


Fig. 1. The FIA system for penicillin measurement.

considering the boundary condition $[PA^-] = 0$ when $[H^+] = [H^+]_b$, where $[H^+]_b$ is the base line concentration of hydrogen ion in the FIA readout curve, K_c is an instrument correction factor, V_c is the volumetric flow rate of carrier solution, V_s is the sample volume, and t is the elapsed time. t_0 is the time before the readout curve, which is the hydrogen ion concentration measured in the flow cell, starts to rise, and t_1 is the time the readout curve returns to the base line. The hydrogen ion concentration is calculated using

$$[H^+] = \exp(-2.30258 \text{ pH}) \quad (4)$$

The instrument correction factor K_c is a factor considering the non-ideal situation of the system including the dispersion of the samples in the carrier stream, the response delay of the pH sensor, etc.

EXPERIMENTAL

Immobilization of enzyme. Silica gel 60 for column chromatography (70–160 mesh, Merck, Darmstadt) was silanized with 10% *r*-aminopropyltrimethoxy silane (adjusted to pH 7.0 with 2 M HCl) at 50°C for 2 h. The silanized silicon gel was rinsed with deionised water and dried overnight in a 100°C oven. Penicillinase (E.C. 3.5.2.6. from *Bacillus cereus*, Sigma (St. Louis, MO) 325 U mg^{-1}) and bovine serum albumin (Sigma) in a ratio of 1:2 by weight, total 6 mg, were dissolved in 200 μl pH 7.0 phosphate buffer solution (0.02 M). 100 μl of 2.5% glutaraldehyde (Sigma) was added to the solution and stirred for 1 min. Then the silanized silica gel (80 mg) was poured into the mixed solution. After gentle shaking for 10 min, 0.1 M DL-lysine monochloride was added to the mixture to stop the cross-linking reaction. The gel particles with immobilized enzyme on their surface were washed with 0.02 M phosphate buffer (pH 7.0) and dried in a vacuum-desiccator for 2 h.

Enzymatic reactor. The enzymatic micro-reactor was packed with 30–60 mg of the gel particles with immobilized enzyme. The appropriate enzyme loading was determined by trial-and-error. The particle size and size distribution of the silica

gel, the immobilization conditions, as well as the amount of gel with immobilized enzyme loaded in the reactor could affect the enzyme loading. When the loading was insufficient to ensure that the penicillin reached hydrolysis equilibrium after passing through the reactor, further increases of enzyme loading could increase the signal output of the pH electrode. For a specific enzymatic reactor, an increase in the flow-rate of the carrier solution could reduce the residence time of the penicillin in the reactor. Therefore, an appropriate loading was found when a further increase of the amount of gel particles loaded did not increase the signal output of the pH electrode, even at the highest anticipated flow-rate.

Carrier solution. The carrier solution was 1 mM phosphate buffer solution at pH 7.0 with 0.1 M NaCl. Since the hydrogen ions, those being generated by the hydrolysis of penicillin, could be neutralized by the buffer, a low buffer capacity solution is used as the carrier solution. In preparation of the carrier solution, 0.1 M NaCl solution was made up first, and its pH was adjusted carefully to 7.0 by adding HCl or NaOH solution. Then the calculated amount of phosphate salt was added to the NaCl solution.

Sample solution. Various amounts of penicillin-G potassium salt (Sigma) was dissolved in 0.1 M NaCl solution (pH 7.0) to make up the standard sample solution at concentration between 1 to 100 mM. The samples were prepared each day to avoid the possible error induced by the slow hydrolysis of penicillin in water.

Instruments. HPLC pump (Bio-Rad, Richmond, CA, Model 1350) was used to pump the carrier solution. The flow cell with pH glass electrode (Cole Parmer, Chicago, IL) was connected downstream of the micro-reactor (stainless steel, 30 \times 2 mm i.d.). The A/D board (Metrabyte, Taunton, MA, Model DSA8, EXP 16) converted the analogue output of the pH electrode to a digital signal for data acquisition with an IBM compatible microcomputer. Software was developed for data acquisition and data processing.

Measurement of the hydrolysis equilibrium constant of penicillin with enzyme. 60 mg silica gel with immobilized penicillinase was placed in a beaker containing 5 ml penicillin-G solution (0.01

M initially). The mixture was stirred with magnetic stirrer until the pH of the mixture dropped to a steady value. The equilibrium constant was calculated based on the final concentration of hydrogen ion and the initial penicillin concentration with Eqn. 2.

Measurement of penicillin concentrations in FIA system. The flow-rate of carrier solution was 4 ml min^{-1} . The sample with known penicillin concentration was injected into the injection port (20–50 μl /sample). The output of the pH electrode was processed by the computer.

RESULTS AND DISCUSSION

A typical readout curve of the FIA system is shown in Fig. 2. It is presented as the hydrogen ion concentration detected in the flow cell versus the elapsed time. Three duplicate samples were injected for each penicillin concentration level. It was observed that the peak area remained nearly constant for duplicate samples, but the peak heights for samples with the same penicillin concentration showed notable differences. This could be caused by a small change of the speed of the sample injection process, which was not very well controlled in our system.

Two methods were used to correlate the FIA readouts with the penicillin concentration in sam-

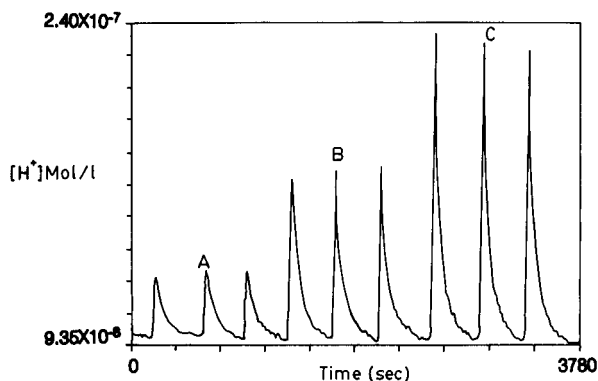


Fig. 2. Readout curve of the FIA system: Hydrogen ion concentration detected in the flow cell versus time. Conditions: flow-rate of carrier solution = 4.0 ml min^{-1} , sample volume = $30 \mu\text{l}$. Penicillin concentrations in samples: A = 20 mM, B = 40 mM, C = 60 mM.

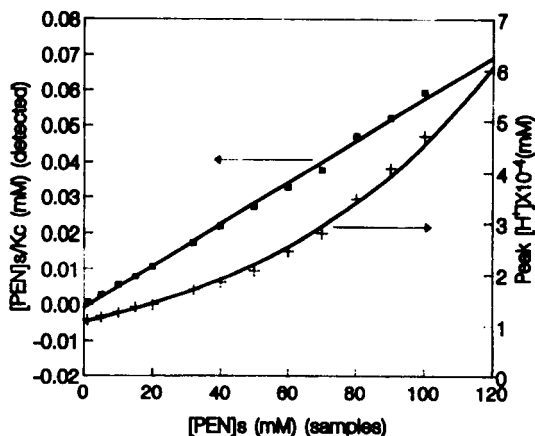


Fig. 3. The correlations of the FIA readouts.

ples. One method was to use Eqn. 3 to calculate the predicted penicillin concentration in the injected sample based on the hydrogen ion concentration measured in the flow cell. The other was found simply by using the peak height of the readout curve, similar to many other FIA systems, to correlate the sample concentrations. The predicted concentrations divided by the instrument correction constant (based on Eqn. 3) and the peak height of various samples are both plotted against sample concentration in Fig. 3. The results show that the linearity of using our correlation method is superior to that of using the peak height. Effects of sample volumes on the FIA readouts were investigated by using samples with the same penicillin concentration but different injection volume. The results are shown in Fig. 4, which indicates that the readouts based on Eqn. 3 were not sensitive to the changes in the sample volumes. The consequences of this are twofold. First, the correlation method for FIA readouts based on Eqn. 3 can provide more precise measurement than that from simply using the peak height if the measurement errors of the sample volumes are the same. Second, it is feasible to use different sample volume for samples of unknown concentration to enlarge the range of measurement of the FIA system.

The applicable life-time of the enzymatic reactor is dependent on the activity of the enzyme immobilized in silica gel, the enzyme loading in

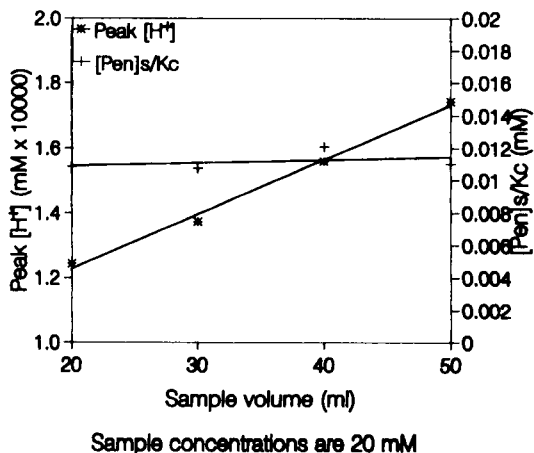


Fig. 4. Effects of the sample volumes on the FIA readouts.

the reactor, and the maximum penicillin concentration expected to be encountered in the carrier stream. When the activity of enzyme declined to a certain level, the readout of the pH electrode for the measurement of the highest concentration sample was the first to show a decline. This reveals that the penicillin in the carrier stream could not reach hydrolysis equilibrium after passing through the enzymatic reactor. A simple way to prolong the applicable life-time of the enzymatic reactor was to increase the enzyme loading of the reactor. Our experimental results showed that a loading of 30 mg of gel particles (70–230 mesh) with immobilized enzyme in the reactor

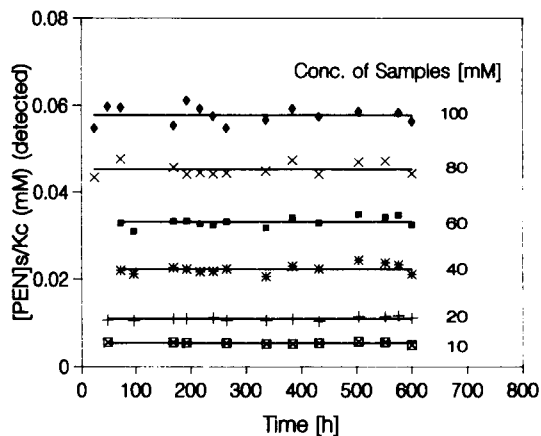


Fig. 5. Life-time testing of the FIA system.

TABLE 1

Interferences of CaCl_2 on the penicillin measurements ^a

Penicillin concentration in samples (mM)	(Readout with salt)/(readout without salt) ^b	
	(1)	(2)
1.0	0.960	0.997
10.0	0.996	1.018
20.0	0.995	0.994
40.0	0.930	0.971
60.0	1.057	0.985

^a All readouts were calculated using Eqn. 3 with experimental data. 1% (weight) of CaCl_2 was added to the sample for conducting the interference tests at various levels of penicillin concentration. ^b Columns (1) and (2) in the table represent the results obtained from two duplicate runs.

had a life-time of about 400 h for a maximum sample concentration of 100 mM. A reactor loaded with 60 mg of gel particles (70–160 mesh) with immobilized enzyme had about 600 h of applicable life-time as shown in Fig. 5. The procedure and conditions of enzyme immobilization for both loadings were the same as that presented in the Experimental.

Interference of CaCl_2 and MgSO_4 on the measurement of penicillin in the FIA system were also investigated. These salts are commonly encountered in fermentation broth. The interference tests were conducted by comparing the FIA readouts for samples with and without added salt but for the same penicillin concentration. Duplicate measurements were made for each test. The results, listed in Tables 1 and 2, do not show any

TABLE 2

Interference of MgSO_4 on the penicillin measurements ^a

Penicillin concentration in samples (mM)	(Readout with salt)/(readout without salt) ^b	
	(1)	(2)
10.0	1.010	1.025
20.0	1.010	0.939
40.0	1.017	1.002
60.0	0.998	1.001

^a All readouts were calculated using Eqn. 3 with experimental data. 1% (weight) of MgSO_4 was added to the sample for conducting the interference tests at various levels of penicillin concentration. ^b Columns (1) and (2) in the table represent the results obtained from two duplicate runs.

significant interference of these salts on the measurement of penicillin.

We thank the Hong Kong Polytechnic for the financial support of this research project.

REFERENCES

- 1 U. Prinzing, I. Ogbomo, C. Lehn and H.-L. Schmidt, *Sensors Actuators*, B1 (1990) 542.
- 2 G.K. Chandler, J.R. Dodgson and M.J. Eddowes, *Sensors Actuators*, B1 (1990) 433.
- 3 K. Matsumoto, H. Kamikado, H. Matsubara, and Y. Osajima, *Anal. Chem.*, 60 (1988) 147.
- 4 A. Manz, N. Graber and H.M. Widmer, *Sensors Actuators*, B1 (1990) 244.
- 5 M. Gern, M. Gisin, C. Thommen, P. Cevey, *Biotechnol. Bioeng.*, 34 (1989) 423.
- 6 J. Ruzicka and E.H. Hansen, *Flow Injection Analysis*, 2nd edn., Wiley, New York, 1988.
- 7 J.J. Murtaugh and G.B. Levy, *J. Am. Chem. Soc.*, 67 (1945) 1042.
- 8 S. Caras and J. Janata, *Anal. Chem.*, 52 (1980) 1935.
- 9 T.J. Kulp, I. Camins, S.M. Angel, C. Munkholm, and D.R. Walt, *Anal. Chem.*, 59 (1987) 2849.
- 10 M.-R.S. Fuh, L.W. Burgess and G.D. Christian, *Anal. Chem.*, 60 (1988) 433.
- 11 S. Luo, and D.R. Walt, *Anal. Chem.*, 61 (1989) 1069.
- 12 D.R. Thatcher, in J.H. Hash (Ed.), *Methods in Enzymology*, Vol. 18, Academic, New York, 1975, p. 640.
- 13 J.F. Rusling, G.H. Luttrell, L.F. Culler and G.J. Pappariello, *Anal. Chem.*, 48 (1976) 1211.
- 14 R. Gnanasekaran and H.A. Mottola, *Anal. Chem.*, 69 (1985) 415.
- 15 B. Olsson, *Anal. Chim. Acta*, 209 (1988) 123.

Amperometric techniques in flow-injection analysis: determination of magnesium in sera and natural waters

Alison J. Downard, Joanne B. Hart, H. Kipton J. Powell and Shuanghua Xu

Department of Chemistry, University of Canterbury, Private Bag, Christchurch (New Zealand)

(Received 5th May 1992)

Abstract

Magnesium was determined in a flow-injection system by formation of the magnesium–Eriochrome Black T (EBT) complex at pH 11.5 (5% 1,2-diaminoethane in 0.1 M KCl) and amperometric measurement of the excess of EBT at +0.175 V on a glassy carbon electrode. From modelling calculations, pH and concentrations of EBT (3.75×10^{-5} M) and masking agent EGTA (1.12×10^{-4} M) were chosen so as to minimize interference from calcium. Electrode fouling from EBT oxidation products was countered by use of 0.2% surfactant (Hostapur SA 93) in the carrier stream. Iron(III) was masked with triethanolamine. For analysis of natural waters the linear working range was 0.027–1.8 mg kg⁻¹ Mg and the R.S.D. was 0.7% at 1.6 mg kg⁻¹ Mg ($n = 11$); the detection limit was 5.5 μ g kg⁻¹. Analysis of human blood serum samples was effected by two methods: direct injection of serum after a 20-fold dilution (Hostapur SA 93 countered the association of EBT with serum albumin) and after dialysis (2.5 min) to separate Mg from acidified serum in the flow system. The linear working range for direct injection was as above and the R.S.D. was 0.4% ($n = 9$) at 1.0 mg kg⁻¹ Mg. For each method the results were compared with those from flame atomic absorption spectrometry.

Keywords: Amperometry; Flow injection; Magnesium; Serum; Waters

The determination of magnesium in natural waters and human sera is routine. The standard methods for analysis include atomic absorption spectrometry (AAS) and UV–visible spectrophotometry [1]. Magnesium may also be determined using electrochemical techniques after complexation by an electroactive ligand. Thus, An et al. [2] determined Mg in water and serum by measurement of the adsorptive reduction peak for the Mg–Eriochrome Black T (EBT) complex at a mercury electrode [2] and the method was subsequently adapted for flow-injection analysis (FIA) for serum magnesium [3]. Up to 35 samples h⁻¹

could be processed but the flow-injection system incorporated several complex features, viz., a dropping mercury electrode assembly, a thin-film deaerator and a rapid potential-scanning detector.

As part of a project to develop amperometric detection techniques for strongly electropositive elements, this paper reports an FIA method for Mg determination. The method is based on complexation of Mg by EBT with monitoring of the current due to oxidation of the excess of EBT at a fixed potential on a glassy carbon electrode without solution deaeration. The FIA system and electrochemical instrumentation required are relatively simple and inexpensive and the method has been applied to determination of Mg in natural waters and blood serum.

Correspondence to: H.K.J. Powell, Department of Chemistry, University of Canterbury, Private Bag, Christchurch (New Zealand).

EXPERIMENTAL

Reagents

1,2-Diaminoethane (BDH), Ethylene glycol bis(β -aminoethyl ether)- N,N,N',N' -tetraacetic acid (EGTA) (Sigma) and triethanolamine (BDH, AnalaR) were used as supplied. All solutions were prepared in doubly distilled water (DDW). Magnesium standards were prepared from $MgSO_4 \cdot 7H_2O$ (BDH, AnalaR). Hostapur SAS 93 was kindly supplied by Hoechst (New Zealand).

Equipment and procedure

Amperometric measurements in the flow cell, or in static solution, were obtained using a PAR 174A polarograph and a Graphtec WX1200 recorder. Voltammetric measurements were made with a PAR 273 potentiostat coupled to a laboratory-built waveform generator.

For water analyses the flow system consisted of two Alitea C4-XV peristaltic pumps and the flow manifold shown in Fig. 1a. The flow-rates

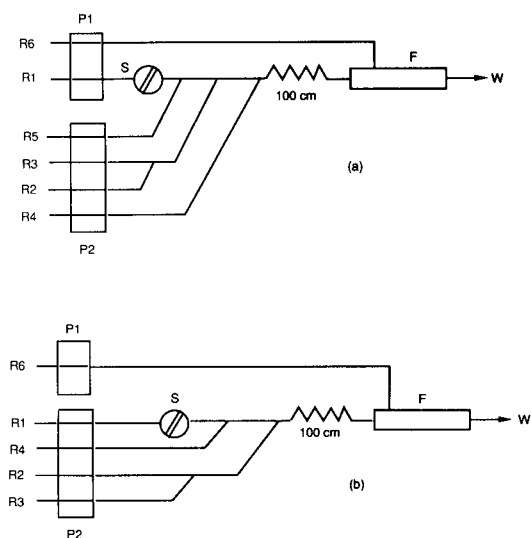


Fig. 1. (a) Manifold for determination of Mg in water. R1 = doubly distilled water; R2 = 1.5×10^{-4} M EBT; R3 = 15% 1,2-diaminoethane in 0.3 M KCl (pH 11.5); R4 = 0.2% Hostapur SAS 93; R5 = 4.5×10^{-5} M EGTA, 4×10^{-2} M triethanolamine; R6 = 0.1 M KCl; S = sample (50 μ l); F = flow cell; W = waste. (b) Manifold for direct determination of Mg in diluted serum. Reagents as in (a); masking agents (R5) not required.

for the carrier (R1 = water), reagent (R2 = 1.5×10^{-4} M EBT), buffer (R3 = 15% 1,2-diaminoethane in 0.3 M KCl, pH 11.5), surfactant (R4 = 0.2% Hostapur SAS 93), masking agents (R5 = 4.5×10^{-4} M EGTA; 4×10^{-2} M triethanolamine) and reference electrode electrolyte (R6 = 0.1 M KCl) were 0.6 ml min^{-1} (R1–R5) and 0.2 ml min^{-1} (R6). EBT solutions decomposed slowly at pH 11.5, therefore buffering of the EBT from neutral pH was effected on-line. The reaction coil consisted of 100 cm \times 0.51 mm i.d. knitted microline tubing (Cole-Palmer). The detector (D) consisted of a wall-jet microflow cell as described previously [4] but with the gold electrode replaced with a 3 mm diameter glassy carbon electrode. Prior to use the electrodes were hand polished with 1- μ m diamond paste. The rotary injection valve had a 50- μ l sample loop. The dispersion coefficient (D) for the injected solution was 5.2 and the elapsed time from merging of the sample and reagent zones was 8 s.

For direct analysis of serum the masking reagents (R5) were not necessary; the manifold was modified to effect binding of surfactant to serum proteins before merging with EBT–buffer (Fig. 1b). Analysis of serum by dialysis–FIA used the manifold shown in Fig. 2. R1, R4 and R6 were as above, R2 = 0.03 M HCl, R3 = 0.01 M HCl and R5 = EBT (1.0×10^{-4} M) + buffer (15% 1,2-diaminoethane–0.3 M KCl, pH 11.5). Flow-rates for R1–R6 were 0.6 ml min^{-1} (R2–R5) and 0.2 ml min^{-1} (R1, R6). The dialyser consisted of two blocks of acetal (Delrin), $120 \times 62 \times 12$ mm, with complimentary channels $0.5 \times 1.5 \times 500$ mm

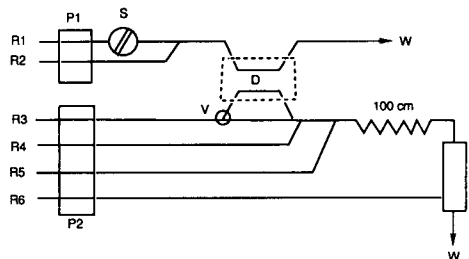


Fig. 2. Manifold for analysis of serum following dialysis. R1, R4, R6 as in Fig. 1. R2 = 0.03 M HCl; R3 = 0.01 M HCl; R5 = 1.0×10^{-4} M EBT, 15% 1,2-diaminoethane, 0.1 M KCl (pH 11.5); D = dialysis unit; V = switching valve.

separated by 30000 molecular weight cut-off (MWCO) dialysis membrane. Flow was stopped in R1 for 150 s after the injected serum sample was contained in the dialyser; during this period the valve V was switched to provide stationary solution in contact with the membrane but maintain a constant reagent flow through the detector.

Analyses for magnesium by AAS were obtained on a Varian Model 1475 spectrophotometer using the 282.8-nm resonance line. Serum samples were diluted 20-fold with DDW; samples and standards contained $1500 \text{ mg Sr kg}^{-1}$.

Samples

Blood was taken in heparinized tubes, chilled (4°C) and centrifuged within 2 h of collection; the serum was removed from the erythrocytes and stored at 4°C . Water samples were provided by DSIR (NZ) Chemistry Division, who carried out independent analyses for Mg (AAS), Fe (AAS), Al (FIA; Eriochrome Cyanine R) and PO_4^{3-} (FIA); the samples were selected to provide a wide range of concentrations for Mg, Ca and Fe ($0.6\text{--}5.2$, $1.3\text{--}134$ and $<0.1\text{--}2.9 \text{ mg kg}^{-1}$, respectively). Freeze-dried serum (Moni-Trol) was obtained from Baxter Healthcare.

Speciation calculations

Speciation calculations were performed with the program SIAS [5]. Protonation and metal-ligand stability constants used were as follows (log values): H_nEBT , $K_1 = 11.55$, $K_2 = 7.00$; $\text{Mg}(\text{EBT})$, $K_1 = 7.00$; $\text{Ca}(\text{EBT})$, $K_1 = 5.30$ [6]; CaOH , $*K_1 = -11.70$; MgOH , $*K_1 = -11.40$ [7]; H_nEGTA , $K_1 = 9.54$, $K_2 = 8.93$, $K_3 = 2.73$, $K_4 = 2.08$; $\text{Mg}(\text{EGTA})$, $K_1 = 5.21$; $\text{Ca}(\text{EGTA})$, $K_1 = 11.00$ [8].

RESULTS

Voltammetry

The cyclic voltammogram for EBT ($1 \times 10^{-4} \text{ M}$) on a glassy carbon electrode at pH 11.8 showed anodic and cathodic peaks at ca. 0.12 and 0.05 V, respectively. On addition of Mg ($1 \times 10^{-4} \text{ M}$) the anodic peak shifted to 0.23 V. In the presence of $1 \times 10^{-4} \text{ M Ca}$ there was no measurable change in the cyclic voltammogram for EBT.

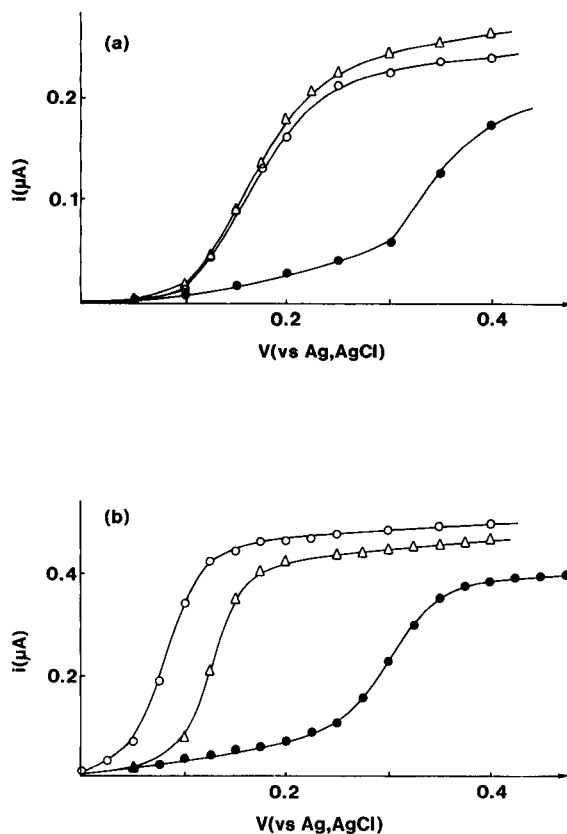


Fig. 3. Hydrodynamic voltammograms for preformed EBT-buffer and M-EBT-buffer solutions, (a) with surfactant (0.2% Hostapur, R4) and (b) without surfactant; pH 11.5. Manifold as in Fig. 1a, R2 and R5 omitted. $\circ = 2.0 \times 10^{-4} \text{ M EBT}$; $\triangle = 2.0 \times 10^{-4} \text{ M EBT}$, $6.0 \times 10^{-4} \text{ M Ca}$; $\bullet = 2.0 \times 10^{-4} \text{ M EBT}$, $4.0 \times 10^{-4} \text{ M Mg}$.

Hydrodynamic voltammograms (Fig. 3) were constructed by injecting preformed EBT-buffer or M(EBT)-buffer solutions into the flow system (Fig. 1a, R2 and R5 omitted) with and without surfactant (R4). In the absence of surfactant, $E_{1/2}$ values for EBT, Ca(EBT) and Mg(EBT) were ca. +85, +125 and +300 mV (vs. Ag/AgCl; 0.10 M KCl). The greater shift in $E_{1/2}$ and decrease in limiting current for Mg indicated the formation of a more stable complex with Mg than with Ca and a smaller diffusion coefficient for metal-bound EBT.

In the presence of surfactant, $E_{1/2}$ values moved in the positive direction [by 75, 45 and 40 mV for EBT, Ca(EBT) and Mg(EBT), respec-

tively]. The $E_{1/2}$ values for EBT and Ca(EBT) were very similar, with the limiting current slightly higher in the presence of Ca. For amperometric measurements the analytical voltage was +175 mV, chosen to minimize the effect of Ca on the difference in anodic currents for EBT and Mg(EBT).

Speciation calculations

For Mg alone the formation of Mg(EBT) was calculated to be nearly quantitative at pH 11.5 and $[EBT] \geq 1 \times 10^{-4}$ M ($> 2 \times 10^{-5}$ M in the detector) for 1×10^{-7} – 1×10^{-5} M Mg (98–96% complexation). Although forming a weaker complex, Ca, typically present at higher concentration in natural waters, competes for EBT; for 1×10^{-5} M Mg and 4×10^{-5} M Ca, 18% and 89% M(EBT) were formed, respectively.

To model the masking of Ca (and Mg) by EGTA, ratios of $[EGTA]:[EBT]$ of 1:1 to 8:1 were considered, with Ca:Mg = 3:1 and 6:1. EGTA binds Ca quantitatively, but at $[EGTA]:[EBT] = 8:1$, 4:1 and 2:1, and Ca:Mg = 3:1, EGTA also binds 23%, 12% and 4%, respectively, of Mg. Optimum conditions chosen were $[EGTA]:[EBT] = 3:1$ which, for 2×10^{-5} M Mg and 3.75×10^{-5} M EBT (both at the detector) and Ca:Mg = 6.0, 4.0, 2.0 and 1.0, gave 100% formation of Ca(EGTA) and 92–95% formation of Mg(EBT).

Electrode activity and chemical interferences

The electrode activity decreased with time, as evidenced by a steady decrease in anodic current

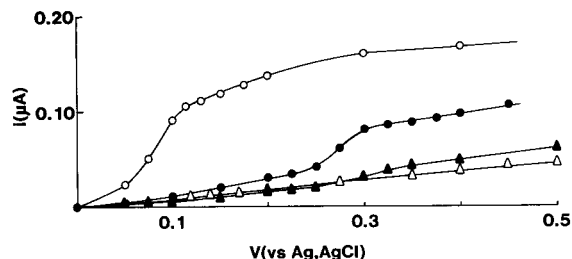


Fig. 4. Hydrodynamic voltammograms for preformed EBT–buffer, EBT–serum–buffer and M–EBT–serum–buffer solutions, pH 11.5, and 7.5×10^{-5} M EBT. \circ = EBT; \bullet = EBT + $1 \mu\text{g ml}^{-1}$ Mg; \blacktriangle = EBT + $1 \mu\text{g ml}^{-1}$ Mg + albumin (0.5 g dl^{-1}); \triangle = EBT + albumin (0.5 g dl^{-1}).

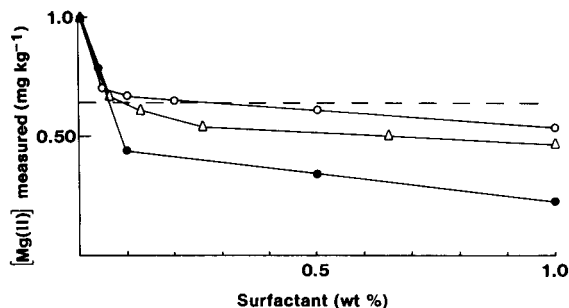


Fig. 5. Effect of surfactant type and concentration (pumped) on apparent Mg concentration measured with the FIA manifold in Fig. 1b. \circ = Hostapur SAS 93; \triangle = Gafac RM710; \bullet = Brij-35. Dashed line represents correct (AAS) value for serum Mg.

for the carrier–reagent stream (EBT–buffer) and a decrease of ca. 0.7% per injection in the peak resulting from complexation of EBT with $1.6 \text{ mg Mg kg}^{-1}$. This deactivation was countered by the presence of 0.2% Hostapur SAS 93 in the flow line (i.e., 0.04% in the detector).

It was established that EBT binds to serum albumin under the experimental conditions used (Fig. 4); thus serum protein caused a large positive error in the current measured for Mg in serum. This ionic association can be masked by addition of anionic surfactants. Again, Hostapur SAS 93 was the most effective of those studied, as indicated in Fig. 5, in which the dashed line represents the ‘correct’ value for Mg in serum (from AAS). Figure 6 shows typical output for replicate injections of serum (diluted 1:20 with DDW), using the manifold in Fig. 1b.

The dialysis unit (Fig. 2) permitted the determination of serum magnesium in the absence of serum proteins. For a 30 000 MWCO membrane,

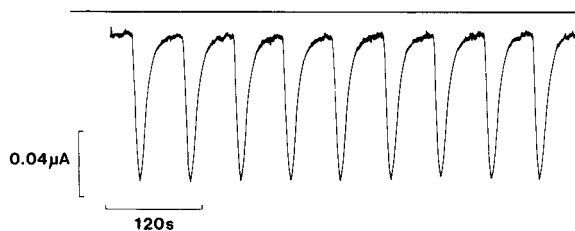


Fig. 6. Amperometric signals for injection of $50 \mu\text{l}$ of serum (diluted 1:20 with distilled water) with the manifold in Fig. 1b.

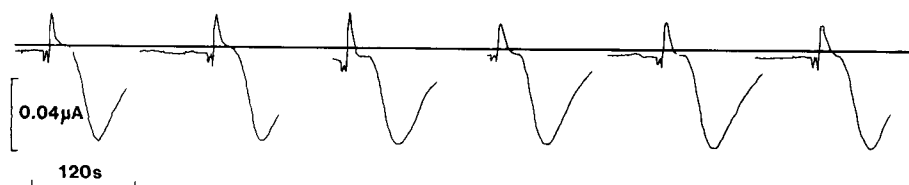


Fig. 7. Amperometric signals for replicate analyses of serum (diluted 1:1 with distilled water) following dialysis (stopped-flow 150 s) with the manifold in Fig. 2.

14% of serum magnesium passed through the membrane in 150 s during stopped flow. Serum was acidified (0.03 M HCl) on-line before dialysis to release Mg from albumin. For undiluted serum samples membrane efficiency decreased by ca. 1.1% per injection; this was countered by a twofold dilution before injection. Figure 7 shows typical output for replicate analyses of serum samples by dialysis–FIA.

Interferences were studied by pre-equilibration of an Mg standard solution with various concentrations of interferent before injection in the FIA system. Fe(III) interfered strongly; on a molar basis the interference was equivalent to 60–90% of the Fe(III) concentration. Fe(III) was effectively masked by triethanolamine [9], but not by EGTA or CN^- . In the presence of EGTA and triethanolamine there was no measurable interference up to (injected concentration) 5×10^{-4} M PO_4^{3-} , Fe^{3+} , Ca^{2+} or Al^{3+} , or up to 1×10^{-3} M F^- at 5×10^{-5} M Mg and 1.5×10^{-4} M EBT.

Water analyses

By use of the manifold in Fig. 1a, multiple injections of a $1.6 \text{ mg Mg kg}^{-1}$ standard gave an R.S.D. of 0.7% ($n = 11$); for $0.10 \text{ mg Mg kg}^{-1}$,

the R.S.D. was 2.5% ($n = 9$). The detection limit, determined as 2σ for a 0.05 mg kg^{-1} standard, was $5.5 \mu\text{g kg}^{-1}$ ($n = 11$), giving a linear working range of $0.027\text{--}1.8 \text{ mg kg}^{-1}$ ($1 \times 10^{-6}\text{--}75 \times 10^{-6}$ M).

Sixteen samples received from DSIR (NZ) Chemistry Division were analysed by FIA and AAS. In the absence of triethanolamine, samples with high concentrations of Fe ($> 0.5 \text{ mg kg}^{-1}$) gave anomalously high values by FIA. In the absence of EGTA, samples with high concentrations of Ca ($> 10 \text{ mg kg}^{-1}$) and a high Ca:Mg ratio (≥ 12) gave anomalously low values by FIA. With the use of masking agents Mg values determined by FIA and AAS correlated well: $\text{Mg(AAS)} = 0.990 \text{ Mg(FIA)}$; $R^2 = 0.996$ ($n = 16$).

Serum analyses

Serum samples were analysed by FIA by direct injection after 20-fold dilution ($60 \text{ samples h}^{-1}$) or by dialysis–FIA ($20 \text{ samples h}^{-1}$). For direct injection, replicate analyses had an R.S.D. of 0.4% ($n = 9$) for $1.0 \text{ mg Mg kg}^{-1}$. The results are given in Table 1 and compared with those for analyses by AAS. Samples 1–5 were serum separated from freshly taken whole blood, sample 6 was serum from aged blood that had partly lysed and sample 7 was reconstituted freeze-dried serum.

TABLE 1

Determination of Mg in serum samples

Sample	Mg (mg kg^{-1})		
	FIA	Dialysis–FIA	AAS
1	18.4	18.3	18.3
2	18.4	18.7	18.7
3	20.8	20.0	19.5
4	19.7	20.8	19.7
5	18.4	17.9	18.3
6 (freeze-dried)	62.8	44.2	44.4
7 (aged)	62.2	35.0	33.4

DISCUSSION

Voltammetry

Cyclic voltammetry and hydrodynamic voltammograms (Fig. 3) established the feasibility of using the EBT oxidation process for the indirect determination of Mg. Oxidation involves the azo or α -hydroxy substituents [10] which are involved

in binding to Mg. Thus, the formation of a stable complex affects the ease of oxidation and results in a shift in $E_{1/2}$. The concentration of metal ion in the system can be established by measuring the current of the additional redox peak (cf., differential-pulse polarography of the Al(alizarin) complex [11]) or, in the case of a flow system, measuring the decrease in the oxidation current of the uncomplexed ligand (e.g., FIA of Al(DASA) [4]). For the Mg–EBT system, use of the oxidation process results in a measuring potential at which O_2 reduction does not occur and hence deaeration of solutions is not necessary.

The hydrodynamic voltammograms measured by injection of preformed solutions into the flow manifold indicated that Mg forms a stable complex with EBT which has a smaller diffusion coefficient than EBT (Fig. 3a). Quantitative complexation of EBT by Ca was forced by addition of excess ($3 \times$) Ca; the lower stability of this complex is evidenced by the smaller shift in $E_{1/2}$ relative to EBT. In the presence of surfactant the slope of each voltammogram was decreased, indicating decreased electrochemical reversibility.

Electrode activity

It is common for oxidation products of azo, phenolic or 1,2-dihydroxyaryl systems to deactivate the electrode by strong adsorption. For EBT, repetitive cyclic voltammograms and amperometric measurements on glassy carbon (GC), Au or Pt electrodes under hydrodynamic conditions ($E = +175$ mV), established significant electrode deactivation with time, especially at high ligand concentrations. Gold was not an appropriate electrode because of its ready oxidation under strongly alkaline conditions. Voltage pulse reactivation of Pt, as used for Al(DASA) [4], was examined. Of several voltage patterns tested, activation at -500 mV (60 s) was most successful; however, this was considered too slow for a flow system. It was established that deactivation of GC could be countered by use of a low EBT concentration (ca. 3.75×10^{-5} M in the detector) and an anionic surfactant in the carrier stream. Surfactants tested included Brij-35, Empigen BB, Empigen OB, Gafac (RM710, RM510, RS410) and Hostapur SAS 93. All caused a concentration-de-

pendent decrease in oxidation current for EBT; this was least and approximately linear for Hostapur SAS 93 (-23% for 1% surfactant pumped) and a proportional change occurred in the FIA peak for Mg. A 0.2% solution of Hostapur SAS 93 was used (0.04% in the detector); baseline (EBT) and peak (Mg) currents did not change measurably over extended use (1 h or 20 injections, respectively).

The maximum current for Ca(EBT) was greater than that for EBT. Consistent with this, the FIA baseline current for oxidation of EBT was increased on inclusion of Ca in the carrier stream; however, in the presence of Mg, and with no Ca masking agent present, the Mg peak was decreased when Ca at high concentration competed for EBT. Setting the analytical voltage at $+175$ mV did not achieve maximum sensitivity for Mg, but minimized errors associated with Ca binding to EBT.

Speciation

Speciation calculations provide only an approximate measure of solution composition. They are limited by the accuracy of and experimental conditions used for the stability constant measurements and, in FIA systems, by reaction kinetics. Competing ligands or metals in environmental or biological samples, if omitted from the model, will also limit the validity of the calculations.

The objective was to determine the optimum pH and minimum EBT concentration required for quantitative formation of Mg(EBT) in the most dilute environmental samples and to determine the concentration of EGTA that would most effectively mask the Ca–EBT reaction without sequestering Mg.

For 3.75×10^{-5} M EBT at the detector, formation of Mg(EBT) was calculated to be nearly quantitative ($\geq 96\%$) up to 2.0×10^{-5} M Mg (2.5 mg kg $^{-1}$ injected) but then decreased significantly. This was demonstrated by the calibration graph, which was linear up to 1.45×10^{-5} M Mg (1.8 mg kg $^{-1}$ or 7.5×10^{-5} M injected); $R^2 = 0.999$ ($n = 5$).

Although Ca forms a significantly weaker complex than Mg with EBT, its higher concentration

in environmental samples and in serum makes it a potential interferent.

In the absence of a Ca masking agent the positive error associated with binding of EBT to Ca increased linearly with Ca concentration and was also dependent on the Ca:Mg ratio. For $[Ca] = 16 \text{ mg kg}^{-1}$ ($4.0 \times 10^{-4} \text{ M}$) and $[EBT] = 3.75 \times 10^{-5} \text{ M}$, the error (at the detector) was +9.8, 5.3, 3.2 and 2.3% for $[Mg] = 3.0 \times 10^{-5}$, 2.0×10^{-5} , 1.0×10^{-5} and $0.1 \times 10^{-5} \text{ M}$ (3.7–0.12 mg kg^{-1} injected), respectively. This established the need to use a masking agent for Ca in environmental samples. In contrast, for diluted serum samples, the concentrations of Ca and Mg in the detector are ca. 3.1×10^{-5} and $7.7 \times 10^{-6} \text{ M}$, respectively; under these conditions, the calculated error associated with Ca(EBT) formation (no EGTA added) is only 1.5%.

EGTA binds Ca quantitatively under the experimental conditions ($\log K_1 = 11.00$) [8]. It is necessary to use an excess EGTA concentration ($> [Ca]$) to ensure that excess of Ca does not bind to EBT; however, EGTA also competes weakly for Mg ($\log K_1 = 5.20$) so the $[EGTA]:[EBT]$ ratio is critical. A ratio of 3:1 was chosen (see Results); under these conditions, the formation of Mg(EBT) was calculated to vary by only 3% for a wide range of Ca:Mg ratios. FIA experiments on samples with Ca:Mg = 12, 13 and 26, with $[EGTA]:[EBT] = 4.0, 3.0, 2.0$ and 1.0, established that there was minimal deviation from Mg(AAS) values for $[EGTA]:[EBT] = 3.0$.

Sample analyses

A feature of the present method is its ability to achieve accurate analyses in waters which are high in Fe(III) or Al. Cañete et al. [12] described an FIA–titration method for Ca + Mg in water using EBT–EDTA. However, they made no attempt to characterize or mask interference from Fe(III) or Al and hence the method may not be suitable for natural waters.

In serum, 22% of Mg is bound to albumin and 7% to globulins [13]. For the dialysis experiments protein-bound Mg was released by merging the carrier stream (R1 = water) with 0.03 M HCl (R2; Fig. 2); this gave a sample pH of ca. 2.0. Without this acidification the results were suppressed by

75%. For direct FIA analysis of serum, the initial 20-fold dilution of serum samples, plus the effects of dispersion, were sufficient to release all protein-bound Mg in the presence of EBT; no acidification was necessary.

Albumin has a propensity to bind dye molecules, either by hydrophobic interaction or by electrostatic attraction between cationic sites on the protein and anionic dye molecules. Hydrodynamic voltammograms of equilibrated EBT–serum samples established a strong interaction under the experimental conditions. Further, the Mg(EBT) complex also associated with the protein (Fig. 4). These interactions were effectively countered by including 0.04% of the *n*-alkyl sulphonate surfactant Hostapur SAS 93 in the reagent stream. Thus, in the absence of surfactant, the ‘apparent’ Mg concentration measured by this amperometric technique was ca. 50% higher than the total Mg concentration determined by AAS (Fig. 5); in the presence of surfactant ($> 0.1\%$ pumped) the FIA amperometric value approached the ‘correct’ value, although excess of surfactant led to negative errors. The surfactant Hostapur SAS 93 was selected because it gave rise to the smallest errors at high concentration, and the smaller slope of the Mg (measured) vs. % surfactant curve gave the widest window of surfactant concentrations which provided a close correlation between AAS and FIA values for Mg.

Hence the surfactant had two roles, to suppress electrode deactivation and to mask binding of EBT to serum. For direct analysis of serum the FIA manifold (Fig. 1b) merged surfactant (R4) with the carrier–sample stream (R1) to mask serum–EBT binding prior to introduction of EBT and buffer. The masking agents for Fe(III) and Ca were not necessary for the analysis of serum (Figs. 1b and 2).

Injection of undiluted serum into the dialysis unit caused fouling of the dialysis membrane; the FIA peak heights decreased by ca. 1.1% per injection. Attempts to rectify this problem by washing with dilute acid, dilute alkali, dilute surfactant or ethanol–water mixtures were unsuccessful. The problem was countered effectively by an initial twofold dilution of the serum samples.

For fresh serum samples there was excellent agreement between the measurements by direct FIA, by dialysis–FIA and by AAS (Table 1). However it is evident that serum from an aged blood sample (partly lysed) contained protein constituents that do not pass the dialyser but which interfere with the chemistry or electrochemistry of the Mg–EBT reaction or which bind with EBT in the presence of surfactant. It is possible that a similar effect arises for the freeze-dried serum.

For routine analysis, the method of choice is by direct FIA using serum samples diluted 20-fold. This permits approximately 60 analyses h^{-1} , compared with ca. 15 h^{-1} by dialysis–FIA. This throughput is very favourable compared with the FIA–adsorptive stripping method [3] and AAS, and the delay from sample preparation to completed analyses for a single sample is very short compared with the automated calmagite spectrophotometric method.

REFERENCES

1 A. Jensen and E. Riber, in H. Sigel (Ed.), *Metal Ions in Biological Systems*, Vol. 16, Dekker, New York, 1984, pp. 151–165.

- 2 J. An, J. Zhou and X. Wen, *Talanta*, 32 (1985) 479.
- 3 R. Goldik, C. Yarnitzky and M. Ariel, *Anal. Chim. Acta*, 234 (1990) 161.
- 4 A.J. Downard, H.K.J. Powell and S. Xu, *Anal. Chim. Acta*, 256 (1992) 117.
- 5 J.J. Fardy and R.N. Sylva, SIAS, a Computer Program for the Generalized Calculation of Speciation in Mixed Metal–Ligand Aqueous Systems, Australian Atomic Energy Commission Report AAEC/E445, 1978, pp. 1–20.
- 6 G. Schwarzenbach and W. Biederman, *Helv. Chim. Acta*, 31 (1948) 678.
- 7 E. Högfeldt, *Stability Constants of Metal–Ion Complexes. Part A: Inorganic Ligands (IUPAC Chemical Data Series, No. 21)*, Pergamon, Oxford, 1982.
- 8 L.G. Sillen, *Stability Constants of Metal–Ion Complexes, Supplement No. 1 (Special Publication No. 25)*, Chemical Society, London, 1971.
- 9 H. Wada and G. Nakagawa, *Anal. Chim. Acta*, 159 (1984) 289.
- 10 A.J. Bard (Ed.), *Encyclopaedia of Electrochemistry of the Elements*, Vol. XIII, Dekker, New York, 1979, pp. 187–189.
- 11 A.J. Downard, H.K.J. Powell and S. Xu, *Anal. Chim. Acta*, 251 (1991) 157.
- 12 F. Cañete, A. Rios, M.D. Luque de Castro and M. Valcárel, *Analyst*, 112 (1987) 267.
- 13 R.J. Henry, D.C. Cannon and J.W. Winkelman, *Clinical Chemistry Principles and Techniques*, Harper and Row, New York, 2nd edn., 1974.

Pressure insensitive solid state reference electrode for in-situ voltammetric measurements in lake water

R. Jermann, M.-L. Tercier and J. Buffle

Département de Chimie Minérale, Analytique et Appliquée, Université de Genève, 1211 Geneva 4 (Switzerland)

(Received 13th April 1992)

Abstract

A pressure insensitive solid state reference electrode was prepared for in-situ voltammetric measurements in lake water in conjunction with a submersible flow-through cell. The dependence of the measured electrode potential on applied pressure, temperature, and the nature and concentration of the electrolyte solution is reported. Reversibility tests (cyclic measurements of the current as a function of applied potential) provided a qualitative indication of the state of the electrode. Its lifetime is approximately two weeks, but electrodes are easily prepared and can be stored for several months before use. The electrode was also successfully used for voltammetric measurements (differential pulse, square wave and linear sweep voltammetry) in the laboratory.

Keywords: Voltammetry; Solid state reference electrode; Waters

Voltammetric measurements are particularly suitable for determining metal concentrations in lake water due to the possibility of multi-element analysis and to their sensitivity. However, measurement of metal concentrations in the nanomolar range and lower is generally hampered by contaminations during sampling or sample handling before its analysis. In addition, due to the change in conditions during sampling (temperature, pressure, light), the sample often undergoes chemical changes such as degassing of, or contamination by, O₂, CO₂, and/or H₂S resulting in changes in pH or redox conditions, and in the corresponding changes in the speciation of many compounds or elements. In-situ voltammetric measurements using an immersible flow-through cell can overcome these problems [1]. However,

liquid junction reference electrodes are not suitable for such measurements because of irreproducibility due to changes in pressure and liquid junction potential. To perform in-situ measurements at depths such as in a lake, a pressure insensitive reference electrode is needed. In addition the reference electrode should be virtually temperature independent, be small in size, be unaffected by adsorbed organic material, be reasonably priced and easy to fabricate.

Commercial liquid junction reference electrodes are pressure dependent; the diffusion potential changes and contact problems may arise from compression of the organic material adsorbed in the frit. A commercial, so-called "pressure insensitive", Xerolyt reference electrode has been used in a previous work [1] (Xerolyt is not a solid state reference electrode; it contains a polyelectrolyte swollen with an electrolyte solution). However, it has been found to exhibit excessive diffusion through the membrane leading to solu-

Correspondence to: J. Buffle, Département de Chimie Minérale, Analytique et Appliquée, Université de Genève, 1211 Geneva 4 (Switzerland).

tion contamination. The use of a liquid bridge could overcome this particular problem, but renders the electrode pressure dependent.

True solid state reference electrodes could provide a convenient solution to the above problems. Three different kinds of such electrodes have been reported to date: (a) solid state reference electrodes made of a pressed pellet containing KCl, alumina and PTFE, in which a silver chloride coated silver wire has been immersed [2,3], (b) electrodes composed of a paste of mercury, calomel, KCl and graphite, fixed in PVC tubing with a PTFE glass membrane [4–6], (c) solid state reference electrodes having a swollen conducting polymer [7–9].

Type (b) and (c) electrodes may show “memory” effects because the solutes of the test solution may diffuse into the swollen electrolyte (c) or adsorb inside the graphite pellet (b), thus contaminating subsequent test solutions. Therefore a type (a) solid state reference electrode was developed in the present work. Only preliminary reports have been published on this topic up to now. The purpose of this work was to study in detail the best conditions for its preparation and its behaviour. This electrode was successfully used for in-situ voltammetric measurements of manganese in lake water (at depths to 20 m).

EXPERIMENTAL

Materials and apparatus

All solutions were prepared with Milli-Q purified water ($18 \Omega \text{ cm}^{-1}$). All the chemicals used (KCl, PTFE powder, Al_2O_3 , HCl, NaNO_3 , $\text{Mg}(\text{NO}_3)_2$ and $\text{Al}(\text{NO}_3)_3$) were puriss p.a. The silver wire (0.30 mm diameter; Johnson Matthey, UK) was of 99.99% purity. The commercial liquid junction reference electrode was a Ag/AgCl/sat. KCl// electrode from Metrohm (No. 6.0719.000).

Electrodeposition of AgCl was effected with a Metrohm Coulometer (E 211 A). All potential measurements were made with a Tacussel Millivoltmeter (Aries 20000) and recorded on a Metrohm Labograph (E 586). The micropolarisation measurements were performed with a Tacus-

sel Potentiostat (PRGE) in conjunction with the above recorder.

Electrolysis of the silver wire

The following procedure results from preliminary tests based on procedures described by Janz and Taniguchi [10].

The silver wire was cleaned in the following manner: Approximately 2 cm of the wire were immersed in nitric acid 60% for 30 s. After rinsing thoroughly with water, the wire was placed as a cathode in a two electrode electrolysis cell with 0.1 M NaClO_4 as electrolyte; a platinum wire was used as anode. A potential of -2.0 V was then applied for 5 min to reduce the excess of silver ions on the surface. This wire was then fixed in a two electrode electrolysis cell protected from light. The silver wire was connected as the anode and a platinum wire acted as the cathode. The electrolyte, 0.1 M HCl, was degassed with nitrogen both before and during the electrolysis. The silver wire was immersed (2 cm) into the solution and a constant current of 0.1 mA was maintained for 30–40 min. After this time a porous dark grey silver chloride layer was obtained on the immersed surface. This wire was then kept in 0.1 M KCl shorted together with other Ag/AgCl wires fabricated in the same way. After 4–6 days their potentials were measured in 0.1 M KCl against the commercial Ag/AgCl/sat. KCl// reference electrode and if correct, they were used for preparation of the solid state electrodes.

Preparation of the powder mixtures

The pellet was made of two layers containing both KCl, Al_2O_3 and PTFE in different proportions. These mixtures of the two layers were prepared in the following way: Al_2O_3 (particle size $0.3 \mu\text{m}$) and KCl were mixed together to give compositions Al_2O_3 : KCl of 7:6 and 7:4 respectively. Each of these two mixtures was ground in a mortar together with a few drops of water to dissolve the KCl and give a paste. These pastes were dried at 80°C for 5 h. During this process the KCl recrystallizes on the surface of the alumina particles [3]. PTFE powder was then added to yield the mixtures PTFE: Al_2O_3 : KCl of 7:7:6 and 9:7:4 respectively. Ethanol was added (to

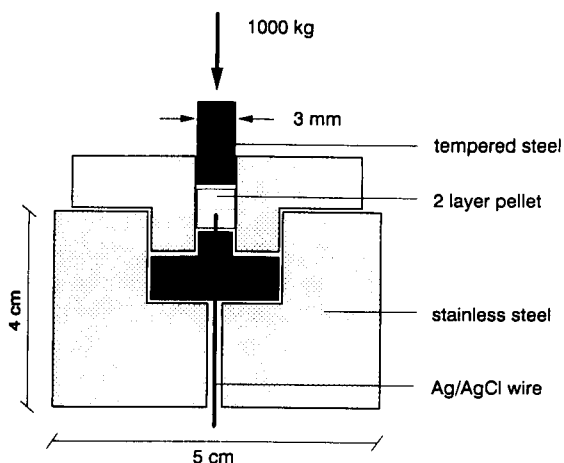


Fig. 1. Pressing system for the pellets.

achieve a 1:1 volume/volume ratio) to act as insoluble solvent. The resulting suspensions were stirred in a beaker for 3–5 h to ensure homogeneity. After drying at 80°C for 12 h the resulting powder mixtures were stored in closed bottles to minimize contact with humid air.

Pellet formation

A pressing system (Fig. 1) was built to prepare pellets with Ag/AgCl wires imbedded in the upper layer (Fig. 2). 60 mg of the 7:7:6 powder

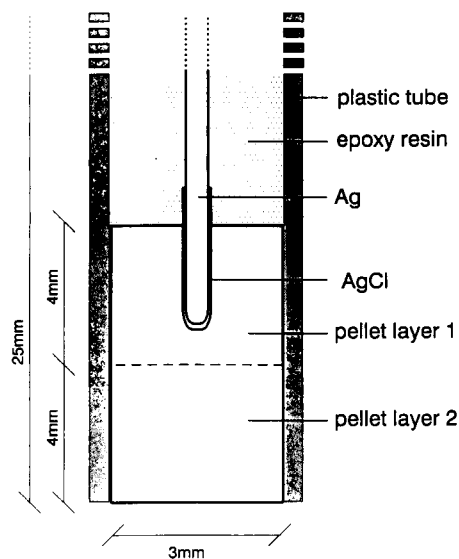


Fig. 2. The cross-section of the solid state reference electrode. Layer 1: PTFE:alumina:KCl = 7:7:6; layer 2: PTFE:alumina:KCl = 9:7:4.

were poured into the bottom of the press to surround the Ag/AgCl wire. This powder was gently pressed by hand, then 60 mg of 9:7:4 powder were placed on the top and the entire mixture was pressed to a pellet (8 min at 14 t cm⁻²). The resulting electrode was sintered at

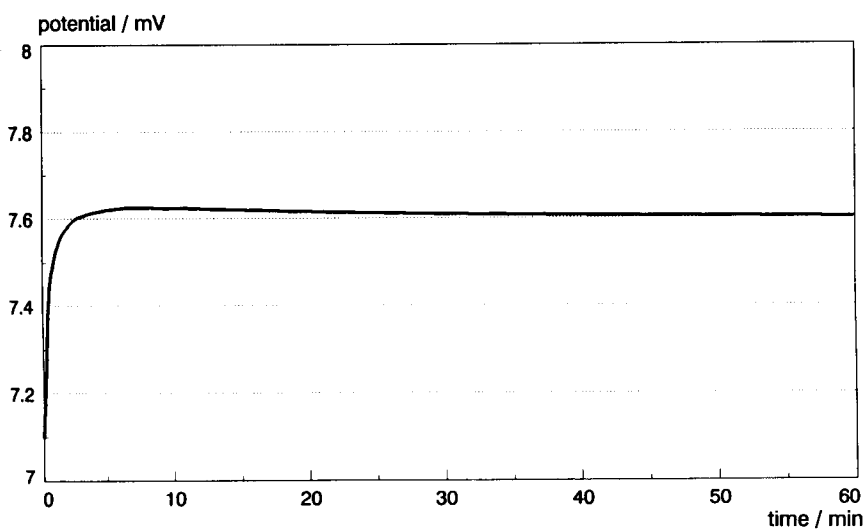


Fig. 3. A single potential measurement of a solid state reference electrode (stored in Milli-Q purified water) versus the commercial Ag/AgCl/sat. KCl// electrode in 0.1 M KCl during the stable potential period (i.e. during its useful "lifetime"; Fig. 4).

350°C for 1 h. Finally the side of the pellet with the protruding wire was covered with epoxy resin (Araldite, Ciba Geigy) and the whole electrode was sealed in a plastic tube (thermo retractable). Electrodes stored under dry conditions (silica gel) were stable for several months. An electrical contact between the external surface of the pellet layer and the Ag/AgCl wire could not be established until the electrode had been soaked in water for approximately 10–20 h. An additional 24 h period was required to obtain a stable electrode potential.

RESULTS

The only tests reported previously [2,3] were potential measurements in different electrolytes at different concentrations. No potential versus time measurements were reported. As a result of the more extensive tests performed in the present work and reported below, the composition of the lower pellet layer of our electrodes (PTFE: alumina: KCl = 9:7:4) differs from those of other workers (PTFE: alumina: KCl = 9:9:2 [2,3]).

Comparison of the results with different pellet compositions is briefly discussed below.

The potential

The potential of our solid state reference electrode with respect to that of the commercial electrode was measured as a function of time in 0.1 M KCl. Typical results over a short and long time period are shown in Figs. 3 and 4 respectively. The response time in 0.1 M KCl depended on the solution in which the electrode was stored. When the electrode was stored in Milli-Q purified water a stable potential in 0.1 M KCl was obtained after 2–5 min, whereas the response time increased to between 30 and 120 min when stored in 1 M KCl. For the long time scale stability measurements the electrode was stored in the preconditioning solution and the potential was measured daily in 0.1 M KCl by leaving the electrode in this solution for 1 h. During the period in which the potential was “stable” (2nd to 13–15th day, Fig. 4) a gradual increase of 0.3–0.5 mV day⁻¹ was observed. The lifetime of each solid state reference electrode was approximately 14 days when the storing solution was

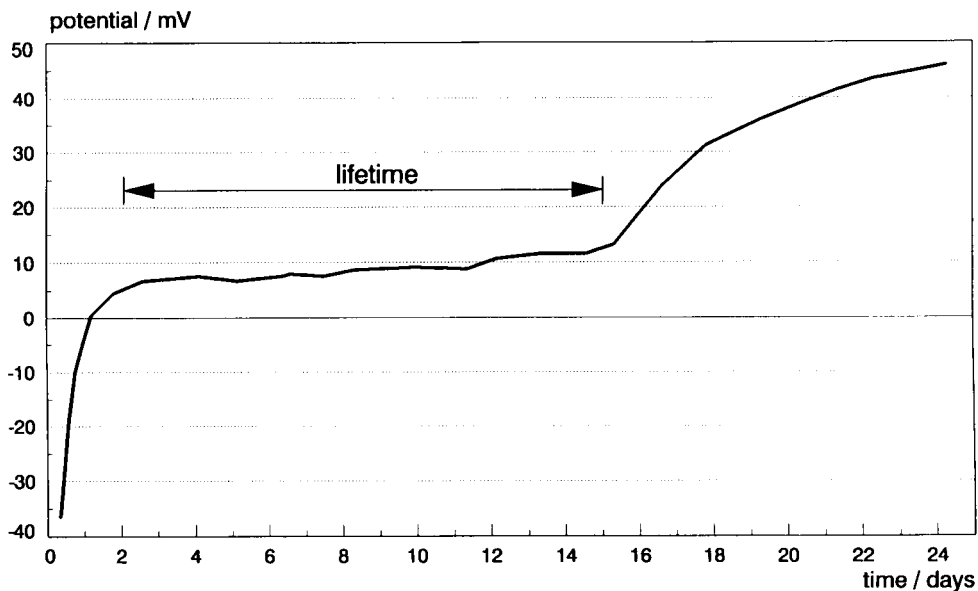


Fig. 4. The potential of a solid state reference electrode (stored in Milli-Q purified water) versus the commercial Ag/AgCl/sat. KCl// electrode in 0.1 M KCl over time. This graph results from a series of daily potential measurements.

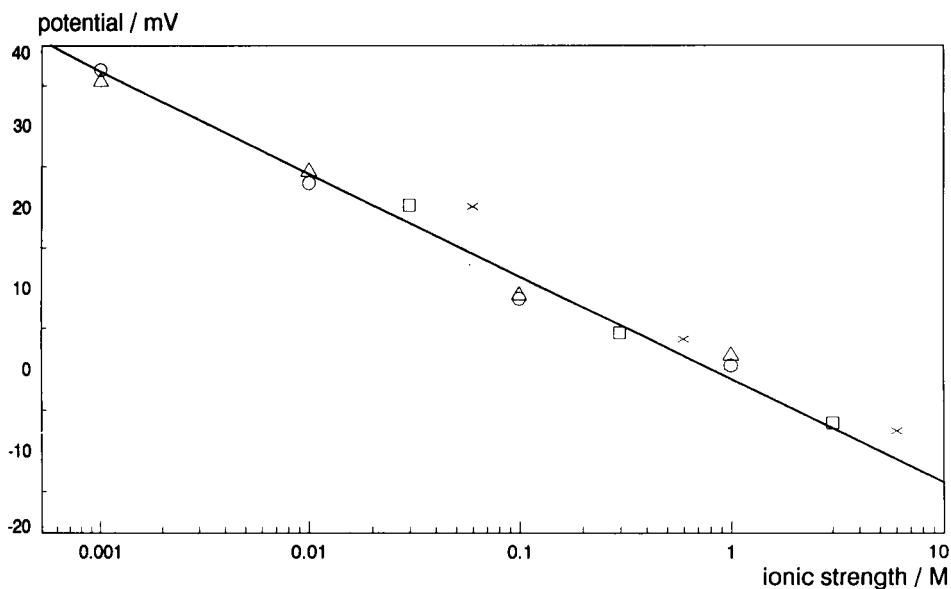


Fig. 5. The potential of a solid state reference electrode (stored in Milli-Q purified water) versus the commercial Ag/AgCl/sat. KCl// electrode in electrolytes of different concentrations plotted as a function of the ionic strength. Key: Δ KCl, \circ NaNO₃, \square Mg(NO₃)₂, \times Al(NO₃)₃.

Milli-Q purified water. Storing the electrode in 1 M KCl increased the lifetime to 25 days, but as mentioned above, the response time was very

long under these conditions. After the preparation, and before the initial soaking in water, the solid state reference electrode could be stored in

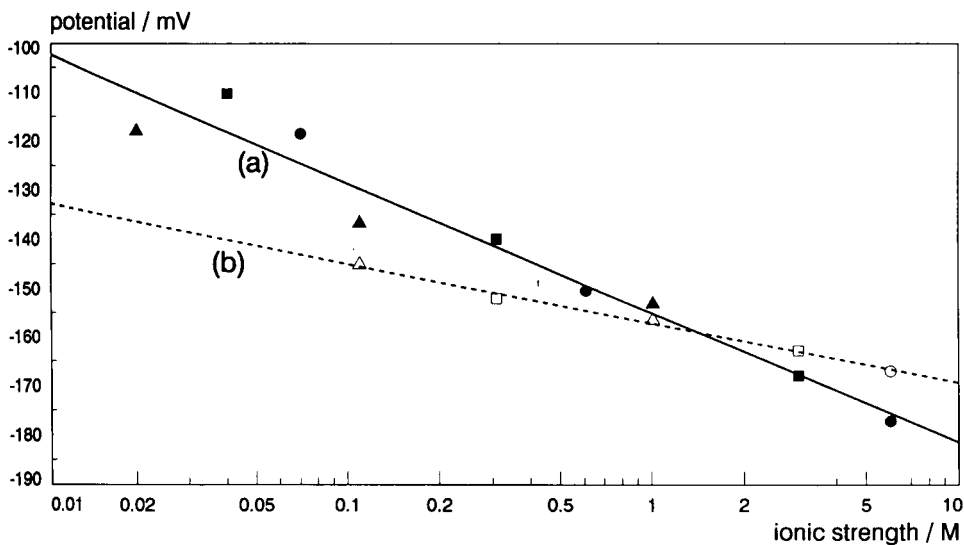


Fig. 6. The potential of either a solid state reference electrode (stored in Milli-Q purified water, (a)) or the commercial Ag/AgCl/sat. KCl// electrode (b) versus a Ag/AgCl wire in 0.01 M KCl + another electrolyte, plotted as a function of the ionic strength. Key: Δ , \blacktriangle NaNO₃; \square , \blacksquare Mg(NO₃)₂; \circ , \bullet Al(NO₃)₃.

TABLE 1

The potential (mV) between a solid state electrode (as described in Experimental, stored in Milli-Q purified water) and the commercial Ag/AgCl/sat. KCl// electrode in different electrolytes at different concentrations

Electrolyte concentration (M)	Electrolyte			
	KCl	NaNO ₃	Mg(NO ₃) ₂	Al(NO ₃) ₃
1	-1.7	-0.5	6.5	7.5
0.1	-9.2	-8.8	-4.5	-3.7
0.01	-24.4	-23.0	-20.3	-20.1
0.001	-35.5	-37.0	-	-

the dry state (over silica gel) for several months to one year with no detrimental effects. The electrodes could also be stored in dry closed bottles after they had been soaked once; a stable potential was restored on soaking in water for 24 h. Storing the electrode under humid conditions decreased its lifetime to 5–6 days.

The potentials measured for the solid state reference electrode in several electrolytes are given in Table 1. In Fig. 5 these data are plotted as a function of the ionic strength, I . On a logarithmic scale a linear plot is obtained with a slope of -12.6 mV/log I . The potential of the solid state reference electrode and that of the commercial reference electrode were also measured separately with respect to an Ag/AgCl wire. These measurements were performed in the presence of 0.01 M KCl plus another electrolyte, as shown in Table 2. In Fig. 6 these data are plotted as a function of ionic strength. A straight line plot was obtained for each electrode with slopes of -26.4 and -14.0 mV/log I for the solid state and the commercial reference electrodes respectively. This figure shows that the results presented in Fig. 5 can be explained by the fact that the potential of both types of electrodes varies in a similar manner with ionic strength, irrespective of the nature of the salt; but variation of the solid state electrode is more marked. This effect is dealt with in the Discussion.

Pressure test

The cell constructed for this test is shown in Fig. 7. For these measurements the potential was

measured with respect to a Hg/Hg₂Cl₂/0.1 M KCl/electrode. Pressure was applied with nitrogen (up to 5 bar) and the potential was recorded as a function of time (Fig. 8). The change in potential was 0.2–0.3 mV/bar. On re-equilibration of the electrode at atmospheric pressure the potential remained 1–2 mV more negative than the initial value. If pressure was again applied to the same electrode (after 24 h) no further shift in potential was observed. In contrast, the solid state electrode previously reported [2,3] with a composition of the lower pellet layer PTFE:alumina:KCl of 9:9:2 showed more pressure dependence (Fig. 8). In addition a pressure test decreased its lifetime by approximately 20%, which does not occur with our electrode.

Reversibility

Cyclic micropolarisation, in which the current passing through the electrode is measured as a function of the applied potential, provides a measure of electrode reversibility (Fig. 9). These measurements were performed in a three electrode cell with a platinum wire as counter electrode and a commercial Ag/AgCl/sat. KCl// reference electrode. If the electrode is completely reversible no hysteresis effect will be observed. In addition, this test provides a qualitative indication of the magnitude of the exchange current, determined from the slope of the above plot. The steeper the slope, the higher the exchange current and the better the reference electrode [11]. Figure 9 shows that the reversibility of the solid state reference electrodes was not as good as, but similar to that of the commercial Ag/AgCl/sat.

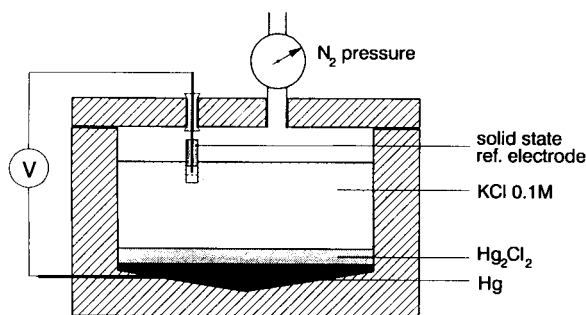


Fig. 7. The pressure test system.

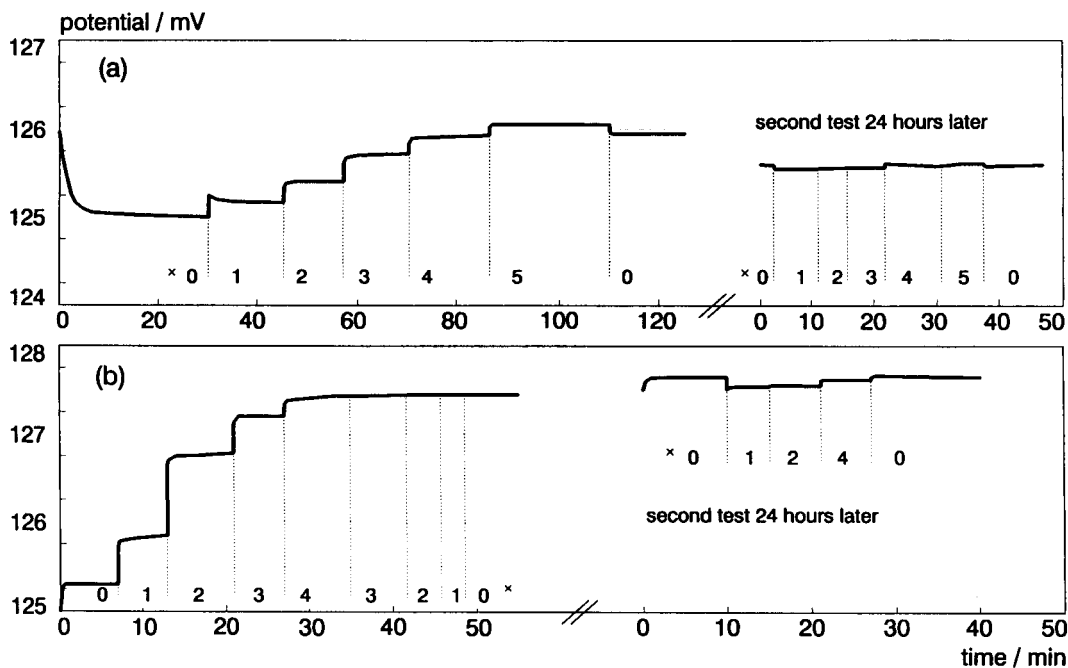


Fig. 8. The potential of two solid state reference electrodes (stored in Milli-Q purified water) with different compositions of the lower layer of the pellet (PTFE : alumina : KCl = 9 : 7 : 4 (a) and 9 : 9 : 2 (b)) as a function of time and pressure. Comparison of the first pressure test and the next, one day after. × applied pressure (bar).

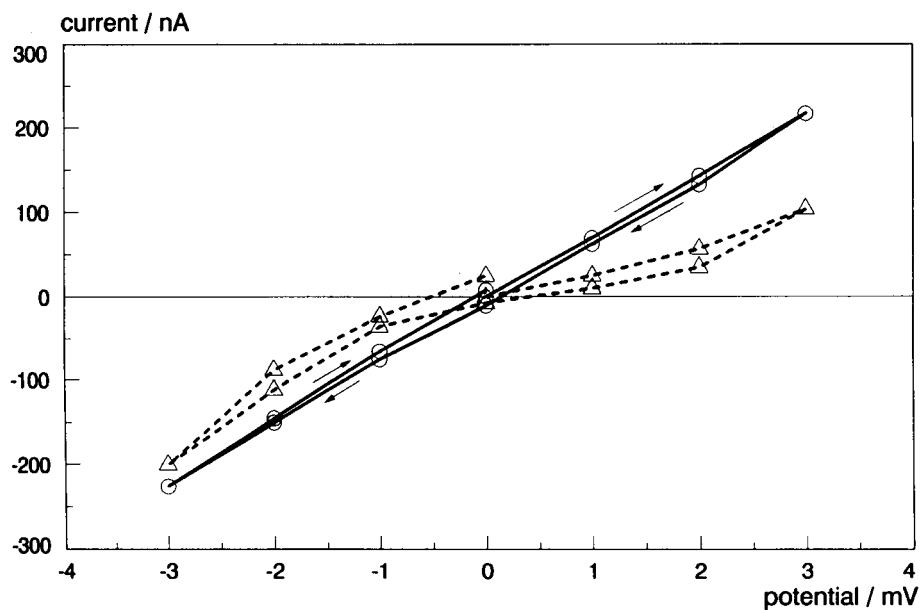


Fig. 9. Reversibility test in 0.1 M KCl. Comparison of a solid state reference electrode (Δ) with the commercial Ag/AgCl/sat. KCl// electrode (\circ).

TABLE 2

The potentials (mV) of a solid state electrode (stored in Milli-Q purified water) and of a commercial Ag/AgCl/sat. KCl// electrode versus a Ag/AgCl wire in 0.01 M KCl+ another electrolyte

Electrolyte concentration (M)	Electrolyte		
	NaNO ₃	Mg(NO ₃) ₂	Al(NO ₃) ₃
<i>Solid state electrode</i>			
1	-153.1	-167.9	-177.2
0.1	-136.8	-140.0	-150.4
0.01	-118.0	-110.3	-118.5
<i>Commercial Ag / AgCl / sat. KCl // electrode</i>			
1	-156.5	-162.8	-169.0
0.1	-143.1	-152.0	-
0.01	-	-	-

KCl// reference electrode. Furthermore, the exchange current was smaller in magnitude. The micropolarisation curves for the electrodes with the composition of the lower layer PTFE: alumina: KCl of 9:9:2 [2,3] were also similar.

Temperature test

In lakes the water temperature is typically within the range of 5–25°C. In the range from 5 to 20°C the temperature dependence of a cell including the solid state reference electrode and

a Hg/Hg₂Cl₂/0.1 M KCl/reference electrode without liquid junction was $-0.73 \pm 0.04 \text{ mV } ^\circ\text{C}^{-1}$ (Fig. 10). Since the temperature dependence of Hg/Hg₂Cl₂/0.1 M KCl is $-0.088 \text{ mV } ^\circ\text{C}^{-1}$ [12], the temperature dependence of the solid state reference electrode is $-0.82 \text{ mV } ^\circ\text{C}^{-1}$. From this value it is possible to estimate the temperature dependence of the electrical junction of the pellet and its associated liquid junction. Indeed it has been shown that the temperature dependence of the Ag/AgCl/0.1 M KCl/Hg₂Cl₂/Hg system is $-0.35 \text{ mV } ^\circ\text{C}^{-1}$ in the range from 20 to 30°C, [12]. Therefore the temperature dependence of the pellet and the associated liquid junction can be estimated to be $-0.38 \text{ mV } ^\circ\text{C}^{-1}$.

Reproducibility

The solid state reference electrodes were always prepared in sets of 5. Within each set the stable potential value was the same within $\pm 1.2 \text{ mV}$. For 6 sets the average stable potential value varied in a range of $\pm 2.5 \text{ mV}$. For three electrodes the change of potential under pressure varied by $\pm 0.05 \text{ mV bar}^{-1}$. Results from reversibility tests were similar.

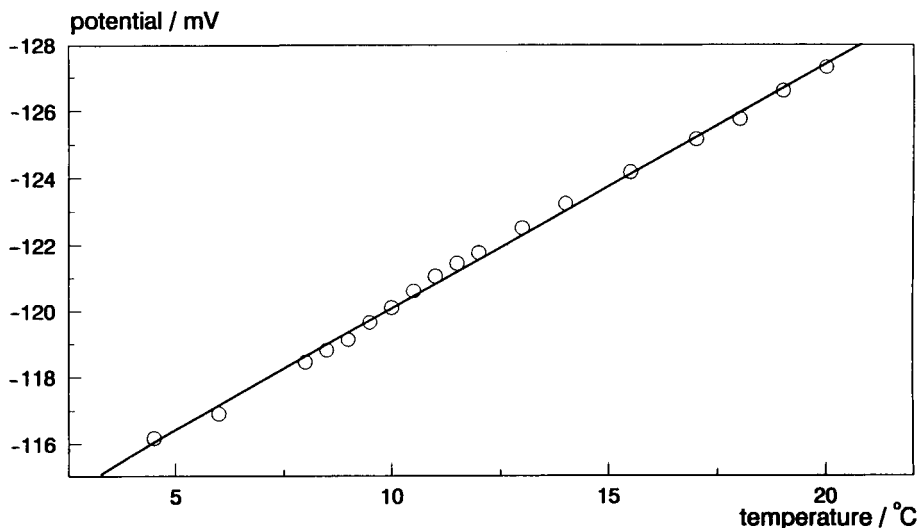


Fig. 10. The potential of a solid state reference electrode versus a Hg/Hg₂Cl₂/0.1 M KCl/reference electrode without liquid junction as a function of temperature.

Utility for *in-situ* measurements

The solid state reference electrodes reported here have been used for voltammetric measurements in the laboratory as well as in *in-situ* measurements in a lake (down to 20 m). All the measurements performed under laboratory conditions (atmospheric pressure, light, room temperature) with either differential pulse, square wave or linear sweep voltammetry were identical to those obtained with the commercial reference electrode. However, for *in-situ* measurements the solid state reference electrode has been found to be much more convenient in terms of potential stability under pressure, size and handling.

DISCUSSION

The physico-chemical processes controlling the potential of the solid state reference electrode are not completely understood. However, all the results obtained in this work are consistent with the following assumptions. Diffusion of water into the porous pellet during the soaking process generates an internal KCl solution which surrounds the Ag/AgCl wire. This internal KCl solution diffuses out of the pellet thus establishing a junction potential in the diffusion layer between the test solution and the pellet. Because of this the solid KCl remaining in the pellet will be gradually depleted over time. After some time (14 days in Milli-Q purified water, 25 days in 1 M KCl), the solid KCl is completely depleted and the electrode potential shifts abruptly to more positive values (Fig. 4). This general process is confirmed by the fact that storing the electrode in 1 M KCl increased its lifetime by more than 10 days. Indeed, the rate of diffusion of KCl out of the electrode will decrease as the concentration difference between the internal solution and the storing solution decreases, thus increasing the electrode lifetime.

The precise roles of PTFE and Al₂O₃ in the pellet have not been proved unambiguously. It is, however, probable that PTFE being hydrophobic prevents the pellet from becoming hydrated too quickly and therefore the subsequent rapid dissolution of KCl, whereas Al₂O₃ being hydrophilic

maintains the existing hydrated films inside the pellet, allowing K⁺ and Cl⁻ to diffuse between the external solution and the Ag/AgCl wire. A good solid state reference electrode is therefore largely dependent on the PTFE:Al₂O₃:KCl ratio.

The different composition of the lower layer of the pellet compared to that previously reported [2,3] results from the more extensive tests performed in the present work. With the new composition it was possible to increase the stability under pressure. In addition, by increasing the thickness of the two pellet layers, it has also been possible to increase the lifetime of the electrode from 7–8 days to 13–15 days.

It has been reported [2,3] that the potential of the electrode in electrolytes of different concentrations was dependent on the composition of the pellet. Since the composition of the pellet prepared in the present work was different from those previously reported, it is difficult to directly compare the results. However, in all cases a positive shift in potential was observed in different electrolytes as the ionic strength was decreased, irrespective of the nature of the electrolyte (Figs. 5 and 6). The potential of a reference electrode is the sum of the electrode and the junction potentials. The latter depends on the logarithm of the electrolyte concentration, the Henderson equation [13]. A linear relationship is indeed observed between the logarithm of the ionic strength and the potential of the commercial Ag/AgCl/sat. KCl// electrode with a slope of -14.0 mV/log I . For the solid state electrode, the potential has also been found to be logarithmically dependent on the ionic strength (slope = -26.4 mV/log I). This suggests that the liquid junction potential of this electrode in the diffusion layer of the pellet–solution interface also plays a primary role in this dependency. The larger slope for the solid state electrode (-26.4 mV/log I) compared to the commercial Ag/AgCl/sat. KCl// electrode (-14.0 mV/log I) might be due to a lower rate of electrolyte diffusion (which establishes the junction potential) inside the pellet. This larger slope should not present a problem for measurements in natural waters. Indeed, for a given water system (e.g. river, lake, ocean) the

ionic strength is most often invariant. Furthermore, the above slope obtained for the ionic strength dependence allows one to calculate the theoretical potential shift of the electrode in different water types, and thus to easily compare results obtained in natural waters of different ionic strength.

The reversibility test is a simple measure of the state of a reference electrode. That is, the micropolarisation curves recorded for solid state electrodes during the period in which the potential was not stable had much flatter slopes, i.e. lower exchange currents than during the period of stable potential. Furthermore, the slope of the micropolarisation curves for electrodes which had been subjected to pressure was slightly greater, indicating a larger exchange current. A second pressure test showed little further influence either on the potential or on the reversibility. That is, a pressure insensitive system was established. All these observations confirm that the exchange current is strongly linked to the diffusion of K^+ and Cl^- ions in a film of solution around grains inside the pellet. Such a film is not well formed before the preconditioning period and the application of pressure allows the electrolyte solution to be forced into empty pores of the pellet, thus increasing the "active" surface on the Ag/AgCl wire.

In conclusion, we have developed a method by which stable, pressure insensitive solid state reference electrodes can be both prepared and used

reproducibly for both in-situ and laboratory based measurements.

The authors thank C. Bernard, F. Bujard and S. Rodak for the design and construction of the different apparatus needed. This work was supported by the Swiss National Foundation, project No. 20-31192.91.

REFERENCES

- 1 M.-L. Tercier, J. Buffle, A. Zirino and R.R. De Vitre, *Anal. Chim. Acta*, 237 (1990) 429.
- 2 G.P. Bound and B. Fleet, *J. Sci. Food Agric.*, 28 (1977) 432.
- 3 S. Zhao, N. Hu, J. Zhao and J. Wang, *Zhongguo Kexue Jishu Daxue Xuebao*, 18 (1988) 312.
- 4 J. Ruzicka, C.G. Lamm and J.C. Tjell, *Anal. Chim. Acta*, 62 (1972) 15.
- 5 J. Ruzicka, E.H. Hansen and J.C. Tjell, *Anal. Chim. Acta*, 67 (1973) 155.
- 6 C.G. Lamm, E.H. Hansen and J. Ruzicka, *Anal. Lett.*, 5 (1972) 451.
- 7 R.M. Neti and R.H. Jones, *ISA Trans.*, 10 (1971) 90.
- 8 J.E. Heider and P.J. Kinien, *Eur. Pat. Appl.*, 0 267 862 A2 (1988).
- 9 D. Hoaf, A. Gemmler and Th. Bloch, *Ger. Pat.*, DE 3823327 A1 (1990).
- 10 G.J. Janz and H. Taniguchi, *Chem. Rev.*, 52 (1953) 397.
- 11 G.J. Janz and D.J.G. Ives, *Ann. N.Y. Acad. Sci.*, 148 (1968) 210.
- 12 M. Quintin, *Electrochimie*, Press Universitaires de France, Paris, 1970.
- 13 L.I. Antropov, *Theoretical Electrochemistry*, Mir, Moscow, 1977.

Blocking of chemically modified graphite electrodes by surfactants

Mikael Skoog, Karin Kronkvist and Gillis Johansson

Department of Analytical Chemistry, University of Lund, S-221 00 Lund (Sweden)

(Received 15th April 1992; revised manuscript received 23rd July 1992)

Abstract

The blocking effect of selected surfactants on phenoxazine-modified graphite electrodes was studied by amperometry and cyclic voltammetry. Non-ionic surfactants such as Tween 20, 60 and 80 caused an almost irreversible blocking of NADH oxidation at the electrode. Hexacyanoferrate(II)/(III) and protons, however, could penetrate the adsorbed surfactant layer. Cationic and anionic surfactants produced reversible blocking, i.e. the current was depressed when the surfactants were present, but returned to its original value after the system had been flushed with pure buffer. Adsorbed non-ionic surfactants could easily be removed by a solution of SDS at a concentration above cmc, thus restoring the original current for NADH oxidation.

Keywords: Amperometry; Cyclic voltammetry; Graphite electrodes; Surfactants

Bioelectrochemical systems based on nicotinamide adenine dinucleotide (NAD⁺) dependent dehydrogenases are receiving increasing interest, and the subject has recently been reviewed [1,2]. The large number of commercially available dehydrogenases opens the prospect for a general detection scheme for a corresponding number of analytes, many of them important in biological and medical applications.

Direct electrochemical oxidation of reduced nicotinamide adenine dinucleotide (NADH) at graphite electrodes is feasible, though at an overpotential of about 1 V, and at the expense of side reactions and possibly interferences from organic compounds in the matrix. With phenoxazine mediators adsorbed to the electrode surface the potential can, however, be lowered to around 0

mV vs. SCE [1–3]. NADH can thus be determined amperometrically with high selectivity and sensitivity.

The possible extension of these detection systems to immunoassays has prompted us to investigate the effect of surfactants on chemically modified graphite electrodes. In particular the non-ionic surfactant Tween 20 (polyoxyethylene sorbitan monolaurate ester) is extensively used in immunochemistry due to its ability to suppress non-specific interactions of antibodies and antigens in assay systems [4]. It also enables hydrophobic antigens, such as steroids, to remain in solution [5].

Amphiphilic molecules are known to aggregate on solid surfaces and reduce the rate of charge transfer from redox couples in solution to gold, tin oxide [6,7] and carbonaceous [8] electrodes. Some surfactants have been shown to self-assemble, forming stable compact layers even when present in micro-molar concentrations. Adsorption to graphite may involve an arrangement with

Correspondence to: G. Johansson, Department of Analytical Chemistry, University of Lund, P.O. Box 124, S-221 00 Lund (Sweden).

the molecules parallel or normal to the surface depending on the surfactant concentration [9].

EXPERIMENTAL

Instrumentation

The experiments were done in a flow system with a peristaltic pump (Gilson Minipuls 2) at a total flow-rate of 1 ml min⁻¹. A pneumatic valve (Cheminert SVA 8031) was used to switch between solutions with or without surfactants. All solutions were made with 0.25 M phosphate buffers, pH 7.0. Amperometric measurements were carried out by means of a potentiostat (LKB 2143) connected to an electrochemical three-electrode cell of wall-jet type [10]. The working graphite electrode was kept at 0 mV vs. SCE, unless otherwise specified. Cyclic voltammograms were obtained with a BAS 100A electrochemical analyzer (Bioanalytical Systems) and a batch cell.

Materials

The electrode material was spectrographic graphite, RW0, diameter 3.1 mm (Ringsdorff-Werke). The phenoxazine mediator, 5,5'-[1,4-phenylenebis-(carbonylimino)]bis-9-(diethylamino)benzo[*a*]phenoxazin-7-ium, CA reg. number 135656-95-0, synthesized according to Polasek et al. [3], was used as an electron transfer mediator.

Tween 20, 60 and 80 [poly(oxyethylene)sorbitan monocarboxylates], and NADH were purchased from Sigma Chemicals. Triton X-100 came from BDH Chemicals. Sodium dodecylsulphate (SDS) and tetradecyltrimethylammonium bromide (TTAB) were purchased from KEBO lab. All other chemicals were supplied by Merck and were of analytical grade.

Electrode pretreatment

Prior to use the graphite rods were cut, polished on wet emery paper and thoroughly washed with deionized water. After 30 min in 60°C they were heated in a muffle furnace at 700°C for 90 s. The pretreated electrodes were stored in a desiccator.

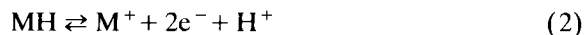
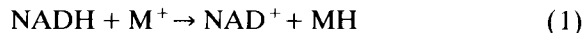
Electrodes were chemically modified by immersion in an acetone solution of the phenoxazine for 2 min and subsequently allowed to dry completely in air. Before they were inserted into the flow system, cyclic voltammetry was employed to ascertain that the surface coverage was within the optimal range 5–10 nmol/cm² [3].

Determination of the critical micelle concentration

The literature is inconclusive on values of the critical micelle concentration, cmc, for Tween 20, 60 and 80 [11–13], which is thought to reflect the inhomogeneity of the commercial preparations [14]. Determinations of cmc were therefore carried out by cyclic voltammetry using a platinum electrode in the presence of hexacyanoferrate(II) according to Mandal [11]. The oxidative peak currents of hexacyanoferrate(II) were plotted versus surfactant concentration and the cmc was defined as the intersection of the resulting two straight lines. Cmc values obtained in the experiments were 16, 20 and 17 mg/l for Tween 20, 60 and 80, respectively.

RESULTS AND DISCUSSION

The blocking kinetics of different surfactants was studied in a flow system using a carrier containing 100 μM NADH, which was oxidized in a steady-state fashion at the chemically modified graphite electrode. The NADH oxidation follows the scheme:



where M denotes the phenoxazine mediator adsorbed on the surface. Reaction 2 is very fast and the equilibrium lies completely to the right at an applied voltage of 0 mV. Reaction 1 is then rate determining with a rate that is partially under kinetic and partially under diffusional control at pH 7.0. The amperometric response is linear over at least three decades of concentration under these conditions [3,10].

The blocking experiment was initiated by switching the flow from buffer without to buffer with surfactant, both containing the same concentration of NADH. Tween 20, a non-ionic surfactant, caused a rapid decrease of the signal, indicating that the hydrophilic, negatively charged NADH molecule was hindered to reach the mediator (Fig. 1). A more concentrated surfactant solution caused a more rapid drop. In both cases the Tween 20 concentrations were well above cmc. This concentration-dependent blocking indicates either that the micelle concentration affects the rate or that the monomer composition varies because of the heterogeneity of the commercial preparation.

The concentration dependence of the current decrease was studied in more detail by comparing Tween 20 solutions with concentrations under and above cmc, 0.5 mg/l–5 g/l. Figure 2 shows the remaining signal after a 5-min surfactant supply. A total blocking of the NADH oxidation with time was observed for all concentrations, al-

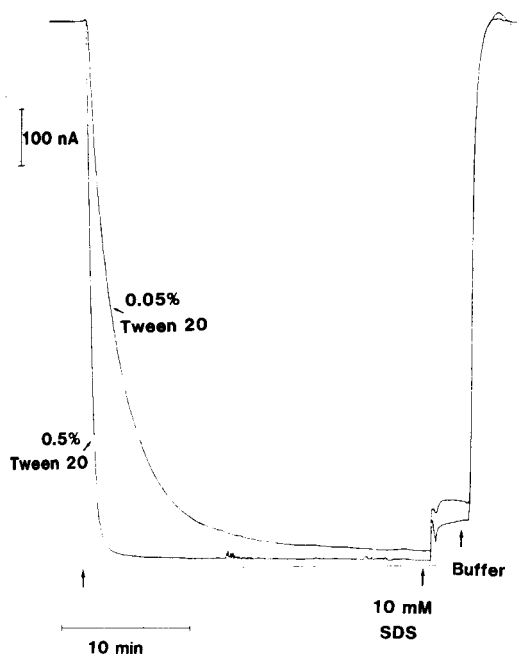


Fig. 1. Current versus time during blocking of the oxidation of 100 μ M NADH by 0.5 and 5 g/l Tween 20 followed by restoration of the signal with 10 mM SDS.

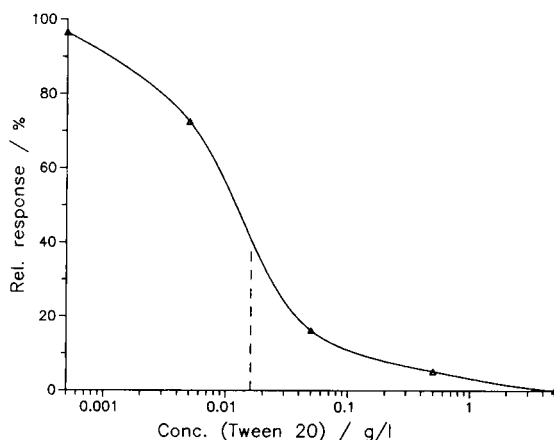


Fig. 2. Remaining signal from NADH oxidation versus concentration of Tween 20 after 5 min exposure of the electrode in the flow system. Cmc for the surfactant (16 mg/l) is indicated with a dashed line.

though several hours were required for the most dilute solutions.

The blockage seemed to be fairly permanent and remained stable when a surfactant-free solution was pumped through the system for 30 min. By the addition of the anionic surfactant SDS, the blocking could be completely reversed. A 3-min exposure of the electrode to a 10 mM solution of SDS (cmc = 8 mM [15]) proved to be sufficient to regain the original signal (Fig. 1). Cationic surfactants like tetradecyltrimethylammonium bromide (TTAB) bromide (DTAB) restored some of the activity, although not as efficiently as SDS. The mediator surface coverage remained the same after Tween treatment and after a following treatment with SDS, which proves that this mediator, which adheres strongly to graphite, is not washed away by the surfactant solutions.

Effects of Tween 20 on the direct oxidation of NADH at 400 mV on naked graphite electrodes was studied in the same way as above. The resulting blocking was comparable with that on chemically modified electrodes, showing that the surfactant adsorbs on the graphite surface independently of the mediator.

Cyclic voltammograms of the adsorbed mediator were almost identical whether a layer of Tween 20 was adsorbed or not. The formal po-

corrected 12 Mar. 92 / AP

12th line in the right column "bromide (DTAB)" should be deleted

tential of the mediator, taken as the mean of the anodic and cathodic peak positions, was -200 mV in both cases. The left peak in Fig. 3 shows cyclic voltammograms of the mediator at a Tween-covered electrode for different sweep rates. No NADH was present and the graph displays a reversible reaction according to reaction 2. The peak current increased linearly with scan rate up to 100 mV s^{-1} , as expected for an adsorbed redox couple. A negative deviation towards a square-root dependence was observed above 100 mV s^{-1} , indicating a beginning influence of diffusional control by the protons necessary for the redox reaction. The electrochemical properties are thus comparable to those of other phenoxazine mediators adsorbed on graphite [10,16]. The break point at which the current switches from a linear to a square root dependence on sweep rate varies with pH and the buffer capacity of the solution [10,16]. These data thus indicate that the protons necessary for the redox reaction of the mediator could pass the surfactant layer essentially unhindered by the Tween 20 layer.

Addition of 3 mM hexacyanoferrate(II)/(III) results in a second redox couple with an $E^{0'}$ of 200 mV, see Fig. 3, the right peak. There was a strictly linear relation between the peak current and the square root of the sweep rate over the

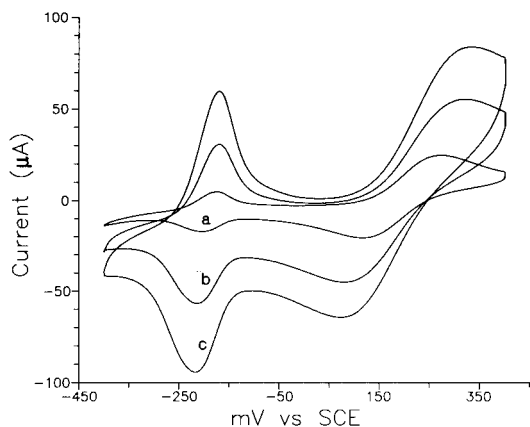


Fig. 3. Cyclic voltammograms of the phenoxazine mediator and 3 mM hexacyanoferrate(II)/(III) at different sweep rates for an electrode treated with Tween 20. (a) 10 mV/s, (b) 50 mV/s and (c) 100 mV/s.

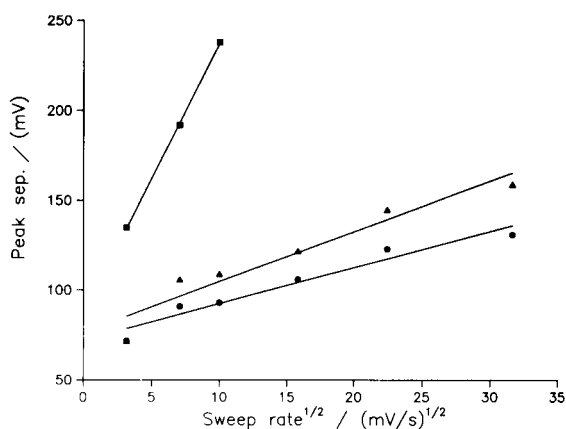


Fig. 4. Peak separation versus square root of the sweep rate for a 3 mM solution of hexacyanoferrate(II)/(III). The electrode (●) before treatment, (■) after treatment with Tween 20 for 10 min and (▲) after washing with SDS also for 10 min.

range $10\text{--}100 \text{ mV s}^{-1}$. Higher sweep rates could not be investigated for the Tween-covered electrode, because of the large peak separation. This square-root dependence confirms that the electrochemical redox reactions of hexacyanoferrate are diffusion controlled even in the presence of a Tween layer. The peak currents were practically identical before and after a Tween treatment, which shows that hexacyanoferrate can pass the surfactant layer unhindered.

The peak separation for different sweep rates was studied in a batch cell before and after a 10-min exposure of the electrode to 5 g/l of Tween 20, as well as after removal of the surfactant layer with SDS. The peak separations for the hexacyanoferrate couple give straight lines when plotted versus the square root of the sweep rate (see Fig. 4). Uncompensated solution resistance is a major source of increases in peak separation with sweep rate. It will shift the peak potential more when the current increases and since the current varies with the square root of the sweep rate, the same type of dependence will hold for the peak separation [17]. The much larger slope of the plot for the Tween-covered electrode is interpreted as the effect of interposing a low-conducting layer between solution and electrode. The original slope was not completely restored by a 15-min SDS treatment and this indicates that some Tween remains on the surface.

Peak separation for the mediator was fairly independent of sweep rate up to 100 mV s^{-1} , but increased rapidly after that. The increase was slightly larger for the Tween-covered electrode than for the one with mediator only. The peak shifts are of the same size and the scan rate dependence is very similar to those observed earlier for other phenoxazines under similar conditions.

A substantial penetration of carrier electrolyte into the Tween layer should have dominated the resistive behavior. This is not the case, as shown by the large peak separations for hexacyanoferrate, and it must therefore be assumed that much of the charge is carried across the Tween layer by the reacting species. The absence of increased peak shifts for the mediator at low sweep rates can be explained if it is supposed that protons are the main charge carriers during this part of the sweep. Protons can be exchanged between the layer and phosphate ions in the solution and they should therefore be readily available at low sweep rates.

Blocking of the NADH oxidation at a chemically modified electrode was also studied for some other surfactants as specified in Table 1. All surfactant concentrations were kept at 1.2 times their cmc. The most efficient blockers were the Tweens, differing only in blocking rate. Their behavior was in agreement with what could be expected from their substituent aliphatic chains (monolaurate, monostearate, and monooleate for Tween 20, 60, and 80, respectively). Triton X-100,

TABLE 1

Blocking efficiency of selected surfactants measured as the remaining current for the oxidation of $100 \mu\text{M}$ NADH at a chemically modified electrode after 10 min exposure to a surfactant solution of the concentration 1.2 times cmc

Surfactant	cmc	Remaining signal after 10 min (%)
Tween 20	16^a mg/l	1.7
Tween 60	20^a mg/l	2.8
Tween 80	17^a mg/l	1.6
Triton X-100	0.3^b mM	17
SDS	8^c mM	12
TTAB	0.28^d mM	46

^a This work. ^b Ref. 11. ^c Ref. 15. ^d Ref. 19.

another non-ionic surfactant, left 17% of the original signal remaining after 10 min of exposure. When the surfactant solution was substituted with pure buffer the signal was gradually restored and after 10 min it amounted to 31% of the value measured prior to the blocking. Cationic and anionic surfactants caused a temporary blocking, i.e. the original signal was restored immediately after pure buffer was introduced into the flow system.

The measurements presented above show that some non-ionic surfactants will adhere permanently to the graphite surface, whereas the ionic surfactants used in this study attach themselves temporarily. The hydrophobic surfactant layer is impermeable to the very hydrophilic NADH but not for protons or for the negatively charged hexacyanoferrate(II)/(III) molecules.

Fouling of phenoxazine-modified electrodes has previously been observed in this department. The electrode sensitivity for NADH oxidation decreased, although it could be shown with cyclic voltammetry that the mediator surface coverage remained constant. The effect was initially ascribed to a chemical or electrochemical degradation to a compound with similar electrochemical properties as the parent phenoxazine. In view of the results presented above it seems likely that the effects are due to blocking by self-assembled unknown amphiphilic impurities. The effects are particularly pronounced when phosphoenolpyruvate is used as a reagent [18]. It has been confirmed that occasional injections of SDS will keep the electrodes active and solubilization of impurity molecules by SDS can therefore prolong the lifetime of NADH-selective graphite electrodes.

Discussions with Professor B. Lindman, Dept. of Physical Chemistry is gratefully acknowledged. Financial support was obtained from the Swedish Natural Research Council.

REFERENCES

- 1 L. Gorton, E. Csöregi, E. Dominguez, J. Emneus, G. Jönsson-Petterson, G. Marko-Varga and B. Persson, *Anal. Chim. Acta*, 250 (1991) 203.

- 2 P.N. Bartlett, P. Tebbutt, R.G. Whitaker, *Prog. React. Kinet.*, 16 (1991) 55.
- 3 M. Polasek, R. Appelqvist, G. Marko-Varga and G. Johansson, *Anal. Chim. Acta*, 246 (1991) 283.
- 4 S.H. Jenkins, W.R. Heineman and H.B. Halsall, *Anal. Biochem.*, 168 (1988) 292.
- 5 K. Kronkvist, U. Lövgren, L.-E. Edholm and G. Johansson, submitted for publication.
- 6 H.O. Finklea, S. Avery, M. Lynch and T. Furtch, *Langmuir*, 3 (1987) 409.
- 7 M. Gomez, J. Li and A.E. Kaifer, *Langmuir*, 7 (1991) 1797.
- 8 R.E. Panzer and P.J. Elving, *J. Electrochem. Soc.*, 119 (1972) 864.
- 9 G.H. Findenegg, B. Pasucha and H. Strunk, *Colloids Surf.*, 37 (1988) 223.
- 10 R. Appelqvist, G. Marko-Varga, L. Gorton, A. Torstensson and G. Johansson, *Anal. Chim. Acta*, 169 (1985) 237.
- 11 A.B. Mandal, B.U. Nair and D. Ramaswamy, *Bull. Electrochem.*, 4 (1988) 565.
- 12 P. Becher, in M.J. Schick (Ed.), *Non-ionic Surfactants*, Marcel Dekker, New York, 1967, Vol. 1, p. 478.
- 13 N.H. Choulis and L.H. Loh, *Can. J. Pharm. Sci.*, 6 (1971) 93.
- 14 A. Helenius, D.R. McCaslin, E. Fries and C. Tanford, *Methods Enzymol.*, 56 (1979) 739.
- 15 M.F. Emerson and A. Holtzer, *J. Phys. Chem.*, 71 (1967) 1898.
- 16 L. Gorton, A. Torstensson, H. Jägfeldt and G. Johansson, *J. Electroanal. Chem.*, 161 (1984) 103.
- 17 A.J. Bard and L.R. Faulkner, *Electrochemical Methods*, Wiley, New York, 1980.
- 18 X. Yang, D. Pfeiffer, G. Johansson and F. Scheller, *Anal. Lett.*, 24 (1991) 1401.
- 19 Sigma Chemical, General catalogue (1992), p. 1538.

Plasticized poly(vinyl chloride) as a permselective barrier membrane for high-selectivity amperometric sensors and biosensors

I.M. Christie, P.H. Treloar and P. Vadgama

University of Manchester, Department of Clinical Biochemistry, Hope Hospital, Eccles Old Road, Salford M6 8HD (UK)

(Received 9th March 1992)

Abstract

A poly(vinyl chloride) (PVC) membrane system is described for use as a high-selectivity barrier in amperometric sensors and biosensors. Membrane casting and electrode fabrication techniques are presented. The membrane properties, both physical and with respect to permselectivity, are outlined. This new form of homogeneous membrane barrier shows very much greater selectivity for H_2O_2 in oxidase-based enzyme electrodes than any previously reported barrier. Selectivity for the phenolic compounds catechol, hydrocaffeic acid, 4-aminophenol and paracetamol, as model electrochemically active compounds, is described and related to interference from ascorbate and urate; the responses of equimolar catechol:ascorbate and catechol:urate are both 61 500:1, and that of 1 mM catechol:undiluted serum is 60 000:1. Comparative results for a low molecular weight cut-off cellulose acetate layer, commonly employed in amperometric sensors and biosensors for clinical monitoring, demonstrates the superior selectivity of PVC, showing the PVC to have 7 and 180 times greater selectivity for H_2O_2 and paracetamol, respectively, against ascorbate. Biocompatibility is also excellent, with no loss of signal after prolonged exposure to serum.

Keywords: Amperometry; Biosensors; Sensors; Enzyme electrodes; Poly(vinyl chloride)

The development of chemical sensors and biosensors for clinical monitoring, based on amperometric detection, has highlighted the need for selective membranes to exclude interferents from the electrically polarized working electrode [1,2]. In serum, such interferents are primarily the charged species urate, ascorbate, glutathione and certain amino acids. Interference has been a particular problem for classical oxidase-based enzyme electrodes designed for metabolite measurement; here the high electrode polarizing voltages (ca. +0.6 V vs. Ag/AgCl), used to detect the product of the enzyme reaction, H_2O_2 , also

result in signals from biological interferents. In addition, dehydrogenase-based sensors involving NADH generation from NAD^+ co-substrate may need to incorporate indicator enzymes to generate a species more suitable for selective electrochemical detection, but which again require high polarizing voltages for detection [3].

To date, selective membranes have largely been cellulosic in nature [4]. Cellulose acetate is known to be permeable to uncharged organic compounds [5], particularly with molecular weights below 200–300, whilst having the capacity, to a variable extent depending on the casting method, to decrease anion permeation. The performance of these membranes is adequate for producing acceptable analyte:interferent signal ratios when H_2O_2 is detected by glucose oxidase-based sen-

Correspondence to: I.M. Christie, University of Manchester, Department of Clinical Biochemistry, Hope Hospital, Eccles Old Road, Salford M6 8HD (UK).

sors in blood. However, nearly total exclusion of interferents would be an advantage for many other biological fluids or where direct electrochemical detection of an organic compound is attempted in a complex mixture, particularly when the analyte is present at very low concentrations (\ll mM).

Among the most selective of membrane barriers available is poly(vinyl chloride) (PVC), already successfully and widely used in ion-selective electrodes (ISEs) [6,7]. PVC here is used as a continuous separate phase, unlike the porous or mesh-like membranes of many biosensors, and is also impermeable to ions. ISEs obtain their selectivity by specific relaxation in total ionic exclusion by the membrane, due to the incorporation of plasticizer, ion exchanger or neutral carrier molecules [7]. One important drawback from the ISE standpoint is the response to lipophilic ions, e.g., SCN^- , and phenols [7,8], even without an ion exchanger, a consequence at least partially of ion partitioning into the organic polymer phase. ISEs in general depend on interfacial potential changes, without large-scale fluxes of ions to generate the potential response.

Work on phenolics, with dioctyl phthalate plasticizer [8], indicated some permeation of non-ionized phenol through PVC membranes for potentiometric devices, independent of any transmembrane potentials built up to oppose ion flux. Hitherto, it has not been considered that such fluxes across PVC were sufficient for amperometric detection. Accordingly, a combination of the selective power of PVC, for uncharged species, particularly without the incorporation of an ion exchanger, coupled with conventional amperometric oxidation was attempted in this study. In addition to direct electrochemical detection of uncharged electrochemically active species, consideration was given to the combination of PVC with transduction schemes of a range of possible biosensor types.

This paper describes the casting of appropriate PVC membranes and their inclusion in electrodes of several configurations. Also, an evaluation of selectivity properties for amperometric devices is given, for oxidase-based biosensors and direct paracetamol monitoring, and an example of an

application to clinical measurement of alkaline phosphatase (ALP) in serum.

EXPERIMENTAL

Most experiments were performed using a chloride–phosphate buffer (pH 7.4) containing 2.44 g $\text{NaH}_2\text{PO}_4 \cdot 4\text{H}_2\text{O}$, 7.5 g Na_2HPO_4 , 3.0 g NaCl and 0.6 g EDTA per litre. Na_2SO_3 (6%, w/v) was added to prevent oxidation of catechol and hydrocaffeic acid solutions when the buffer pH was adjusted to alkaline conditions. Other chemicals were of analytical-reagent grade. For ALP assay, the buffer was 2-amino-2-methylpropanol (AMP) [9,10], based on the IFCC recommended method for ALP assay [9,10]. For the interference voltammograms, the chloride–phosphate buffer was used. Bovine intestinal ALP, type VII-S (E.C. 3.1.3.1) was obtained from Sigma (Poole). 4-Aminophenyl phosphate was synthesized as described previously [9].

Polycarbonate membranes of pore size 0.03 and 0.05 μm were obtained from Nuclepore (Pleasanton, CA). Cuprophane dialysis membranes were removed from a haemodialysis cartridge (Gambro, Lund, Sweden). Cellulose acetate membranes were prepared by dissolving 2.0 g of polymer (39.8% acetyl content) in 100 ml of acetone. A 1.0-ml volume of this solution was spread on a $5 \times 5 \text{ cm}^2$ glass plate and the plate was rotated manually for 2 min (ca. 30 rpm). Membranes were left to dry at room temperature for 1 h. Cellulose acetate was used with a covering polycarbonate membrane, pore size 0.03 μm . Both polycarbonate alone and the cellulose acetate–polycarbonate membrane were evaluated in the amperometric cell.

Casting of PVC membranes

A 10-ml volume of tetrahydrofuran (THF) (Fisons, Loughborough) was placed in a beaker and plasticizer added [8,11]. The plasticizers used were dioctyl phthalate (DOP) and isopropyl myristate (IPM), in volumes of 50–300 μl . A 0.06-g amount of PVC powder (MW 200 000) (BDH, Poole) was added to the THF and plasticizer and the mixture stirred until the PVC had fully dissolved. A 9-cm

SAMPLE

PVC

CUPROPHAN + BUFFER

ELECTRODE

Fig. 1. Arrangement of membranes covering the electrode.

Petri dish was rinsed with THF, then the PVC solution (10 ml) was poured in and the lid replaced. The dish was left at room temperature ($20 \pm 2^\circ\text{C}$) for 2-3 days, until the THF had evaporated, leaving a film of PVC on the glass dish. A 1.5×1.5 cm piece of the thin membrane (ca. 0.05 mm) was cut out, overlaid with a matching dialysis membrane and the membrane pair lifted from the glass with a scalpel blade.

PVC membranes could also be cast directly on dialysis membranes. A piece of dialysis membrane was stuck to a sheet of paper with adhesive tape; further tape was stuck over the dialysis membrane to form a window (1.5×1.5 cm). A $15\text{-}\mu\text{l}$ volume of PVC solution (10 ml of THF, 0.06 g of PVC, 0.15 ml of IPM) was pipetted and spread on the dialysis membrane. The tape window confined the solution to the desired area, and also prevented curling of the resulting membrane. When dry, after evaporation of the THF, the membrane sandwich was cut within the window, allowing ready removal of the PVC-coated dialysis membrane. The discrete PVC films could be peeled off the dialysis membranes, but normally the membranes were used in combination.

Assembly of electrodes

Composite membranes were used in an amperometric cell designed for oxygen measurement (Rank, Bottisham, Cambridge) [5]. This consisted of a platinum working electrode and a silver cathode functioning as a pseudo-reference electrode. Before use the electrodes were polished with alumina powder, then conditioned by polarization at $+0.65$ V vs. Ag, in phosphate buffer until a baseline was achieved. To assemble the cell, the electrode was covered with a small volume of aqueous buffer and the membrane composite was placed on top. In some instances this involved a combination of polycarbonate membrane overlying cellulose acetate, polycarbonate alone or a dialysis membrane alone. For the PVC system, the final arrangement is as shown in Fig. 1, the PVC being used in conjunction with the dialysis membrane. The sample chamber and O-ring were then mounted over the electrode; this served to stretch the membrane over the raised anode, and the locking ring was tightened. The sample chamber was then rinsed and filled with any chosen solution.

Dipstick configuration sensor

To avoid possible damage to the thin PVC membrane when the electrode was assembled, a "dipstick" configuration was also studied, whereby the PVC was cast directly over an in-house electrode (Fig. 2). For this, a piece of platinum wire 1 mm diameter and 10 mm long was sol-

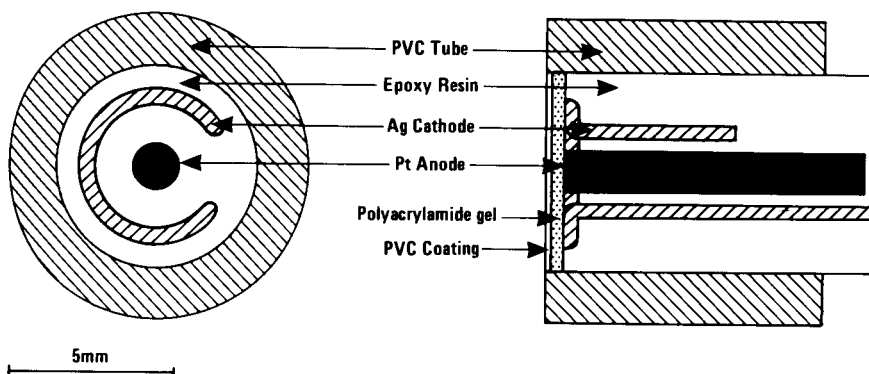


Fig. 2. Schematic diagram of the "dipstick" electrode.

dered to one lead of a two-core coaxial cable. The platinum and lead were covered in epoxy resin over a length of 30 mm from the tip. A section of PVC tubing (Gallenkamp) of 2.5 mm i.d. was pushed over the platinum–epoxy resin, and resin was inserted to fill any air pockets, with adjustments made to position the platinum and lead fully within the epoxy. After the epoxy resin had set, the PVC was removed leaving the platinum embedded in a cylinder of epoxy resin. A silver wire, 0.5 mm diameter, looped around the end of the cast cylinder, served as the pseudo-reference electrode and was itself fixed in position with epoxy resin moulded to a PVC tube (6.5 mm i.d.).

A 25-mm length of 6.5 mm i.d. PVC tube was fitted over the epoxy resin so that it projected 0.5 mm beyond the end face of the electrode. Polyacrylamide gelling solution [12] was prepared by mixing aqueous solutions of 30% acrylamide (electrophoresis grade) (300 μ l), 2.6% *N,N'*-methylenebisacrylamide (electrophoresis grade) (100 μ l) and 2% *N',N',N',N'*-tetraethylmethylenediamine (TEMED) (100 μ l) and then adding 100 μ l of 2.8% potassium peroxodisulphate solution. After mixing, 10 μ l were immediately spread on the end face of the upturned dipstick to form an electrolytic gel layer, and allowed to set for several hours. A 40- μ l volume of PVC solution containing 0.024 g of PVC and 0.06 ml of IPM in 1.5 ml of THF was then spread on top of the gel, ensuring film continuity with the PVC tubing. After evaporation of the THF overnight and conditioning in phosphate buffer, the electrode was ready for use.

Measurements were made with the platinum anode polarized at +0.65 V vs. Ag after a 2-h conditioning period at this voltage in buffer. A potentiostat, constructed by the School of Chemistry Workshops, University of Newcastle-upon Tyne, allowed polarization of the cell in the range +1.2 to -1.2 V and continuous current measurements from 0.1 nA to 2.0 mA to be made via a strip-chart recorder (SE 120, Goertz-Metrawatt, Vienna).

Generally, measurements were made by adding small volumes of stock buffered solutions to the assay buffer; changes in current output were

recorded at plateau values, with solutions stirred in all experiments.

For the ALP assay, the polarized cell was allowed to achieve a low current baseline (ca. 10 nA) in chloride–phosphate buffer, before exposure to substrate in 2-amino-2-methylpropanol buffer and reattainment of a baseline as an apparent second conditioning stage. Substrate was added to give a final concentration of 4 mM. Use of a low polarizing voltage (+0.135 V) minimized the electrochemical response to substrate, while retaining the maximum 4-aminophenol signal [13]. The enzyme reaction was initiated by adding 0.02 ml of sample/standard enzyme solution to 1 ml of the assay mixture, to give a 1:51 dilution in accordance with IFCC recommendations [10]. The slope of the current response (nA min^{-1}), was compared with that of a calibration graph for a commercial enzyme.

RESULTS

The cast PVC membranes were transparent and colourless, possessed slight elasticity and retained their structural integrity provided that they were carefully handled.

Slow solvent evaporation during casting resulted in full incorporation of IPM into the membrane, but if THF was allowed to evaporate rapidly, some plasticizer inevitably remained in liquid form on the membrane surface; such membranes gave less response (25%) to electroactive species. The casting procedure did not influence the incorporation of dioctyl phthalate.

The thickness of the membranes was ca. 0.05 mm, compared with ≤ 1 mm used for ISE membranes [8], although some variation was likely in individual cases. Inclusion of a dialysis membrane below the PVC layer maintained a stable electrolyte film and gave reliable, reproducible responses. Also, the problem of PVC insulating the electrodes and preventing completion of the electrochemical cell was avoided. With the dialysis membrane in place, and the cell sealed and found to be impermeable to ascorbate, the response was 17 nA for 30 μ M catechol, compared with only a slightly greater signal (25 nA) for a dialysis mem-

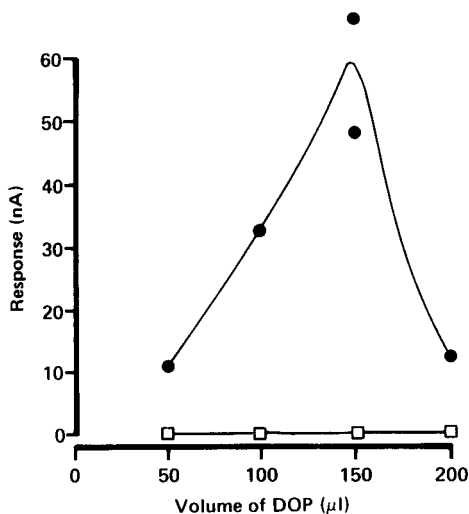


Fig. 3. Responses to (●) 0.1 mM catechol and (□) 1.0 mM ascorbate with various amounts of DOP added to 0.06 g of PVC in the membrane casting mixture. Phosphate buffer (pH 7.4), +0.65 V vs. Ag.

brane alone. Equally important, response times were similar (2 min for t_{95} , time for 95% of maximum response), and therefore the Cuprophan membranes were included with the PVC for all work using the Rank cell.

Figure 3 shows the electrode response to catechol in comparison with ascorbate. For membranes cast with 0.06 g of PVC, with various amounts of DOP included in the casting mixture, the optimum catechol response was obtained for 150 μl of DOP, without compromising selectivity, as manifested by the negligible ascorbate response (0.02 nA at 1.0 mM, compared with 0.8 μA obtained for 0.1 mM ascorbate with the Cuprophan-mounted electrode).

With IPM as plasticizer (Fig. 4), no clear optimum plasticizer content was noted, although the signal size was approximately three times greater than the DOP maximum for equivalent concentrations. Again, no significant ascorbate interference was observed.

The superimposition of several PVC membranes, (cast from 0.06 g of PVC and 0.2 ml of IPM) above an electrode and a single dialysis membrane showed a decrease in signal from 42 nA for a single PVC membrane to 40 and 33 nA with two and three layers, respectively, for 0.03

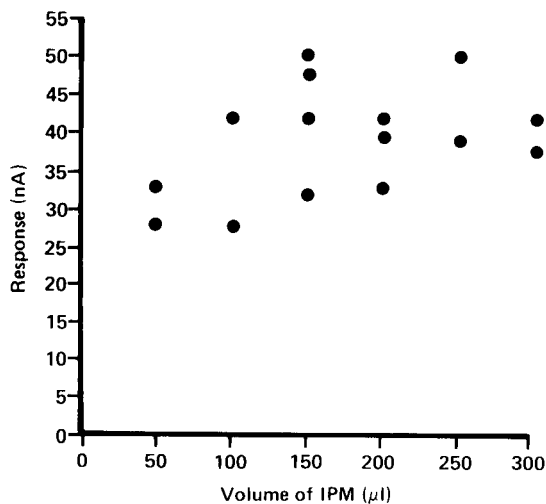


Fig. 4. Responses to 30 μM catechol with various amounts of IPM added to 0.06 g of PVC in the membrane casting mixture. Measurement conditions as in Fig. 3.

mM catechol, with no significant change in response dynamics (Fig. 5).

Casting PVC on to a dialysis membrane enabled the thin films to be easily handled, although the electrode construction still rendered them liable to damage when the cell was assembled. A doubled signal size was obtained compared with a conventional PVC casting using an identical amount of material per unit area of membrane, but the response times were similar.

Casting PVC on polyacrylamide gel, in a dipstick configuration, led to a sensor that was moderately selective for catechol against ascorbate (51 nA for 0.1 mM catechol and 1 nA for 1 mM

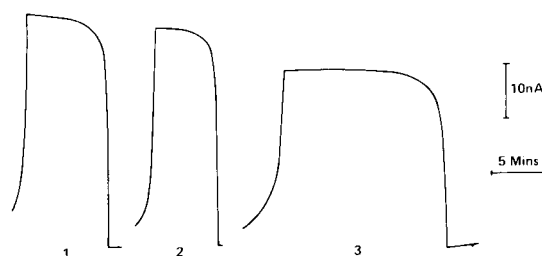


Fig. 5. Responses to 30 μM catechol with the electrode covered with one, two or three PVC membranes. PVC cast using 0.06 g of PVC and 200 μl of IPM. Measurement conditions as Fig. 3.

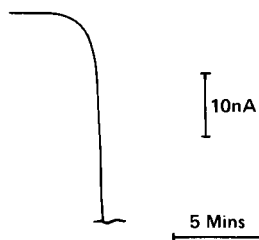


Fig. 6. Response time course to 30 μM catechol with dipstick configuration electrode. Measurement conditions as in Fig. 3.

ascorbate), as shown in Fig. 6, with a short response time (ca. 3 min) in a stirred solution.

The permeabilities of membranes commonly used in biosensors are indicated in Fig. 7. The non-selective microporous polycarbonate membrane (pore size 0.05 μm) provided a guide to the basic electroactive properties of the species used, and served as a control. PVC (prepared from 0.06 g of PVC and 150 μl of IPM) is seen to eliminate almost totally the responses to ascorbate, urate and NADH and, although the response to perox-

ide is attenuated, it is not affected to a similar extent. Retention of relatively large responses to phenolic compounds, particularly catechol, was also an important feature of PVC. The responses obtained with cellulose acetate (2%) and polycarbonate (0.03 μm), a combination commonly used in sensor fabrication [1], are also shown; the paracetamol and 4-aminophenol responses are similar to those obtained with PVC, but much less selectivity against ascorbate was noted.

For practical sensors, the determinand:interference signal ratio may be of greater significance than the magnitude of the signal. The ratios of the current sizes for relevant species are shown in Table 1. These demonstrate the high degree of selectivity of the PVC membrane, in particular for phenolic compounds, over the common interferences ascorbate and urate. Comparison with values for the cellulose acetate–polycarbonate used at present shows that PVC membranes gave greatly improved determinand:interference signal ratios, by a factor of seven for hydrogen

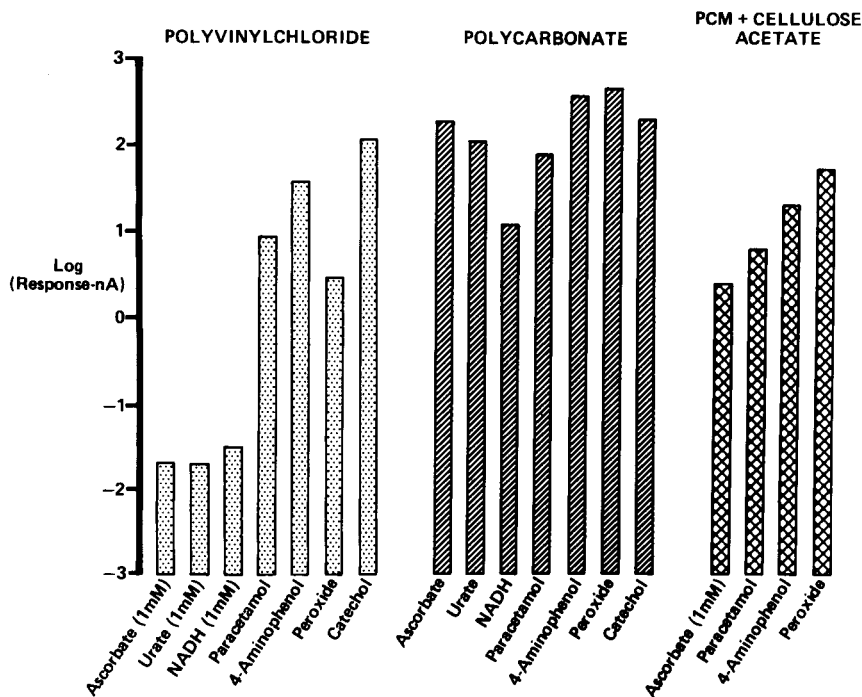


Fig. 7. Responses to 0.1 mM solutions, except where shown, comparing PVC (0.06 g of PVC + 150 μl of IPM), polycarbonate (0.05 μm) and combined polycarbonate (0.03 μm)–cellulose acetate (2%) membranes. Measurement conditions as in Fig. 3.

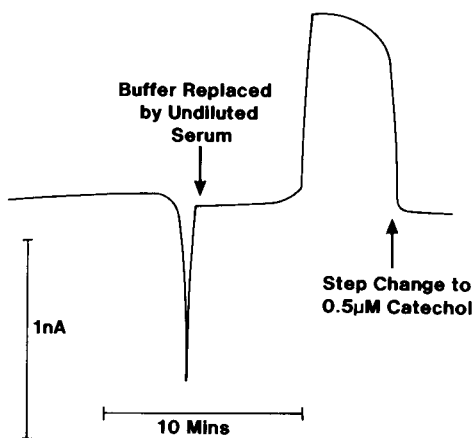


Fig. 8. Current changes in response to a step change from buffer to $0.5 \mu\text{M}$ catechol, and replacement of buffer with undiluted serum.

peroxide, 180 for paracetamol and 230 for 4-aminophenol.

Changes in current at a PVC-covered electrode were monitored when buffer was replaced with undiluted patient serum samples obtained from the Department of Clinical Biochemistry, Hope Hospital, Salford. After 3 min, six samples gave changes within $\pm 0.016 \text{ nA}$, the remaining two being -0.04 and -0.06 nA . During this work, no fouling of the membrane (0.06 g of PVC, 150 μl of IPM) by serum, and consequent loss of response to other species, was seen. To assess this apparent biocompatibility of PVC (Fig. 8), responses to $0.5 \mu\text{M}$ catechol were recorded

TABLE I

Comparison of selectivity ratios for PVC and cellulose acetate membranes

Measurand: interferent	Signal ratios	
	PVC membrane + dialysis	2% cellulose acetate membrane + polycarbonate
H_2O_2 : ascorbate	1500	200
H_2O_2 : urate	1500	–
Paracetamol: ascorbate	4500	25
Paracetamol: urate	4500	–
4-Aminophenol: ascorbate	18500	80
4-Aminophenol: urate	18500	–
Catechol: ascorbate	61500	–
Catechol: urate	61500	–

before and after a 90-min exposure of the membrane to undiluted serum; the responses were 0.98 and 1.02 nA, respectively. Similarly, catechol responses before and after 20 patients' serum samples were each in contact with the membrane for 10 min were within 0.02 nA.

It was believed that permeation through PVC was likely to be affected by solute charge, and therefore likely to show a pH dependence for ionizable species. Signals obtained for catechol ($\text{p}K_{\text{a}} = 9.46$) and hydrocaffeic acid (carboxylic $\text{p}K_{\text{a}} = 4.8$), with varying pH (Fig. 9), confirm the pH effect, with signal size attenuated at $\text{pH} > \text{p}K_{\text{a}}$.

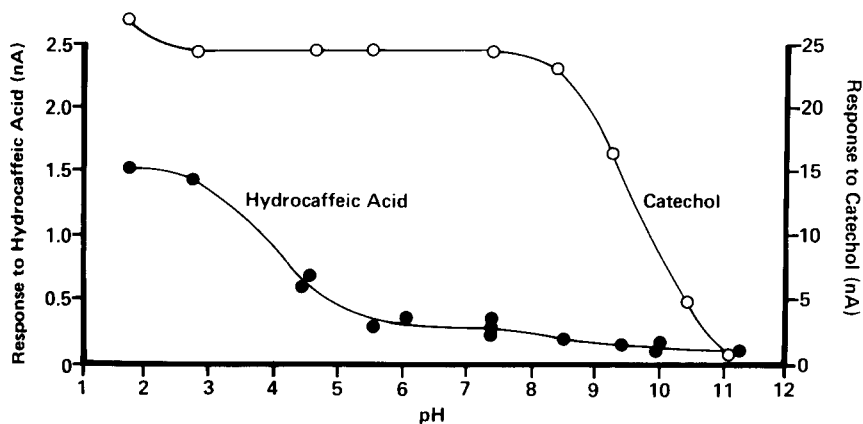


Fig. 9. Responses to $30 \mu\text{M}$ (○) catechol and (●) hydrocaffeic acid with varying external pH. Electrode polarized at +0.65 V vs. Ag, PVC membrane (0.06 g of PVC + 150 μl of IPM) covering the electrode and pH 7.4 buffer between membrane and electrode.

DISCUSSION

PVC has been well tried as a matrix for retaining ion affinity ligands in ISE methodology. Recent investigations with a PVC-coated amperometric electrode [14] indicated a degree of selectivity, although the integrity of the very thin film was open to question. Also, the membranes included an ion exchanger, which may have implications for ion flux through the membrane, necessary to maintain electrical continuity with a coated electrode. The PVC membranes resembled those used previously for ISEs [6,8], but were approximately 10% of the thickness in order to ensure maximum response, although this did lead to some handling problems. Work on ISEs [8] indicated that a flux of non-ionized phenol was possible through PVC, but gave no indication of the large fluxes resulting in the signals described in this work. The fuller incorporation possible with DOP would make its use the preferred method; however, if maximum response size was important for the membrane application, then the enhanced responses obtained with IPM plasticized membranes might dictate the use of the latter, despite the more controlled casting technique required.

The decreased signal size for the DOP–PVC membranes above 150 μl (Fig. 3) was a possible result of increased membrane thickness. However, IPM probably reached “saturation” in the membrane, and further increases of IPM in the casting mixture were not incorporated into the PVC bulk, but formed a discrete layer which was subsequently removed.

The requirement for a liquid layer below the PVC was readily provided by a dialysis membrane spacer, with little effect on signal size or response time; this suggested that PVC acted as the main diffusion limiting barrier.

Multiple PVC layers (not separated by buffer) gave smaller signals, but not to the extent expected for increased diffusion distances through PVC. The inevitable presence of IPM liquid on the membrane surface may have served to link the membranes into a single quasi-continuous phase, and it is possible that solute transfer at the

membrane/solution interface was the main rate-limiting step.

Casting of PVC on dialysis membrane or on a dipstick did not affect the permeability properties. Therefore, the alternative electrode structures could be developed as suitable means of deploying PVC; in particular, the gelled internal electrolyte can provide a “solid” surface for casting.

The pattern of selectivity seen with PVC membranes is that predicted on the basis of the properties seen in ISE work, although no quantification of fluxes was attempted [8]. Ions (ascorbate, urate and NADH) are excluded to a very large extent. Uncharged species such as catechol and paracetamol permeate as expected on the basis of previous work, although the signal size, approximating that with 0.05- μm polycarbonate, is remarkable for a highly selective membrane. 4-Aminophenol, although charged at neutral pH, did permeate PVC, but its aromatic character may have facilitated its partitioning into the organic phase. Ion-pair formation may be involved [7], or homoconjugation of charged and uncharged phenolics [8,15]. Hydrogen peroxide, although uncharged, is polar, and showed relatively limited PVC permeation. Addition of ion exchangers would be likely to alter the permeability properties of the membrane. The greatest selectivity appears to be for aromatics with no ion exchanger present, as these species cannot be excluded when selectivity is relaxed by the addition of ion exchangers to permit fluxes of charged species.

The response ratios in Table 1 show the extent to which PVC selectivity greatly exceeds that of cellulose acetate. The extremely high selectivity possible with PVC could be exploited for new types of chemical sensors and biosensors, in addition to bringing improvements to existing devices. The selectivity of direct paracetamol measurements is greater, as shown by a 180-fold improvement in paracetamol:ascorbate signal ratio compared with existing cellulose acetate membranes. Similarly, despite small signals, the selectivity for hydrogen peroxide is increased, which may be of benefit to oxidase-based sensor systems.

In addition, enzyme systems generating a phenolic product would gain from the selective properties of PVC to such an extent that advantage could be gained by devising systems to generate such signal species suitable for the PVC membrane. Such an approach may be more fruitful than grafting PVC membranes on to existing sensor formats.

The absence of fouling noted with PVC exposed to serum could be due to the hydrophobic and quasi-liquid PVC surface reducing the adherence of serum proteins compared with other membrane materials. PVC therefore appears to be an ideal material for an outer membrane exposed to clinical samples.

The nature of the selectivity obtained was investigated with respect to charge (Fig. 9), and the ionization of carboxylic and phenolic groups decreased the membrane permeation of catechol and hydrocaffeic acid. Some molecules permeated the membrane when the COOH group was ionized, probably owing to the favourable partitioning conferred by the aromatic ring. Similarly, moderate responses were obtained at pH 7.4 to 4-aminophenol, which is charged at this pH. Hence, although the general basis for selectivity appears to be charge and partitioning, for individual species the situation may require further elucidation.

The ALP assay represents the first use of this PVC membrane for a practical assay. This method (y , U l^{-1}) appears to correlate well ($y = 1.32135x + 18.6295$; $r = 0.9931$, $n = 10$) with spectrophotometric data (x , U l^{-1}), and could be developed into a viable clinical technique. The data confirms the acceptability of response times for kinetic monitoring of the enzymic reaction products, and indicates that PVC could be used for enzyme electrodes operating in the kinetic mode and for steady-state measurements.

Conclusion

PVC membranes similar to those used in ISE, but without specific affinity molecules, can be used successfully as permeability barriers to confer selectivity to amperometric sensors. Fluxes of certain classes of molecule of those investigated, mainly uncharged aromatic compounds, give large

electrode responses, coupled with extreme selectivity against ions. Particularly important is the virtual exclusion of the interferents found in serum, which pose problems in amperometric biosensor development. Equally important is the total prevention of signal loss by fouling. The resulting electrodes have the operational reliability of electrodes employed in simple aqueous solution. The selectivity offered by PVC is far in advance of existing membranes used for this purpose, and future biosensor development could gain from the simultaneous development of PVC membranes and reaction schemes generating permeating signal species.

This work was supported by the SERC and ICI.

REFERENCES

- 1 W.H. Mullen, F.H. Keedy and S.J. Churchouse, *Anal. Chim. Acta*, 183 (1986) 59.
- 2 G. Palleschi, M.A.N. Rahni, G.J. Lubrano and J.N. Ngwainbi, *Anal. Biochem.*, 159 (1986) 114.
- 3 M.F. Cardosi, S.W. Birch, C.J. Storey, A. Johannson and A.P.F. Turner, *Int. Biotech. Lab.*, 1 (1989) 8.
- 4 T. Tsuchida and K. Yoda, *Enzyme Microb. Technol.*, 3 (1981) 326.
- 5 Z. Koochaki, I.M. Christie and P. Vadgama, *J. Membr. Sci.*, 57 (1991) 83.
- 6 G.J. Moody, R.B. Oke and J.D.R. Thomas, *Analyst*, 95 (1970) 910.
- 7 W.E. Morf and W. Simon, in H. Freiser (Ed.), *Ion-Selective Electrodes in Analytical Chemistry*, Vol. 1, Plenum Press, New York, 1978, p. 236.
- 8 I.M. Christie, PhD Thesis, University of Wales, 1988.
- 9 I.M. Christie, P.H. Treloar, G.N. Smith, Z.B. Koochaki and P.M. Vadgama, *Anal. Chim. Acta*, 257 (1992) 21.
- 10 N.W. Tietz, A.D. Rinker and L.M. Shaw, *Clin. Chim. Acta*, 135 (1983) 339F.
- 11 P.L. Bailey, *Analysis with Ion-Selective Electrodes*, Heyden, London, 1976, p. 238.
- 12 C.V. Nicholas, M.A. Desai, P.M. Vadgama, M.B. McDonnell and S. Lucas, *J. Chem. Soc., Faraday Trans.*, 87 (1991) 293.
- 13 H.T. Tang, C.E. Lunte, H.B. Halsall and W.R. Heineman, *Anal. Chim. Acta*, 214 (1988) 187.
- 14 M. Fujihira, H. Ogura, T. Saji and S. Aoyagi, *J. Chem. Soc. Jpn., Pure Chem. Sect.*, (1985) 1167.
- 15 L.P. Hammett, *Physical Organic Chemistry*, McGraw-Hill-Kogahusha, Tokyo, 2nd edn., 1970, p. 221.

Silicon-based chlorine sensor with on-wafer deposited chemically anchored diffusion membrane

Part I. Basic sensor concept

Albert van den Berg, Milena Koudelka-Hep, Bart H. van der Schoot and Nico F. de Rooij

Institute of Microtechnology, University of Neuchâtel, Rue A.-L. Breguet 2, CH-2000 Neuchâtel (Switzerland)

Elisabeth Verney-Norberg

G.I.E. Recherche du Pôle Energie Chaleur, C.E.R.C.L.E., Groupe Lyonnaise des Eaux, L'Orée d'Ecully, Chemin de la Forestière, 69130 Ecully (France)

Alain Grisel

Microsens S.A., Rue Jaquet Droz 7, CH-2000 Neuchâtel (Switzerland)

(Received 12th May 1992)

Abstract

A method for on-wafer fabrication of free-chlorine sensors is described. The sensor structure consists of a planar three-electrode electrochemical cell covered with a poly(hydroxyethyl methacrylate) hydrogel membrane. This membrane is photolithographically patterned on-wafer. In order to guarantee good adhesion of the membrane to the electrode surface a special oxidation step consisting of a treatment in an oxygen plasma followed by a silanization procedure has been developed. The optimal operational polarization voltage of the integrated sensor for detection of hypochlorous acid was found to be 0 mV vs. the on-chip Ag/AgCl reference electrode in a solution of 0.1 M KCl. Sensors with membrane thicknesses of 10 and 50 μm are found to give linear calibration curves between 0.1 and 5 mg l^{-1} free chlorine, with sensitivities of 2.0 and 0.4 $\text{nA (mg l}^{-1})^{-1}$, respectively.

Keywords: Sensors; Chlorine detection; Diffusion membrane; Silicon based sensor

There is an increasing need for the determination and continuous on-line monitoring of residual water disinfectant. Although several alternatives, like ozone, bromide, iodine or chlorine dioxide, exist for disinfecting purposes, none can compete with chlorine with respect to its effectiveness, easy applicability, persistence and low

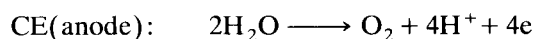
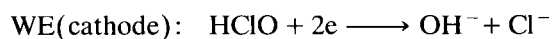
cost [1]. At the normal pH values of drinking water (pH 6.5–9), chlorine is present in the form of hypochlorous acid, HClO, or its conjugated base, the ClO^- anion [2]. However, since the disinfecting reactivity of HClO is about 10 000 times higher than that of the ClO^- anion [3,4], we will focus on the detection of hypochlorous acid.

Different methods exist to detect dissolved chlorine, most of them based on electrochemical principles. A potentiometric approach, as pro-

Correspondence to: A. van den Berg, Institute of Microtechnology, University of Neuchâtel, Rue A.-L. Breguet 2, CH-2000 Neuchâtel (Switzerland).

posed by Schlechtriemen and Sohège [5] for the detection of chlorine gas is less appropriate for on-line monitoring because of its logarithmic response, giving the sensor a large dynamic range but a relatively low precision. Detectors based on amperometric detection respond linearly to concentration variations, and are thus more promising. In this case, use is made of the strong oxidative nature of the hypochlorous acid, which enables its electrochemical reduction at a relatively anodic potential thus excluding interference of other oxidants like dissolved oxygen. Conventional analyzers often use rotating disk electrodes that provide sufficient sensitivity and selectivity, but are rather bulky systems that are not easily introduced on a large scale for on-line monitoring [6]. The same holds for FIA-based systems that use iodometric [7,8] or direct amperometric detection [9]. A macroscopic membrane-covered amperometric detector fabricated by conventional techniques with good sensing properties has been described by Ben-Yaakov [10], but this approach lacks the possibility of easy mass-fabrication. Finally, an alternative optical detection as recently proposed by Piraud et al. [11] for the moment does not attain the required detection limit of about 0.01 mg l^{-1} and the measurement system cannot be easily miniaturised.

The sensor we present here is based on a Clark-type device. It uses a planar three-electrode electrochemical cell covered with a thin hydrogel membrane to detect the hypochlorous acid. The distinctive feature of our approach is that the entire sensing element is realized on silicon with standard IC-fabrication techniques, implying that the sensing element can be easily and reproducibly mass-produced. Thin-film platinum working- and counter-electrodes, and a partially chloridized silver reference electrode were used. The latter can be used as a reference electrode since the Cl^- concentration in drinking water is fairly constant. The electrode reactions taking place at the working electrode (WE) and counter electrode (CE) are respectively:



To prevent the convective effects such as stirring from influencing the mass flow to the working electrode, we used a diffusion limiting membrane (DLM) to define a stagnant surface layer in which diffusion is the only process determining the mass transfer and thus the measured current. Under potentiostatic operation at a properly chosen working potential, the measured current is proportional to the amount of reduced free chlorine.

Recently, we have proposed the use of a poly(hydroxyethyl methacrylate) (polyHEMA) hydrogel layer as DLM for the detection of hydrogen peroxide and oxygen [12]. This membrane has the advantage that it can be photolithographically polymerized and patterned enabling the fabrication of the complete cell with IC-compatible methods. With this technology, polyHEMA layer thicknesses of between 10 and $100 \mu\text{m}$ can be realized. In this way an optimal trade-off between a high sensor current and a rapid response on one hand (thin membrane) and a signal insensitive to stirring on the other hand (thick membrane) can be chosen.

Special attention has been paid to the adhesion of the polyHEMA membrane. It is known that chemical pretreatment of oxide surfaces such as SiO_2 and Al_2O_3 with methacrylic functional silane strongly improves the adhesion [13]. However, such a treatment can not be directly applied to the surface of a platinum electrode. Therefore we investigated methods to oxidize and subsequently functionalize a platinum electrode, with the extra requirement that the method should be applicable on-wafer.

EXPERIMENTAL

Basic device fabrication

The basic structure consists of a three-electrode cell realized on a silicon wafer. The working- and counter-electrodes consist of a 1500 \AA thick Pt layer on top of a 500 \AA thick Ti adhesion layer. The reference electrode is made by chemical chloridisation of a $1 \mu\text{m}$ thick Ag layer. Further details of the fabrication of the device are given in [14].

Instrumentation and methods

Cyclic voltammetry measurements were performed using a PAR 273 potentiostat. For all cyclic voltammetric measurements a solution of 1 M H_2SO_4 and a scan rate of 100 mV s^{-1} were used, except for the determination of the interference of oxygen reduction relative to the hypochlorous acid reduction, where a solution of 0.1 M KCl with 0.01 M phosphate buffer (pH 5.8) and a scan rate of 10 mV s^{-1} were used. For potentiostatic measurements a potentiostat built in-house was used. The plasma oxidation of the platinum electrodes was carried out using an oxygen plasma in an Alcatel GIR 300 plasma etch machine. Measurements of polyHEMA membrane thicknesses were carried out with an Alphastep 200 step height profiler. Visual inspections after the measurements confirmed that the scan of the stylus did not cause any damage to the membranes.

Electrode surface modification

Electrochemical oxidation of the platinum electrode surface was carried out by polarizing the electrodes in 1 M H_2SO_4 at +2.5 V vs. SCE during 5 min. Chemical oxidation was carried out in 0.25 M $(\text{NH}_4)_2\text{S}_2\text{O}_8$, 0.5 M HClO, or 1 M HNO_3 . Plasma oxidation was carried out in an oxygen plasma at a frequency of 13.5 MHz, a pressure of 0.1 mbar, and using a power of 100 W.

Silanization of the electrode surface was carried out by dipping the electrodes in hexamethyldisilazane (HMDS) (Fluka). Subsequently, the electrodes were blown dry in nitrogen. Functionalization of the surface with methacrylic groups was performed by treating the electrodes for 1 min with a solution of 10% (trimethoxysilyl)propyl methacrylate (TMSM) (Aldrich) and 0.5% H_2O in toluene at 60°C .

Membrane deposition

The monomer mixture consisting of 57.5 wt.% hydroxyethyl methacrylate (HEMA) (Fluka), 38 wt.% ethyleneglycol (EG) (Merck), 1 wt.% dimethoxyphenylacetophenone (DMAP) (Aldrich), 2.5 wt.% polyvinylpyrrolidone K90 (PVP) (Aldrich) and 1 wt.% tetraethyleneglycol

dimethacrylate (TEGDM) (Fluka) was placed by pipette on the wafer in an amount corresponding to the required membrane thickness. A Mylar sheet was then pressed onto the mixture which was allowed to spread out over the wafer until the required coverage of the wafer was obtained. Then the monomer mixture was selectively photopolymerized with UV light. Exposure times of 30 s to 3 min were used. This was followed by development in ethanol. The sensors were pre-conditioned in 0.1 M KCl prior to measurement.

RESULTS AND DISCUSSION

Surface modification of the electrodes

In the fabrication process of the completed cell with hydrogel membrane, a crucial element concerning the durability is the membrane adhesion to the electrode surface. In order to be able to apply the frequently used method of surface silanization, the surface of the platinum electrodes must first be oxidized. A well-known standard method to do this is electrochemical oxidation [15]. The formation of oxide (mono)layers at the electrode surface can be monitored by reducing the oxide in a cathodic scan starting at high anodic potential. In Fig. 1 stripping voltammo-

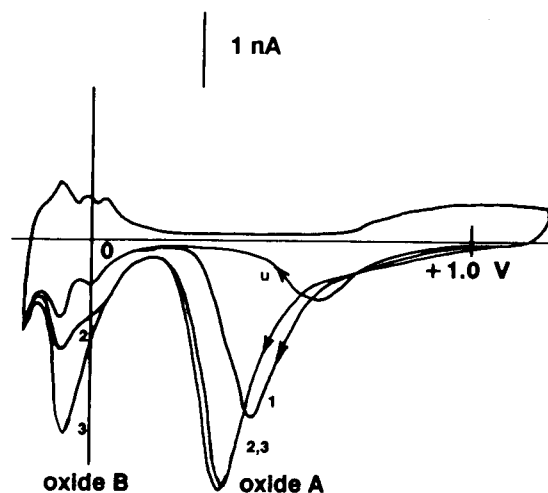


Fig. 1. Cathodic stripping voltammograms of bare Pt electrodes in 1 M H_2SO_4 after anodic polarization at +2.5 V vs. SCE. u: untreated; 1: 1 s, 2: 2 min, 3: 5 min.

grams of platinum, untreated and electrochemically oxidized for 1 s, 3 min and 5 min, respectively, are shown. In this figure, two different cathodic waves can be clearly distinguished: one corresponding to a quickly formed, and easily reduced oxide (reduction potential about +400 mV vs. SCE), and a second wave corresponding to an oxide form that is only formed after a few minutes of polarization at +2.5 V vs. SCE, and reduced at approximately -50 mV vs. SCE. The presence of these two waves is in good correspondence with the results reported in [14], where they were attributed to two different forms of platinum oxide. We will also designate the two waves as A and B for the more anodic and more cathodic waves, respectively, in accord with the nomenclature used in [15].

In order to see which one of the two oxides is necessary for the silanization, we performed a simple silanization reaction with HMDS which is comparable to the somewhat more elaborate reaction with TMSM. Such a reaction should passivate the formed oxide, and disable its electrochemical reduction. In Fig. 2 the effects of the silanization on the appearance of both oxide peaks is shown. From the three curves representing untreated oxide, oxide treated in HMDS for

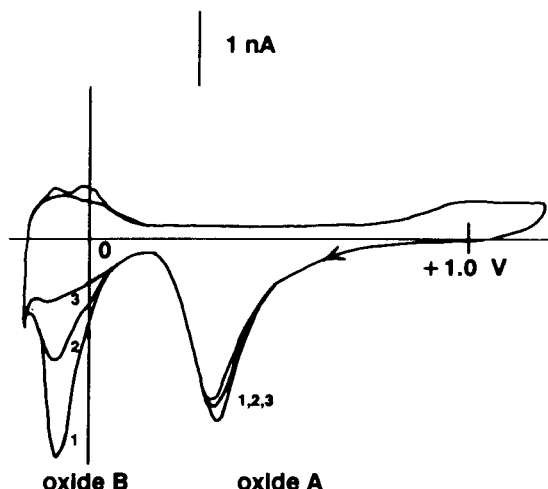


Fig. 2. Cathodic stripping voltammograms of Pt electrodes, electrochemically oxidized during 5 min in 1 M H_2SO_4 , and treated with HMDS. 1: no HMDS treatment, 2: 30 s HMDS, 3: 5 min HMDS.

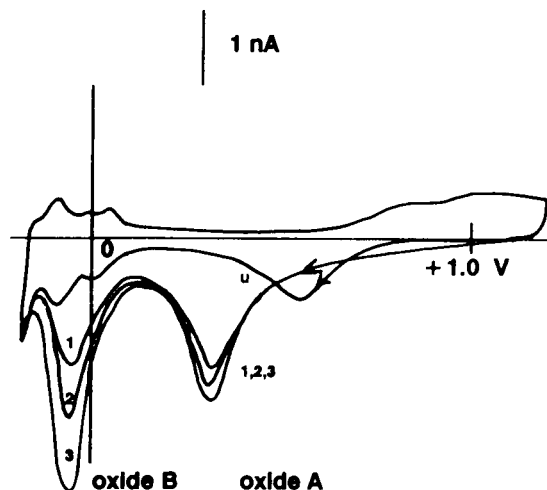


Fig. 3. Cathodic stripping voltammograms of bare Pt electrodes in 1 M H_2SO_4 after treatment in oxygen plasma. u: untreated; 1: 30 s, 2: 2 min, 3: 5 min.

30 s, and oxide treated in HMDS for 5 min, two conclusions can be drawn: The first and most important conclusion is that the oxide represented by wave A does not react with HMDS. The second conclusion is that wave B reacts only relatively slowly with HMDS, and that it takes about 5 min to obtain a fully silanized oxide.

From the above results it can be concluded that in order to be able to silanize the electrode surface, the formation of platinum oxide of type B is necessary. Since electrochemical oxidation is not easily applicable on whole wafers, we investigated other chemical treatments that could provide the platinum type B oxide. Unfortunately, treatments with oxidants such as nitric acid, and ammonium peroxodisulfate did not result in the appearance of the type B oxide. The only treatment which did give both oxide waves was a treatment in oxygen plasma, as shown in Fig. 3. From this figure it can be concluded that a 5-min treatment of the platinum electrode in an oxygen plasma results in similar A- and B-type oxide waves as obtained with the electrochemical oxidation.

Membrane deposition

The deposition of the polyHEMA hydrogel membranes was carried out as described in the

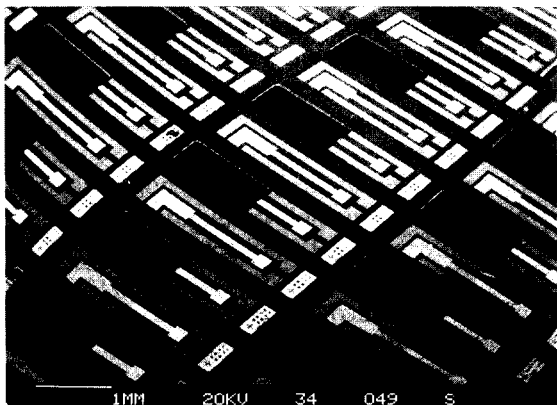


Fig. 4. SEM micrograph of part of a wafer with a photopolymerized hydrogel membrane on every second device.

experimental part. Some difficulties were encountered when we tried to wash away the unpolymersed regions from the wafer in the development step. Therefore we had to modify the mask in such a way that only every second basic electrode was covered with the polyHEMA membrane. A SEM micrograph of a part of a wafer covered with membranes is shown in Fig. 4. From this figure, it can be concluded that a satisfactory lateral resolution of some tens of microns is obtained, which is largely sufficient for our purpose. The homogeneity of the membrane thickness over the wafer was investigated by step-height measurements. On 32 evenly distributed membranes over the wafer a mean thickness of $61.8 \mu\text{m}$ was found with a standard deviation of $7.3 \mu\text{m}$. An important part of the thickness variation was caused by a continuous varying thickness of the membranes over the wafer. If closely located membranes were considered, typical standard deviations of $3\text{--}4 \mu\text{m}$ were found.

Sensor characterization

A first characterization of the electrodes was carried out to determine the optimal polarization potential for the detection of free chlorine. Therefore, cyclic voltammograms were taken of the bare platinum electrodes in background electrolyte under nitrogen and with added sodium hypochlorite. A background electrolyte a solution of 0.1 M KCl with 0.01 M potassium dihydrogen-

phosphate (pH 5.8) was taken to ensure that all the free chlorine was present as hypochlorous acid. In order to examine the interference of oxygen, a third cyclic voltammogram was recorded in background electrolyte and ambient air, as shown in Fig. 5.

From the cyclic voltammogram of the reduction of hypochlorous acid (at $E < +700 \text{ mV}$ vs. SCE) and of oxygen reduction ($E < +300 \text{ mV}$ vs. SCE), a polarization potential "window" between $+300$ and $+400 \text{ mV}$ vs. SCE can be determined where the hypochlorous acid reduction is relatively potential independent, and there is no oxygen reduction interference. It must be remarked here that the finally desired detection limit for free chlorine is in the micromolar range, whereas the figure shown is obtained with a concentration of 1 mM hypochlorous acid.

The above mentioned conclusions were verified with potentiostatic measurements carried out with mounted and encapsulated three-electrode devices covered with a polyHEMA membrane of approximately $10 \mu\text{m}$ thickness. In Fig. 6, the sensor current as a function of the free chlorine concentration at three different polarization potentials is measured. At the most cathodic potential (-100 mV vs. on-chip reference electrode) an offset current due to oxygen reduction is found. At 0 mV this offset current is largely suppressed, whereas the same sensitivity to free chlorine is

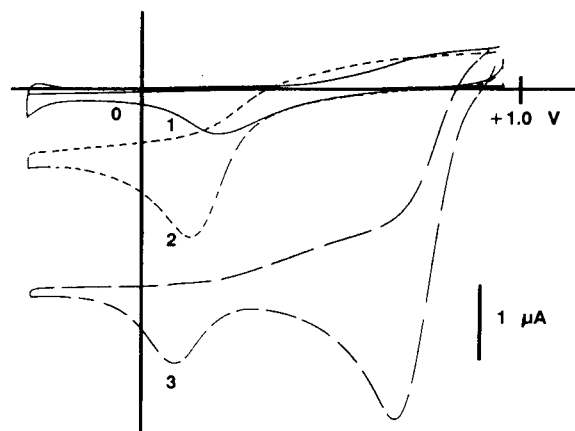


Fig. 5. Cyclic voltammograms of platinum electrodes in 0.1 M KCl , 0.01 M phosphate buffer, pH 5.8. 1: under N_2 , 2: with 10^{-3} M HClO , 3: as 1, in ambient air. Scan rate: 10 mV s^{-1} .

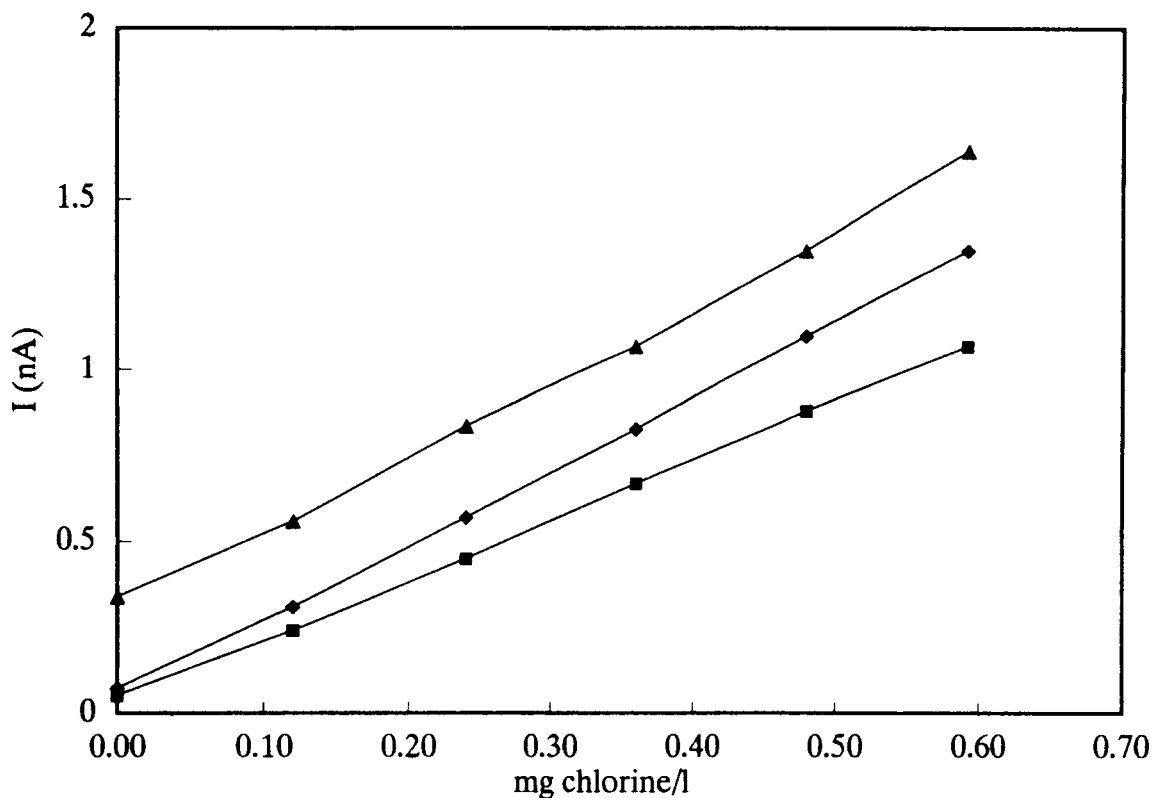


Fig. 6. Sensitivity curves of completed sensors with a ca. 10- μm thick polyHEMA membrane in 0.1 M KCl, pH 7. Polarization potentials: upper curve: -100 mV, middle curve: 0 mV, lower curve: $+100$ mV vs. on-chip Ag/AgCl reference electrode.

maintained. A further increase of the polarization potential results in no further decrease of the offset current, while the sensitivity starts to decrease. There is a difference in polarization potential as compared to the cyclic voltammetric measurements which can be explained by a combination of the different reference electrode (Ag/AgCl in 0.1 M KCl, instead of a SCE), a different pH (7 instead of 5.8), and the presence of the polyHEMA membrane on the electrodes. Thus, 0 mV vs. on-chip Ag/AgCl has been taken as the optimal polarization potential in 0.1 M chloride solutions.

Finally, calibration curves of two completed sensors with membranes of thickness 10 and 50 μm are shown in Fig. 7. A slight difference in the sensitivity is observed for both sensors between low and high free chlorine concentrations: 2.2 and 1.8, $\text{nA} (\text{mg l}^{-1})^{-1}$ for 10 μm polyHEMA,

0.45 respectively 0.3 $\text{nA} (\text{mg l}^{-1})^{-1}$ for 50 μm polyHEMA. The approximate sensitivity ratio of 5.5 ± 0.5 closely reflects the thickness ratio of the membranes.

Conclusions

It has been shown that membrane-covered electrochemical cells can be realized on-wafer. A special oxidation procedure was found to be necessary for the platinum electrodes to be able to carry out the surface silanization, since the standard electrochemical oxidation is not easily performed on whole wafers. Using cathodic stripping voltammetry, it was found that oxidation in oxygen plasma resulted in the same oxidized surface state of the platinum electrode as with the electrochemical oxidation.

Cyclic voltammetric measurements using bare electrodes showed that a polarization potential

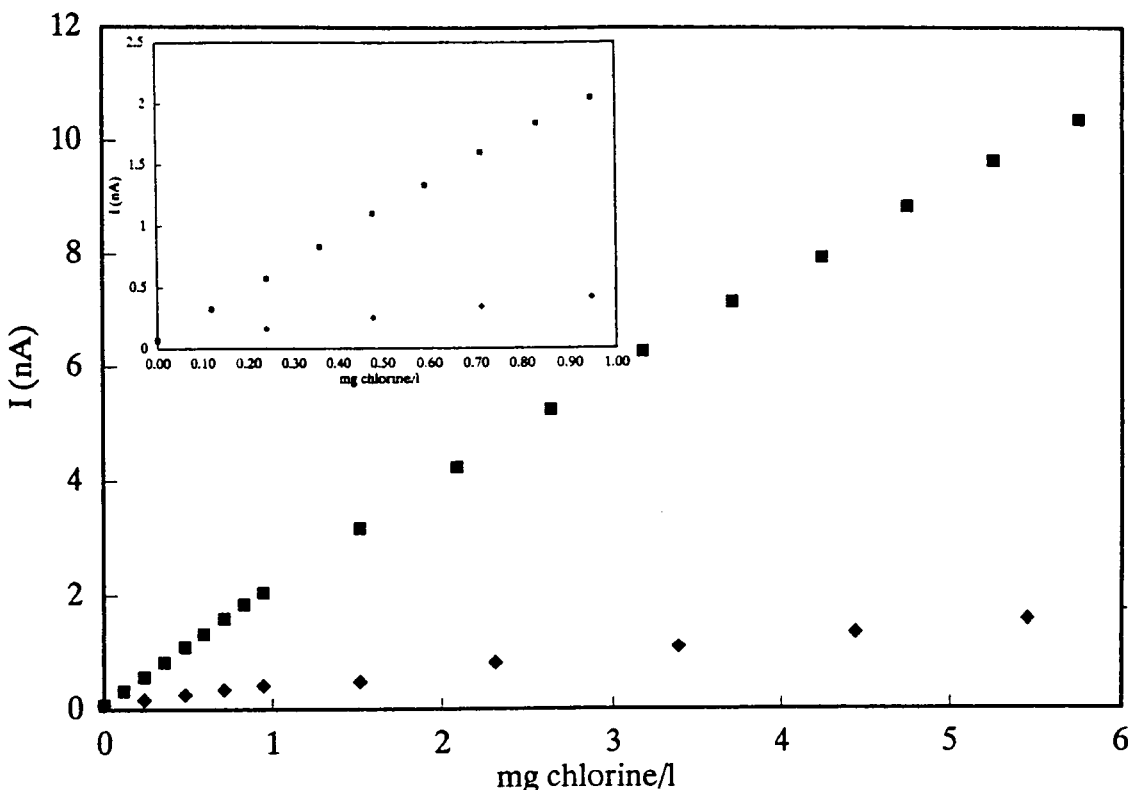


Fig. 7. Calibration curve of two sensors with 10 μm (upper curve) and 50 μm (lower curve) thick polyHEMA membranes, respectively. Polarization potential: 0 mV vs. on-chip Ag/AgCl electrode. The insert shows the low concentration part of the curve in more detail.

can be found where the hypochlorous acid reduction is relatively potential independent and dissolved oxygen does not interfere. The calibration curves obtained with sensors having two different membrane thicknesses using the optimally chosen polarization potential revealed a nearly linear sensor response over the range 0.1–5 mg l^{-1} free chlorine.

Since the desired measurement range for the determination of chlorine in drinking water is in the range 0–0.2 mg l^{-1} , with a desired detection limit of 0.01 mg l^{-1} , the sensor range must be extended in the lower concentration range. Unfortunately, the sensor current becomes very low in this region. Therefore a new electrode design with a larger surface area will be studied as a first solution in the near future. Other investigations will concern the study of interference by chlo-

ramines, and optimization of the long term stability of the Ag/AgCl reference electrode.

The financial support of the Lyonnaise des Eaux-Dumez group and SAGEP is gratefully acknowledged. The authors thank G. Mondin and J.D. Cretin for their technical assistance.

REFERENCES

- 1 G.C. White, *The Handbook of Chlorination*, Van Nostrand Reinhold, New York, 1986, p. 256.
- 2 V.L. Snoeyink and D. Jenkins, *Water Chemistry*, John Wiley and Sons, New York, 1980, p. 388.
- 3 J.C. Morris, *Water Chlorination: Environ. Impact Health Eff.*, 1 (1978) 27.
- 4 R.L. Jolley and J.H. Carpenter, *Water Chlorination: Environ. Impact Health Eff.*, 4 (1983) 3.

- 5 G.-L. Schleichriemen and J. Sohège, *Ber. Bunsenges. Phys. Chem.*, 94 (1990) 991.
- 6 V. Grangirard, *L'Eau, L'Industrie, Les Nuisances*, 153 (1982) 46.
- 7 W. Matuszewski and M. Trojanowicz, *Anal. Chim. Acta*, 207 (1988) 59.
- 8 A.M. Dietrich, T.D. Ledder, D.L. Gallagher, M.N. Grabeel and R.C. Hoehn, *Anal. Chem.*, 64 (1992) 496.
- 9 A.N. Tsaousis and C.O. Huber, *Anal. Chim. Acta*, 178 (1985) 319.
- 10 S. Ben-Yaakov, *J. Electroanal. Chem.*, 98 (1979) 15.
- 11 C. Piraud, E. Mwarania, G. Wylangowski, J. Wilkinson, K. O'Dwyer and D.J. Schriffin, *Anal. Chem.*, 64 (1992) 651.
- 12 A. van den Berg, A. Grisel, M. Koudelka and B.H. van der Schoot, *Sensors Actuators B*, 5 (1991) 71.
- 13 E.J.R. Sudhölter, P.D. van der Wal, M. Skowronska-Ptasinska, A. van den Berg, P. Bergveld and D.N. Reinhoudt, *Anal. Chim. Acta*, 230 (1990) 59.
- 14 M. Koudelka, S. Gernet and N.F. de Rooij, *Sensors Actuators*, 18 (1989) 57.
- 15 J. Facci and R.W. Murray, *J. Electroanal. Chem.*, 112 (1980) 221.

Development of an optical–chemical sensor for the detection of ammonium ions

W. Sellien, R. Czolk, J. Reichert and H.J. Ache

Kernforschungszentrum Karlsruhe GmbH, Institut für Radiochemie, P.O. Box 3640, W-7500 Karlsruhe 1 (Germany)

(Received 3rd January 1992; revised manuscript received 2nd June 1992)

Abstract

An optical–chemical sensor for monitoring ammonium ions in aqueous solutions was developed. The properties of the sensor, which is based on an immobilized pH indicator were investigated. For the immobilization microporous PTFE membranes were used and the changes in the reflectance spectra were measured. The detection limit is dependent on the pK_a value of the pH indicator used and on the pH and the temperature of the sample. With *p*-Xylenol Blue ($pK_a = 2.0$) the detection limit is $1 \times 10^{-6} \text{ mol l}^{-1} \text{ NH}_4^+$ (pH = 6.8; $T = 22^\circ\text{C}$). The response time depends on the ammonium ion concentration and ranges from 1 to 60 min. The long-term stability of the sensors is better than 6 months. The sensor was optimized to analyse waste water without pretreatment of the sample. The measured ammonium ion concentration correlated well with the results obtained by conventional analytical methods.

Keywords: Sensors; Ammonia; pH; Waters

There is growing interest in the development of selective chemical sensors for analytical applications. Sensors with optical transduction have several advantages over potentiometric systems. Different approaches toward optical ammonia or ammonium ion sensors have been published [1–9]. These sensors are based on the deprotonation of an immobilized pH indicator. An ammonium ion sensor can be constructed by entrapment or immobilization of an appropriate indicator in or behind a gas-permeable membrane (Fig. 1). In aqueous solutions the ammonium ion is in equilibrium with ammonia. Diffusion of ammonia through the gas-permeable membrane leads to deprotonation of the immobilized pH indicator. This deprotonation by ammonia varies according to the concentration of ammonium ions in the solution and can be detected spectroscopically.

As reported previously [10], the immobilization of Bromophenyl Blue in silicone-rubber layers resulted in ammonium ion optrodes with limited stability. To overcome this, microporous PTFE membranes were used for adsorptive immobilization of the pH indicator in these membranes. In order to develop an optical–chemical sensor that fulfils the requirements for the determination of ammonium ions in waters, the effects of the indicator used and of the temperature and pH of the sample were investigated. To illustrate the suitability of the sensor, it was applied to the determination of ammonium ions in waste-water samples.

EXPERIMENTAL

Reagents

All chemicals were purchased from Merck (Darmstadt, Germany) and used as received. Deionized water was used throughout. Standard

Correspondence to: R. Czolk, Kernforschungszentrum Karlsruhe GmbH, Institut für Radiochemie, P.O. Box 3640, W-7500 Karlsruhe 1 (Germany).

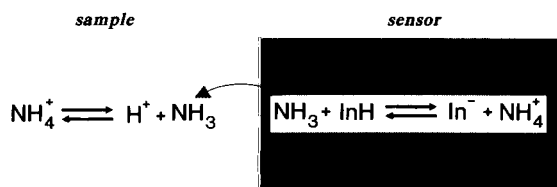


Fig. 1. Principle of optical-chemical ammonium ion sensor. The sample solution containing ammonium ions is separated from the immobilized pH indicator by a gas-permeable membrane. The ammonia in equilibrium with ammonium ions passes through this membrane and deprotonates the indicator.

ammonium solutions were prepared fresh daily by diluting an aqueous solution of 53.5 g l^{-1} NH_4Cl (0.1 mol l^{-1}) with phosphate buffer solution (0.06 mol l^{-1} ; pH 6.8). The following triphenylmethane derivatives were used as pH-sensitive indicators: *p*-Xylenol Blue (PXB), Bromophenol Blue (BPB), Bromocresol Green (BCG) and Bromocresol Purple (BCP).

Sensor preparation

A $50\text{-}\mu\text{mol}$ amount of the pH indicator was dissolved in 50 ml of tetrahydrofuran (THF). A microporous PTFE membrane (47 mm diameter, $0.5 \mu\text{m}$ pore diameter, $60 \mu\text{m}$ thickness, type FHUP04700; Millipore, Eschborn, Germany) was dipped in the solution of the indicator for a few seconds and dried in air at ambient temperature. According to this procedure it was possible to immobilize the hydrophilic indicators in a non-aqueous environment. To remove excess of indicator the membrane was stirred in buffer solution for 12 h. Plexiglas discs were used as a membrane support, and were mounted in a flow cell (Fig. 2).

Apparatus

The reflectance spectra were measured with a UV-visible spectrophotometer (Shimadzu Model UV-2100 with the Integrating Sphere Assembly ISR-260). In this assembly the reflectance of the sensitive membrane is measured relative to a BaSO_4 standard. The membranes showed a transmission of about 0.05%. Reference analyses were performed with an ion chromatograph (Dionex Model 2000i SP with an HPIC-CS1 cation-separating column), an ammonia-selective elec-

trode (Orion Model 95-12) and a spectrophotometric determination kit for ammonium ions (Spectroquant, Merck).

Measurement of waste water

In all instances the concentration of ammonium ions was determined by the standard addition method.

Sensor. All measurements were performed with thermostated solutions ($T = 22^\circ\text{C}$). The sensor was calibrated with four standard solutions at pH 6.8. The pH of the sample was controlled with a pH electrode. The sample solution was pumped through the measuring flow cell until constant signals were reached and the cell was subsequently washed with buffer solutions.

Ion chromatography. The ion chromatograph was calibrated with four standard solutions. The sample was filtered with microporous filter membranes before injection into the chromatograph.

Ion-selective electrode. After adding 0.5 ml of 8.8 mol l^{-1} NaOH solution to 25 ml of a stirred sample solution in a narrow-necked flask, the ammonia-selective electrode was immediately im-

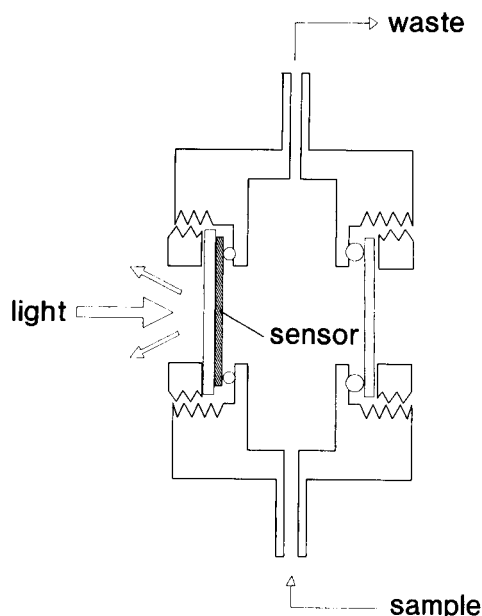


Fig. 2. Measurement assembly. The sensor membrane was fixed in a flow cell on a Plexiglas disc. The reflectance spectra were measured from the rear side.

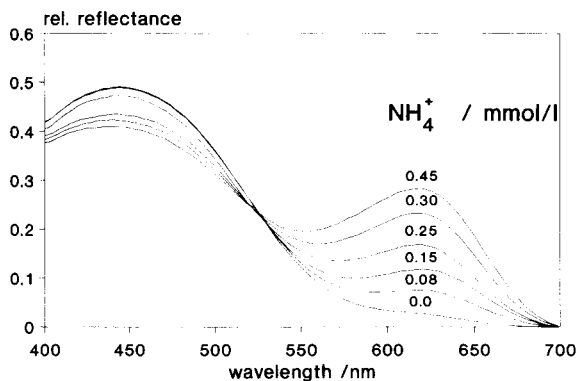


Fig. 3. Reflectance spectra. The pH indicator is deprotonated with increasing ammonium ion concentration which can be followed by the alkaline absorption band. Indicator, Bromocresol Green; temperature, 22°C; pH, 6.8; spectra recorded after 30 min.

mersed and the potential was measured after 5 min.

Spectrophotometric measurement. The Spectroquant assay for ammonium ions is based on the Berthelot reaction. A 5-ml volume of the sample was treated according to the recommended procedure with 600 μl of “ $\text{NH}_4\text{-1B}$ ” (alkaline tartrate reagent) and 150 mg of “ $\text{NH}_4\text{-2B}$ ” (chlorination reagent). After 4 min 100 μl of “ $\text{NH}_4\text{-3B}$ ” (Thymol and catalyst) were added and the absorbance of the indophenol dye was measured at 690 nm against a blank.

RESULTS AND DISCUSSION

Sensor characteristics

According to the principle described (Fig. 1), the concentration of ammonium ions in solution is correlated with the deprotonation of the pH indicator. As can be seen in Fig. 3, an increase in the concentration of ammonium ions (i.e., increasing content of free ammonia in solution) results in an increasing flux of ammonia into the membrane. This can be detected by an increase in the absorbance of the deprotonated form. If the ammonium ion concentration in the solution is decreased (i.e., decreasing content of free ammonia), ammonia diffuses out of the membrane,

TABLE 1

Spectral characteristics of immobilized triphenylmethane derivatives: wavelength (nm) of the isosbestic point and the absorption maxima of the protonated and deprotonated forms of the indicators

	Indicator			
	PXB	BPB	BCG	BCP
Protonated form	450	447	444	432
Deprotonated form	562	595	622	600
Isosbestic point	496	496	521	500

so that the indicator is protonated. This reversible mechanism was only observed if the sensitive membrane was in contact with an aqueous solution. The necessity for water vapour in the non-polar matrix was also found with a previously described ammonia sensor [4]. The wavelength maximum of the alkaline absorbance peak depends on the indicator used. In Table 1 the absorption maxima and isosbestic points for the four different immobilized triphenylmethane derivatives used are given.

The response time of the sensor ranges from 1 to 60 min. This time is dependent on the concentration of ammonium ions (i.e., free ammonia in solution). For an ammonium ion concentration of 0.1 mmol l^{-1} (pH = 6.8; $T = 22^\circ\text{C}$) a response time of 10 min is observed (Fig. 4). When the ammonium ion concentration was lowered, the

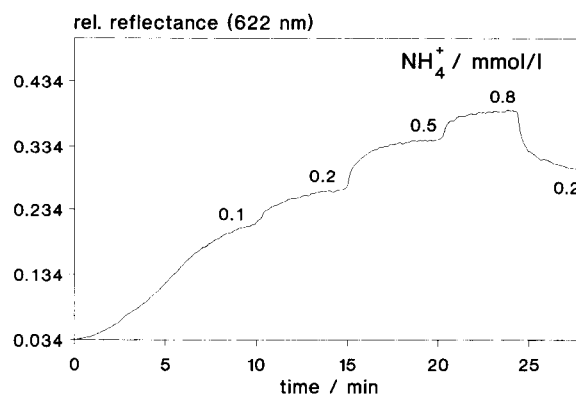


Fig. 4. Response time. The response time of the sensor ranges from 1 to 60 min depending on the concentration of ammonium ions. Indicator, BCG; temperature, 22°C; pH, 6.8; measuring wavelength, 622 nm.

signal decreased. Changing from an ammonium solution to a blank solution (i.e., buffer at pH 6.8) caused a decrease in the signal down to the starting value. At low concentrations the flux of ammonia into the membrane limits the response.

If excess of indicator was removed after immobilization by buffer solutions as described, no loss of indicator was detected within 6 months. During this period sensors with BCG showed no decrease in sensitivity. Leaching of the indicator was only found in solutions with a high ammonium ion concentration. A decrease in the absorbance of the protonated form of about 5% was observed if the sensor was in contact for 24 h with a solution containing as much ammonium ion as is necessary to deprotonate the indicator completely.

The reproducibility of sensor fabrication was determined by measurement of the relative reflectance at 432 nm (protonated form). The relative reflectance varies within 8.9% ($n = 4$). The calibration graph for a sensor measured on different days has a regression coefficient $r = 0.9986$ ($n = 30$; sum of data for four different runs).

Effect of indicator used

First, the pH indicator used has to remain in its protonated form after being dissolved in tetrahydrofuran. It turned out that indicators such as dimethylaminoazobenzene and Methyl Orange were deprotonated after preparing the sensor, which led to irreversible systems. The protonation of the indicator, before or after immobilization, on addition of hydrochloric acid or acetic acid did not overcome this problem. It was found that the use of triphenylmethane derivatives for the described procedure resulted in reversible sensors. The sensitivity should vary with the protonation–deprotonation behaviour of the indicator (i.e., pK_a value of the indicator). Higher sensitivities were observed when more acidic pH indicators were used (Fig. 5). The pK_a values in solution for the tested indicators decrease in the order BCP ($pK_a = 6.0$), BCG ($pK_a = 4.6$), BPB ($pK_a = 3.8$) and PXB ($pK_a = 2.0$). An estimation of the pK_a values of the immobilized indicators gave an increase on these values which is caused by adsorption on a non-polar surface, as reported

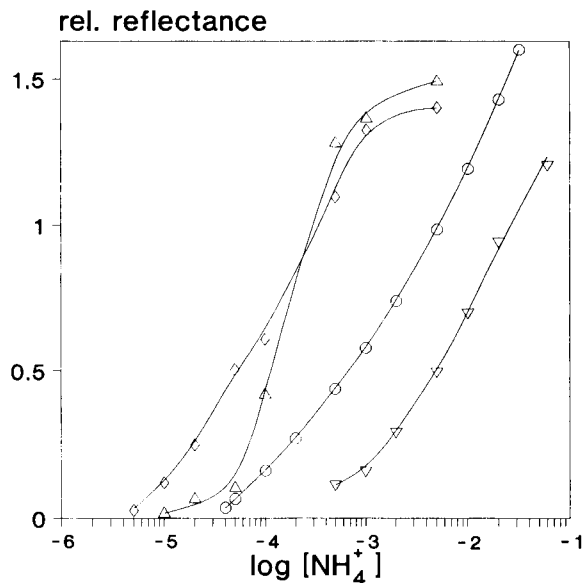


Fig. 5. Influence of pH indicator on sensitivity. The sensitivity of the sensors is dependent on the acidity of the pH indicator used. Most sensitive devices are obtained using acidic pH indicators: \diamond = PXB (562 nm); \circ = BCG (622 nm); \triangle = BPB (600 nm); ∇ = BCP (595 nm).

previously [11]. The sensitivity increased in that order (detection limits for sensors with BCP, BCG, BPB and PXB are 130, 20, 8 and $1 \mu\text{mol NH}_4^+ \text{l}^{-1}$, respectively). For further investigations, sensors with Bromocresol Green (BCG) were used.

Temperature dependence

Temperature affects the equilibria of the buffer components and of ammonium–ammonia. With increasing temperature, the pH of the buffer becomes more acidic and the ammonium–ammonia equilibrium is shifted in the direction of ammonia. Thus the effect of temperature on the free ammonia determined is nearly compensated. With a phosphate buffer solution an increase in temperature from 0 to 50°C would double the content of free ammonia in solution. However, as can be seen in Fig. 6 there is a more distinct temperature dependence of the sensor signal. Therefore, there has to be a further effect of temperature change on the signal. This can be explained by a third equilibrium. This is illus-

trated in Fig. 7, where the titration curves of BCG in aqueous solution at two different temperatures are shown. With increasing temperature the pK_a value is shifted to the acidic region. As already described, this increases the sensitivity of the sensor.

pH dependence

The pH of the sample solution affects the ammonium–ammonia equilibrium. For a constant ammonium ion concentration the signal of the sensor increases with increasing pH, the relative reflectances at a constant ammonium ion concentration of 1 mmol l^{-1} being 0.29, 0.34, 0.37 and 0.43 at pH 6.80, 7.00, 7.25 and 7.65, respectively.

The pH dependence should be corrected by converting the calibration graph for ammonium ion measured at constant pH value into a graph of ammonia versus pH. The ammonia concentration in the sample solution can be calculated from the deprotonation constant for ammonium ($K = 10^{-9.24} \text{ mol l}^{-1}$ at 22°C). With a concentra-

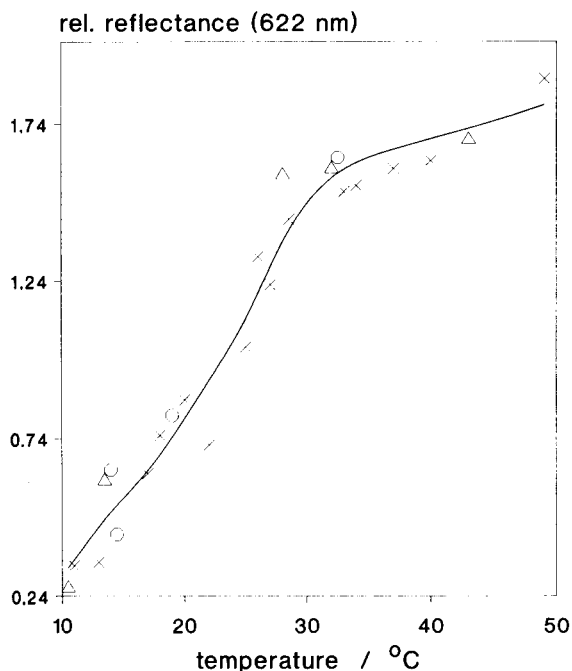


Fig. 6. Influence of temperature on the signal of the sensor. The ammonium ion content in solution was constant (1 mmol l^{-1}). Indicator, BCG; pH, 6.8; temperature, 22°C . The data are from three different runs.

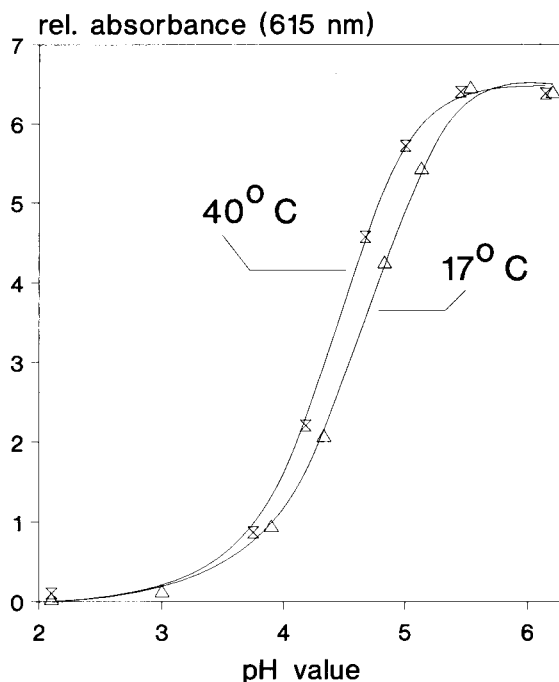


Fig. 7. Influence of temperature on the pK_a value of the pH indicator. The titration curves were measured with an aqueous solution of BCG ($1 \times 10^{-5} \text{ mol l}^{-1}$). The pH scale was corrected with respect to temperature.

tion of ammonia N of a sample at a pH value A the ammonium ion concentration is given by the equation

$$[\text{NH}_4^+] = N \times 10^{-A} \times K^{-1}$$

When the data for ammonium ions are corrected according this equation, it turns out that it is possible to overcome the intrinsic pH sensitivity of the sensor and correct the signal to the real content of ammonium ions in the sample.

Test of the sensor with real samples

The sensor was applied to the analysis of real samples. The samples, consisting of purified waste water, were taken from a tank where the water is collected for release into the municipal wastewater treatment plant. As previous studies have shown [8], acidic compounds such as carbon dioxide or acetic acid do not interfere significantly, hence the determination of ammonium ions in thermostated real samples should be possible with the pH-correction described above. Chemical

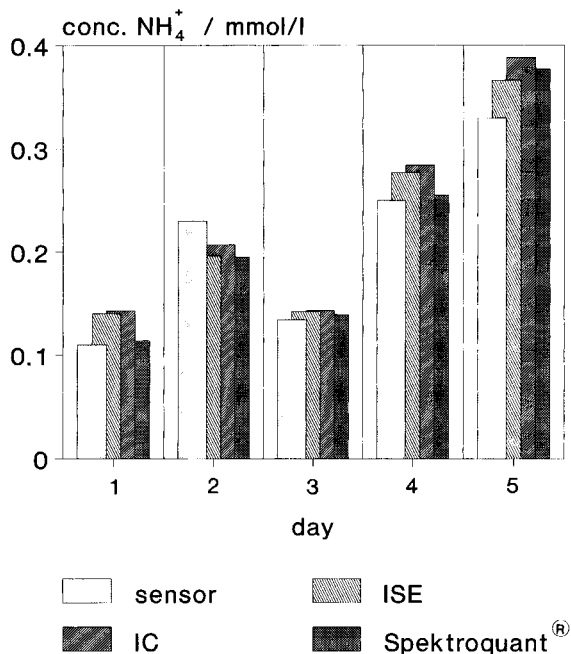


Fig. 8. Measurement of chemical waste water. The ammonium ion content of the chemical waste water (purified sewage) was analysed with the sensor (indicator, BCG) and the results were compared with those obtained by ion chromatography (IC), a spectrophotometric determination kit (Spektroquant) and an ammonia-selective electrode (ISE).

waste water was used that had been chemically sewage treated. The ammonium ion concentration detected with the sensor was compared with the results of analyses of the same samples by ion chromatography, a spectrophotometric assay and with an ammonia-selective electrode (Fig. 8). The results from the sensor correlated well with those obtained by the conventional analytical methods. No interferences from organic pollutants or carbon dioxide were found.

Conclusions

The adsorptive immobilization of pH-sensitive triphenylmethane derivatives on a microporous

PTFE membrane results in an ammonium-sensitive optical sensor. The sensitivity of the sensor varies with the pK_a value of the indicator used. If the pH of the sample is known, its influence on the sensor signal can be eliminated. The optical-chemical sensor is suitable for waste-water analysis without pretreatment of the sample. For an accurate determination the temperature of the sample should be kept constant. It should be possible to determine the concentration of ammonium ions continuously if the optical-chemical sensor is combined with a sensor array with sensors for pH and temperature. Finally, the absorption characteristics of the indicators allow the use of light-emitting diodes as light sources. In combination with optical fibres and other optoelectronic systems it should be possible to develop a microsensing device for the detection of ammonium ions.

REFERENCES

- 1 J.F. Giuliani, H. Wohltjen and N.L. Jarvis, *Opt. Lett.*, 8 (1983) 54.
- 2 Q.S. Wolfbeis and H.E. Posch, *Anal. Chim. Acta*, 185 (1986) 321.
- 3 M.A. Arnold and R.J. Ostler, *Anal. Chem.*, 58 (1986) 1137.
- 4 P. Caglar and R. Narayanaswamy, *Analyst*, 112 (1987) 1285.
- 5 T.D. Rhines and M.A. Arnold, *Anal. Chem.*, 60 (1988) 75.
- 6 S. Muto, A. Ando, T. Ochiai, H. Ito, H. Sawada and A. Tanaka, *Jpn. J. Appl. Phys.*, 28 (1989) 125.
- 7 Q. Zhou, D. Kritz, L. Bonnell and G.H. Sigel, Jr., *Appl. Opt.*, 28 (1989) 2022.
- 8 F.L. Dickert, S.K. Schreiner, G.R. Mages and H. Kimmel, *Anal. Chem.*, 61 (1989) 2306.
- 9 S. Ozawa, P.C. Hauser, K. Seiler, S.S.S. Tan, W.E. Morf and W. Simon, *Anal. Chem.*, 63 (1991) 640.
- 10 J. Reichert, W. Sellien and H.J. Ache, *Fresenius' J. Anal. Chem.*, 337 (1990) 74.
- 11 R. Narayanaswamy and F. Sevilla, III, *Anal. Chim. Acta*, 189 (1986) 365.

Noise analysis of the reflected power signal from a microwave-induced plasma gas chromatographic detector

Rosa M. Alvarez Bolainez and Charles B. Boss

Department of Chemistry, Box 8204, North Carolina State University, Raleigh, NC 27695-8204 (USA)

(Received 5th January 1992; revised manuscript received 13th May 1992)

Abstract

Noise analysis of the signal from a non-optical microwave plasma detector for gas chromatography is presented. The signal in this detector is the reflected microwave power. White noise, low-frequency $1/f$ noise and high-frequency discrete noise were the major noise types observed in the frequency window considered (0–200 Hz). The overall magnitude of the noise spectra exhibited a marked dependence on the degree of coupling of power to the microwave cavity and, to a lesser extent, on the flow-rate of the plasma gas. The noise did not change consistently as the plasma tube cooling-water flow-rate was changed.

Keywords: Gas chromatography; Microwave-induced plasma; Noise spectra; Plasmas

The knowledge of the magnitude and characteristics of the noise phenomena involved in the operation of any analytical system constitutes a powerful tool for the evaluation and improvement of the system's performance. Identification of the noise components and their sources has proved useful in the characterization of several spectrometric sources [1–6]. Evaluation of the inductively coupled plasma (ICP) noise power spectra [3] revealed valuable diagnostic information with respect to nebulizer performance and design and important physical characteristics of the ICP spectral source. Deutsch and Hieftje [4] studied the noise associated with the emission signal from the microwave-induced nitrogen discharge at atmospheric pressure (MINDAP). They found that a dominant noise source is the power supply and indicated that the precision and sensitivity of the MINDAP could be improved through better filtering and stabilization of the microwave source.

Correspondence to: C.B. Boss, Department of Chemistry, Box 8204, North Carolina State University, Raleigh, NC 27695-8204 (USA).

This paper presents a study of the noise associated with the reflected power signal from the highly efficient, atmospheric pressure microwave-induced argon plasma. The use of the reflected power measurement as a means of detection for gas chromatography has been investigated previously [7]. Limits of detection reported in that study are higher than those reported for microwave-induced plasma emission detectors [8–11].

As with any other analytical method, the limit of detection for the reflected power microwave-induced plasma detector is limited by the magnitude of the background noise. Therefore, improvement of the limits of detection might be achieved by a careful analysis of the noise power spectra of the reflected power signals. Since these spectra allow the identification of each noise component and its origin, they help in devising methods for noise reduction or elimination.

Noise magnitude spectra for plasma background reflected power signals were recorded and the major types of noise characterized. The magnitude of the most prominent feature in the spectra was studied as a function of the degree of

coupling of power to the microwave cavity (tuning and matching), plasma gas flow-rate and plasma torch cooling-water flow-rate.

EXPERIMENTAL

Microwave-induced plasma (MIP) system

The atmospheric pressure argon plasma was sustained in the highly efficient microwave TM₀₁₀ resonant cavity [12,13]. The microwave generator employed (KIVA MPG-4-195; KIVA Instrument, Rockville, MD) had a 0–120-W, 2.45-GHz microwave output. A laboratory-built, water-cooled capillary plasma torch [14] was used to contain the plasma discharge. Plasma tube cooling water flow rates of 96–144 ml min⁻¹ were employed. In the experiments to evaluate the effect of the degree of coupling of power to the cavity on the noise spectra of the reflected power signal, a forward power of 32 W was used to maintain the plasma. The same incident power level was also employed in studies considering the effect of plasma gas flow-rate and discharge tube cooling water-flow-rate.

Gas chromatographic system

For the study of the analytical significance of the 0-Hz noise component of the reflected power noise magnitude spectra, a laboratory-built gas chromatograph equipped with an 8 ft × 1/8 in o.d. stainless-steel column coated with 2% OV-1 stationary phase on 100–200-mesh CG-Q packing material was used. The injector temperature was kept at 90°C and the column temperature at 75°C. The argon carrier gas flow-rate through the column was 349 ml min⁻¹. The analyte used was pentane (Fisher Scientific, Pittsburgh, PA).

Data collection system

The reflected power data collection system consisted of a Hewlett-Packard (Palo Alto, CA) 413B power meter equipped with a Hewlett-Packard 478A thermistor mount, which was connected to a Telonic Engineering (Laguna Beach, CA) bandpass filter to discriminate power at 2.45 GHz from other harmonic modes. The signal from the power meter was sent to an Apple II

Plus computer through a 10 gain, LF411CN operational amplifier and a 12-bit, 10-V unipolar A/D converter (Analog Devices AD574A). In the experiments investigating the analytical significance of the 0-Hz feature, data sets containing 512 points were collected using a data collection rate of 73 ms per point. In the experiments to evaluate how the noise spectrum of the reflected power signal is affected by the three parameters studied, a data collection rate of 2.3 ms per point was employed. For each data set a total of 1024 points were acquired.

To calibrate the data collection rates, sine waves from a signal generator, at various known frequencies, were input into the data collection system. The data collection program used allowed different data collection rate settings to be made. For each known frequency, the data collected at three different digitization rates were fast Fourier transformed and the data collection rates were determined from the resulting single-line spectrum.

Argon plasma emission data were also collected. Emission from the highly efficient argon MIP was collected with a fiber-optic cable, dispersed with a monochromator (Series EU-700, Heath, Benton Harbor, MI) and detected with a 1P28A RCA photomultiplier (PMT) tube operated at a bias of -900 V. The PMT anode current was sent to a preamplifier/current-to-voltage converter (Model 244/2441, Keithley Instruments, Cleveland, OH) and then to an LF356N laboratory-built operational amplifier circuit for a 30-fold amplification. The amplified signal was digitized and analyzed with the same equipment as used for the reflected power signals.

For both reflected power measurements and emission measurements, five replicates of time-domain data sets containing 1024 points were collected.

Data processing method

The noise magnitude spectra were obtained by fast Fourier transformation of the time-domain measured reflected power and emission signals. A noise spectra program was written in Turbo Pascal (version 5.0, Boreland International) which

used the fast Fourier transform from the Turbo Pascal Numerical Methods Toolbox (Boreland International) to process the data. The program generates the magnitude and the phase of the frequency-domain data by taking the square root of the sum of the squares of the real and imaginary components of the transformed data and the arctan of the imaginary part divided by the real part, respectively. The magnitude information was then used to obtain magnitude diagrams of the frequency components of the time-domain signals. Only plots of the magnitude information versus frequency were obtained because, for the purpose of this work, the knowledge of the frequencies and magnitudes of the transformed time-domain signals is sufficient for the identification and characterization of the noise components. No effort was made to calibrate the ordinate values of the noise magnitude spectra in terms of units such as root mean square current or voltage. They represent, however, a numerical value proportional to noise magnitude.

With exception of the spectra shown in Fig. 6b, which contains 256 points, all noise magnitude spectra presented here contain 512 points over the given frequency range. In all instances, only half of the collected frequency window was plotted (since the second half is the mirror image of the first).

RESULTS AND DISCUSSION

Reflected power noise magnitude spectra

A typical noise magnitude spectrum for the reflected power background signal is shown in Fig. 1. The time-domain data used to obtain this spectrum were acquired with the microwave cavity being operated under critically coupled conditions with 32 W forward power and 5 μW reflected power. Below 10 Hz, the spectrum displays a $1/f$ dependence of the noise components in addition to several superimposed interference peaks. The 10–200 Hz region of the spectrum shows distinct spikes at discrete frequencies over a white noise baseline.

In the low-frequency region (0–10 Hz) the spectrum is dominated by the $1/f$ feature. As will

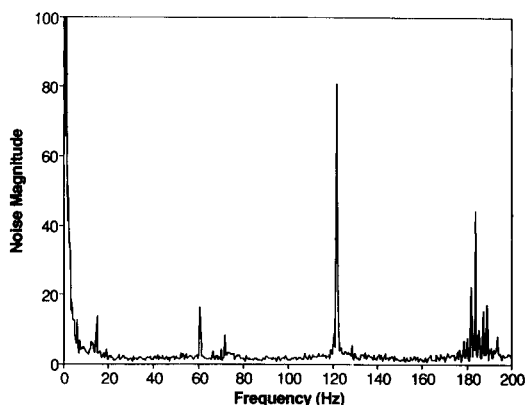


Fig. 1. Noise magnitude spectrum of the reflected power background signal from the highly efficient, atmospheric pressure microwave-induced argon plasma. Time domain data were collected while running the plasma with a forward power of 32 W. The baseline reflected power, as registered by the power meter, was ca. 5 μW . The plasma gas flow-rate and the plasma tube cooling-water flow-rate were 186 and 96 min^{-1} , respectively.

be shown later, the magnitude of the 0-Hz component of the $1/f$ feature is proportional to the d.c. level imposed by the analyte peak area. For this reason, the $1/f$ noise component of the spectrum is not considered in the following ranking of the reflected power measurement noises. The ranking, based on the contribution of each noise feature to the total noise area, places the 120-Hz peak as the most important noise component in the spectrum, followed by the peak at ca. 180 Hz and the 60-Hz peak, with the remaining peaks last.

Over the course of several weeks of experiments, the noise features in the low frequency region (0–10 Hz) and the peaks at 60, 120 and 180 Hz were regularly observed. Discrete noise features at 60 and 120 Hz were identified as power line noise that is always present, to varying extents, in the noise power spectra of emission signals from an inductively coupled plasma [3], a microwave-induced nitrogen discharge at atmospheric pressure [4] and a surfatron helium MIP [6]. It has been suggested that the 60-Hz noise is due to pickup of alternating current [4,6] and that the 120-Hz interference noise is the resulting modulation of the plasma caused by the ripple

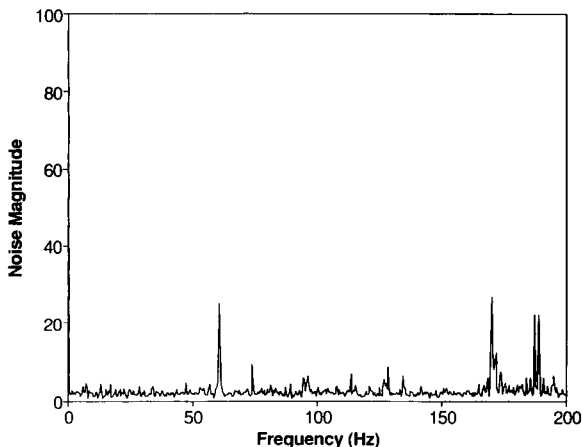


Fig. 2. Noise magnitude spectrum of the detection electronics (blank signal). To collect the time-domain data of the blank signal, the thermistor mount was disconnected from the microwave generator at the bandpass filter so that no microwave power was fed into the power meter.

noise from the microwave power supply filtering circuit [4,6].

The results suggested that the 60-Hz spike originated in the power supply line voltage and that the 120 Hz peak, and the features in the low-frequency region (0–10 Hz), originate in the microwave generator.

Figure 2 shows a noise magnitude spectrum for the detector blank signal. Collection of the detector blank signal was done by removing the thermistor mount from the set-up so that no microwave power was being fed into the power meter. Note that the predominant features in this spectrum are the 60-Hz peak and the groups of peaks in the 160–200-Hz region. The strong 120-Hz noise feature in Fig. 1 is virtually absent in the detector blank signal noise magnitude spectrum (Fig. 2).

Figure 3a and b display the noise magnitude spectrum of a 12-W forward power signal and that of the reflected power signal from a plasma sustained with 12-W incident power, respectively. Comparison of the magnitude spectra for the detector blank signal (Fig. 2) and that for a 12-W forward power signal (Fig. 3a) reveals that the magnitude of the 60-Hz noise component in Fig. 3a is significantly greater than that in Fig. 2,

which suggests that the magnitude of the power line-originated noise features is augmented at the microwave generator.

The existence of the 120-Hz peak in both the forward power (Fig. 3a) and the reflected power noise magnitude spectra (Figs. 1 and 3b), and its absence in the spectrum of the detector blank signal, support the idea of this noise component originating in the microwave generator. This idea was confirmed by the presence of a 120-Hz ripple on the microwave generator output. The ripple from the microwave generator can originate from two sources: the high-voltage supply to the magnetron and the magnetron's filament power supply. To establish the origin of the ripple, its amplitude was measured on the high-voltage side

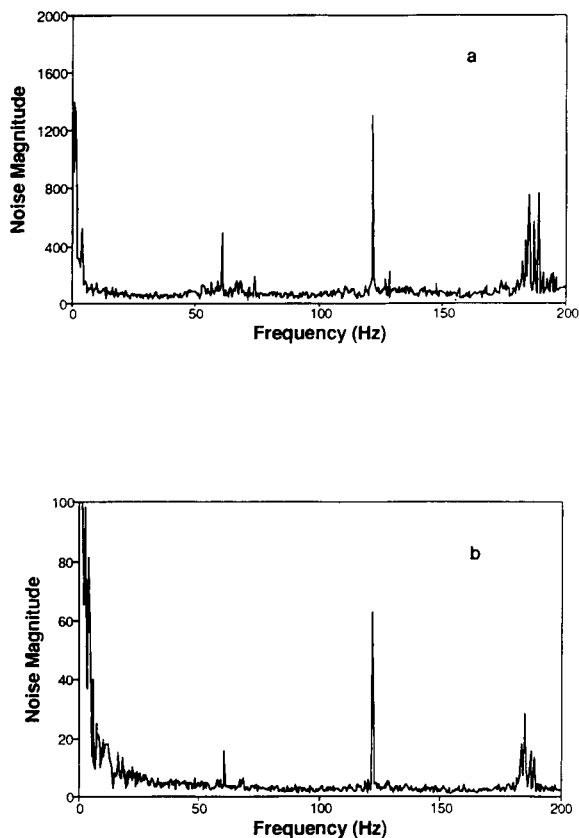


Fig. 3. Noise magnitude spectra of (a) 12-W forward power signal and (b) reflected power signal from a plasma sustained with 12-W input power. The flow-rate of the plasma gas and plasma tube cooling water were the same as in Fig. 1.

of the magnetron supply with both the high-voltage and filament supplies on and with the high-voltage supply off and filament supply on. With the high-voltage supply off, the ripple amplitude decreased by 86% of the value it had with the high-voltage supply on and an output power of 30 W. These results indicate that the most significant source of ripple on the microwave generator employed is the high-voltage power instead of the filament d.c. power supply.

Figure 3b shows the noise magnitude spectrum for the time-domain reflected power signal produced when the MIP system was being operated with 12 W forward power. Note that, although the magnitude of the noise components in the noise spectrum of the reflected power signal is only a fraction of that in the forward power signal spectrum (Fig. 3a), the relative magnitudes of the major peaks in both spectra remain about the same. The similarities in both frequency distribution and characteristics of the noise features among the spectra in Fig. 3a and b indicate that the augmented power line noise components along with the noise features originating in the microwave generator are transmitted to and reflected from the plasma.

The origin of the peaks in the 180–190-Hz frequency range of the noise magnitude spectra for the forward power signal (Fig. 3a) and the reflected power signal (Figs. 1 and 3b) is unknown. Note that, in the same frequency range of the detector blank signal noise spectrum (Fig. 2), there is a group of peaks of significant magnitude. Based on this observation, it is reasonable to believe that some of the noise components in the noise magnitude spectra for the reflected power signal, in this frequency range, originate in the detection electronics, as seen in the spectrum for the detector blank signal. Comparison of Figs. 1–3 also shows that the distribution and relative intensity of such noise components vary from experiment to experiment. In addition to the noise components originating in the detection electronics, it is considered that the multiplet-like noise feature observed in the noise spectrum of the reflected and forward power signals has contributions from the 180-Hz overtone of the 60-Hz noise.

Based on the experimental observations described above, it is concluded that the 60-Hz noise feature in the typical noise magnitude spectrum of the reflected power signal arises from the power line voltage and that the noise feature dominating (120-Hz) the spectrum originates in the microwave power generator.

To investigate whether or not the major noise component (120-Hz peak) in the noise spectra of the reflected power signal is transmitted into the plasma emission signals, the background emission from an argon plasma sustained with 32 W forward power was monitored. Emission measurements were done at 416.89 nm by viewing the plasma both axially and laterally with a fiber-optic probe. The noise magnitude spectra obtained (not shown) provided no evidence of the transmission of the 120-Hz noise component into the optical emission signal.

Mistuning and mismatching effect on noise magnitude spectra

To study the effect of mistuning and mismatching on the noise magnitude spectrum of the reflected power signal, noise spectra were acquired under critically coupled, mistuned and mismatched microwave cavity coupling conditions. The critically coupled condition was achieved by monitoring the reflected power while moving the quartz rods and the coupling probe to the minimum reflected power point. When the loaded cavity is close to the critically coupled condition, movement of the quartz rods affects tuning and movement of the coupling probe affects matching [12]. The mistuned and mismatched conditions were accomplished by sliding one of the tuning rods and the coupling probe in and out from the critically coupled position, respectively.

The effect of mistuning and mismatching on the noise power spectra is illustrated in Fig. 4. The spectra corresponding to the mistuned, critically coupled and mismatched conditions are shown from top to bottom. In each instance, several spectral features are reproducibly present: a $1/f$ noise component with superimposed peaks in the low-frequency region (0–20 Hz) and distinct spikes at discrete frequencies displayed in the high-frequency region (20–200 Hz). Notice

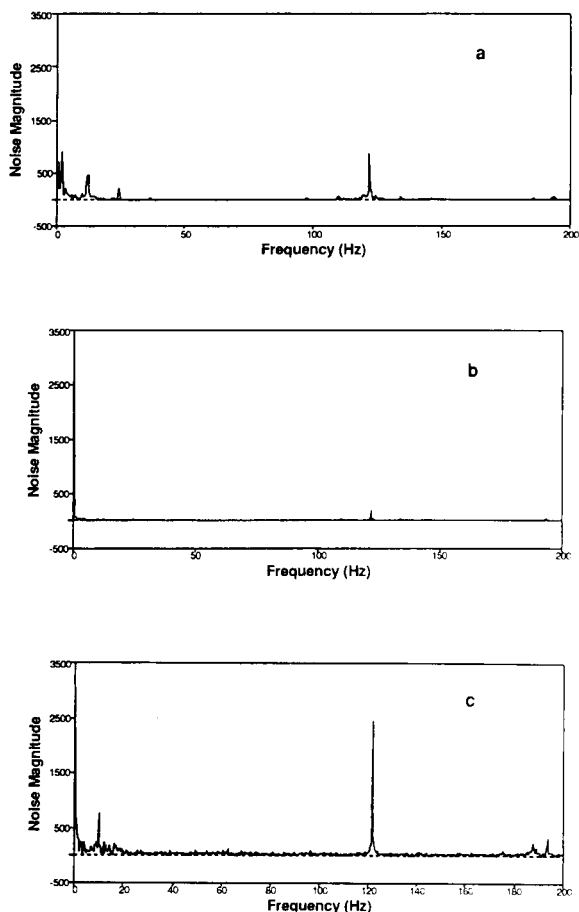


Fig. 4. Noise magnitude spectra of the reflected power background signal obtained with the cavity being (a) mistuned, (b) critically coupled and (c) mismatched. A 32-W forward power plasma with a baseline reflected power of $40 \mu\text{W}$ was employed. The tube cooling-water flow-rate and the plasma gas flow-rate were 125 and 186 ml min^{-1} , respectively.

that the overall noise magnitude increases significantly on going from a critically coupled condition (Fig. 4b) to either a mistuned (Fig. 4a) or mismatched (Fig. 4c) condition. To have a more quantitative appreciation of this effect, the magnitude of the most prominent noise feature (peak at 120 Hz) in the noise power spectra was plotted as a function of the position of the tuning rod and the coupling probe and the results are shown in Fig. 5. Negative numbers on the abscissa on the mistuning plot (Fig. 5a) are indicative of an out-

ward motion of the tuning rod from the critically coupled position, which is represented by the zero position. Positive numbers, on the other hand, indicate inward motion. Similarly, negative numbers on the mismatching plot (Fig. 5b) correspond to coupling probe positions away from the critically coupled point toward the edge of the cavity and positive numbers represent coupling probe positions closer to the center of the cavity.

The results shown here indicate that the magnitude of the 120-Hz noise increases as the cavity is either mistuned or mismatched. In each instance, an increment in the noise magnitude occurs regardless of the direction in which the coupling device (the probe or the tuning rod) is moved away from the critically coupled point,

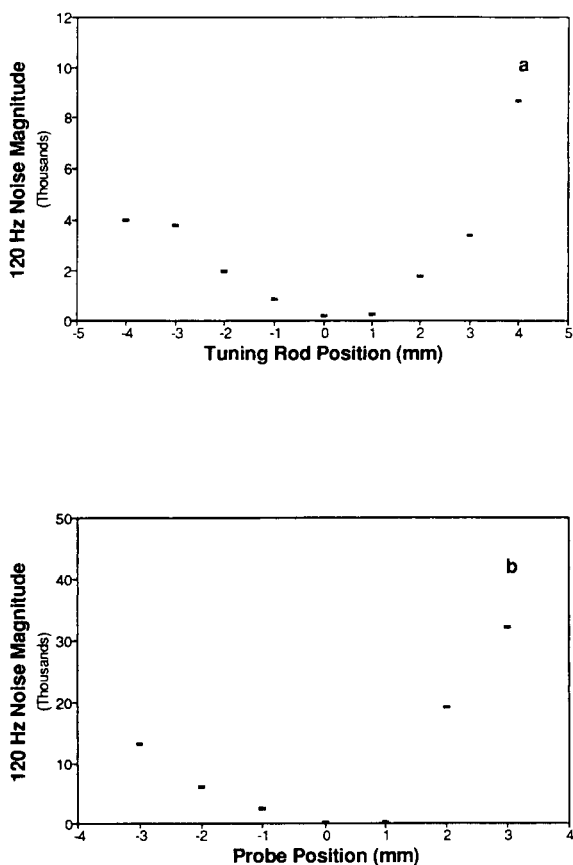


Fig. 5. Effect of (a) mistuning and (b) mismatching on the magnitude of the 120-Hz noise feature.

where a minimum magnitude is observed. This pattern was also observed when the magnitude of the white noise was plotted against the positions of the tuning rod and the coupling probe (plots not shown). The magnitude of the white noise was calculated as the peak-to-peak variation of the baseline frequency domain data lying in the frequency range 150–175 Hz, where no interference peaks are present.

For both noise features (white noise and the 120-Hz peak) the trend described was reproducibly observed from experiment to experiment in the course of several days. The shape of the noise magnitude versus degree of mistuning and mismatching plots, on the other hand, was not reproducible from experiment to experiment.

Effect of plasma gas flow-rate

Plasma gas flow-rates in the range 40–400 ml min⁻¹ were considered to investigate the effect of this experimental parameter on the noise magnitude spectra of the reflected power signal. In this study, the microwave cavity was properly re-tuned and re-matched prior to collecting the time-domain data at each different flow-rate setting. The noise spectra obtained in these experiments were very similar to the typical noise power spectrum shown in Fig. 1. Once again, the major feature in the spectra was the 120-Hz noise peak. Plots of the magnitudes of the white noise feature and the 120-Hz peak versus plasma gas flow-rate (not shown) exhibited similar shapes to those displaying the effect of mistuning and mismatching on the magnitude of the mentioned noise components. Within the gas flow-rate range studied, a minimum noise magnitude was observed at 186 ml min⁻¹. At flow-rate settings higher than 186 ml min⁻¹, the noise magnitude increased with increasing flow-rate; similarly, at flow-rate settings lower than 186 ml min⁻¹, the noise magnitude increased with decreasing flow-rate.

The extent of the increase in the magnitudes of the white noise and the 120-Hz spike produced by moving off the optimum setting was not as great as that produced by either mistuning or mismatching. These results indicate that the magnitudes of those noise components are affected in the same fashion, but to different extents, by the

three experimental parameters studied, suggesting that there is an interdependence among those parameters. Burns [13] showed that the achievement of a tuned and matched condition in the highly efficient microwave cavity depends not only on the position of the coupling probe and the tuning rods but also on the plasma gas flow-rate. He found that higher flow-rates are associated with lower plasma electron number density pro-

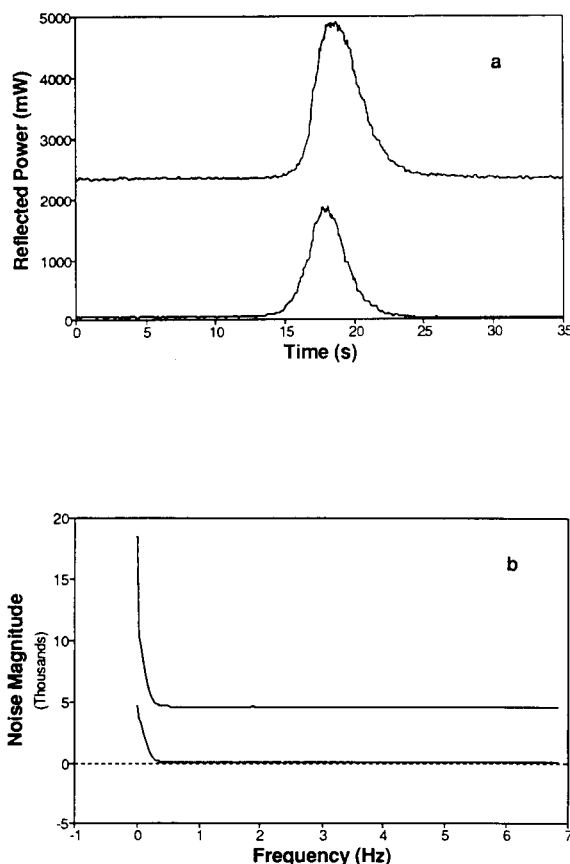


Fig. 6. Relationship between the total area of (a) pentane chromatographic peaks and the magnitude of the 0-Hz noise component of their corresponding (b) noise spectra. The top and bottom chromatographic peaks in (a) correspond to the change in reflected power observed on injection of 0.2 and 0.1 μ l of pentane, respectively. The argon plasma was sustained with a forward power of 30 W. The baseline reflected power registered at the power meter was 0.1 mW. The flow-rates of the plasma tube cooling water and the plasma gas were 144 and 186 ml min⁻¹, respectively.

ductions, which in turn affects the degree of coupling.

Effect of discharge tube cooling-water flow-rate

To investigate the effect of the discharge tube cooling-water flow-rate on the noise magnitude spectrum of the reflected power background signal, noise magnitude spectra were obtained at eleven different cooling-water flow-rates within the range 30–350 ml min⁻¹. In general, the characteristics of the spectrum remained the same at the various flow-rates studied. No trend of the magnitudes of the white noise and the 120-Hz noise feature as a function of cooling-water flow-rate was observed. A possible explanation of this phenomena might be that the effect of this experimental parameter, if any, on the microwave power coupling efficiency is insignificant compared with that exerted by the plasma gas flow-rate and by the degree of tuning and matching of the cavity. Therefore, its effect on the magnitudes of the white noise and the 120-Hz peak, which have shown to be strongly correlated with the degree of coupling, would also be insignificant.

Analytical significance of the 0-Hz noise component

It is believed that the information of the analyte signal from the reflected power measurement is contained in the 0-Hz feature of the noise power spectrum. Figure 6 shows (a) two pentane chromatographic peaks and (b) their corresponding noise power spectra. The upper and lower plots in Fig. 6a correspond to the change in reflected power obtained on the injection of 0.2 and 0.1 μ l of pentane, respectively. The calculated total area (not background corrected) of the whole data set corresponding to the top chromatogram in Fig. 6a (315 832 arbitrary units) was found to be three times larger than that corresponding to the bottom chromatogram (104 117 arbitrary units). Note that the same relationship holds true for the corresponding 0-Hz frequency component in the noise power spectra (Fig. 6b), which suggested that the magnitude of such spectral feature is proportional to the total chromatographic area.

Conclusions

An attempt to isolate the most dominant experimental factors in the generation of the noise associated with reflected power measurements has been made. Noise magnitude spectra covering the 0–200-Hz frequency range showed that the reflected power signal noise is governed by a $1/f$ noise component with superimposed peaks at frequencies below 10-Hz. In the 10–200-Hz frequency range, the spectra are characterized by white noise containing well defined interfering peaks at 60, 120 and 180 Hz, with the 120-Hz spike dominating that region. The deterministic features in the high-frequency range, also observed in the noise power spectra for emission signals from an ICP [3], an MIP [4] and a surfatron helium plasma [6], have been previously explained as arising from the microwave power supply.

The results obtained in conjunction with the findings mentioned above, indicate that fluctuations in the microwave power supply output constitute the main source of the noise present in the reflected power background signal. The results also indicate that the magnitude of such noise is greatly reduced by operating the microwave cavity under critically coupled conditions.

REFERENCES

- 1 Y. Talmi, R. Crosmun and N.M. Larson, *Anal. Chem.*, 48 (1976) 326.
- 2 G.L. Walden, J.N. Bower, S. Nikdel, D.L. Bolton and J.D. Winefordner, *Spectrochim. Acta, Part B*, 35 (1980) 535.
- 3 R.M. Belchamber and G. Horlick, *Spectrochim. Acta, Part B*, 37 (1982) 17.
- 4 R.D. Deutsch and G.M. Hieftje, *Appl. Spectrosc.*, 39 (1985) 19.
- 5 C.A. Monnig and G.M. Hieftje, *Appl. Spectrosc.*, 43 (1989) 742.
- 6 R.L.A. Sing and J. Hubert, *Appl. Spectrosc.*, 44 (1990) 1605.
- 7 R.M. Alvarez Bolainez and C.B. Boss, *Anal. Chem.*, 63 (1990) 159.
- 8 C.I.M. Beenakker, *Spectrochim. Acta, Part B* 32 (1977) 173.
- 9 S.A. Estes, P.C. Uden and R.M. Barnes, *Anal. Chem.*, 53 (1981) 1829.

- 10 S.R. Goode, B. Chambers and N.P. Budin, *Appl. Spectrosc.*, 37 (1983) 439.
- 11 B.D. Quimby and J.M. Sullivan, *Anal. Chem.*, 62 (1990) 1027.
- 12 L.G. Matus, C.B. Boss and A.N. Riddle, *Rev. Sci. Instrum.*, 54 (1983) 1667.
- 13 B.A. Burns, PhD Dissertation, North Carolina State University, Raleigh, NC, 1987.
- 14 R.M. Alvarez Bolainez, M.P. Dziewatkoski and C.B. Boss, *Anal. Chem.*, 64 (1992) 541.

Light emission from bilirubin using the peroxyoxalate chemiluminescence reaction

Nian Wu, William J. Horvath and Carmen W. Huie

Department of Chemistry, University Center at Binghamton, State University of New York, Binghamton NY 13902–6000 (USA)

(Received 27th February 1992; revised manuscript received 27th May 1992)

Abstract

The observation of light emission from bilirubin in an organic solvent as a result of the peroxyoxalate chemiluminescence reaction is reported for the first time. The results presented herein indicate that bilirubin chemiluminescence can be detected in *N,N'* dimethylformamide but not in chloroform, dimethylsulfoxide, or pyridine. To elucidate this phenomenon, the effects of solvent on the chemiluminescence intensity were examined as a function of solvent composition. Furthermore, analytical utilization of the present observation for the determination of bilirubin in biological materials was evaluated. Relative and absolute limits of detection were found to be 8.5 nmol l⁻¹ and 5.0 ng, respectively, and the response was found to be linear at least over three orders of magnitude. Selectivity for the detection of bilirubin in the presence of a number of common interference species was also examined. Finally, the visible spectrum of bovine serum in the blue–green region was obtained using the present chemiluminescence method and was briefly compared with those obtained from absorption and fluorescence methods.

Keywords: Chemiluminescence; Bilirubin; Peroxyoxalate reaction

Bilirubin, a metabolic breakdown product of blood heme, is a highly significant biological molecule. Abnormal concentrations of bilirubin found in human serum or plasma usually signify the presence of a variety of diseases associated with liver dysfunctions, ranging from neonatal jaundice to infectious hepatitis [1,2]. In spite of enormous quantities of work that have been published on bilirubin, the lack of analytical methods capable of accurate determination of bilirubin and/or its conjugates still remains a challenging and difficult problem. This is especially true for routine clinical laboratories which require not only reliable, but also simple and inexpensive methods for the rapid screening and/or quantitation of total bilirubin concentrations as well as

individual bilirubin species present in biological materials.

The simplest method for the determination of bilirubin is perhaps direct absorptimetry in which light absorption by bilirubin in the blue-green region of the visible spectrum is monitored [3]. However, this method is not very sensitive and is prone to interference problems. To increase sensitivity and selectivity, the most widely used approach has been the coupling of bilirubin with suitable diazonium salts to form colored azo derivatives. A large number of papers have been published based on this approach for the absorption measurement of the derivatized bilirubin [1,2]. Unfortunately, all these methods still lack the simplicity and reliability required for routine analysis in clinical laboratories. It has been known for a long time that fluorescence of free bilirubin is difficult to detect due to very efficient radiationless decay paths that return the excited bilirubin

Correspondence to: C.W. Huie, Department of Chemistry, State University of New York – Binghamton, P.O. Box 6000, Binghamton, NY, 13902-6000 (USA).

bin rapidly to the ground electronic state [4]. However, it has been clearly established that relatively strong fluorescence from bilirubin can be detected when bilirubin is bound to albumin or micelles [5,6]. In fact, standard fluorometric methods have been developed for the determination of bilirubin in the presence of albumin [2,7]. However, these methods are not very popular in routine clinical laboratories, perhaps in part due to the complexities and expensive instrumentation associated with fluorometric techniques.

In recent years chemiluminescence has shown great promise as a powerful analytical technique for routine usage in clinical laboratories due to its outstanding analytical advantages in terms of detectability, speed, simplicity and linear dynamic range [8,9]. The peroxyoxalate chemiluminescence reaction, which is based on the oxidation of aryl oxalate esters by hydrogen peroxide in the presence of a suitable fluorescent species (sensitizer), has been successfully exploited for the detection of a number of highly fluorescent sensitizers, e.g., polyaromatic hydrocarbons and urinary porphyrins [10,11]. To the best of our knowledge, the fluorescent emission of bilirubin generated by chemical excitation via a chemiluminescence reaction has never been reported. This is perhaps not surprising since the fluorescent quantum yield (ϕ_{FL}) of bilirubin is extremely low near room temperature ($\leq 10^{-5}$ in water or chloroform). Indeed, whether free bilirubin fluoresces or whether the fluorescence can be detected via excitation at ca. 430 nm has been a subject of controversy [12].

In this paper the observation of light emission from bilirubin dissolved in an organic solvent as a result of the peroxyoxalate chemiluminescence system involving the reaction of bis(2,4,6-trichlorophenyl)oxalate and hydrogen peroxide is reported for the first time. The effects of various solvents on the chemiluminescence intensity were briefly investigated. To evaluate the analytical potential of the present chemiluminescence method for the determination of bilirubin, the limit of detection (LOD), selectivity, and linear dynamic range were examined. Furthermore, the total bilirubin contents in a real biological sample (bovine serum) were determined using the pre-

sent chemiluminescence method and were compared with those obtained from absorption and fluorescence techniques.

EXPERIMENTAL

Materials

Bis(2,4,6-trichlorophenyl)oxalate (TCPO) was synthesized and purified by the procedure of Mohan and Turro [13]. Hydrogen peroxide (30%) was obtained from Fisher (Springfield, IL). HPLC grade ethyl acetate and acetonitrile were used as the solvents for TCPO and H_2O_2 , respectively. Hemoglobin, protoporphyrin, β -carotene, riboflavin, bovine serum, benzo[*a*]pyrene and phosphoric acid were all purchased from Sigma (St. Louis, MO).

Bilirubin (unconjugated bilirubin IX) and its conjugate, bilirubin ditaurite, were obtained from US Biochemical (Cleveland, OH) and were used as received since their extinction coefficients were in agreement with the accepted values for pure pigments and, furthermore, the thin-layer chromatography on silica gel showed bilirubin and bilirubin ditaurite to migrate as single spots without the presence of any detectable impurities [14]. *N,N'*-dimethylformamide, pyridine, chloroform and dimethylsulfoxide were purchased from Fisher and used as solvents for bilirubin or bilirubin ditaurite. Stock solutions were made up just before each experiment and used immediately.

Methods

Absorption spectra. Direct absorptimetry of bovine serum samples were carried out using a 8451A diode-array spectrophotometer (Hewlett Packard, Palo Alto, CA). Sample preparation procedures for the extraction of total bilirubin from bovine serum were as follows: 200 μ l of bovine serum was placed in a centrifuge tube containing 4 ml of the solvent system: ethylacetate–DMF–pyridine 15.00:84.99:0.01 (v/v/v) and was shaken vigorously for 30 s. The tube was then placed in a centrifuge and run at 2500 r.p.m. (950 g) for 2 min. The supernatant (3 ml) was then transferred to a 1-cm cell and the absorbance spectrum was measured.

Fluorescence and chemiluminescence spectra. The fluorescence spectra were recorded using an SLM–Aminco (Urbana, IL) Model 8000 photon-counting spectrofluorometer. The excitation wavelength was set at 435 nm and the bandpass was set at 16 nm. For the measurement of fluorescence spectra of benzo-[a]pyrene appropriate amounts of benzo[a]-pyrene were dissolved in the various solvents studied and placed in a 1-cm quartz cell. For the measurement of the bilirubin spectra from bovine serum, sample preparation and measurement procedures were adopted from a standard fluorescence method [2]. In a 1-cm quartz cell, 50 μ l of bovine serum was added and mixed with 0.5 ml of phosphoric acid. After 5 min, 3 ml of water was added to the cell and mixed. Procedures for obtaining the spectra of the blank were the same except that 50 μ l of water was added instead of bovine serum.

The chemiluminescence spectra were also recorded using the SLM–Aminco Model 8000 photon-counting spectrofluorometer but with the light source turned off. Emission slit was set for a bandpass of 16 nm. A spectrum was obtained for a single scan by photon-counting for 0.5 s at intervals of 5 nm. Five scans were averaged for each spectrum reported. For the measurement of the chemiluminescence spectra, appropriate amounts of benzo[a]pyrene, bilirubin or bilirubin ditaurite standards dissolved in a particular solvent were mixed with 1 ml of 1–5 mM TCPO in a 1-cm quartz cell; 3–5% H_2O_2 (1 ml) was then added to generate chemiluminescence emission. For the measurement of chemiluminescence spectra of total bilirubin from bovine serum, procedures used in the absorption experiment for the extraction of total bilirubin from 100 μ l bovine serum was performed. Afterward, 1 ml of 2 mM TCPO was added to 2 ml of the supernatant in a 1-cm quartz cell. A spectrum was recorded after the addition of 1 ml of 5% H_2O_2 . The chemiluminescence spectra of the blanks were obtained similarly but without the presence of bilirubin standards or bovine serum.

Quantitative chemiluminescence measurements.

A home-built luminometer was used for the recording of chemiluminescence intensity as a function of time. Basically, it consists of a 5-ml

glass test tube (sample cell) housed within a light-tight compartment. Chemiluminescence emission from the sample cell passes through a filter and a series of focusing lenses before reaching a photomultiplier tube (R928, Hamamatsu, Bridgewater, NJ). A 10-nm bandpass filter centered at 520 nm (Corion, Holliston, MA) was used to isolate chemiluminescence emission from bilirubin. The photocurrent was fed to a picoammeter (Oriel, Stratford, CT) and the output signal was filtered through a 1.0 s time constant before recording on a strip-chart recorder. To make measurements of chemiluminescence intensity of bilirubin, 1 ml of the bovine serum extract or bilirubin standards dissolved in DMF–pyridine was mixed with 1 ml of 2 mM TCPO in the sample cell and was stirred continuously with a magnetic stir bar; 1 ml of 3% H_2O_2 was then added to the sample cell to generate chemiluminescence emission

RESULTS AND DISCUSSION

Figure 1 shows the chemiluminescence spectrum of bilirubin dissolved in *N,N'*-dimethylformamide (DMF). It is important to note that the spectral distribution of chemiluminescence is sim-

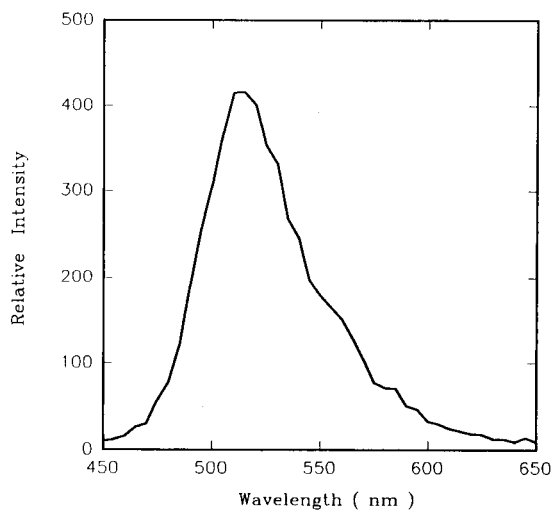


Fig. 1. Chemiluminescence spectrum of 4.5×10^{-4} M bilirubin in DMF. Concentrations of TCPO and H_2O_2 were 5×10^{-3} M and 5% (v/v), respectively.

ilar to the fluorescence spectra of bilirubin reported in the literature [5,6], suggesting that the chemiluminescence emission may also be a result of a radiative transition of electrons from the first singlet excited electronic state to the ground state of bilirubin. It can be seen that the chemiluminescence maximum of bilirubin is centered at ca. 512 nm, which is within the 505–545 nm range reported for the fluorescence maxima of bilirubin bound to micelles or albumin. It has been suggested that the variation in the fluorescence maximum may be due to differences in the conformation and/or ionization of bilirubin in these different environments [12].

The relative fluorescence intensity of bilirubin was measured for a number of organic solvents and the results were as follows: pyridine > dimethylsulfoxide (DMSO) > DMF > chloroform (CHCl_3). It was observed that the fluorescence of bilirubin in chloroform (ϕ_{FL} ca. 10^{-5}), for which an intramolecularly hydrogen-bonded form of bilirubin is known to predominate [15], was barely detectable above the Raman scattering of the solvent. The fluorescence intensity increased slightly when bilirubin was dissolved in the other three organic solvents (ϕ_{FL} ca. 10^{-4}). These results are similar to those reported in the literature [16], which indicated that fluorescence of bilirubin usually increases with increasing polarity, dielectric constant, and basicity of the solvent, probably due to more effective disruption of the intramolecular hydrogen bonding and/or ionization of bilirubin. The same solvent series was employed for the observation of chemiluminescence from bilirubin. It was surprising to find that chemiluminescence was detected in DMF and not in the other solvents studied. In order to understand this phenomenon, it is important to remember that in the peroxyoxalate chemiluminescence reaction the luminescence intensity is directly proportional to the product of the efficiency of chemiluminescence (ϕ_{CL}) and rate of the reaction, and ϕ_{CL} is the product of the efficiency of chemical excitation (ϕ_{CE}) and ϕ_{FL} [17]. Thus, it is possible that a relatively large ϕ_{FL} of bilirubin in a particular solvent may be offset by a low ϕ_{CE} and/or slow kinetics, leading to an undetectable luminescence intensity. To investigate

this possibility, we have studied the effects of this solvent series on the relative fluorescence and chemiluminescence intensity of benzo[*a*]pyrene because this probe molecule gave comparable relative fluorescence intensity over the above range of solvents and thus allowed for a qualitative evaluation of solvent effects on ϕ_{CE} and/or rate of the reaction.

The relative fluorescence intensity of benzo[*a*]pyrene (normalized intensity) has the following trend: DMSO (1.00) > DMF (0.60) > CHCl_3 (0.35) > pyridine (0.25), while the trend for the relative chemiluminescence intensity was very different: CHCl_3 (1.00) > DMF (0.40) > DMSO (0.08) > pyridine (0.06). These results suggest that DMSO and pyridine could be more effectively quenching the ϕ_{CE} and/or slowing down the kinetics of the peroxyoxalate chemiluminescence reaction relative to DMF or CHCl_3 . Further evidence of this postulation are shown in Fig. 2a which shows that the chemiluminescence intensity of benzo[*a*]pyrene in CHCl_3 increased slightly with the presence of small amounts of DMF (probably due to an increase in the ϕ_{FL}) but began to decrease significantly after a certain threshold concentration of DMF (ca. 8%) was exceeded. With the presence of DMSO or pyridine in CHCl_3 it can be seen that the chemiluminescence intensity decreased dramatically as the percentage of CHCl_3 in the solution became smaller, suggesting that pyridine and DMSO severely quench the ϕ_{CE} and/or decrease the rate of the reaction. It has been suggested that the peroxyoxalate reaction mechanisms probably involve nucleophilic attack of the hydrogen peroxide on the oxalate carbonyl [17]. Thus, it is possible that nucleophilic solvents such as DMF, DMSO and pyridine could also attack the chemiluminescence reagent and consume it in non-chemiluminescence side reactions. However, other factors such as interference of the donor-acceptor complex formation and/or inhibition of electron transfer due to solvent effects are also possible [17–19].

The question of why chemiluminescence of bilirubin can only be detected in DMF among the solvent series studied can be partly addressed in terms of the balance between efficiency and ki-

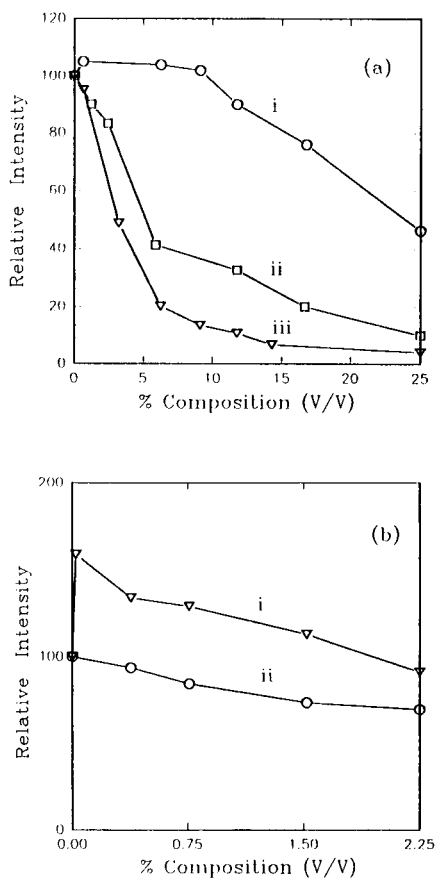


Fig. 2. (a) Chemiluminescence intensity of 2.4×10^{-6} M benzo[a]pyrene as a function of percentage of (i) DMF, (ii) DMSO and (iii) pyridine present in chloroform. Concentrations of TCPO and H_2O_2 were 1×10^{-3} M and 3% (v/v), respectively, and (b) chemiluminescence intensity of 4.0×10^{-5} M bilirubin as a function of percentage of (i) pyridine and (ii) DMSO present in DMF. Concentrations of TCPO and H_2O_2 were 5×10^{-3} M and 5% (v/v), respectively.

sent experimental conditions, no chemiluminescence emission was detectable from the mixing of chemiluminescence reagents with the solvents studied without the presence of bilirubin (i.e. the blanks); however, at higher detection sensitivity, a small amount of background chemiluminescence signal can be detected from the blanks, which has been shown to occur for a variety of aryl oxalate esters [20].

Figure 2b shows that the chemiluminescence intensity of bilirubin in DMF increased in the presence of small amounts of pyridine but not with the addition of DMSO. The addition of small amounts of pyridine may catalyze the peroxyoxalate chemiluminescence reaction [17] and/or cause an increase in the chemiluminescence intensity by effectively slowing down the twisting motion of bilirubin and thereby increasing its ϕ_{FL} [6,16,21]. Furthermore, it has been suggested that exciplex formation may occur between bilirubin and the solvent molecule in the presence of pyridine, leading to possible enhancement in the rate of excitation of the peroxyoxalate chemiluminescence reaction [16,22]. With further increases in the pyridine concentration above ca. 0.01% in DMF, however, it can be seen that the chemiluminescence intensity of bilirubin begins to decrease, probably due to the negative effect of pyridine on the ϕ_{CE} and/or rate of the reaction.

Figure 3a shows that chemiluminescence signal of bilirubin near the LOD in the solvent system of DMF–pyridine 99.99:0.01 (v/v). The solvents chosen for TCPO and H_2O_2 were ethyl acetate and acetonitrile, respectively, since these solvents have been shown to provide the optimum experimental performances in terms of solubility, stability, chemiluminescence intensity and lifetime for the measurement of a number of fluorophores in static systems [18,23]. Based on a signal-to-noise ratio (S/N) of three, the absolute and relative LODs calculated from calibration plots using peak heights as shown in Fig. 3a were found to be 5.0 ng and 8.5 nM, respectively. Calibration plots drawn for a series of bilirubin standards exhibited linearity from the LOD up to 20 μM and the corresponding linear regression constant was 0.997.

netic parameters for this system. For bilirubin in CHCl_3 it is possible that the ϕ_{FL} of bilirubin (ca. 10^{-5}) is too low to yield any detectable chemiluminescence signals. On the other hand, bilirubin in DMSO and pyridine may reduce the ϕ_{CE} and/or rate of the reaction to such an extent that luminescence intensity becomes undetectable. However, it appears that bilirubin in DMF provides an optimum balance between ϕ_{FL} , ϕ_{CE} and/or kinetics among the solvent series studied, allowing the chemiluminescence of bilirubin to be detected. It should be noted that under the pre-

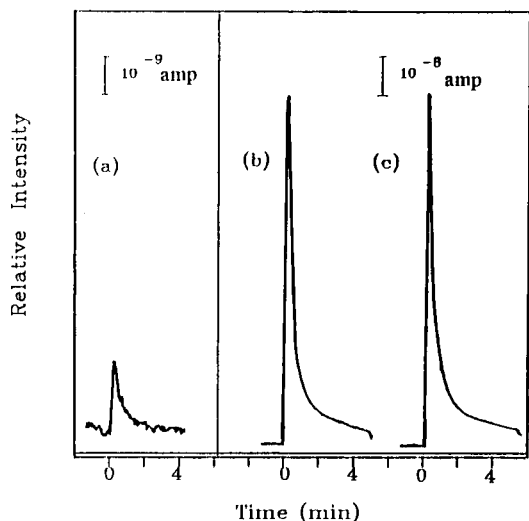


Fig. 3. Chemiluminescence intensity as a function of time: (a) 25 nM bilirubin, (b) 6.0 μM bilirubin and (c) 6.0 μM bilirubin mixed with 20 mg l^{-1} hemoglobin, 600 $\mu\text{g l}^{-1}$ β -carotene, 35 $\mu\text{g l}^{-1}$ protoporphyrin and 20 $\mu\text{g l}^{-1}$ riboflavin in 99.99:0.01 (v/v) of the solvent system: DMF–pyridine. Concentrations of TCPO and H_2O_2 were 2×10^{-3} M and 3% (v/v), respectively.

Considering the relatively low ϕ_{FL} of bilirubin in DMF and pyridine (ca. 10^{-4}) and the effects of solvents on ϕ_{CE} and/or rate of the reaction, the LODs that can be achieved using the present chemiluminescence methods are quite good. For comparison an absolute LOD of 134 pg has been reported for albumin-bound bilirubin using a laser-based fluorometric technique [6]; a laser-based photothermal technique for the detection of free bilirubin adsorbed on thin-layer chromatographic plates, yielded an absolute LOD of 2.5 ng [24]. It should be noted that the normal concentrations of bilirubin present in human serum or plasma are relatively high, which falls in the range of 6–17 μM [2]. Figure 3b shows that with a bilirubin concentration of 6.0 μM spiked into the DMF–pyridine solvent system, the chemiluminescence signal is significantly higher than the background level, suggesting that the sensitivity of the present chemiluminescence method should be more than sufficient for the detection of elevated levels of bilirubin in human serum or plasma.

The selectivity of this chemiluminescence method for the detection of bilirubin in the presence of a number of common interference species in serum or plasma was examined. Figure 3c shows the chemiluminescence signal of 6.0 μM of bilirubin in the presence of a mixture of hemoglobin, protoporphyrin, β -carotene and riboflavin. The concentrations of these interference species as shown in Fig. 3c are representative of the normal concentrations usually found in human serum or plasma [25]. It can be seen that the chemiluminescence signal of bilirubin with and without the presence of these common interference species as shown in Fig. 3b and c were about the same, suggesting that these particular species present in normal concentrations in serum should have negligible effects on the chemiluminescence detection of bilirubin using the present approach.

The threshold concentrations at which the above interference substances could cause a noticeable variation in the chemiluminescence intensity ($\pm 3\%$) of bilirubin were determined by spiking these species individually into the solvent system. Hemoglobin and β -carotene are known to cause interference problems when using direct absorptimetry for the determination of bilirubin in plasma [2]. Fortunately, it was found that hemoglobin is highly insoluble in DMF and there was no noticeable change in the chemiluminescence intensity of bilirubin even when concentrations of hemoglobin ten times larger than the normal concentration were present. However, β -carotene in large excess (4000 $\mu\text{g l}^{-1}$) did consistently cause a decrease in the maximum chemiluminescence intensity of 6.0 μM of bilirubin. This is not surprising since there is an overlap between the emission band of bilirubin and the absorption band of β -carotene at ca. 510 nm. On the other hand, it is interesting to note that protoporphyrin and riboflavin present in relatively large concentrations (440 $\mu\text{g l}^{-1}$ and 900 $\mu\text{g l}^{-1}$, respectively), as compared to their normal concentrations in human serum, were shown to cause a consistent increase in the chemiluminescence intensity of 6.0 μM of bilirubin. This is, again, not surprising since these are highly fluorescent species capable of emitting relatively intense radiation in the yel-

low-red region of the visible spectrum. In fact, chemiluminescence emission from urinary porphyrins generated from the peroxyoxalate chemiluminescence system has already been demonstrated to be a sensitive and selective technique for the screening of various forms of porphyrias in clinical laboratories [11].

Comparisons were made between the present chemiluminescence method and absorption and fluorescence methods for the determination of total bilirubin concentration, i.e., bilirubin and its conjugate, in bovine serum. It should be noted that the normal total bilirubin concentration in bovine serum falls in the range of 1 to 5 mg l⁻¹, consisting mostly of bilirubin (unconjugated form) [26]. Figure 4a shows an absorption spectrum of a

bovine serum sample. It can be seen that a fairly diffuse band barely distinguishable from the background was observed between 400 and 500 nm. Although it is known that bilirubin absorbs in the range 420–460 nm, it is difficult to tell whether or not this weak absorption band, as shown in Fig. 4a was due to absorption by bilirubin and/or interference species present in the serum. This result is consistent with those reported in the literature which stated the lack of sensitivity of direct absorptimetry for the determination of bilirubin in human serum at the borderline level (ca. 4 mg l⁻¹) [2].

To increase the detection sensitivity, a standard fluorescence method [2] was employed for the measurement of the fluorescence spectrum of

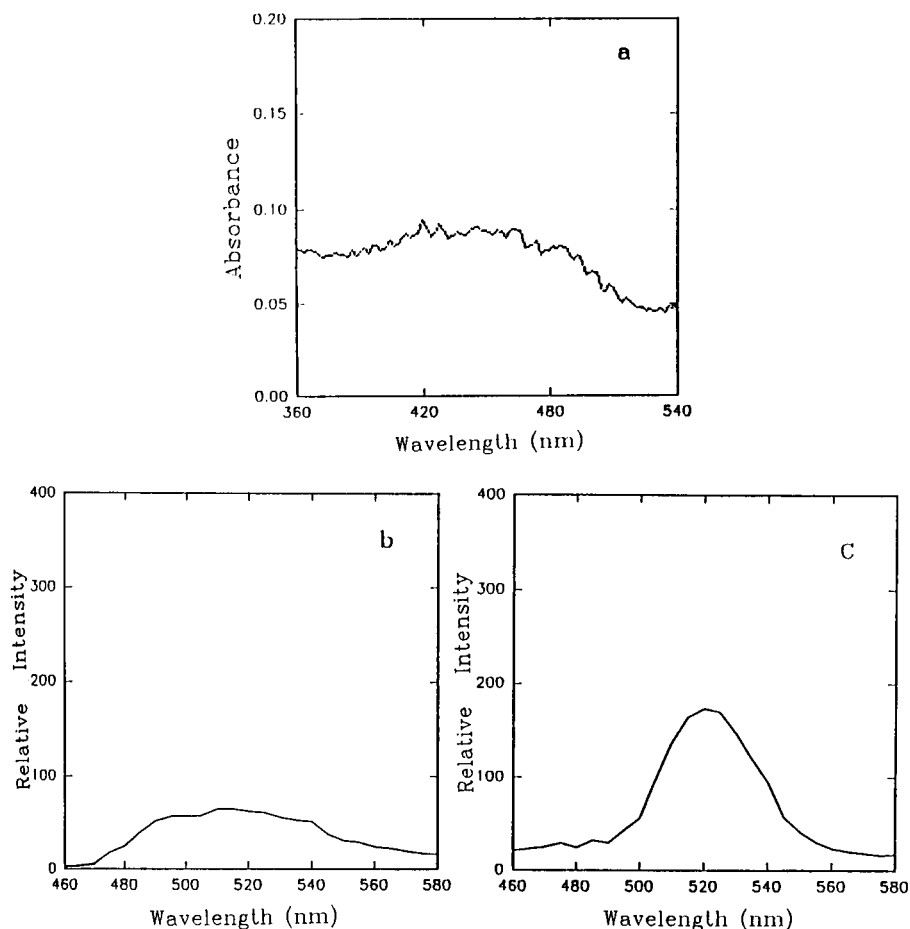


Fig. 4. Spectrum of bovine serum: (a) absorption, (b) fluorescence, and (c) chemiluminescence.

bovine serum as shown in Fig. 4b. For comparison, Fig. 4c shows the chemiluminescence spectrum of the bovine serum sample dissolved in a solvent system of ethyl acetate–DMF–pyridine 15.00:84.99:0.01 (v/v/v). Ethyl acetate was added to accelerate the precipitation of the proteins present in the serum. It is interesting to see that the chemiluminescence spectrum of the bovine serum is very similar to that obtained from the bilirubin standard as shown in Fig. 1, suggesting that the chemiluminescence emission from the bovine serum was probably due to bilirubin and its conjugate present in the sample. It should be noted that the chemiluminescence spectrum of conjugated bilirubin (bilirubin ditaurite) has also been obtained using the present chemiluminescence method and it was found that the chemiluminescence intensity and spectral distribution were similar to those obtained from bilirubin (unconjugated), except there was a slight red shift of about 20 nm in the peak maximum for conjugated bilirubin. Similar shifts in peak maxima can also be observed for fluorescence spectra of bilirubin and bilirubin ditaurite, which has been proposed as a mean for the differential determination of these two forms of bilirubin in serum [27]. By measuring the chemiluminescence intensity of the bovine serum sample and a series of bilirubin standards at ca. 520 nm, the total bilirubin concentration in bovine serum was calculated to be 2.7 mg l^{-1} , which is consistent with the total bilirubin concentration range normally found in bovine serum ($1\text{--}5 \text{ mg l}^{-1}$).

In comparing the fluorescence and chemiluminescence spectra of the bovine serum sample as shown in Figs. 4b and c, respectively, it can be seen that the locations of the peak maxima were about the same for both methods and the magnitudes of the fluorescence and chemiluminescence signals were comparable. However, an important difference is that in the fluorescence method a relatively large background signal was obtained from the blank, i.e., phosphoric acid and water, probably due to the combination of emission from fluorescent impurities and Raman scattering from the blank. To obtain a fluorescence spectrum as shown in Fig. 4b, subtraction of background from

the sample spectra was necessary. It is interesting to note that the bandwidth of the fluorescence spectrum was slightly broader than that of the chemiluminescence spectrum, suggesting that there could be fluorescence contributions from fluorescent interference species present in the bovine serum sample such as riboflavin and flavin-type compounds, which are capable of emitting relatively intense radiation in the spectral region between 450 and 600 nm [28].

In summary, the present study shows for the first time that the chemiluminescence of bilirubin can be detected in an organic solvent system using the peroxyoxalate chemiluminescence reaction. The effects of solvents on the ϕ_{FL} , ϕ_{CE} and/or rate of the reaction appear to play an important role in the optimization of the chemiluminescence intensity of bilirubin. Although the sensitivity of the present chemiluminescence method does not appear to be significantly better than the standard fluorescence method, it should be more than adequate for the determination of elevated levels of total bilirubin concentrations in human serum or plasma. When compared to fluorescence methods, the major advantages of the present chemiluminescence method are simplicity, wide linear dynamic range, less expensive instrumentation and perhaps better selectivity, which are important criteria for routine usage in clinical laboratories. Further investigations of the selectivity of the present chemiluminescence method for the detection of bilirubin should be performed. It may be possible to modify the present chemiluminescence detection scheme for the rapid screening of total bilirubin concentration in human serum or plasma by direct injection of samples into a flow injection analysis system. If quantitation of individual bilirubin species is required, the use of high-performance liquid chromatography in conjunction with chemiluminescence detection could potentially offer a number of unique analytical advantages [29].

We would like to thank Professor Alistair J. Lees for helpful discussions.

REFERENCES

- 1 J.R. Chowdhury, A.W. Wolkoff and I.M. Arias, in C.R. Scriver, A.L. Beaudet, W.S. Sly and D. Valle (Eds.), *The Metabolic Basis of Inherited Diseases*, Vol. 1, Part 8, McGraw-Hill, New York, 1989, pp. 1367–1408.
- 2 M. Roth, in H. Ch. Curtius and M. Roth (Eds.), *Clinical Biochemistry: Principles and Methods*, Vol. H, Part XII, Walter de Gruyter, New York, 1974, pp. 1372–1389.
- 3 D. White, G.A. Haidar and J.G. Reinhold, *Clin. Chem.*, 4 (1958) 211.
- 4 A.A. Lamola, *J. Invest. Dermatol.*, 31 (1981) 114.
- 5 R.F. Chen, *Arch. Biochem. Biophys.*, 160 (1974) 106.
- 6 J.H. Aiken and C.W. Huie, *Anal. Lett.*, 24 (1991) 167.
- 7 M. Roth, *Clin. Chim. Acta*, 17 (1967) 487.
- 8 A. Townshend, *Analyst (London)*, 115 (1990) 495.
- 9 L.J. Kricka, *Clin. Chem.*, 37 (1991) 1472.
- 10 K. Sigvardson and J.W. Birks, *Anal. Chem.*, 55 (1983) 432.
- 11 S. Albrecht, H. Brandl and E. Köstler, *Z. Klin. Med.*, 23 (1989) 2071.
- 12 A. Cu, G. Bellah and D.A. Lightner, *J. Am. Chem. Soc.*, 97 (1975) 2579.
- 13 A.G. Mohan and N.J. Turro, *J. Chem. Educ.*, 51 (1974) 528.
- 14 A.F. McDonagh and F. Assisi, *Fed. Eur. Biochem. Soc. Lett.*, 18 (1971) 315.
- 15 J. Fog and E. Jellum, *Nature (London)*, 198 (1963) 88.
- 16 J.J. Lee and G.D. Gillispie, *Photochem. Photobiol.*, 33 (1981) 757.
- 17 M.M. Rauhut, *Acc. Chem. Res.*, 2 (1969) 80.
- 18 R. Weinberger, *J. Chromatogr.*, 314 (1984) 155.
- 19 C. Gooijer, P. van Zoonen, N.H. Velthorst and R.W. Frei, *J. Bioluminesc. Chemiluminesc.*, 4 (1989) 479.
- 20 B. Mann and M.L. Grayeski, *Anal. Chem.*, 62 (1990) 1532.
- 21 C.D. Tran and G.S. Beddard, *J. Am. Chem. Soc.*, 104 (1982) 6741.
- 22 C.D. Tran and G.S. Beddard, *Biochim. Biophys. Acta*, 687 (1981) 497.
- 23 S. Kobayashi and K. Imai, *Anal. Chem.*, 52 (1980) 424.
- 24 C.D. Tran, *Appl. Spectrosc.*, 41 (1987) 512.
- 25 D. O'Brien and D.O. Rodgeron, in C.H. Kempe, H.K. Silver and D. O'Brien (Eds.), *Current Pediatric Diagnosis and Treatment*, 3rd edn., Lange Medical Publications, Los Altos, CA, 1974, pp. 987–994.
- 26 C.E. Cornelius, in J.J. Kaneko and C.E. Cornelius (Eds.), *Clinical Biochemistry of Domestic Animals*, Vol. 1, Academic Press, New York, 1970, pp. 166–167.
- 27 J. Fog and A.F. Bakkeh, *Scand. J. Clin. Lab. Invest.*, 20 (1967) 88.
- 28 O.S. Wolfbeis and M. Leiner, *Anal. Chim. Acta*, 167 (1985) 203.
- 29 A.J. Weber and M.L. Grayeski, *Anal. Chem.*, 59 (1987) 1452.

Flow injection and liquid chromatographic postcolumn detection of amino acids by mimetic peroxidase-catalysed chemiluminescence reaction

Yun-Xiang Ci, Jian-Ke Tie, Qin-Wei Wang and Wen-Bao Chang

Department of Chemistry, Beijing University, Beijing 100871 (China)

(Received 3rd March 1992; revised manuscript received 12th May 1992)

Abstract

Four amino acids were determined on the basis of the finding that the catalytic activity of mimetic peroxidase (metalloporphyrin) in the chemiluminescence reaction between luminol and hydrogen peroxide is inhibited in the presence of an amino acid. The degree of chemiluminescence inhibition is a measure of the amino acid concentration. The electrostatic interaction between amino acid and metalloporphyrin was confirmed by comparing the degree of inhibition of cationic and anionic metalloporphyrin-catalysed chemiluminescence reactions. More than 20 amino acids were tested, and only L-cysteine, L-tyrosine, L-tryptophan and L-cystine significantly quenched the chemiluminescence intensity. Detection limits were 6.8×10^{-8} , 1.3×10^{-7} , 8.5×10^{-6} and 2.2×10^{-5} M, respectively. The detection approach is demonstrated with a silica-based liquid chromatographic separation of amino acids using phosphate buffer (pH 7.3) as mobile phase. Compared with other chemiluminescence analyses, this method is faster, can be run at room temperature and, in favourable cases, has a lower detection limit.

Keywords: Chemiluminescence; Flow injection; Liquid chromatography; Amino acids; Metalloporphyrins

It is well established that amino acids can be determined by measuring the amount of hydrogen peroxide formed during the reaction of the amino acid with its oxidase. The hydrogen peroxide that is formed is typically determined via the use of a chemiluminescence (CL) reaction. Of the different CL reagents available, peroxyoxalate or luminol appear to be the most popular [1]. Several oxalates have been investigated for their stability in the presence of hydrogen peroxide and CL intensity. Unfortunately, none of them combines all the required characteristics and often compromises have to be made. In the luminol CL system, the high pH required for efficient

light productions is not compatible with most enzymatic reactions. Consequently, the most significant problem with such enzyme-coupled CL detection reaction schemes is that a two-stage reaction sequence must be employed [2,3]. Nieman and co-workers [4,5] developed a liquid chromatographic (LC) detection method for amino acids based on the suppression of CL in the Co(II)- and Cu(II)-luminol-peroxide systems.

Our interest has been in the use of metalloporphyrins (M-Pr) as a substitute for peroxidase in analytical applications. Various M-Pr have been used as mimetic peroxidase in fluorescence and CL analysis [6–8]. Recently, it was found that the catalytic activity of M-Pr in the CL reaction of luminol and hydrogen peroxide is inhibited in the presence of an amino acid and approaches a

Correspondence to: Yun-Xiang Ci, Department of Chemistry, Beijing University, Beijing 100871 (China).

definite value with an increasing amount of the acid. This was considered to be the result of the formation of a mixed ligand complex between the amino acid and M-Pr [9]. In the complex, the two axial coordination sites of M-Pr, which are the catalytic activity centre for the CL reaction, were occupied by amino acid, and thus the catalytic activity of M-Pr was inhibited. The inhibition effects of cationic and anionic M-Pr were compared and the results confirmed the conclusion that the electrostatic interaction is an important factor that affects the stability of the mixed ligand complex [9]. In this work, the possibility of the sensitive determination of amino acids by using this phenomenon was investigated. The detection method is demonstrated with a silica-based LC separation of amino acids.

EXPERIMENTAL

Reagents

L-Arginine monohydrochloride, L-histidine monohydrochloride and L-lysine monohydrochloride (chromatographically pure) were kindly provided by E. Merck (Darmstadt). All other amino acids (chromatographically pure) were obtained from the Institute of Microbiology, Academia Sinica. Luminol (analytical-reagent grade) was obtained from Beijing Chemical Works. All other reagents were of analytical-reagent grade and all aqueous solutions were prepared with doubly distilled water.

Luminol was dissolved in 0.10 M NaOH to give a 2.5×10^{-2} M stock standard solution. A working standard solution (2.5×10^{-4} M) was prepared by diluting the stock solution with 0.1 M NaHCO_3 -NaOH buffer (pH 12) containing 1×10^{-4} M EDTA. Stock solutions of amino acids (1×10^{-2} or 5×10^{-3} M) were prepared by weighing accurately and dissolving in water or 1×10^{-3} M NaOH (for L-cystine, L-tyrosine and L-aspartic acid). Serial dilutions of the stock standard solution with water yielded the required working standard solutions, which were prepared immediately prior to use. The stock standard solutions were prepared fresh weekly and stored refrigerated.

Mn-TPPS₄ [tetrakis(sulphophenyl)porphyrin] and Fe-TMPyP [tetrakis(*N*-methylpyridiniumyl)porphyrin] solutions were prepared as described previously [7,8].

Apparatus

A schematic diagram of the flow system used is shown in Fig. 1. The flow system was constructed with a solenoid valve to control the movements of sample and reagents. Valve operation was controlled by a microprocessor for the precise timing of events. Luminol and hydrogen peroxide reagent solution were pumped at a rate of 4.0 ml min^{-1} (silicon tube, i.d. 1.0 mm) and mixed by one peristaltic pump (B) of the intelligent flow-injection sampler and delivered directly to the flow cell. M-Pr and water or amino acid were pumped at a rate of 1.0 ml min^{-1} and mixed by another pump (A) and a certain amount of the mixed solution was injected automatically into the luminol-hydrogen peroxide stream by the solenoid valve.

The CL produced was monitored by a GD-1 luminometer (Northwest Research Institute of Geology) and the signal was recorded with an LKB 2210 recorder. The LC detection system consisted of a Model 650 high-pressure pump (Waters), a Model U6K injection valve equipped with a $100\text{-}\mu\text{l}$ sample loop (Waters) and an analytical C₁₈ ($10 \mu\text{m}$) column ($300 \times 2 \text{ mm i.d.}$) (Waters). Separation was performed by using 0.01 M phosphate buffer (pH 7.3) as mobile phase at a flow-rate of 1.0 ml min^{-1} . The eluent was mixed

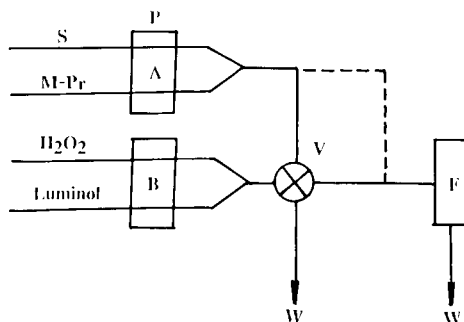


Fig. 1. Schematic diagram of the LC flow system. P, pump; S, water-amino acid-LC eluent, F, flow cell; V, 16-V solenoid valve; W, waste.

with M-Pr followed by a short delay loop (10 cm \times 1.0 mm i.d.) before this solution was mixed with the luminol–hydrogen peroxide stream which was delivered directly to the flow cell (dashed line in Fig. 1).

RESULTS AND DISCUSSION

Optimization of M-Pr-catalysed CL reaction

Acidity is a major factor influencing the M-Pr-catalysed CL reaction. A 0.1 M NaHCO₃–NaOH buffer (pH 12) was chosen for the recommended procedure [8]. The effects of the concentrations of H₂O₂ and luminol on the CL reaction were tested. The relative CL intensity increased rapidly as the concentration of luminol increased; with regard to CL inhibition measurement and economic considerations, 2.5×10^{-4} M luminol was selected as the optimum concentration. The CL intensity increased slightly with increasing H₂O₂ concentration in the range 5×10^{-3} – 2×10^{-2} M. At higher or lower concentrations, the CL intensity decreased rapidly; 1×10^{-2} M H₂O₂ was chosen as the optimum. Under the optimum conditions, the CL intensity–concentration relationship was linear over more than five orders of magnitude of concentration of M-Pr (10^{-1} – 10^4 $\mu\text{g l}^{-1}$). This is the principle of amino acid determination.

Optimization of amino acid complex with M-Pr

Effect of pH. L-Tyrosine was used as a model amino acid for this examination and different buffers were used for pH control. The dependence of blank-to-signal ratio (B/S) on pH is shown in Fig. 2. It is evident that the B/S remains constant from pH 8 to 9.6. Comparison of the pK_a values of L-tyrosine (2.2 for COOH, 9.11 for NH₃⁺, 10.07 for phenol), the predominant species in this pH range is RCH(NH₂)COO[−]. This indicates that the amino acid is bound to M-Pr through its NH₂ group in anionic form (Fig. 3). With increase in pH, the anionic form of L-tyrosine is deprotonated, which gives a doubly negatively charged species. This will weaken the electrostatic interaction between the amino acid and anionic M-Pr (Mn-TPPS₄), as Fig. 2 shows. A

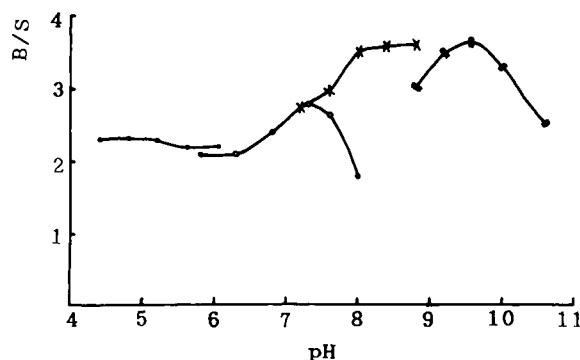
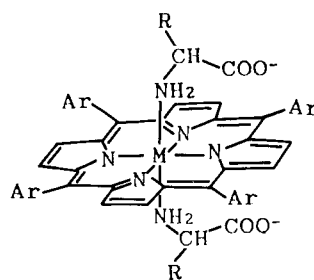


Fig. 2. Effect of pH on the mixed ligand complex formation between amino acid and Mn-TPPS₄. ● = 0.01 M NaOAc–HOAc buffer; ○ = 1/15 M Na₂HPO₄–KH₂PO₄ buffer; × = 0.05 M glycine–HCl buffer; ■ = 0.05 M Tris–HCl buffer. Mn-TPPS₄, 10 $\mu\text{g l}^{-1}$; L-tyrosine, 5×10^{-3} M.

pH of 7.3 (0.01 M phosphate buffer) was selected for use in subsequent studies.

Effect of M-Pr concentration. Figure 4 shows the effect of the concentration of M-Pr on the calibration graph for L-tyrosine. A 10 $\mu\text{g l}^{-1}$ Mn-TPPS₄ concentration shows a relatively wide working range and an easily detectable signal. To study the compatibility with LC separation, the inhibitory effect of more than 20 amino acids was tested at 10 $\mu\text{g l}^{-1}$ Mn-TPPS₄ and pH 7.3; the results are summarized in Table 1. Only L-tyrosine, L-cystine, L-cysteine and L-tryptophan significantly inhibit the CL intensity. Fe-TMPyP (a



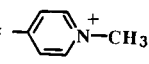
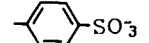
- 1, Ar =  M = Fe Fe-TMPyP
- 2, Ar =  M = Mn Mn-TPPS₄

Fig. 3. Structure of mixed ligand complex of amino acid with M-Pr.

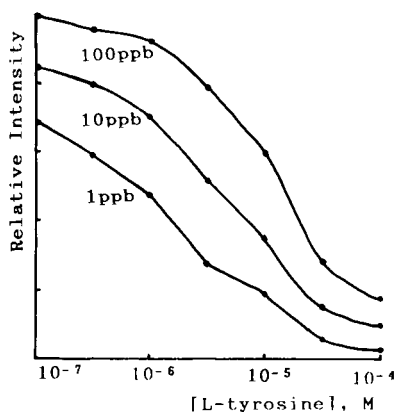


Fig. 4. Effect of the concentration of Mn-TPPS₄ on L-tyrosine calibration graph.

cationic M-Pr) was used as the catalyst to investigate the inhibitory effect of amino acids on the CL reaction. The results are given in Table 1. The inhibitory effect of most amino acids on the Fe-TMPyP-catalysed CL reaction is greater than that with Mn-TPPS₄. These results indicate that in addition to the coordination effect there is an electrostatic interaction between the amino acids and M-Pr. Further, the effects of L-aspartic acid and DL-aspartic acid on the Fe-TMPyP-catalysed CL reaction are different. The former enhances the CL intensity whereas the latter inhibits it, suggesting that there is a stereoselective effect of

amino acids on the Fe-TMPyP-catalysed CL reaction. The reason for this is unclear.

Relative response of amino acids

The theoretical response of a complexation mechanism was proposed by MacDonald and Nieman [4]. If only the free, uncomplexed M-Pr catalyses the CL reaction, then the CL intensity would vary as the concentration of free M-Pr. In the absence of a chelating ligand, the background light intensity remains at a high, constant level. In the presence of a chelating ligand the fraction of free M-Pr is given by the ligand concentration and the complex formation constants. A decrease in the background intensity is observed due to the complexation of some of the M-Pr by the analyte. The relative responses of L-cysteine, L-tyrosine, L-tryptophan and L-cystine were examined. The results are shown in Fig. 5. They agree with the theoretical response. The detection limits (signal-to-noise ratio = 3) of the four amino acids were 6.8×10^{-8} , 1.3×10^{-7} , 8.5×10^{-6} and 2.2×10^{-5} M, respectively; all values were measured without the chromatographic column. In general, the limit of detection for amino acids based on complex formation between amino acids and the catalyst of the CL reaction is related to their formation constants. However, in the present system, most of the amino acids do not inhibit the M-Pr-catalysed CL reaction although complexes are formed.

TABLE 1

Effect of amino acids on M-Pr-catalysed CL reaction^a

Amino acid	Blank/signal ^b		Amino acid	Blank/signal ^b	
	Mn-TPPS ₄	Fe-TMPyP		Mn-TPPS ₄	Fe-TMPyP
L-Cysteine	14.69	74.00	L-Alanine	1.04	1.14
L-Tyrosine	14.50	10.05	L-Glutamine	1.03	1.60
L-Tryptophan	4.77	17.00	L-Glycine	1.00	1.07
L-Cystine	4.20	3.00	L-Asparagine	0.99	1.64
L-Lysine	2.43	2.64	L-Isoleucine	0.98	1.56
DL-Serine	1.20	1.02	L-Hydroxyproline	0.98	1.58
L-Glutamic acid	1.14	1.75	L-Leucine	0.92	1.27
L-Aspartic acid	1.08	0.67	L-Histidine	0.91	1.61
DL-Aspartic acid	1.07	1.29	L-Phenylalanine	0.88	1.66
L-Arginine monohydrochloride	0.95	1.38	L-Arginine	0.87	1.22
L-Lysine monohydrochloride	0.91	1.50	L-Histidine monohydrochloride	0.75	1.64

^a M-Pr, $10 \mu\text{g l}^{-1}$; amino acid, 10^{-3} M. ^b Blank/signal values > 1 mean that the amino acid inhibits the CL reaction; values < 1 mean that the amino acid enhances the CL reaction.

In addition, some amino acids inhibit the Mn-TPPS₄-catalysed CL reaction but they enhance the Fe-TMPyP-catalysed CL reaction. The reasons for this still remain unclear.

LC considerations

As with all postcolumn reaction schemes, the selection of a mobile phase that is compatible with the detection reaction is a critical step in the development of the method. The constraints that the M-Pr–luminol reaction system for the detection of amino acids imposes on the selection of the mobile phase are that a non-complexing buffer of low capacity should be used. A standard method for the separation of amino acids is to elute them from a strong cation-exchange column using citrate buffer, pH and ionic strength appropriate for a specific application [10]. Citrate buffers are incompatible with the present CL system for two reasons: under acidic conditions, less complexation occurs between amino acids and M-Pr, and the buffer is acidic whereas the CL reaction of luminol proceeds optimally at pH \approx 12. Although a polymeric column is often used in ion-exchange separations of amino acids [11,12], a silica-based ODS C₁₈ column was available here so it was used in this instance. In order to use the ODS C₁₈ column, it is necessary to use an acidic mobile phase, as aqueous solutions of pH > 8 will damage the silica column. Phosphate buffer of pH 7.3 (0.01 M) was chosen as the

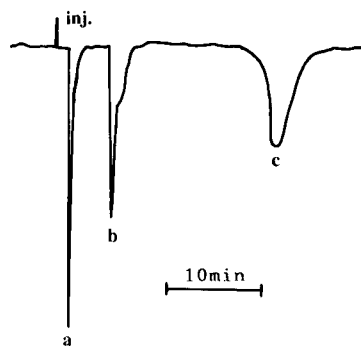


Fig. 6. Chromatogram obtained with 0.01 M phosphate buffer (pH 7.3) as the mobile phase at a flow-rate of 1.0 ml min⁻¹. (a) L-Cysteine, 10 nmol; (b) L-tyrosine, 40 nmol; (c) tryptophan, 450 nmol.

mobile phase for this CL detection scheme (Tris-HCl buffer quenches the CL intensity and was not used in the present system).

Figure 6 shows the chromatogram obtained for L-cysteine, L-tyrosine and L-tryptophan. L-Tyrosine and L-cysteine have the same retention time.

Conclusion

A simple and rapid detection method for amino acids has been established based on the suppression of CL in the M-Pr–luminol–hydrogen peroxide system. It is considered that mixed ligand complex formation between the amino acid and M-Pr occurs. The detection approach was demonstrated successfully with a silica-based LC separation and it is hoped that the method will be applicable to the detection of various species containing NH₂ groups.

REFERENCES

- G.J. De Jong and P.J.M. Kwakman, *J. Chromatogr.*, 492 (1989) 319.
- W.R. Seitz, *Methods Enzymol.*, 57 (1985) 445.
- M.L. Grayeski, in J.G. Burr (Ed.), *Chemical and Bioluminescence*, Dekker, New York, 1985, Chap. 12, p. 469.
- A. MacDonald and T.A. Nieman, *Anal. Chem.*, 57 (1985) 936.
- P.J. Koerner, Jr., and T.A. Nieman, *Mikrochim Acta II* (1987) 79.
- Y.X. Ci and F. Wang, *Anal. Chim. Acta*, 233 (1990) 299.
- Y.X. Ci and F. Wang, *Fresenius' J. Anal. Chem.*, 339 (1991) 46.

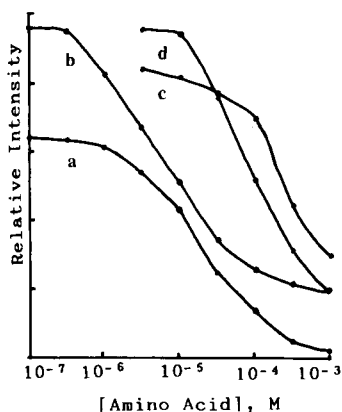


Fig. 5. Calibration graphs for (a) L-tyrosine, (b) L-cysteine, (c) L-cystine and (d) L-tryptophan. Mn-TPPS₄, 10 μ g l⁻¹.

- 8 Y.X. Ci, H.B. He, W.B. Chang and J.S. Liu, *Anal. Chim. Acta*, 237 (1990) 497.
- 9 E. Mikros, F. Gaudemer and A. Gaudemer, *Inorg. Chem.*, 30 (1991) 1806.
- 10 A. Niederwieser, in E. Heftmann (Ed.), *Chromatography: a Lab Handbook of Chromatographic and Electrophoretic Methods*, Van Nostrand Reinhold, New York, 3rd edn., 1975.
- 11 D.P. Lee, *LC Mag.*, 2 (1984) 828.
- 12 M.W. Dong and J.L. DiCesare, *LC Mag.*, 1 (1983) 222.

Multi-element analysis of biological tissues by inductively coupled plasma mass spectrometry: healthy Sprague Dawley rats

Yves G elinas, Massayon Youla, Richard B eliveau and Jean-Pierre Schmit

Universit e du Qu ebec  a Montr eal, D epartement de Chimie and GEOTOP, B.P. 8888, Succursale A, Montr eal, Qu ebec H3C 3P8 (Canada)

Jocelyne Ferraris

CRODT, B.P. 2241, Dakar (Senegal)

(Received 24th March 1992; revised manuscript received 11th May 1992)

Abstract

The normal inorganic contents of bone, brain, erythrocyte, heart, kidney cortex, kidney medulla, liver, lung, muscle and plasma from healthy Sprague Dawley rats were established by using a general method developed for inductively coupled plasma mass spectrometric multi-element determinations of most of the elements present in biological tissues. The most characteristic elemental pattern of each tissue was identified via a statistical multivariate analysis and a principal component analysis helped to elucidate the correlations between elements and tissues.

Keywords: Inductively coupled plasma-mass spectrometry; Biological samples; Rats; Trace elements

Since the appearance of the first biological cells, inorganic exchanges between living organisms have always given rise to self-regulated cycles in self-equilibrated ecological systems. Every plant and animal lived in complete symbiosis with its natural environment. However, serious problems arose with the undue development of human technology and its capacity to modify greatly its natural inorganic surroundings. Acid rains, chemical fertilizers, heavy industries, metallic extractions, toxic wastes disposal sites, ecological disasters and excessive urbanization are only a few of the numerous factors that have drastically

changed the world distribution of most of the bioavailable elements of the Periodic Table. Today, living organisms are increasingly obligated to deal with an inorganic environment that departs considerably from its natural composition. It is therefore essential to deepen our knowledge of the inevitable implications of such severe changes for living species.

Until recently, in spite of the wide literature on the subject [1–5], only partial information has been published on the total inorganic content of biological tissues measured under conditions that allow direct comparison of elemental concentrations. Most reference books on the subject gather results from disparate studies done by workers using distinct techniques and a wide variety of instruments. This situation mainly results from the lack of a single technique capable to perform

Correspondence to: Y. G elinas, Universit e du Qu ebec  a Montr eal, D epartement de Chimie and GEOTOP, B.P. 8888, Succursale A, Montr eal, Qu ebec H3C 3P8 (Canada).

rapid determinations of almost the totality of the elements of the Periodic Table on the small amounts of biological tissues usually available. Up to now, atomic absorption and emission spectrometry and neutron activation analysis have been the most commonly used methods. However, none of them permits routine multi-elemental determinations for most of the elements.

In the early 1980s, inductively coupled plasma–mass spectrometry (ICP–MS) became available for trace element determinations. Its potential for the simultaneous analysis of biological samples has recently been summarized [6–9], and it is now becoming established as one of the most powerful and sensitive methods for multi-element analyses.

Multi-element analysis is a very important feature of ICP–MS as it allows access to studies of synergistic effects that can hardly be achieved when using conventional analytical techniques. Indeed, it is well known that not only is the concentration variation of most of the elements closely related to the presence of the other elements, but also that the pathological effects of many elements are modulated by the presence of the others. For example, rubidium and thallium use the same pathway as potassium for cell penetration [10]. Calcium and strontium concentrations are also closely correlated in most tissues [1]. In fact, more than 54 interrelations between two distinct elements have been demonstrated so far, and a modification of the concentration of a single element, e.g., sodium, can exert an influence on as many as thirteen others [11]. This interdependence is often at the origin of synergistic relationships that can enhance the evolution of many diseases. As a consequence, it is clear that each element must be considered as part of a highly organized and interrelated open system that cannot be simplified to the sum of its components.

In recent years, we have developed and optimized a general ICP–MS method for the multi-element determination of most of the elements present in biological tissues [12]. This work was aimed at establishing the normal inorganic contents of bone, brain, erythrocyte, heart, kidney cortex and medulla, liver, lung, muscle and plasma

of healthy Sprague Dawley rats and at pinpointing their most characteristic elements.

EXPERIMENTAL

Instrumentation

The measurements were made on an Elan Model 250 ICP–MS instrument from Sciex/Perkin-Elmer under the following conditions: plasma argon flow-rate, 16.0 l min⁻¹; nebulizer argon flow-rate, 0.5 l min⁻¹; auxiliary argon flow-rates 1.2 l min⁻¹; r.f. power, 1.1 kW; and reflected power, < 2 W. The standard torch was used throughout. Sample uptake for the Meinhard concentric nebulizer was controlled by a Gilson Minipuls 2 peristaltic pump working at a flow-rate of 0.4 ml min⁻¹. The ion sampling depth, defined as the distance between the aperture of the sampler cone and the downstream turn of the r.f. coils, was fixed at 15 mm. The sampler and skimmer nickel cone apertures were 1.1 and 0.9 mm, respectively.

Reagents and solutions

Standard reference solutions were prepared from SCP-Science 1000 µg ml⁻¹ ICP standards diluted with ultrapure water obtained with a Milli-Q system (Millipore). High dilutions of ICP standards necessary for most analyses decreased their trace element contamination to negligible levels. Merck Suprapur 65% nitric acid was used for tissue digestion in a microwave acid digestion bomb. NBS SRM 1577a Bovine Liver standard reference material was used throughout for calibration and reference purposes.

Tissue preparation and digestion

Male Sprague Dawley rats (ca. 300 g) of the same line were killed by decapitation and the studied organs were immediately taken apart, perfused with a 300 mM mannitol solution (buffered at pH 7.5) and frozen at -22°C. A 500-mg amount of crude tissue and 1.25 ml of ultrapure 8 M nitric acid were mixed in the internal PTFE cup (30 ml) of a Parr microwave acid digestion bomb and allowed to digest for 2 min at medium power inside a standard mi-

crowave oven. After cooling for 30 min at room temperature and a further 30 min in dry-ice, the digest was poured into a 25-ml calibrated flask and the internal PTFE cup was rinsed three times with ultrapure (Milli-Q) water. All the fractions were collected in the flask and an internal standard of 100 ng ml⁻¹ of rhodium was added. The resulting volume was adjusted to 25 ml with ultrapure (Milli-Q) water. Aliquots of solution were pipetted into polypropylene flasks and appropriate solutions of standards were added for element determination by the standard addition method.

All sample manipulations were done inside a class 100 clean room. Samples were introduced via an automatic sample introduction system working on a class 100 clean surface.

Element determination

The standard addition subroutine from the instrument software was used. Linear regression on a minimum of three additions (four measurements, $r \geq 0.999$) was performed throughout for element determination. A blank solution was analysed for every sample in order to subtract for reagent contamination. Considering the relatively elevated inorganic content of the tissues, blank levels were not problematic for any of the elements. Each measurement represents the average of four replicates. An NBS SRM 1577a Bovine Liver digest solution was inserted every ten measurements. Because of their much higher concentrations in the SRM 1577a Bovine Liver and the consequently higher dilution factor that they necessitate, Cu, Fe and Zn were determined independently. Each measurement was done after 2 min of rinsing with ultrapure (Milli-Q) water and an additional 2 min of sample introduction to allow for stabilization of the instrument response. Rinsing and stabilization times were determined in preliminary experiments as appropriate to avoid memory effects and sample introduction instabilities, respectively.

As spectral interferences are much more frequent in the low-mass region, the total analysed mass range ($m/z = 5$ to 238) was divided into two different zones: the low-mass range (from $m/z = 5$ to 90) and the high-mass range (from $m/z = 91$

to 238). The elements in the low-mass range were determined in the high-resolution mode (resolution of 0.6 u at 10% peak height), while the elements in the high-mass range were determined in the low-resolution mode (resolution of 1.0 u at 10% peak height). The division of the full mass range into two distinct and contiguous zones also allows a better optimization of the ion lens system of the instrument. This helps to compensate for the mass effect during ion transmission and thus improves the detection limits. The optimized voltages applied to the lens system in the high- and low-resolution modes were +2.99 and +3.98 V (barrel lens), -7.44 and -5.56 V (plate lens), -17.75 and -19.63 v (Einzel lens unit) and -5.28 and -6.05 V (stop lens), respectively.

Precision

Confidence limits are given by the mean value $\pm ts/\sqrt{n}$, where s is the standard deviation and t is the t -table value at a 90% confidence level. The estimated uncertainties are based on the combined effects of the digestion method, the imprecision and instabilities of the instrument, and the biological material variability.

Statistical multivariate analysis

Statistical multivariate analysis was used to establish the most characteristic elemental pattern of the ten analysed tissues. In a first step, SAS software was used to perform a discriminant analysis which tests tissue differences by comparing variances within and between each kind of tissue and which extracts the most significant elements. Second, principal component analysis (SPAD software), applied to the previously calculated correlation matrices, was used to elucidate the main discriminant sources of the different tissues.

RESULTS AND DISCUSSION

Exhaustive screening of the inorganic content of tissues allows the detection of a pool of about 45 different elements. Among them, C, N and O are not currently measurable by ICP-MS. P, S,

Cl and Br determinations necessitate specific manipulations which are not compatible with multi-element analysis [13,14]. Although they can be determined by ICP–MS [15–17], Ca, Mg, Na and K are more easily measured by atomic absorption spectrometry because of their usually high concentrations in the studied tissues. These elements are the most common and the best described in the literature. As such, there is no specific need for the analytical power of the ICP–MS technique for this type of element.

Detection limits

Precision and quantitative detection limits of the method have been established in a recent study [12]. They were evaluated via repeated spike recoveries in an organic matrix similar to that generated by the digestion of the rat tissues, and lay between 0.125 and 1.0 ng ml⁻¹ for most of the elements (Table 1). Only Bi, Fe, Sc, Si and I were not accurately determined below 10 ng g⁻¹.

Inorganic content of rat tissues

Table 2 summarizes the inorganic content of the ten different tissues taken from a group of standardized healthy male Sprague Dawley rats.

As expected, the elemental distribution reflects some known biochemical characteristics of the analysed tissues. Bone (without marrow), a structural tissue physiologically less active than most of the others, acts as an inorganic biological reservoir for some elements, but it also shows marked and unexplained accumulations for many others. This higher inorganic content can be explained by the existence of a passive protection mechanism that results in a long-term immobilization of the excessively absorbed inorganics that could threaten the integrity or function of other organs or tissues. Liver and kidneys also taken an active part in the homeostatic control of numerous elements and are therefore also characterized by their relatively high inorganic content. When the main source of exposure to trace

TABLE 1

Evaluation of elemental detection limits via spike recoveries in a complex organic matrix

Element	Spike (ng ml ⁻¹)	Found (ng ml ⁻¹) ^a	Confidence limit (90%)	Element	Spike (ng ml ⁻¹)	Found (ng ml ⁻¹) ^a	Confidence limit (90%)
Ag	0.125	0.130	0.018	Al	0.50	0.44	0.03
Co	0.125	0.121	0.005	B	0.50	0.49	0.06
Cr	0.125	0.122	0.004	Cu	0.50	0.47	0.03
Li	0.125	0.129	0.006	Ni	0.50	0.46	0.05
Mn	0.125	0.127	0.006	Rb	0.50	0.50	0.05
Mo	0.125	0.124	0.008	Se	0.50	0.51	0.07
Sb	0.125	0.122	0.015	Ti	0.50	0.48	0.03
Sr	0.125	0.123	0.005	W	0.50	0.49	0.03
Tl	0.125	0.117	0.004				
V	0.125	0.128	0.004	Zn	1.00	1.02	0.09
Y	0.125	0.125	0.002				
As	0.250	0.233	0.037	Bi	10.00	7.92	0.24
Ba	0.250	0.253	0.024	Fe	10.00	10.36	0.37
Cd	0.250	0.249	0.022	Sc	10.00	8.34	0.34
Hg	0.250	0.244	0.028	Si	10.00	14.16	1.73
Pb	0.250	0.235	0.036	I	10.00	6.86	0.48
Sn	0.250	0.254	0.025				
Zr	0.250	0.227	0.019				
U	0.250	0.235	0.008				

^a Means of five replicate determinations.

TABLE 2

Inorganic contents of individual male Sprague Dawley rat tissues ^a

Element	Brain		Heart		Erythrocyte		Liver		Muscle	
	Mean ($\mu\text{g ml}^{-1}$)	Confidence limit (90%)	Mean ($\mu\text{g ml}^{-1}$)	Confidence limit (90%)	Mean ($\mu\text{g ml}^{-1}$)	Confidence limit (90%)	Mean ($\mu\text{g ml}^{-1}$)	Confidence limit (90%)	Mean ($\mu\text{g ml}^{-1}$)	Confidence limit (90%)
Ag	0.004	0.001	0.002	0.001	0.004	0.001	0.011	0.001	0.008	0.001
Al	0.568	0.069	0.636	0.063	0.610	0.063	1.072	0.050	0.943	0.146
As	0.092	0.006	0.119	0.024	10.174	0.495	0.174	0.006	0.124	0.008
B	0.081	0.005	0.097	0.008	0.106	0.008	0.303	0.016	0.081	0.018
Ba	0.004	0.001	0.010	0.001	0.063	0.005	0.012	0.001	0.010	0.001
Bi	n.d. ^b		n.d.		n.d.		n.d.		n.d.	
Ca	20.365	1.575	2.671	0.251	37.982	2.991	1.954	0.283	2.958	0.209
Cd	0.001	0.000	0.001	0.000	0.003	0.001	0.004	0.001	0.003	0.001
Co	0.002	0.001	0.011	0.001	0.010	0.001	0.017	0.001	0.003	0.001
Cr	0.214	0.014	0.270	0.009	0.221	0.016	0.294	0.011	0.148	0.007
Cu	2.334	0.124	4.931	0.166	0.991	0.044	3.388	0.062	1.019	0.042
Fe	35.368	1.455	101.080	4.133	862.327	36.143	151.034	4.260	20.781	1.303
Hg	n.d.		0.001	0.001	0.000	0.000	n.d.		0.001	0.001
K	4682.22	39.16	4406.28	72.15	5275.15	244.30	4072.38	233.97	6624.24	173.09
Mg	151.84	5.25	241.73	6.90	89.53	3.50	211.77	4.26	242.26	5.44
Mn	0.279	0.016	0.383	0.024	0.092	0.005	2.107	0.079	0.110	0.007
Mo	0.043	0.005	0.055	0.005	0.004	0.001	0.531	0.020	0.018	0.001
Na	1438.16	47.55	1356.21	53.73	2079.22	56.48	906.99	28.71	546.59	21.21
Ni	0.001	0.001	0.001	0.001	0.028	0.002	0.050	0.006	0.033	0.005
Pb	0.001	0.001	0.010	0.001	0.0003	0.000	0.202	0.016	0.034	0.010
Rb	0.997	0.073	3.005	0.068	2.521	0.122	5.617	0.121	3.552	0.088
Sb	n.d.		0.006	0.001	n.d.		0.030	0.002	0.011	0.001
Sc	n.d.		n.d.		n.d.		n.d.		n.d.	
Se	0.104	0.012	0.246	0.030	0.898	0.047	0.421	0.032	0.207	0.018
Sn	n.d.		0.010	0.002	n.d.		0.092	0.005	0.097	0.006
Sr	0.052	0.007	0.031	0.005	0.056	0.008	0.077	0.008	0.049	0.007
Ti	1.218	0.046	1.497	0.121	0.883	0.070	0.563	0.019	0.263	0.017
Tl	0.001	0.001	0.010	0.001	0.002	0.001	0.001	0.001	0.023	0.002
V	0.025	0.004	0.016	0.003	0.064	0.008	0.048	0.007	0.038	0.002
W	n.d.		0.001	0.001	n.d.		0.001	0.001	0.002	0.001
Y	n.d.		0.006	0.005	0.001	0.000	0.002	0.001	0.001	0.001
Zn	9.725	0.402	17.079	0.661	9.549	0.250	23.024	0.845	12.316	0.737
Zr	0.019	0.002	0.088	0.010	0.020	0.005	0.152	0.011	0.108	0.009

Element	Bone		Plasma		Lung		Kidney cortex		Kidney medulla	
	Mean ($\mu\text{g ml}^{-1}$)	Confidence limit (90%)	Mean ($\mu\text{g ml}^{-1}$)	Confidence limit (90%)	Mean ($\mu\text{g ml}^{-1}$)	Confidence limit (90%)	Mean ($\mu\text{g ml}^{-1}$)	Confidence limit (90%)	Mean ($\mu\text{g ml}^{-1}$)	Confidence limit (90%)
Ag	0.263	0.016	0.001	0.000	0.001	0.000	0.005	0.001	0.005	0.001
Al	1.585	0.053	0.505	0.022	0.893	0.068	0.454	0.055	0.334	0.035
As	0.650	0.040	0.055	0.006	0.623	0.054	0.087	0.011	0.122	0.014
B	1.940	0.073	0.003	0.001	n.d.		0.143	0.014	0.182	0.021
Ba	5.373	0.225	n.d.		0.009	0.001	0.005	0.001	0.005	0.001
Bi	n.d. ^b		n.d.		n.d.		n.d.		n.d.	
Ca	105 418.77	4728.25	62.071	3.613	14.216	1.885	21.923	1.933	10.476	1.191
Cd	0.054	0.008	0.015	0.002	0.001	0.000	0.037	0.004	0.094	0.014
Co	1.366	0.109	0.001	0.001	0.004	0.001	0.047	0.006	0.046	0.005
Cr	0.362	0.025	0.121	0.007	0.266	0.015	0.210	0.016	0.292	0.024
Cu	0.998	0.034	1.055	0.053	0.991	0.035	8.278	0.458	4.731	0.115
Fe	58.393	6.363	2.950	0.249	149.155	8.657	87.474	6.035	82.479	4.539
Hg	0.222	0.018	n.d.		n.d.		0.003	0.001	0.008	0.001

(Continued on p. 120)

TABLE 2 (continued)

Element	Bone		Plasma		Lung		Kidney cortex		Kidney medulla	
	Mean ($\mu\text{g ml}^{-1}$)	Confidence limit (90%)	Mean ($\mu\text{g ml}^{-1}$)	Confidence limit (90%)	Mean ($\mu\text{g ml}^{-1}$)	Confidence limit (90%)	Mean ($\mu\text{g ml}^{-1}$)	Confidence limit (90%)	Mean ($\mu\text{g ml}^{-1}$)	Confidence limit (90%)
K	1002.49	14.62	483.16	8.16	4342.75	108.56	2753.08	129.71	3993.45	94.15
Mg	4842.55	74.13	45.71	3.10	178.20	7.35	279.75	8.68	268.45	8.57
Mn	0.518	0.015	0.003	0.001	0.138	0.009	1.441	0.043	1.778	0.073
Mo	0.215	0.019	n.d.		0.058	0.004	0.394	0.011	0.382	0.015
Na	9673.97	132.46	5802.55	137.70	1819.30	41.14	1217.53	71.03	2333.97	119.23
Ni	0.875	0.052	0.002	0.001	0.011	0.001	0.090	0.010	0.178	0.014
Pb	0.209	0.024	0.002	0.001	0.011	0.001	0.088	0.009	0.098	0.010
Rb	1.021	0.065	0.191	0.014	2.482	0.088	4.890	0.138	6.867	0.112
Sb	0.044	0.006	n.d.		0.055	0.008	n.d.		0.001	0.001
Sc	0.537	0.077	n.d.		n.d.		0.013	0.001	0.019	0.002
Se	0.248	0.027	0.509	0.057	0.395	0.032	1.268	0.061	1.386	0.082
Sn	0.221	0.015	0.002	0.001	0.001	0.001	0.012	0.002	0.021	0.002
Sr	45.058	1.542	0.043	0.006	0.059	0.006	0.033	0.002	0.051	0.007
Ti	1.113	0.092	0.457	0.026	2.090	0.082	1.102	0.046	1.612	0.065
Tl	0.008	0.007	n.d.		0.001	0.000	0.019	0.002	0.128	0.009
V	0.047	0.004	0.074	0.008	0.021	0.002	0.034	0.006	0.057	0.009
W	0.008	0.002	n.d.		n.d.		n.d.		0.002	0.001
Y	0.005	0.001	n.d.		n.d.		n.d.		n.d.	
Zn	168.009	7.513	1.448	0.048	14.384	0.604	28.465	1.328	28.304	0.852
Zr	0.157	0.010	0.048	0.008	0.043	0.005	0.069	0.011	0.105	0.010

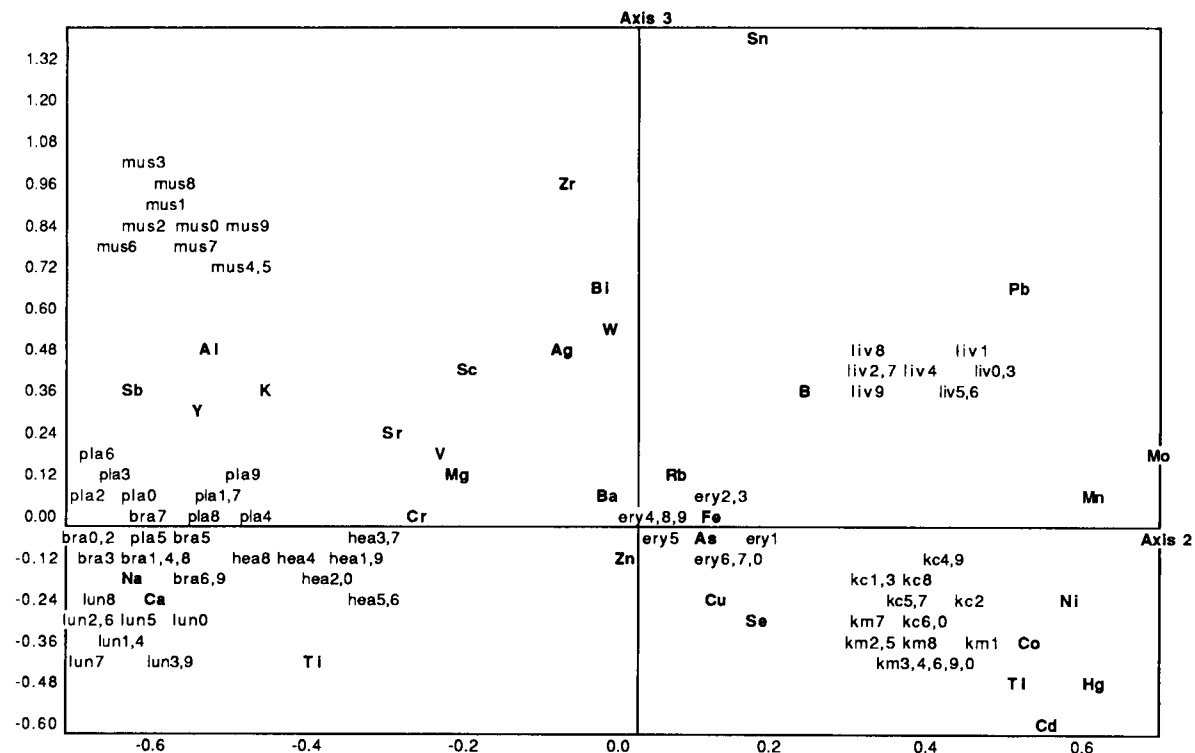
^a Each value is the average of ten independent determinations on each of the ten different tissues. Each determination is the average of four successive measurements. ^b Not determined or below quantitative detection limits

elements pass via the gastrointestinal tract, their distribution and incorporation into other tissues is mostly controlled by the highly active enzymatic system of the liver, which metabolizes, excretes or incorporates them. During long-term exposure, metal-binding proteins such as metallothionein, superoxide dismutase or ceruloplasmin are implicated in the transfer of certain metals towards the kidneys [18]. Incidentally, the concentration of some of the most toxic metals (Cd, Hg, Ni, Tl) is higher in kidneys than in liver. Other less toxic inorganics are also found to be very concentrated in the kidneys and liver, partly because of their intense metabolic activity (Co, Cu, Se, Ti, Zn). In contrast, the brain is characterized by its very low inorganic content, a situation resulting from the action of an effective barrier at the capillary level protecting neurons from inorganic aggressions.

However, in addition to specific considerations on element distributions in biological tissues, one of the main interests of a systematic determination of the elemental content is to permit the definition of their most characteristic inorganic

pattern. This characteristic pattern, best illustrated via a principal component analysis, could then be used as a reference table when analysing tissues from animals affected by a given disorder.

The principal component analysis (PCA), derived from a correlation matrix produced by SAS, generates a multi-dimensional axis system the origin of which is located at the gravity centre of the inter-elemental variations. This system is positioned in a way such that maximum variability is emphasized. Elements and tissues are characterized by coordinates describing their relative positions within the system. Figure 1 shows the existing relationships between biological tissues and elements as expressed by PCA. It summarizes 83% of the corresponding multi-dimensional correlation structure. In this instance, bone was omitted because its inorganic content is so different from the others that the more subtle variations between other tissues and elements are masked. The first axis of the system is not shown as it only gives an idea of the most evident variations between one tissue (erythrocyte) and



Mean coordinates on axis 1 ("z" axis):

Brain (bra):	-0.35	Kidney cortex (kc):	-0.50	Lung (lun):	+0.05
Erythrocytes (ery):	+1.26	Kidney medulla (km):	-0.51	Muscle (mus):	-0.36
Heart (hea):	-0.42	Liver (liv):	-0.64	Plasma (pla):	-0.18

Fig. 1. Relative individual positions of elements and tissues within the three-dimensional axis system generated by the principal component analysis (axis 1 is perpendicular to the plane). Axes 2 and 3 illustrate 83% of total variability.

the eight others. Moreover, major elements (K, Na, Mg, Ca) are presented on this figure even though they were not considered in the PCA calculations (illustrative mode). Axes 2 and 3 illustrate the most evident relationships between elements and tissues.

The first information derived from Fig. 1 is that some elements (Ag, Bi, Cr, Mg, Sc, Sr, V, W and Zr) exhibit no specificity for any of the tissues (bone not considered). They show no correlation between each other or with any tissue following the SAS discriminant analysis, and they occupy a central area in the system where no tissues are found. Table 2 shows that some of them (Cr, Mg, V, Zr) are evenly distributed within the tissues whereas the concentrations of the others (Ag, Bi, Sc, Sr and W) are very low

whatever the tissue. Hence they are not part of any "characteristic" content for any of those tissues. On the other hand, few elements are closely correlated with one specific tissue (As, Ba and Fe in erythrocytes; B and Pb in liver; Ti in lung; Na and Ca in plasma; Ni, Co, Hg, Tl and Cd in kidney). Their concentrations in those tissues are significantly (90% confidence limit) different than in the others. Cd, Hg and Tl are even responsible for the separation of the kidney medulla from the cortex as their concentration is higher in the former. A third class of elements shows a preference for two or three tissues and they are found mid-way between them in Fig. 1 (Sn between muscle and liver; Mn and Mo between kidney and liver; Cu and Se between kidney and heart; Al, K, Y and Sb between muscle, brain and lung;

Rb between heart, muscle, erythrocytes, liver and kidney; and Zn between heart, liver and kidney). Consequently, it is obvious that many elements exhibit marked accumulations or very low concentrations in certain tissues, confirming the existence of active mechanisms modulating their accumulation in or exclusion from organs or tissues. Any pathology threatening the integrity or function of a tissue or organ can then be expected to disturb those mechanisms and have a direct or indirect effect on the concentration of the characteristic elements that are specific to the target tissue.

Another important observation derived from Fig. 1 is that all the analysed samples within every kind of tissue are tightly grouped together in specific areas of the axis system. Moreover, kidney cortex can be isolated from the medulla through comparison of their trace inorganic contents. Even if they seem associated, plasma, brain, lung and heart are well separated when their coordinates on the first axis (not illustrated) are considered: lung is located in front of the plane formed by axes 2 and 3 (mean z coordinate = +0.05), whereas heart, brain and plasma lie behind it (-0.42, -0.35 and -0.18, respectively). Erythrocytes, with their +1.26 mean coordinate on the first axis, exhibit distinct particularities in their inorganic composition, mostly their high As, Fe and Ba concentrations, thus isolating them from the others. Heart and muscle are relatively far from each other, emphasizing the differences in their cell structures. Finally, the interest in studying erythrocytes and plasma separately instead of whole blood when trace elements are concerned is evident when their relative positions are compared.

The variance between the inorganic contents of the ten samples of a given tissue is, as expected, lower than that between any pair of different tissues. The precision of the ICP-MS technique combined with multivariate discriminant analysis can even separate two distinct areas of the same organ (e.g., kidney cortex and medulla) solely on the basis of a comparative evaluation of their trace element contents, as element determinations cover the whole range of concentrations

of known physiological activity. It could then separate a given organ or tissue from a pathologically marked animal from that from a healthy animal.

Conclusion

The main objective of this work was to take advantage of the capability of multi-element analysis by ICP-MS in order to establish the inorganic contents of ten biological tissues and to pinpoint their most characteristic elemental pattern. This approach, together with PCA, was found to be promising and may open the way to numerous biochemical and medical applications.

REFERENCES

- 1 W. Mertz (Ed.), *Trace Elements in Human and Animal Nutrition*, Academic, San Diego, CA, 5th edn., 1987.
- 2 P. Bratter and P. Schramel (Eds.), *Trace Element Analytical Chemistry in Medicine and Biology*, Vol. 4, De Gruyter, Berlin, 1987.
- 3 H.A.O. Hill (Ed.), *Inorganic Biochemistry*, Royal Society of Chemistry, London, 1979.
- 4 W.G. Hoekstra (Ed.), *Trace Element Metabolism in Animals - 2*, University Park Press, Baltimore, MD, 1974.
- 5 L.S. Hurley (Ed.), *Trace Elements in Man and Animal - 6*, Plenum, New York, 1988.
- 6 R.S. Houk and J.J. Thompson, *Mass. Spectrom. Rev.*, 7 (1988) 425.
- 7 M. Selby and G.M. Hieftje, *Am. Lab.*, August (1987) 16.
- 8 D.J. Douglas, *Can. J. Spectrosc.*, 34 (1989) 38.
- 9 G.M. Hieftje and G.H. Vickers, *Anal. Chim. Acta*, 216 (1989) 1.
- 10 S.G. Schafer and W. Forth, *Biol. Trace Elem. Res.*, 5 (1983) 205.
- 11 T. Rae, *Systemic Aspects of Biocompatibility*, Vol. 1, CRC Press, Boca Raton, FL, 1981, p. 21.
- 12 J.-P. Schmit, M. Youla, J. Ferraris and Y. Gélinas, *Anal. Chim. Acta*, 249 (1991) 495.
- 13 S.-J. Jiang and R.S. Houk, *Spectrochim. Acta*, Part B, 43 (1988) 405.
- 14 A.R. Date and M.E. Stuart, *J. Anal. At. Spectrom.*, 3 (1988) 659.
- 15 J.R. Garbarino and H.E. Taylor, *Anal. Chem.*, 61 (1989) 793.
- 16 S.-J. Jiang, R.S. Houk and M.A. Stevens, *Anal. Chem.*, 60 (1988) 1217.
- 17 S. Schuette, D. Verrault, B.T.G. Ting and M. Janghorbani, *Analyst*, 113 (1988) 1837.
- 18 P.L. Goering and C.D. Klaassen, *Toxicol. Appl. Pharmacol.*, 74 (1984) 321.

Laser-induced plasma atomic emission spectrometry in liquid aerosols

K.C. Ng¹, N.L. Ayala, J.B. Simeonsson² and J.D. Winefordner

Department of Chemistry, University of Florida, Gainesville, FL 32611 (USA)

(Received 18th October 1991; revised manuscript received 25th May 1992)

Abstract

Atomic emission spectrometry was performed in a laser-induced plasma in air. The plasma was produced by focusing the beam of an Ar–F (193 nm) excimer laser into a liquid aerosol nebulizer system. A liquid aerosol was generated with a concentric glass nebulizer–spray chamber assembly and carried into the plasma by the argon (0.5 l min⁻¹) nebulizer gas. In general, the emission signal lasted ca. 35–40 μ s after the laser pulse. The excitation temperature of the plasma decreased from 3994 K at 1 μ s to 3607 K at 35 μ s after the laser pulse. The solution limits of detection (3σ of the blank) were determined for Na, Li, In, Al, Ga, Ca, Mg, K and Sr to be 0.9, 0.3, 10, 3, 3, 8, 3, 2 and 20 μ g ml⁻¹, respectively. The sensitivity obtained with this system is similar to that of a previous Nd:YAG wet droplet system reported in the literature.

Keywords: Atomic emission spectrometry; Laser-induced plasmas; Plasmas

A plasma can be generated by laser-induced breakdown of a gas. Plasma generation processes have been summarized by Raizer [1]. Laser-induced plasmas (LIPs) have been produced by laser excitation using high-power pulsed laser systems such as the Nd:YAG at 532 nm [2] or 1064 nm [3–10], the CO₂ laser at 10.6 μ m [11] and the Ar–F excimer laser at 193 nm [12]. For wavelengths in the visible region, the typical threshold laser irradiances for breakdown to occur in air and inert gas [2] is ca. 10¹¹ W cm⁻² and in the presence of water droplets it is ca. 10⁹ W cm⁻².

The decrease in the laser irradiance threshold for wet systems is due to the focusing and amplification effects of the droplets [2].

LIPs offer several attractive features for analytical atomic emission spectrometry (AES): the laser generated plasma has been reported to give excitation temperatures greater than 5000 K [3,8,13], resulting in intense atomic emission; the plasma is produced by a remote laser beam so that direct sampling in a gas atmosphere is feasible; the plasma is electrodeless, thus avoiding spectral contamination from electrodes; the plasma can be sustained in air or in almost any gas, avoiding the high gas consumption cost of other plasmas such as the inductively coupled plasma (ICP), which uses 17 l min⁻¹ of argon; and the plasma can “tolerate” virtually all sample forms and types (e.g., gas, liquid, solid, aqueous, organic). LIP-AES has also been applied to the direct analysis of dry aerosols in air [3,8], vapors

Correspondence to: J.D. Winefordner, Department of Chemistry, University of Florida, Gainesville, FL 32611 (USA).

¹ Present address: Department of Chemistry, California State University at Fresno, Fresno, CA 93740-0070, USA.

² Present address: Department of the Army, US Army Laboratory Command, Ballistic Research Laboratory, Aberdeen Proving Ground, MD 21005-5066, USA.

in air and helium [9], liquids [4,7], metals [5,14], filters [6] and chromatographically separated acetylene [12]. In an attempt to use LIP-AES for solution samples, the most common sample type, Archontaki and Crouch [10] used an isolated droplet generator for sample introduction. Recently, Cheng et al. [15] determined Group III and V hydrides in helium by measuring the emission generated by LIP. They were able to obtain $\mu\text{g ml}^{-1}$ detection limits. Majidi et al. [16] used an electrothermal atomizer for LIP-AES, achieving pg detection limits.

This paper presents the results of an evaluation of an Ar-F excimer laser (193 nm) LIP-AES system for liquid aerosols. The liquid aerosol was generated with a commonly used ICP-type glass concentric nebulizer assembly and carried by the nebulization argon (0.5 l min^{-1}) through a small tube (1 mm i.d.) into an LIP sustained in ambient laboratory air.

EXPERIMENTAL

The experimental set-up is shown in Fig. 1. The Ar-F excimer laser (Model 2110, Questek, Billerica, MA), unless noted otherwise, was operated at 5 Hz with an output energy of 150 mJ per pulse. The glass concentric nebulizer (TR-30-A3, Meinhard, Santa Ana, CA) and spray chamber (dual concentric, laboratory constructed) were those typically used in ICP-AES. The flow rate of nebulization argon was 0.5 l min^{-1} at 35 psi with a solution uptake rate of 2.0 ml min^{-1} . The laser was focused with a quartz lens (270 mm focal length) at ca. 5 mm above the liquid injector tip. The resulting analyte emission was collected by a quartz lens (130 mm focal length) at a 90° angle of the laser beam and the emission was imaged on to the $120 \mu\text{m}$ wide, 12 mm high entrance slit of the monochromator (0.35 m , 1180 lines mm^{-1} grating blazed for 250 nm; EU-700, Heath, Benton Harbor, MI). The photomultiplier (R928, Hamamatsu TV, Japan) tube signal was terminated with a 1-k Ω resistor and processed using an electronic filter (1-s time constant) prior to the boxcar averager. The boxcar averager (SR-250, Stanford Research Systems, Sunnyvale, CA), un-

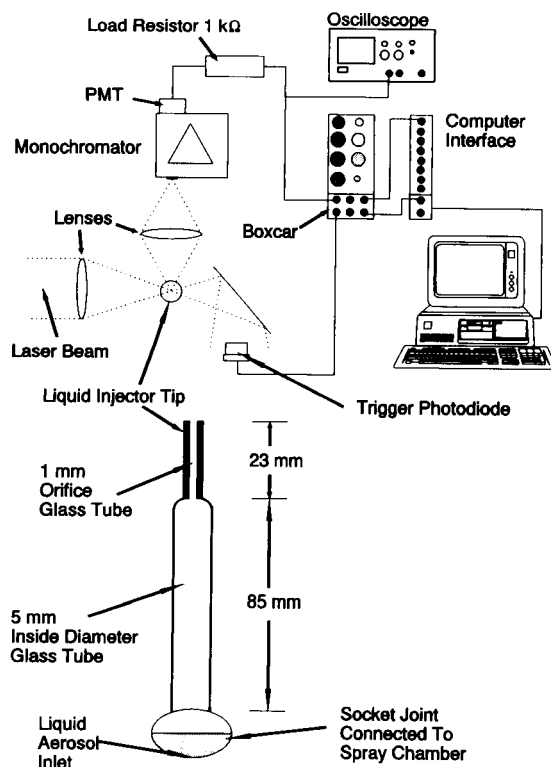


Fig. 1. Experimental set-up of the laser-induced plasma atomic emission spectrometry system. R = 1-k Ω resistor; PD = triggering photodiode; PMT = photomultiplier tube; PC = IBM PC computer.

less noted otherwise, was operated with 100-sample averaging, a 6- μs delay time and a 300-ns gate width. The boxcar was externally triggered by a fast photodiode (FND-100Q, EG&G Electro-Optics, Salem, MA). The boxcar output was statistically processed with an IBM-PC computer using Stanford Research Systems software. The oscilloscope (2430A, Tektronix, Beaverton, OR) was used to observe the signal from the photomultiplier tube.

All standard solutions were prepared from stock solutions ($1000 \mu\text{g g}^{-1}$) (Inorganic Ventures, Lakewood, NJ) recommended for ICP-AES. Deionized, distilled water was employed for dilution and for the blank. The laser filling gases used were of the purity suggested by the manufacturer.

RESULTS AND DISCUSSION

The injector tube (Fig. 1) had an i.d. of 1 mm, which is the typical size used for conventional ICPs. The liquid droplets were confined to a small path owing to the small orifice of the injector tube. The laser beam and the plasma appeared to enclose the entire aerosol path, thus maximizing the reproducibility and the number of droplets excited. Our system is different from that of Essien et al. [3] in that they measured dry aerosols distributed in an air chamber, but is similar to that of Archontaki and Crouch [10], which measured droplets from an isolated droplet generator.

Emission characteristics

Pinnick et al. [17] evaluated the relationship between laser wavelength and plasma production, and found that the breakdown threshold irradiance decreased with a decrease in wavelength. The 193-nm laser used in this work should facilitate plasma formation when compared with other laser systems of higher wavelength. The LIP was visible at the intersection of the laser beam and the liquid aerosol path. Chylek et al. [2] suggested that the LIP was initially created outside the particle and then propagated back into the droplet, from which the observed plume was ejected. The analyte emission lifetime is similar to that for Nd:YAG laser systems. A high background emission was seen at early times ($t \leq 3 \mu\text{s}$). A 6- μs delay time was selected as it was judged to have the best signal-to-noise ratio on the oscilloscope.

Figure 2 shows the oscilloscope traces of the emission for the blank and for a Li standard at 671 nm. The blank trace (A) shows a high background signal at $t < 1 \mu\text{s}$. Figure 2B shows the signal which corresponded to the LIP-AE of a $10 \mu\text{g ml}^{-1}$ solution of Li. The emission signal for the analyte has decreased to half of the maximum intensity at ca. $2 \mu\text{s}$. It was instructive to obtain a background spectrum for the wavelength region of interest (200–800 nm). Figure 3A shows the spectral scan of the LIP blank emission (water aerosol blank, laser repetition rate 40 Hz, monochromator scanning rate 2 \AA s^{-1} , boxcar

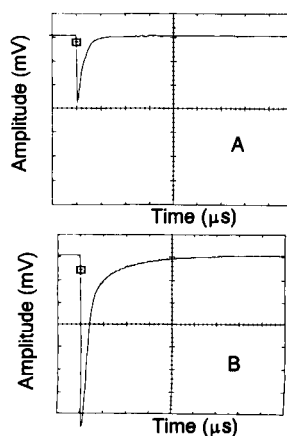


Fig. 2. Oscilloscope traces of the Li emission at 671 nm versus lifetime profile. (A) Blank (deionized water) emission, showing a high background signal at $t < 1 \mu\text{s}$; (B) analyte solution ($10 \mu\text{g Li g}^{-1}$ solution) emission. The cursor (T), which is surrounded by a box, represents where the laser pulse has terminated and is taken as zero time. In both traces, the vertical scale is 20 mV per division and the horizontal scale is $5 \mu\text{s}$ per division.

averaging of 30 samples, delay time $6 \mu\text{s}$ and gate width 300 ns) in the 200–800-nm region. Figure 3B shows the LIP spectral scan without the aerosol blank but with nebulization argon passing through. Figure 3C shows the LIP emission of plain air and Figure 3D shows the background spectrum with the room lights on while both the laser and the nebulizer gas were off. The two intense emission peaks at ca. 386 and ca. 770 nm observed for the LIP in water droplets can be attributed to the second- and fourth-order harmonics of the Ar-F laser emission, respectively.

Excitation temperature

Radziemski et al. [8] have shown evidence that the LIP is at local thermal equilibrium (LTE) after a 1- μs plasma lifetime. By assuming LTE, the two-line intensity method [17] was used to measure the plasma excitation temperature as a function of delay time. Two indium atomic lines, 451.1 and 325.6 nm, were used for this purpose. The temperature was 3994 K at $4 \mu\text{s}$ and decreased to 3607 K at $35 \mu\text{s}$; the standard deviation of the temperature was 300 K. Sneddon et al. [3] used lead in dry aerosol for LIP-AES and found the excitation temperature at 20–40- μs

delay times to be ca. 5500–7000 K. The wet aerosols in our system have apparently reduced the plasma temperature. Zahn and Dietze [19] used a mass spectrometric method to determine the temperature of the plasma and found that the LIP temperature varied with the target material,

ranging from 3300 K for indium to 8200 K for molybdenum.

Analytical figures of merit

The highest precision obtained with this method (ten measurements) was for the determi-

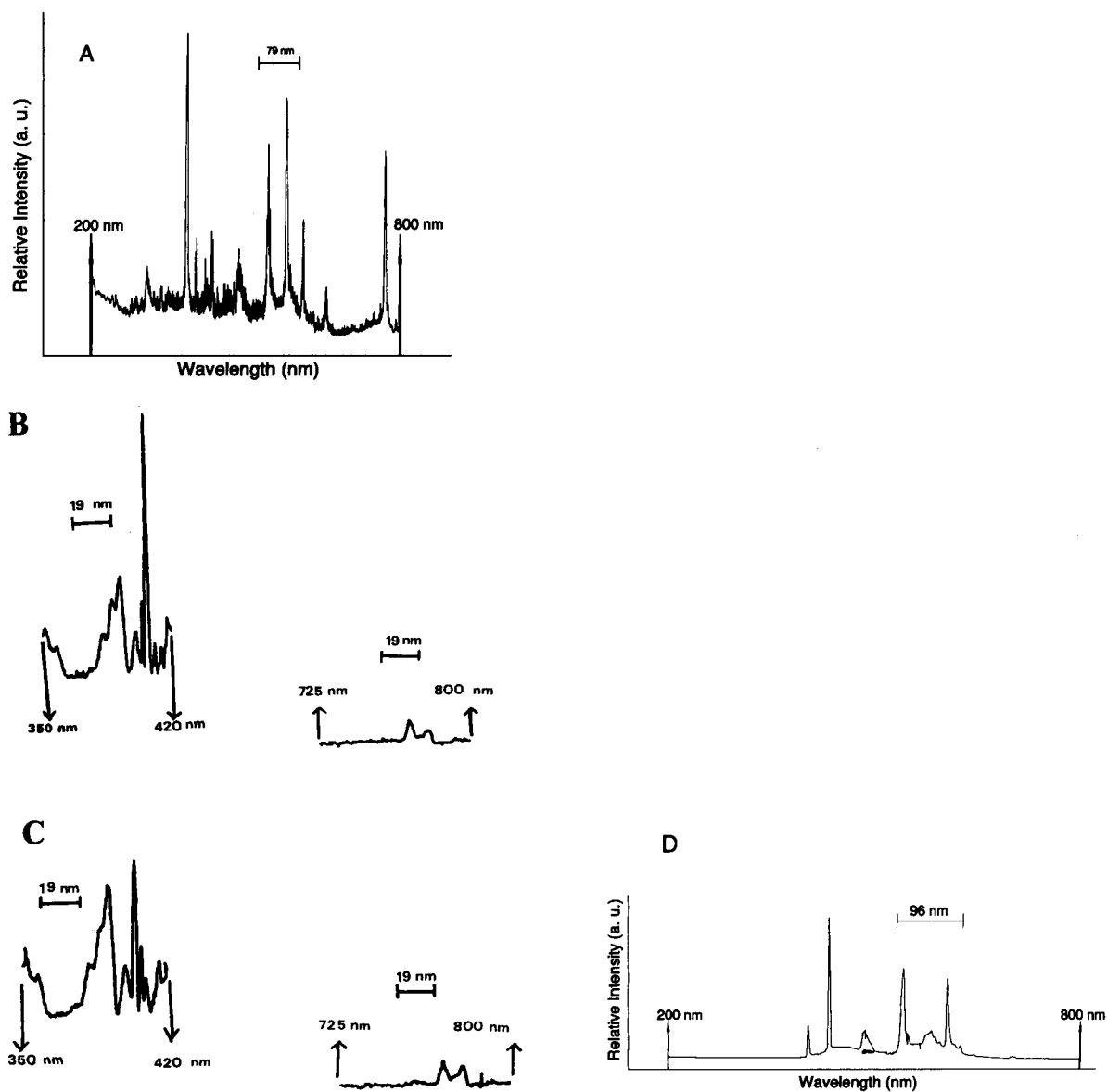


Fig. 3. Spectral scan of the background emission. (A) Spectrum of the blank aerosol (200–800 nm); (B) background spectrum without the blank being aspirated but with the nebulization argon on; (C) emission from just air (nebulizer off); (D) background spectrum with the room lights on (nebulizer off, laser off).

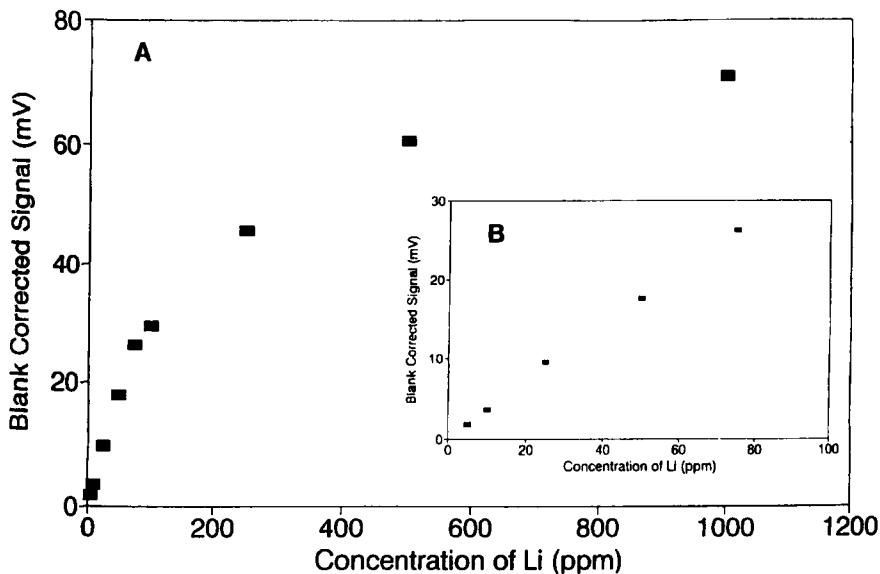


Fig. 4. Calibration graph for the determination of Li by LIP-AES. (A) Calibration graph; (B) expansion of linear portion of the calibration graph. The plasma emission was monitored at 671 nm.

nation of Mg (285.2 nm). The precision, calculated as the relative standard deviation of 100 $\mu\text{g ml}^{-1}$ Mg, was 1.7%. In addition to the background emission, this level of precision includes fluctuation from the laser pulses, the imprecision of the plasma position at the laser beam aerosol plath intersection and changes in the nebulization of the liquid aerosol. Figure 4 shows a calibration

graph for the determination of Li. The linear dynamic range (LDR) for Li was about three orders of magnitude.

Table 1 summarizes the limits of detection (LOD) for the elements studied, which are compared with those obtained by Crouch and co-workers [10,13] using a computer-controlled, hardware-driven isolated droplet generator

TABLE 1

Comparison of limits of detection ($\mu\text{g ml}^{-1}$)

Element	Wavelength (nm)	This work ^a	Droplet LIP-AES ^b	ICP-AES ^c
Li	670.8	0.3	0.3	0.0018
N	589.9	0.9	2.2	0.029
K	766.5	2.0	–	0.060
Mg	285.2	3.0	–	0.0016
	279.55	–	1.9	–
Ca	422.7	8.0	–	0.010
	393.37	–	0.4	–
Mn	257.61	–	7.2	0.0014
Sr	460.7	20.0	–	0.068
Al	396.1	3.0	5.2	0.028
Ga	417.2	3.0	–	0.066
In	451.1	10.0	–	0.140

^a This system; limit of detection = 3σ of the water blank emission. ^b Ref. 10: droplet generation Nd:YAG LIP-AES (LOD = $3 \times$ background). ^c Ref. 20.

Nd:YAG LIP-AES system; both systems show similar detection limits, at the $\mu\text{g ml}^{-1}$ level. The isolated droplet generation Nd:YAG system, which uses a more complicated sample introduction device, although able to give a higher plasma temperature owing to less liquid cooling, did not provide superior detection limits. The LODs obtained for both LIP-AES systems are also compared with those of ICP-AES [14], and are poorer.

Conclusions

An LIP-AES system that was designed for the excitation of analytes in liquids, the most commonly encountered sample type, was evaluated. A simple ICP-type nebulizer–spray chamber–injector assembly was employed. Further optimization of the system should improve the detection limits. LIP-AES offers an alternative approach to trace element analysis and may find application in specific analyses involving air pollution.

This research was supported by NIH-5-R01-GM38434-05.

REFERENCES

- 1 Y.P. Raizer, *Laser-Induced Discharge Phenomena*, Consultants Bureau, New York, 1977.
- 2 P. Chylek, M.A. Jarzembki, V. Srivastava, R.G. Pinnick, J.D. Pendleton and J.P. Crunclenton, *Appl. Opt.*, 26 (1987) 760.
- 3 M. Essien, L.J. Radziemski and J. Sneddon, *J. Anal. At. Spectrom.*, 3 (1988) 985.
- 4 J.R. Wachter and D.A. Cremers, *Appl. Spectrosc.*, 41 (1987) 1042.
- 5 D.A. Cremers, *Appl. Spectrosc.*, 41 (1987) 572.
- 6 D.A. Cremers and L.J. Radziemski, *Appl. Spectrosc.*, 39 (1985) 57.
- 7 D.A. Cremers, L.J. Radziemski and T.R. Loree, *Appl. Spectrosc.*, 38 (1984) 721.
- 8 L.J. Radziemski, T.R. Loree, D.A. Cremers and N.M. Hoffman, *Anal. Chem.*, 55 (1983) 1246.
- 9 D.A. Cremers and L.J. Radziemski, *Anal. Chem.*, 55 (1983) 1252.
- 10 H.A. Archontaki and S.R. Crouch, *Appl. Spectrosc.*, 42 (1988) 741.
- 11 L.J. Radziemski, D.A. Cremers and T.M. Niemczyk, *Spectrochim. Acta, Part B*, 40 (1985) 517.
- 12 J.B. Morris, B.E. Forch and A.W. Miziolek, *Appl. Spectrosc.*, 44 (1990) 1040.
- 13 P.M. Wiegand and S.R. Crouch, *Appl. Spectrosc.*, 42 (1988) 567.
- 14 K.J. Grant, G.L. Paul and J.A. O'Neill, *Appl. Spectrosc.*, 45 (1991) 701.
- 15 E.A.P. Cheng, R.D. Fraser and J.G. Eden, *Appl. Spectrosc.*, 45 (1991) 949.
- 16 V. Majidi, J.T. Rae and J. Ratliff, *Anal. Chem.*, 63 (1991) 1600.
- 17 R.G. Pinnick, P. Chylek, M. Jarzembki, E. Creegan, V. Srivastava, G. Fernandez, J.D. Pendleton and A. Biswas, *Appl. Opt.*, 27 (1988) 987.
- 18 J.M. Mermet, in P.W.J.M. Boumans (Ed.), *Inductively Coupled Plasma Emission Spectroscopy, Part 2 (Chemical Analysis, 90)*, Wiley, New York, 1987, Chap. 10.
- 19 H. Zahn and H.J. Dietze, *Int. J. Mass Spectrom. Ion Phys.*, 22 (1976) 111.
- 20 R.K. Winge, V.J. Peterson and V.A. Fassel, *Appl. Spectrosc.*, 33 (1979) 206.

Development of a laser-excited atomic fluorescence spectrometer and a method for the direct determination of lead in Great Lakes waters

V. Cheam, J. Lechner, I. Sekerka and R. Desrosiers

Research and Applications Branch, National Water Research Institute, Burlington, Ontario L7R 4A6 (Canada)

J. Nriagu and G. Lawson

Lakes Research Branch, National Water Research Institute, Burlington, Ontario L7R 4A6 (Canada)

(Received 19th March 1992; revised manuscript received 25th May 1992)

Abstract

A copper vapor laser-pumped dye laser was used in the development of a laser-excited atomic fluorescence spectrometer, which was optimized to give low-ng l⁻¹ sensitivity. Using the spectrometer, a method was developed for direct determination of lead in Great Lakes water samples. This is the first time that direct analyses of such samples have been successfully achieved. Existing methods require these samples to be preconcentrated before they can be analysed. The following performance characteristics were achieved: satisfactory recoveries (within 3%) for two certified reference materials, a relative standard deviation of 4.9% at the 10 ng l⁻¹ level, 53 spike recoveries within 100 ± 10% and a working detection limit of 0.4 ng l⁻¹ with a 25-μl injection volume (10 fg absolute). The 18-MΩ water used was found to contain less than 0.9 ng l⁻¹ of lead.

Keywords: Atomic fluorescence spectrometry; Laser excitation; Lead; Waters

The determination of lead in water is of great importance because of the well documented toxicity of lead in the aquatic environment and the entire ecosystem. Electrothermal atomic absorption spectrometry (AAS) is commonly used for this determination. The problem with this method is that severe interferences attributed to the matrix effect are usually encountered. The methods have been the subject of debate and dissatisfaction among environmental scientists for many years. Existing graphite furnace AAS or inductively coupled plasma (ICP) methods require sample preconcentration by procedures such as

liquid-liquid extraction/back-extraction or evaporation. These steps not only are time consuming and labor intensive but also are prone to accumulate contamination and tend to give biased high results. For accurate determination of ultratrace amounts, there is an obvious need to develop a very sensitive and effective method to alleviate these problems. Based on the literature and our own experience, laser-excited atomic fluorescence spectrometry (LEAFS) should meet these challenges.

Even though LEAFS has been shown to be an ultrasensitive technique for metals determinations [1–8], it has not become popular owing to its lack of commercial availability. It will be seen that a LEAF spectrometer can be built to provide adequate sensitivity to avoid preconcentration

Correspondence to: V. Cheam, Research and Applications Branch, National Water Research Institute, Burlington, Ontario L7R 4A6 (Canada).

TABLE 1

Equipment and operating conditions

Copper vapor laser:	MLT20 (Metalaser Technologies)
Pulse width	24 ns
Power input, power output ^a	3.6 kW, 6 W
Oscillator/function generator	HP 3311A
Interface box	In-house built
Delay generator	4144, EG&G PAR (delay = 215 ns)
Dye laser:	DL-13 (Laser Photonics)
Dye: Rhodamine 6G	0.2 g l ⁻¹ (4.2 × 10 ⁻⁴ mol l ⁻¹)
Setting for maximum fluorescence	280.60–280.61
Second harmonic generator:	Autotracker II (Inrad)
Crystal	KDP-B
Visible light filter	UG5, 4 mm (Schott Glass Technologies)
Electrothermal atomizer:	Perkin-Elmer HGA 2100
Graphite tube	8 × 28 mm
Dry, char, atomization	120, 500, 2100°C; 40, 40, 5 s
Sample injection, internal gas flow	10–25 μl, stopped-flow (interrupt)
Narrow bandpass filter, 404.7 ± 5 nm	Melles Griot
Monochromator I:	Schoeffel GM 250, 0.25 m
Aperture ratio	f/3.6
Slit width	1.5 mm
Photomultiplier I:	Thorn EMI 9813
Voltage setting	1.7–2.4 kV
Boxcar averager (software):	4121B, EG&G PAR (4162, EG&G PAR)
Gate width, operation mode	1 μs, baseline 2
A/D converter	4161A, EG&G PAR
Lead lamp	EDL lamp, 10 W (Perkin Elmer)
Monochromator II:	GCA/McPherson, EU-700-56, 0.35 m
Aperture ratio	f/6.8 at 200 nm
Slit width	1 mm
Photomultiplier II:	Thorn EMI 9798B
Voltage setting	0.9 kV
Boxcar averager	4121B, EG&G PAR
Multimeter	HP 3468A
Energy meter:	Scientex 36-0201 200 mV
Power range	0.1 mW–25 W

^a With time the power output decreases; this value is less than half the value measured when copper metal was freshly loaded.

To avoid the self-reversal phenomenon (two maxima with a local minimum response), the lamp must be in line with the incoming laser beam and it was found that it is better to focus the laser beam towards the front rather than the middle of the lamp.

Cleaning procedure, Great Lakes waters collection

The rigorous cleaning procedure, which takes over 1 week and involves the use of many agents including soap, acetone, concentrated HCl and HNO₃ and water purified with a Milli-Q system, has been described elsewhere [10] and was used to clean all relevant labware. Surface water samples were collected using a raft rod sampler and depth samples were collected using Go-flo bottles. The samples were immediately brought to a mobile clean laboratory equipped with such facilities as clean suit, clean polyethylene gloves, clean plasticware/glassware and Milli-Q-purified water. Each sample was immediately filtered through 0.4-μm filter into a clean bottle and then acidified to 0.2% nitric acid (Seastar). All samples were collected in the summer of 1991 from various stations in Lakes Ontario, Erie and Superior.

Chemicals, sample preparation and injection

Pure water (18 MΩ), referred to as MQW, was obtained from a Milli-Q water purification system (Waters) installed in a class 100 clean laboratory. Ultra-high-purity nitric acid (Seastar) with a specified lead content of 40 ng l⁻¹ was used. Standards and spikes were prepared in the class 100 clean room using precleaned glassware and plasticware and the 0.2% HNO₃ MQW blank. Lead standards were prepared from a commercial AAS 1000 mg l⁻¹ standard by sequential dilution with MQW blank. The plastic micropipette tips were soaked in 0.4% acid for several days and each tip was rinsed about a dozen times with the solution of interest before use. In spite of very careful sample handling during sample injection into the furnace, occasional contamination from the surrounding air is to be expected as the LEAF spectrometer is located in an ordinary laboratory.

tem by using the spectrometer set-up for LEAFS, but this method of tuning is makes impractical the simultaneous tuning and LEAFS operation.

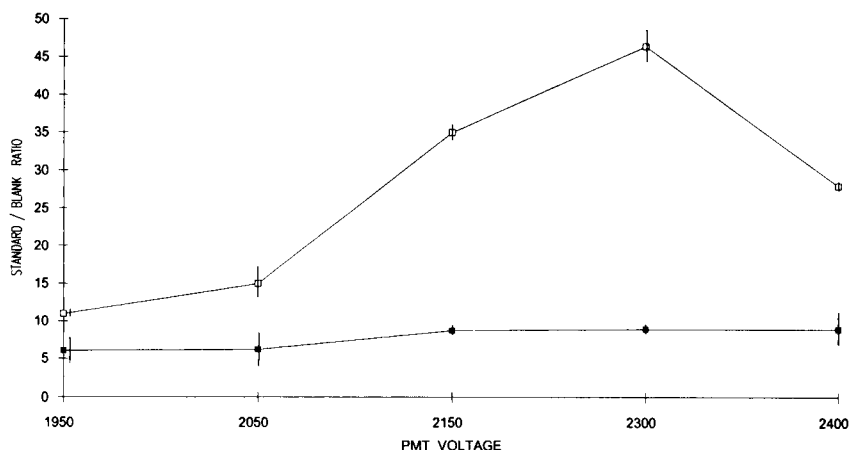


Fig. 2. Voltage dependence of signal-to-blank ratios for a 5 ng l^{-1} standard.

RESULTS AND DISCUSSION

Optimization

The Thorn EMI PMT originally had a gating board to operate as a gating PMT, but the board ceased to function after a brief period of use, probably owing to the high repetition rate (6 kHz) being used. Therefore, it was used as an ordinary PMT and the background subtraction method was relied upon. A logics circuitry of 6 kHz frequency was built and installed to permit the boxcar to subtract the baseline from the output

signal after every laser pulse, thereby significantly improving the sensitivity. With the boxcar set at $1\text{-}\mu\text{s}$ gate width, at 1000 samples averaged and in the baseline mode, a delay of 215 ns gave the best boxcar responses. The delay range 0–305 ns was tested. As was pointed out by Butcher et al. [3], stringent background corrections were found to be unnecessary.

The PMT excitation voltage giving the best signal-to-blank ratio was 2300 V, as can be seen in Fig. 2, in which the length of each vertical line on a point represents twice the standard deviation.

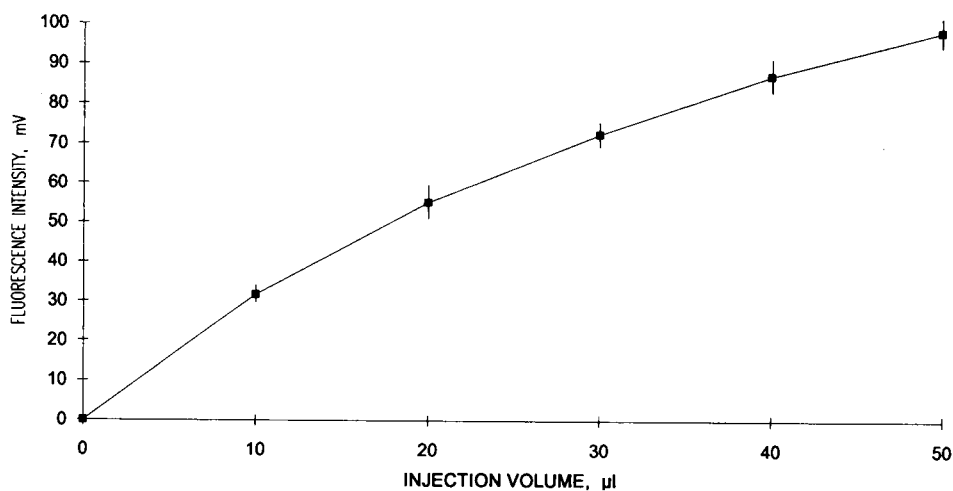


Fig. 3. Dependence of signal (mV) on injection volume.

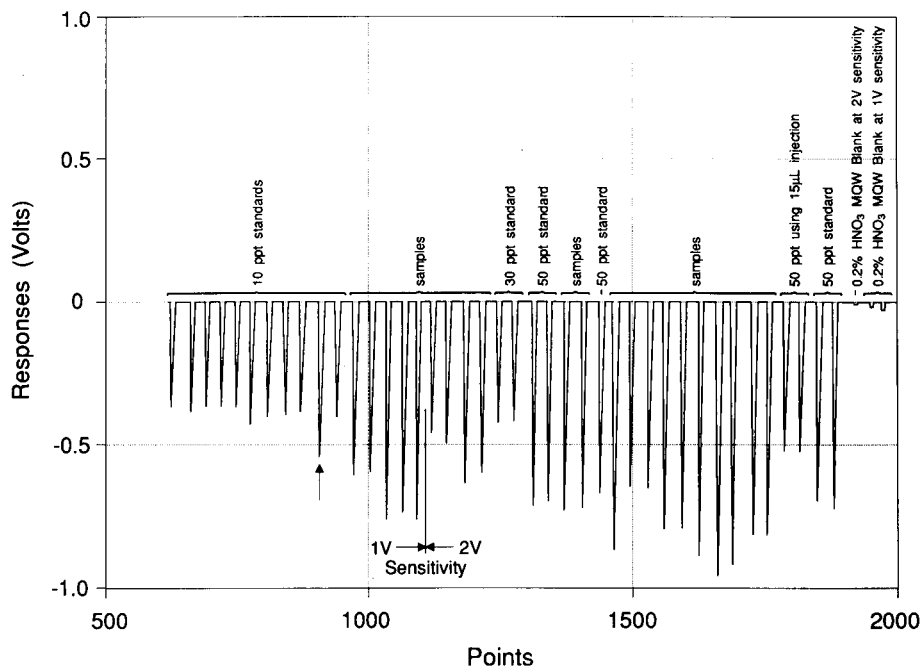


Fig. 4. Typical fluorescence responses for standards and samples containing Pb (20- μ l injection).

tion of the mean for several measurements. The working range was 1.7–2.4 kV, the lower end being used for more concentrated samples and the higher end for lower level samples. The voltage most often used was 2100 V. A ferrite bead

was installed in the PMT signal line to filter out or to reduce electrical noise, thereby improving the signal-to-noise ratio, but was found to make no further improvement.

The atomization temperature ranged from 1800

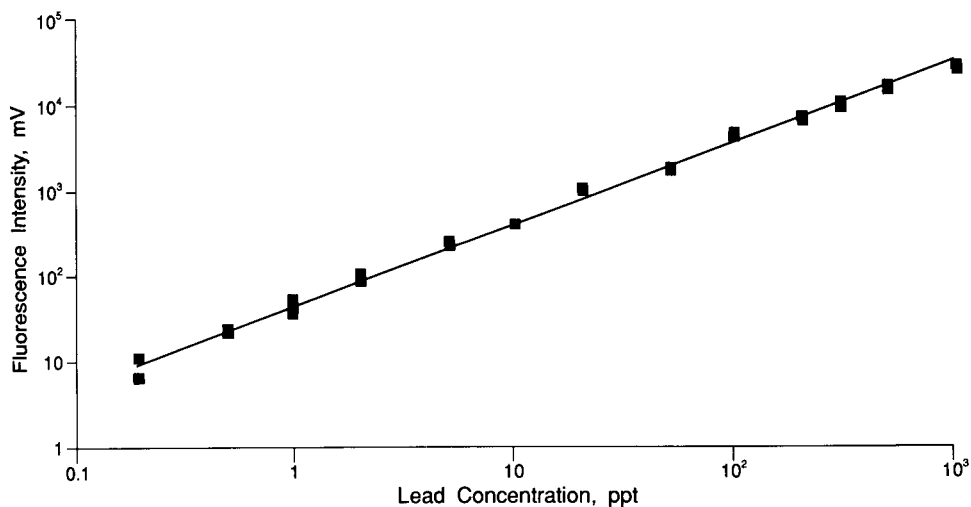


Fig. 5. LEAF calibration graph (25- μ l injection) for direct determination of lead in water.

to 2200°C but the temperature giving optimum recoveries of SLRS-2 (a certified reference material to be discussed below) was 2000–2200°C. The chosen temperature was 2100°C, because 2200°C tended to give overlapping analyte and furnace black-body radiation responses, resulting in less accurate quantification. A slit width of 1.5 mm was found to give optimum responses.

An average power output from the dye laser as low as 0.14 W, corresponding to an irradiance value of 3.5 W cm^{-2} for the 566.6-nm light (0.004 nm measured FWHM), was found to be sufficient to perform LEAFS experiments. Of course, this is far from attaining optical saturation but the benefit of operating at lower power resulted in an extended operating lifetime for the CVL before the replacement of copper inside laser tube became necessary. In fact, 700 h of operation, twice the time quoted by the manufacturer, were possible before new copper ingots were added.

Samples analysis

The sample injection volume can range from 10 to 50 μl , but the response is not linear as it shifts slightly downward with volume increase, as shown in Fig. 3, where each vertical line depicts two standard deviations as in Fig. 2. Volumes of 10–25 μl were most often used. Typical fluorescence responses for lead standards and natural water samples are shown in Fig. 4. The arrow indicates a spurious peak, which occurs about 5–10% of the time; this is probably due to build-

up of residues around the graphite tube sample hole falling into the tube during manual injection. An automated injection system will probably help to alleviate this and make the method more adaptable to routine use.

A LEAF calibration graph for lead standards in a 0.2% HNO_3 matrix is given in Fig. 5, showing duplicate measurements at each concentration level. It is an integrated line covering the 0.2–50 and the 100–1000 ng l^{-1} ranges. For the lower concentration range, normal instrument sensitivity was used; for the high range, lower sensitivity was used so the responses (peak heights in mV) were on a measurable scale and were then multiplied by a common factor so they would be in scale with the lower range (0.2–50 ng l^{-1}).

Twenty-six values of the MQW blank (0.2% acidified MQW) were monitored during a period of 2 months, giving a median value of 0.9 ng l^{-1} , a mean value of $0.94 \pm 0.21 \text{ ng l}^{-1}$ and extreme values of 0.6 and 1.4 ng l^{-1} . The blank includes contributions from the MQW itself, 0.2% acid, furnace blank (black-body radiation) stray light from various scattering processes, surrounding air and electronic noise. Thus the MQW itself should contain less than 0.9 ng l^{-1} of lead. A value of 0.28 ng l^{-1} was reported by Apatin et al. [11] for ultra-pure Grenoble water.

According to Butcher et al. [3], three types of background (concomitant scatter, molecular fluorescence and non-analyte atomic fluorescence) generated by the sample matrix may produce

TABLE 2
Results of accuracy tests

Sample	Origin	Certified (ng l^{-1})	MSA ^a (ng l^{-1})	Found ^b (ng l^{-1})
SRM 1643c	NIST ^c	35.3 ± 0.9 ^d	N.A.	36.4 ± 1.5
SLRS-2	NRC ^e	129 ± 11	N.A.	125.3 ± 10.8
LO-79-19m ^f	Lake Ontario	N.A. ^g	12.45	11.85 ± 0.54
LO-87-20m	Lake Ontario	N.A.	22.85	23.14 ± 1.63
LS-2-12m	Lake Superior	N.A.	25.75	25.46 ± 0.78
LS-125-175m	Lake Superior	N.A.	2.75	2.58 ± 0.21
LE-23-50m	Lake Erie	N.A.	44.83	44.86 ± 2.39
LE-54-6m	Lake Erie	N.A.	18.97	18.22 ± 2.53

^a MSA = results from multiple standard addition technique, field blank included. ^b Direct determination, field blank included for lake samples. ^c NIST = National Institute of Science and Technology. ^d 1000-fold dilution. ^e NRC = National Research Council of Canada. ^f LO-79-19m = Lake Ontario, Station 79, 19 m deep; the other five samples are represented correspondingly. ^g N.A. = not applicable.

signals that interfere with the analyte fluorescence signal. To determine these backgrounds, several signals were obtained for lake samples, 0.2% MQW blank and 10 ng l⁻¹ standard at ± 0.05 nm away from the analytical line, and were found to be insignificantly different from one another. This is in agreement with previous findings [3] that lead background signals for electrothermal LEAFS are negligible compared with the fluorescence signal (as opposed to AAS, where background signals can be larger than the analyte signal).

Performance characteristics

Ten replicate analyses of a 10 ng l⁻¹ standard gave an average fluorescence response of 413.3 mV with an R.S.D. of 4.9%. Table 2 shows the results of accuracy tests using two certified reference materials and six values derived from the multiple standard addition technique [12,13] applied to six different Great Lake water samples, two from each of Lake Ontario, Lake Superior and Lake Erie (different stations, different depths). For each of these samples, three distinct levels of lead standard were added and the recoveries calculated. In total, 53 such determinations of recoveries were made and are summarized in Table 3, showing recoveries well within 100 \pm 10%.

The working detection limit was defined as twice the standard deviation obtained from replicate analyses of a concentration at least five times greater than the lowest concentration that can be distinguished from the blank signal, in this in-

TABLE 3

Summary of recoveries for six different Great Lakes samples (three levels of additions for each sample)

Sample ^a	Recovery (%)	No. of determinations
LO-79-19m	102 \pm 5	17
LO-87-20m	101 \pm 10	10
LS-2-12m	100 \pm 3	8
LS-125-175m	97 \pm 8	6
LE-23-50m	101 \pm 2	6
LE-54-6m	106 \pm 4	6

^a See Table 2, footnote f.

TABLE 4

Results (blank included) for two other Lake Ontario stations

Sample ^a	Result (ng l ⁻¹)	Sample ^a	Result (ng l ⁻¹)
LO-87-field blank	4.78 \pm 1.16	LO-79-field blank 1	2.79 \pm 0.04
LO-87-0m	18.40 \pm 3.51	LO-79-field blank 2	3.52 \pm 0.25
LO-87-10m	26.01 \pm 1.66	LO-79-field blank 3	3.32 \pm 0.04
LO-87-20m	23.14 \pm 1.63	LO-79-2m	12.54 \pm 1.95
LO-87-35m	16.49 \pm 3.36	LO-79-10m	11.54 \pm 0.53
		LO-79-19m	11.85 \pm 0.54

^a See Table 2, footnote f.

stance 0.2 ng l⁻¹ [14]. Replicate analyses of 2 and 5 ng l⁻¹ (i.e., 10 and 25 times greater than 0.2 ng l⁻¹, respectively) were made, and twice the resulting pooled standard deviation [15] was 0.37 ng l⁻¹. For all practical purposes this is equal to twice the standard deviation of the MQW blank (0.42 ng l⁻¹) as discussed above. The working detection limit was then taken as 0.4 ng l⁻¹ (10 fg of lead with a 25- μ l injection).

Concentration of lead in Lake Ontario water

The results summarized in Table 4 show that the lead concentration in the samples from two stations at four different depths is lower than 25 ng l⁻¹. Table 5 shows the results for a profile of another station (LO-33) down to 130 m deep (near bottom sediment) and indicates that the lead level starts at around 18 ng l⁻¹ (surface sample), decreases to about 8 ng l⁻¹ at 100 m deep, but increases to 18 ng l⁻¹ at the deepest sampling site. The results from the fourteen sampling sites (Tables 4 and 5) indicate lead levels below 25 ng l⁻¹, which is much lower than the

TABLE 5

Results (blank included) for a depth profile of a Lake Ontario station (LO-33)

Sample	Results (ng l ⁻¹)	Sample	Result (ng l ⁻¹)
Field blank 1	1.46 \pm 0.08	25 metre depth	18.26 \pm 0.97
Field blank 2	2.24 \pm 0.08	50 metre depth	9.50 \pm 0.39
Field blank 3	1.29 \pm 0.16	75 metre depth	8.76 \pm 0.03
0 metre depth	18.71 \pm 1.25	100 metre depth	8.23 \pm 0.47
10 metre depth	15.49 \pm 1.28	130 metre depth	18.29 \pm 0.25

average value of 300 ng l⁻¹ reported for Lake Ontario up to 1986 [16]. This finding of low lead levels agrees with that reported by Flegal et al. [17], who used a preconcentration–graphite furnace AAS technique and clean-room practices. The high levels of lead reported previously were probably caused by the combination of contamination and insensitive methods used.

Conclusion

A copper vapor laser-based LEAFS has been developed and used in the development of a method for the direct determination of lead in Great Lakes waters. The preconcentration steps required in the conventional methods are no longer necessary. The generation of analytical data is simple and rapid and avoids the possibility of accumulating contamination and of producing biased high results. It appears that lead levels in Lake Ontario are much lower than the average value of 300 ng l⁻¹ reported for this lake up to 1986.

REFERENCES

- 1 M.A. Bolshov, C.F. Boutron, F.M. Ducroz, U. Gorch, O.N. Kompanetz, S.N. Rudniev and B. Hutch, *Anal. Chim. Acta*, 251 (1991) 169.
- 2 J.B. Womack, E.M. Gessler and J.D. Winefordner, *Spectrochim. Acta, Part B*, 46 (1991) 301.
- 3 D.J. Butcher, R.L. Irwin, J. Takahashi, G. Su, G.-T. Wei and R.G. Michel, *Appl. Spectrosc.*, 44 (1990) 1521.
- 4 H. Falk, H.-J. Paetzold, K.P. Schmidt and J. Tilch, *Spectrochim. Acta, Part B*, 43 (1988) 1101.
- 5 B.W. Smith, J.B. Womack, N. Omenetto and J.D. Winefordner, *Appl. Spectrosc.*, 43 (1989) 873.
- 6 G.-T. Wei, J.P. Dougherty, F.R. Preli and R.G. Michel, *J. Anal. At. Spectrom.*, 5 (1990) 249.
- 7 M.A. Bolshov, C.L. Boutron and A.V. Zybin, *Anal. Chem.*, 61 (1989) 1758.
- 8 V. Cheam, I. Sekerka and R. Desrosiers, National Water Research Institute Contribution No. 90-128, National Water Research Institute, Burlington, 1990, pp. 1–13.
- 9 V. Cheam, R. Desrosiers, J. Lechner and I. Sekerka, *Microchem. J.*, in press.
- 10 J. Nriagu, G. Lawson and H. Wong, in preparation.
- 11 V.M. Apatin, B.V. Arkhangel'skii, M.A. Bolshov, V.V. Ermolov, V.G. Koloshnikov, O.N. Kompanetz, N.I. Kuznetsov, E.L. Mikhailov, V.S. Shishkovskii and C.F. Boutron, *Spectrochim. Acta, Part B*, 44 (1989) 253.
- 12 R. Klein, Jr., and C. Hach, *Am. Lab.*, July (1977) 21.
- 13 V. Cheam, A.S.Y. Chau and S. Todd, in A.H. El-Shaarawi and R.E. Kwiatkowski (Eds.), *Statistical Aspects of Water Quality Monitoring (Developments in Water Science, Vol. 27)*, Elsevier, Oxford, 1986, pp. 64–78.
- 14 V. Cheam, *Analyst*, in press.
- 15 H.A. Laitinen, *Chemical Analysis*, McGraw-Hill, Toronto, 1960.
- 16 R. Allen and A.J. Ball, *Water Pollut. Res. J. Can.*, 25 (1990) 465.
- 17 A.R. Flegal, J.O. Nriagu, S. Niemeyer and K.H. Coale, *Nature (London)*, 339 (1989) 455.

Usefulness of stopped-flow mixing methodology for the determination of fluorescent and absorbing species. Spectrofluorimetric determination of imipramine in serum

L. de la Peña, A. Gómez-Hens and D. Pérez-Bendito

Department of Analytical Chemistry, Faculty of Sciences, University of Córdoba, E-14004 Córdoba (Spain)

(Received 19th March 1992; revised manuscript received 29th May 1992)

Abstract

A very simple approach for the determination of fluorescent and absorbing species based on stopped-flow mixing methodology is reported. By using a special procedure to introduce samples and their solvent into the observation cell of a spectrofluorimeter or spectrophotometer with the aid of a stopped-flow module, one can rapidly obtain a kinetic curve, the slope and amplitude of which are proportional to the concentration of the fluorescent or absorbing solute concerned. Various chemical systems, including quinine, imipramine, potassium permanganate and Methylene Blue were examined in order to find a plausible explanation for the kinetic effect observed and whether it applied to any fluorescent or absorbing species. The proposed approach was satisfactorily applied to the determination of imipramine in serum.

Keywords: Fluorimetry; Kinetic methods; UV-Visible spectrophotometry; Imipramine; Serum; Stopped-flow mixing

From a systematic study of the fluorescent behaviour of various therapeutic drugs in the presence of different oxidants, the reaction between carbamazepine and cerium(IV) in an acidic medium was chosen to develop a very fast kinetic spectrofluorimetric method for the determination of carbamazepine in serum based on stopped-flow mixing methodology [1]. Owing to the similar structures of this drug and imipramine, the latter was also subjected to the same systematic study by using a stopped-flow mixing technique. In strongly alkaline media, imipramine showed native fluorescence that was not affected by any of the oxidants tested. However, the fluorescence intensity increased with time when alkaline imipramine was mixed with its solvent (water) in the mixing chamber of the stopped-flow module,

which also served as the observation cell of the instrument. This resulted in the rapid production of a fast kinetic curve, the slope and amplitude of which were proportional to the imipramine concentration. Because this phenomenon could be used for the kinetic spectrofluorimetric determination of imipramine, it was studied in depth in order to find the origin of the signal increase. Other spectrofluorimetric and spectrophotometric systems were tested by using stopped-flow mixing technique and were found to behave similarly. On the other hand, the phenomenon was not observed when the batch technique was used.

EXPERIMENTAL

Instrumentation

Perkin-Elmer LS-50 and SLM 8000 C spectrofluorimeters and a Perkin-Elmer Lambda 5 and a Hitachi U-2000 spectrophotometer were

Correspondence to: D. Pérez-Bendito, Department of Analytical Chemistry, University of Córdoba, E-14004 Córdoba (Spain).

used. The SLM spectrofluorimeter was fitted with an SLM FP-052 stopped-flow module and the other instruments were furnished with a stopped-flow module [2] supplied by Quimi-Sur Instrumentation. Each instrument was connected to a microcomputer.

Reagents

The solutions used included the following: a $500 \mu\text{g ml}^{-1}$ stock solution of imipramine hydrochloride (Sigma) in distilled water, a $100 \mu\text{g ml}^{-1}$ stock solution of quinine (Merck) in 0.05 M sulphuric acid, a 0.01 M stock solution of potassium permanganate (Merck) in distilled water and 0.1% stock solutions of Methylene Blue (Aldrich) in distilled water, ethanol and dimethylformamide.

Working solutions were made by appropriate dilution of the stock solutions. All other reagents were of analytical-reagent grade.

General procedure

One of the two 10-ml reservoir syringes used was filled with a solution containing an adequate amount of the absorbing or fluorescent compound in a final volume of 10 ml. The other syringe was filled with 10 ml of solvent. After the two 2-ml drive syringes had been filled, 0.15 ml of each solution was mixed in the mixing chamber in each run. The variation of the signal (absorbance or fluorescence) was monitored at the maximum absorption or excitation and emission wavelengths of the corresponding system. The measured parameters used were the slope and amplitude of the recorded kinetic curve, which were directly proportional to the initial concentration of the compound. The slope values obtained were processed by linear regression by the microcomputer, furnished with a program for application of the initial-rate method. Each sample was assayed in triplicate.

RESULTS AND DISCUSSION

As stated above, imipramine shows native fluorescence in alkaline media [$\lambda(\text{ex}) = 290 \text{ nm}$, $\lambda(\text{em}) = 400 \text{ nm}$], the intensity of which is not affected by the presence of oxidants such as hy-

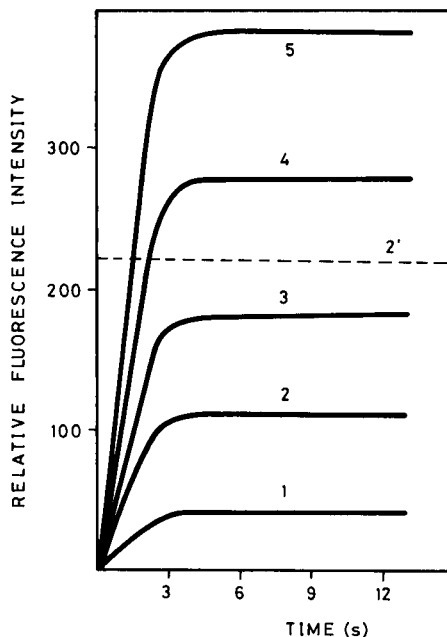


Fig. 1. Kinetic curves obtained for different concentrations of imipramine ($\mu\text{g ml}^{-1}$): 1 = 0.10; 2 = 0.30; 3 = 0.50; 4 = 0.75; 5 = 1.00. 2' = Signal obtained when both syringes were filled with $0.30 \mu\text{g ml}^{-1}$ of imipramine. $\lambda(\text{ex}) = 290 \text{ nm}$, $\lambda(\text{em}) = 400 \text{ nm}$.

drogen peroxide or potassium peroxodisulphate. On mixing an aqueous alkaline solution of imipramine held in one of the syringes of the stopped-flow module and distilled water, which was held in the other syringe, in the mixing chamber, which also acted as the observation cell, a greater variation of the fluorescence with time was observed. The slope and amplitude of the kinetic curve thus recorded were found to be directly proportional to the imipramine concentration. Figure 1 shows the kinetic curves typically obtained, which have been superimposed in order to compare their slopes. However, no signal change was observed when both syringes were filled with the same imipramine solution.

The fact that no reference to this phenomenon was found in the literature and the possibility of extending the application of the stopped-flow mixing technique to the kinetic determination of absorbing and fluorescent species with advantages over direct signal measurements, including the possibility of automation, led us to test other

spectrofluorimetric and spectrophotometric systems.

Figure 2 shows the kinetic curves obtained by using different concentrations of quinine [$\lambda(\text{ex}) = 350 \text{ nm}$, $\lambda(\text{em}) = 450 \text{ nm}$] in one of the syringes of the stopped-flow module and distilled water in the other. The graphs obtained by plotting the slope and signal amplitude against the quinine concentration had Pearson's correlation coefficients (r) of 0.990 and 0.999, respectively. Also, as with imipramine, no signal change was observed when both syringes were filled with the same quinine solution.

A possible reason for the signal change could be poor mixing of the flows from the syringes arising from a low efficiency of the stopped-flow module. The mixing module used to study the imipramine and quinine systems had an observation chamber volume of $100 \mu\text{l}$, a dead time of 20 ms and a flow velocity of 2.2 ml s^{-1} [2]. However, another stopped-flow module, an SLM 052, which featured better specifications (observation chamber volume = $32 \mu\text{l}$, dead time = 2.5 ms, flow velocity = 14 ml s^{-1}) and a mixing efficiency greater than 98%, resulted in similar signal changes, even though the slope values were larger.

In order to study the possibility of obtaining an absorbance change similar to those obtained with

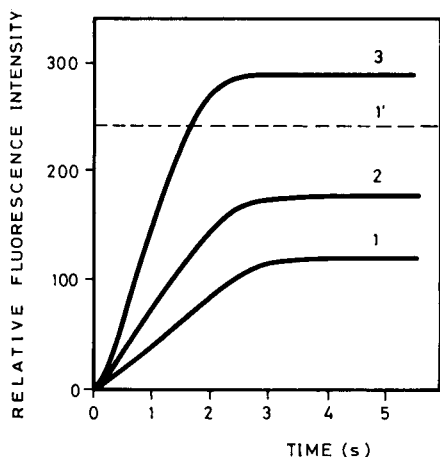


Fig. 2. Kinetic curves obtained for different concentrations of quinine ($\mu\text{g ml}^{-1}$): 1 = 0.2; 2 = 0.4; 3 = 0.8. 1' = Signal obtained when both syringes were filled with $0.2 \mu\text{g ml}^{-1}$ of quinine. $\lambda(\text{ex}) = 350 \text{ nm}$, $\lambda(\text{em}) = 450 \text{ nm}$.

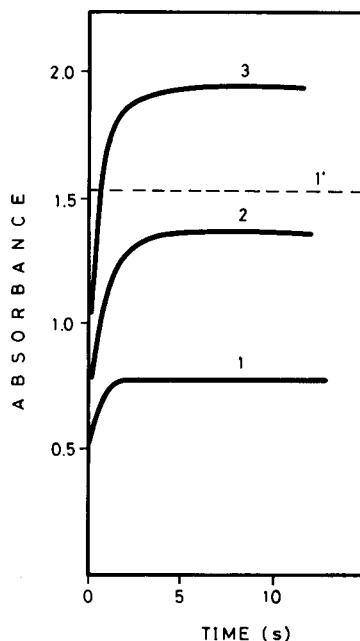


Fig. 3. Kinetic curves obtained for different concentrations of potassium permanganate (M): 1 = 5.0×10^{-4} ; 2 = 1.25×10^{-3} ; 3 = 2.0×10^{-3} . 1' = Signal obtained when both syringes were filled with $5.0 \times 10^{-4} \text{ M}$ potassium permanganate. $\lambda = 530 \text{ nm}$.

the spectrofluorimetric systems, the former mixing module was fitted to a spectrophotometer and different concentrations of potassium permanganate were used. No signal change was observed when both syringes were filled with the same permanganate solution. On the other hand, when one of the syringes was filled with the permanganate solution and the other with distilled water, a transient increase in the absorbance ($\lambda = 530 \text{ nm}$) was obtained (Fig. 3). The slope and the amplitude of the kinetic curve are also related to the permanganate concentration.

The possibility of the signal change being related to the time constant of the instrument or to the pressure (relaxation methods) was discarded because a similar signal change would have been obtained when both syringes were filled with the same fluorescent or coloured solution.

Consistent with the results obtained, a plausible explanation for the observed phenomenon would be solvation or hydration effects. Thus,

although the physical mixing of the flows from the syringes is rapid and virtually complete, the mixing and dilution effects involved might alter the solvation equilibrium and hence result in a rearrangement of the solvent and solute molecules. Accordingly, the change in the variation of the signal with time could be attributed to the rate of hydration or solvation until a new solute–solvent equilibrium is reached. This hypothesis is supported by the fact that the rate of solvation increases (there is an increase in the slope of the kinetic curves) with increase in the solute concentration. However, the fact that the signal does not change when both syringe streams hold the same concentration of solute appears to indicate that the solvation equilibrium is not changed in this instance because no dilution is involved.

Finally, one other spectrophotometric system was tested in order to study the effect of the solvent on the signal change. Three solutions of Methylene Blue, in water, ethanol and dimethylformamide, were prepared for this purpose. Different signal changes were also obtained for each solvent using various Methylene Blue concentrations, but they were very small when ethanol or dimethylformamide was used.

Although no reference to this signal change was found in the literature, the phenomenon seems to be inherent in the stopped-flow mixing technique, particularly when signals are acquired immediately after mixing. Therefore, it should be taken into account whenever a fast chemical reaction (ca. 5–10 s) is monitored spectrophotometrically or spectrofluorimetrically and one of the reactants absorbs or fluoresces at the wavelength used for measuring the analytical signal.

This signal change could be used to study the kinetics of association–dissociation processes between solutes and solvents because, according to our results, they are very fast (ca. 3–5 s). Also, as the rates of these processes are proportional to the solute concentrations, the signal change could be used for quantitative purposes. This would be as simple as the direct determination of a solute based on its native absorbance or fluorescence. However, the use of stopped-flow mixing technique can offer some additional advantages such

as shorter data acquisition times and avoidance of manipulation of reactants, which results in a higher sample throughput and allows methods to be automated for use in routine analyses.

The resolution of mixtures of absorbing or fluorescent compounds would be another tentative analytical application of this phenomenon, provided that the signal change with time is different for each compound.

Spectrofluorimetric determination of imipramine in serum

A kinetic method for the spectrofluorimetric determination of imipramine was developed on the basis of the above-described effect. Only dilution of the sample by the stopped-flow mixing technique was required.

As imipramine is intensely fluorescent in basic media, several tests were conducted in order to determine the optimum conditions for acquiring the kinetic curve. As stated above, no signal change was observed when an alkaline imipramine solution was placed in both stopped-flow drive syringes; on the other hand, only a small signal change was obtained when an aqueous imipramine solution was placed in one of the syringes and the other was filled with sodium hydroxide solution. Further, a significant signal change described above was obtained when the alkaline imipramine solution was held in one of the syringes and the other was filled with distilled water, the slope of the kinetic curve and its amplitude being proportional to the imipramine concentration.

Experimental variables (sodium hydroxide concentration, dielectric constant, temperature and ionic strength) were optimized by the univariate method in order to obtain the maximum possible slope and signal amplitude in the kinetic curves. Each reported result is the average of three measurements.

The effect of sodium hydroxide was studied by assaying different concentrations of this base in the syringe containing imipramine. The slope and the signal amplitude of the fluorescence–time curves were maximum and constant over the range 0.9–1.1 M sodium hydroxide (Fig. 4A). Placing sodium hydroxide in the syringe containing no

imipramine or in both syringes gave rise to poorer results.

The decrease in the dielectric constant of the solutions arising from addition of ethanol concentrations between 0 and 20% to the syringe containing no imipramine resulted in a slight decrease in the slope and signal amplitude of the kinetic curve (Figure 4B). Higher ethanol contents caused an even greater decrease in the parameters. Increasing temperatures in the range 20–60°C resulted in virtually linear decreases in both parameters (slope and signal amplitude) owing to the quenching effect on the fluorescence intensity of imipramine. The system was not affected by the ionic strength in the range 0.2–0.8, which was adjusted with potassium chloride.

Features of the proposed method

The fluorescence–time curves obtained at excitation and emission wavelengths of 290 and 400 nm, respectively, were processed by using a kinetic (initial rate) and an equilibrium (signal amplitude) method. The calibration graphs obtained were linear over the range 0.03–12.0 $\mu\text{g ml}^{-1}$ in both methods, and Pearson's correlation coefficient (r) was 0.997 for the kinetic method and 0.995 for the equilibrium method (both $n = 6$). The detection limit, calculated according to IUPAC recommendations [3], was 0.02 $\mu\text{g ml}^{-1}$.

The relative standard deviation for the methods ($n = 10$) for 0.2 $\mu\text{g ml}^{-1}$ of imipramine was 2.5% for the kinetic method and 3.9% for the equilibrium method. The selectivity of the two methods was assessed by testing various poten-

TABLE 1

Effect of various species on the determination of 1 $\mu\text{g ml}^{-1}$ of imipramine

Tolerated weight ratio (species/analyte)	Species added
100:1	Glucose, urea, uric acid, creatinine, salicylic acid, hydroxylamine, hydrazine sulphate, Cu(II), Mg(II), sulphite
50:1	Fe(III), Ca(II)
10:1	Norepinephrine
5:1	Epinephrine
1:1	Bilirubin

tially interfering compounds. The maximum concentration tested was 100 times that of imipramine. According to the results obtained (Table 1), the most serious interference was posed by bilirubin. One salient feature of the proposed method is its speed: measurements are performed within ca. 5 s, which results in a very high sampling rate.

The method was applied to serum by using the following procedure: 1 ml of human serum was mixed with 0.25 ml of 2 M sodium hydroxide solution, 8 ml of heptane and 0.75 ml of isoamyl alcohol. The mixture was stirred for 5 min and centrifuged at 3000 rpm at room temperature for 5 min. The resulting aqueous layer was removed by aspiration and 0.15 ml of 2 M sodium hydroxide solution was added. The tube was then shaken for 5 min and centrifuged. A volume of 7 ml of the organic phase was transferred into a centrifuge tube containing 2 ml of 0.1 M hydrochloric acid and the tube was shaken for 5 min and subsequently centrifuged. The organic phase was then discarded and 1.5 ml of the acidic phase was mixed with 0.5 ml of 4 M sodium hydroxide solution and placed in one of the two 2-ml drive syringes. The other syringe was filled with distilled water. In each run, 0.15 ml of each solution was mixed in the mixing chamber, which was also the observation cell. The variation of the fluorescence intensity with the time was monitored at $\lambda(\text{ex}) = 290$, and $\lambda(\text{em}) = 400$ nm. Fluorescence values were acquired for 5–10 s and processed by linear regression by the microcomputer furnished with a program (Kinetic Obey) for application of

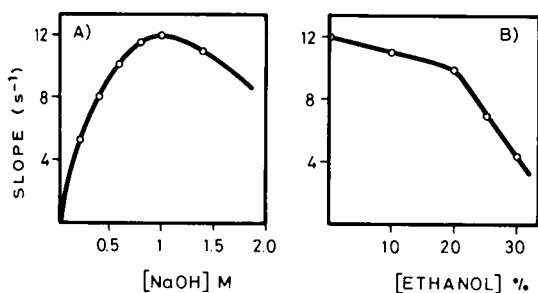


Fig. 4. Effect of (A) sodium hydroxide concentration and (B) percentage of ethanol on the slope of the kinetic curves obtained for imipramine.

TABLE 2

Recovery of imipramine added to serum samples

Sample	Imipramine ($\mu\text{g ml}^{-1}$) ^a		Recovery (%)		
	Added	Found ^b		A	B
		A	B		
1	0.150	0.160	0.164	106.7	109.3
	0.300	0.316	0.318	105.3	104.0
	0.600	0.546	0.556	91.0	92.7
2	0.150	0.158	0.157	105.3	104.7
	0.300	0.324	0.321	108.0	107.0
	0.600	0.620	0.610	103.3	101.7
3	0.150	0.155	0.161	103.3	107.3
	0.300	0.287	0.274	95.7	91.3
	0.600	0.638	0.619	106.3	103.2
4	0.150	0.148	0.148	98.7	98.7
	0.300	0.288	0.295	96.0	98.3
	0.600	0.564	0.579	94.0	96.5
5	0.150	0.140	0.137	93.3	91.3
	0.300	0.288	0.280	96.0	93.3
	0.600	0.555	0.570	92.5	95.0

^a A = kinetic method; B = signal amplitude method. ^b Average of three determinations.

the initial-rate method. The slopes of the fluorescence–time curves were determined in about 3 s and each sample was assayed in triplicate. All measurements were carried out at 20°C. The concentration of imipramine in the samples was determined by interpolation on the calibration graphs constructed using a standard solution of imipramine (final concentration 0.03–12.0 $\mu\text{g ml}^{-1}$) made by adding 1 ml of a previously prepared serum pool to each imipramine standard.

The slowness of the sample pretreatment [4,5] is offset by significantly faster measurements, which take only a few seconds. Table 2 lists the concentrations and analytical recoveries obtained for various serum samples to which were added different amounts of imipramine. The mean recovery obtained for both the kinetic and the equilibrium method was very close to 100%.

Imipramine undergoes extensive first-pass metabolism, chiefly by demethylation to the primary active metabolite desipramine. Thus, on

oral administration of imipramine, about 30% of the amount given is transformed into desipramine within ca. 4 h [6]. However, it was found that desipramine (tested at the same concentration) yielded the same signal change as imipramine, so that it was impossible to distinguish between the two compounds.

Conclusions

The phenomenon observed on applying the stopped-flow mixing technique to the determination of compounds of pharmacological interest has been investigated. The increase in the fluorescence or absorbance with time throughout the mixing of the solute and solvent can be used both to study the kinetics of association–dissociation processes and for the determination of the solute. The main practical advantage of this approach is the great simplicity resulting from the lack of a need for reagent to obtain the analytical signal; in fact, it suffices to fill the second syringe of the stopped-flow module with the same solvent as used for the analyte. In this work this effect was exploited for the determination of imipramine in serum.

The authors acknowledge financial support from the CICyT.

REFERENCES

- 1 L. de la Peña, A. Gómez-Hens and D. Pérez-Bendito, *Fresenius' J. Anal. Chem.*, 338 (1990) 821.
- 2 A. Loriguillo, M. Silva and D. Pérez-Bendito, *Anal. Chim. Acta*, 199 (1987) 29.
- 3 G.L. Long and J.D. Winefordner, *Anal. Chem.*, 55 (1983) 273.
- 4 J.R. Gillette, J.V. Dingell, F. Sulser, R. Kuntzman and B.B. Brodie, *Experientia*, 17 (1961) 377.
- 5 J.V. Dingell, F. Sulser and J.R. Gillette, *J. Pharmacol. Exp. Ther.*, 143 (1964) 14.
- 6 N. Sistovaris, E.E. Dagrosa and A. Killer, *J. Chromatogr.*, 28 (1983) 273.

Versatile stopped-flow apparatus with adjustable pistons

Per-Ola Freskgård, Nils Bergenhem and Uno Carlsson

IFM, Department of Chemistry, Linköping University, S-581 83 Linköping (Sweden)

(Received 14th April 1992)

Abstract

A stopped-flow apparatus with many potential applications is described, in which the vertical design makes operation easier. In addition, the system has adjustable driving pistons that facilitate refilling of syringes and changing of reaction solutions without allowing air to enter the system. This means that the use of reservoir syringes is redundant. The driving pistons can easily be adjusted to withstand different pressures and temperatures and the O-rings are simple to change when worn out. The vertical stopped-flow system is also flexible, as syringes of different size can be used and are easily changed when, for instance, different dilution ratios are needed.

Keywords: Electron spin resonance spectrometry; UV-Visible spectrophotometry; Protein denaturation; Stopped-flow apparatus

The determination of the kinetics of chemical reactions is important in several fields of fundamental and applied research. Many intermediates of chemical and biochemical processes can be detected and characterized only by means of fast kinetic methods. The most rapid method of mixing two solutions is the stopped-flow technique. The aim of this work was to construct a stopped-flow apparatus that has a reasonably short dead time (ca. 10 ms) and that can both efficiently mix solutions of varying viscosity and mix solutions in different ratios. Another aim was that the apparatus should allow reactions to be followed at different temperatures without encountering problems with the liquid system. The present instrument was designed to fulfil the requirements of protein folding studies. In such studies, rapid measurement of kinetics is a method commonly used to reveal kinetic phases and properties of intermediates.

Correspondence to: U. Carlsson, IFM, Department of Chemistry, Linköping University, S-581 83 Linköping (Sweden).

In a conventional stopped-flow apparatus (Fig. 1), the reactant solutions are placed in storage syringes and transferred into the driving syringes. Pneumatic pressure is applied to the horizontal driving syringes by opening a gas reservoir, and this forces a piston forward, against the driving syringes, until it hits the mechanical stop. The mixed solution is pushed through the mixer into the observation cell, where continuous monitoring takes place. The stopped-flow method allows several measurements to be made on only a few millilitres of sample solution, which is preferable when using solutions that are expensive or difficult to obtain. Temperature control is essential when using the stopped-flow apparatus, as the kinetics of chemical and biochemical reactions are strongly temperature dependent. Accurate control of this parameter is normally obtained by using a complete flow circuit, including the driving syringes and reservoirs. The conventional applications of the stopped-flow technique are absorbance and fluorescence measurements, but the method can also be used to measure circular dichroism (CD) and electron spin resonance

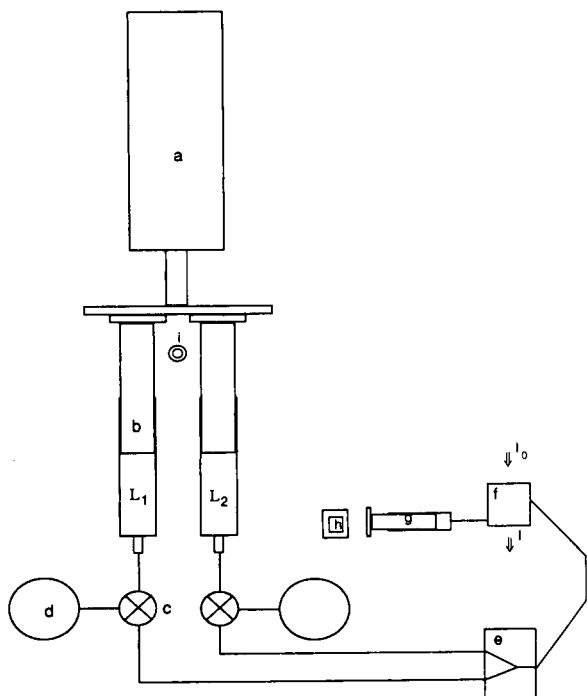


Fig. 1. Schematic diagram of a stopped-flow apparatus. a = Pneumatic drive; b = driving syringes; c = three-port valves; d = solution reservoirs; e = mixer; f = observation cell; g = stop syringe; h = end-stop; i = front-stop.

(ESR). Consequently, the stopped-flow technique is a powerful tool for studying almost any type of reaction.

The vertical stopped-flow apparatus described in this paper was constructed to meet the special requirements of our research. This vertical system has the following characteristics: the two driving syringes are mounted vertically in a thermostated box, which facilitates refilling of the two syringes or changing the reactant solutions and also prevents air from entering the solution system; the system is flexible, as syringes of different size can be used and easily changed, thereby allowing dilution ratios to be varied; the apparatus is designed with driving pistons that are simple to adjust when used at different temperatures, and that are equipped with a number of O-rings, to prevent leakage, which are conveniently changed when they are worn out; and the syringes are manufactured of a material that

withstands high operating pressures, which means that problems with leakage are avoided.

EXPERIMENTAL

Apparatus

The vertical stopped-flow apparatus (Fig. 2) consists of a framework (g) which supports the driving block (d), and a thermostated box which contains the two driving syringes (c). The framework (33 × 80 × 35 cm) is made of cast iron, which gives the whole apparatus the stability and weight needed to hold the stop-plate in a rigid position. The framework also stabilizes the aluminium driving block. There are two horizontal driving plates in the apparatus: the pneumatic drive (a) is connected to the upper and the two driving pistons (b) are connected to the lower plate. Two cylindrical barrels are located at both ends of the driving plate. Steel tubes attached to

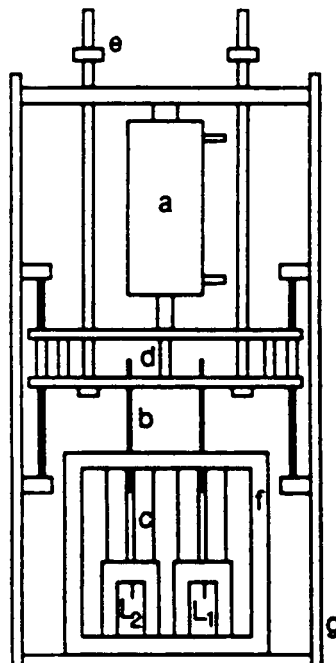


Fig. 2. Vertical stopped-flow apparatus. a = Pneumatic drive; b = driving pistons; c = driving syringes; d = driving block; e = mechanical stop; f = thermostated box; g = framework; L₁ and L₂ = outlet reactant solutions.

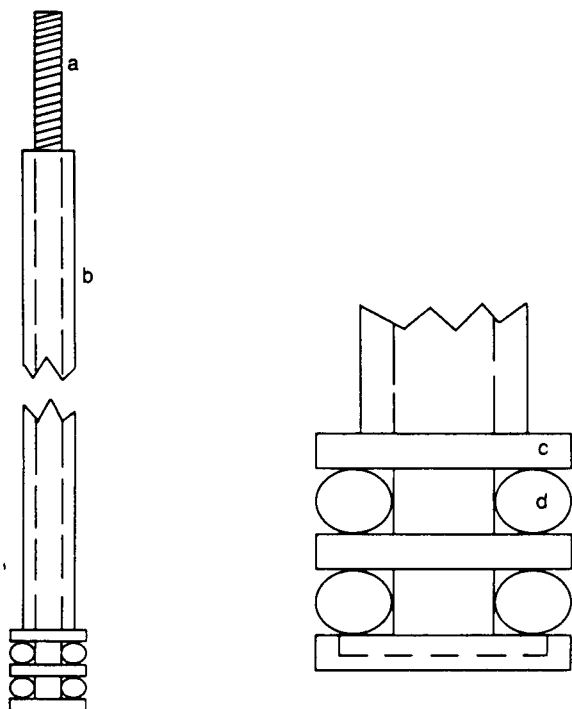


Fig. 3. Structure of the driving piston. a = Inner threaded tube; b = outer pushing tube; c = washer; d = O-ring.

the frame run through the barrels, which are made of Teflon to reduce friction. This set-up ensures an accurately linear motion of the driving block so that equal volumes of liquid will be delivered. When driving syringes of different size are used, the pneumatic drive can be adjusted horizontally to help prevent a non-linear motion. The pneumatic driver can be driven by either air or nitrogen at a pressure controlled by a reservoir tank; the gas flow can be initiated by an electromagnetic valve, either manually or by a computer system. The driving pistons [Figs. 2 (b) and 3] are made of stainless steel, and to prevent the solutions from being contaminated with metal ions the driving surface (which is in contact with the solution) is jacketed with nylon and the two washers are made of nylon. When the driving piston is pressed into the driving syringe and is in full contact with the solution, the nut on the inner tube (a) pushes the outer tube (b) against the washers (c) and squeezes them together so the O-rings (d) expand against the syringe wall. With

this type of piston, reservoir syringes are unnecessary. This is true because the vertical position of the driving syringes allows them to be refilled with solutions or the solutions to be changed without letting air into the system, which is not possible when using syringes with unadjustable pistons. The driving syringes are made of Plexiglas and are of a size that will withstand the pressure. The outside dimension of the syringe is 55 mm and will, for example, give a wall thickness of 10 mm if the syringe diameter is 35 mm. The thickness of the wall is important for the strength of the driving syringe: the thicker the syringe wall, the higher is the operating pressure that can be used.

The mixing device consists of a turbulent two-jet tangential mixing chamber, in which the injection streams of the two solutions meet and create a turbulent mixing stream. The mixer is connected directly with the observation cell (Fig. 4) by two screws and tightened with a washer. The combined mixing device and observation cell are made of Plexiglas with quartz windows. It is of the same size as a standard cell, and can therefore be used in an ordinary spectrophotometer. The photomultiplier signal is digitized by a fast analogue-to-digital A/D converter, which feeds the data directly into the memory of a microcomputer; the sweep time is set on the clock of the microcomputer. The present set-up, a PC Bondwell BW3B1 equipped with a high speed,

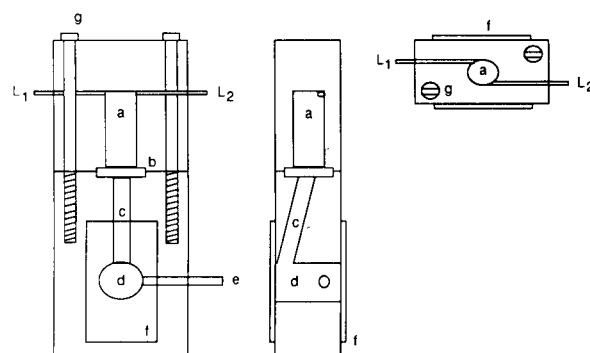


Fig. 4. Combined mixing device and observation cell. L_1 and L_2 = inlets for the two solutions; a = turbulent mixing chamber; b = washer; c = transport tube; d = observation pathway; e = outlet; f = quartz glass; g = screw.

multi-function data acquisition PCL 812 card (Advantech) was used to sample the data. The A/D converted data were transferred under program control to an exponential-fit function program MATLAB.

RESULTS AND DISCUSSION

Mixing and observation

As the reaction in stopped-flow experiments is started by mixing two solutions, the mixing efficiency is one of the most critical factors for a correct estimation of the rate constant. Efficient mixing is essential when using solutions with high viscosity, which might be due to high protein concentrations and/or to high concentrations of different denaturants. Both theoretical and practical problems arise when designing a system that is highly turbulent and yet free of cavitations [1].

Mixing test

The mixing efficiency can be tested simply by mixing a coloured solution with water [2]. An appropriate compound for use in such a test is potassium hexacyanoferrate(III) [$K_3Fe(CN)_6$], which in a 0.03% solution has an absorbance of about 1.0 cm^{-1} at 420 nm. Any incomplete mixing and unbalanced stopping of the two solutions would produce some turbulence immediately after the flow is stopped. This may occur within a few to a few hundred milliseconds. The magnitude of the turbulence should produce less than a 0.5% change in the absorbance of the coloured solution [2]. The efficiency of mixing is delicately dependent on the shape of both the outlet of the mixer and the inlet of the observation cell. In a test of the mixing device, the turbulence after the stop was found to be less than 0.3% of the total absorbance of the coloured solution when using a mixing ratio of 1:1.

Dead-time test

The dead time (i.e., the time required for the solution to flow from the centre of the mixer to the centre of the observation cell) between mixing and observation can be measured as follows [2,3]. As it was known that the reduction of

$K_3Fe(CN)_6$ by L-ascorbic acid proceeds at a suitable rate, a test was carried out with a 0.25 mM solution of this compound in one syringe and water in the other (mixing ratio 1:1). From this, the total absorbance (A_{tot}) of the mixture was determined at 420 nm. A second test experiment was performed with $K_3Fe(CN)_6$ solution (also 0.25 mM) in one syringe and L-ascorbic acid solution (10 mM) in the other. The spectrophotometric trace of the reaction that occurred was found to proceed as a first-order reaction in terms of disappearance of the coloured reactant. If A is the absorbance initially observed and k_{app} the rate constant of the pseudo-first-order reaction, then the dead time (t_d) is given by

$$A = A_{tot} \exp(-kt_d) \quad (1)$$

According to this, the dead time in the present tests was 11 ms.

ESR application

The mixing device (turbulent two-jet tangential mixing chamber) of the apparatus was connected to a standard flat cell in an electron spin resonance (ESR) spectrometer in order to examine the reaction between the spin-label 4-oxo-TEMPO (4-oxo-2,2,6,6-tetramethylpiperidine-*N*-oxyl) and ascorbic acid under basic conditions. The trace of the recorded high-field resonance line is shown in Fig. 5. The amplitude decay is

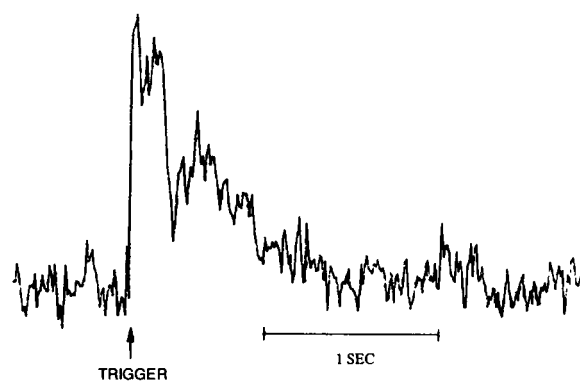


Fig. 5. Reduction of 4-oxo-TEMPO by ascorbic acid at pH 10 (adjusted with KOH). After mixing, the final concentrations of 4-oxo-TEMPO and ascorbate were 0.35 and 0.5 mM, respectively. Mixing ratio, 1:13.2; temperature $23 \pm 0.2^\circ\text{C}$. The trace illustrates the ESR high-field resonance line amplitude of 4-oxo-TEMPO.

first order, with a half-life of ca. 300 ms [4]. Two different syringes were used in the experiment and the mixing ratio of 4-oxo-TEMPO and ascorbic acid was 1:13.2. The significant disturbance in the decay phase was probably caused by microphonics occurring when the liquid flow was arrested, which indicates how important it is that the flat cell is rigidly attached to the ESR cavity. This type of time-dependent measurements of the signal from a spin label attached to a specific site on a protein can give information about local conformational changes in different environments.

Conformational change of proteins

Conformational changes of proteins can be induced by a sudden addition of a denaturing agent such as guanidine hydrochloride (GuHCl). In most instances these changes can be monitored by small accompanying changes in absorbance at 280–300 nm, due to environmental changes around tryptophan and tyrosine residues. Denaturation of human erythrocyte carbonic anhydrase II (HCA II) by GuHCl was registered as the absorbance change at 292 nm, a change caused by the exposure of tryptophan residues to the polar solvent. Proteins are unfolded in GuHCl because the side-chains and the polypeptide backbone are more soluble in GuHCl than in water, and this unfolding leads to an increased exposure of the buried tryptophan residues. A typical stopped-flow trace from this type of reaction is illustrated in the inset in Fig. 6.

A linear relationship between $\log k_u$ and GuHCl concentration can be seen in Fig. 6. Previous experiments [5] have shown that

$$\log k_u = \log k_u^{\text{H}_2\text{O}} + m_{ku}[\text{GuHCl}] \quad (2)$$

where k_u is the rate constant for unfolding $k^{\text{H}_2\text{O}}$ is the rate constant in water and m_{ku} is the slope of the line. Hence experimental results obtained with the present equipment are in accordance with what can be expected from the results of Matouschek et al. [5].

Conclusion

The stopped-flow method is the technique most often used to measure fast reactions. The appara-

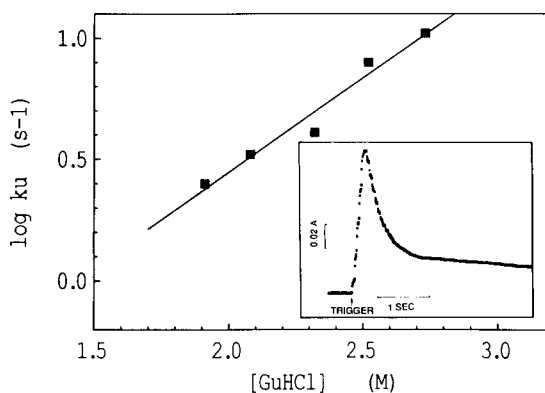


Fig. 6. $\log k_u$ versus [GuHCl] plot for HCA II. The slope (m_{ku} from Eqn. 2) is 0.75. The inset shows time course of denaturation of HCA II observed at 292 nm. The reaction was monitored with a Perkin-Elmer Lambda 5 spectrophotometer equipped with the combined mixing device and observation cell described in the text. Unfolding was initiated by diluting the aqueous protein solution (0.5 mg ml^{-1}) in GuHCl solution (4.64 M) to final GuHCl and protein concentrations of 2.32 M and 0.25 mg ml^{-1} , respectively. The experiment was performed in 0.1 M Tris- H_2SO_4 (pH 7.5) at $23 \pm 0.2^\circ\text{C}$. The ratio of the syringe volumes was 1:1. The data sampled on the PCL 812 Card in a PC Bondwell BW3B1 were transferred to an exponential-fit function program (MATLAB) and analysed to give the curve that best fitted the data. $k = 4.07 \text{ s}^{-1}$ ($t_{1/2} = 170 \text{ ms}$).

tus employed has remained more or less unchanged since it was developed and only the quality of the components have changed over the years. A vertical design is conducive to easier operation, particularly with regard to refilling syringes or changing solutions. The adjustable pistons are the key characteristics of this system, as they can be filled with solution before they are inserted, thereby avoiding air bubbles, which is a great advantage. The vertical design of the driving syringes renders reservoir syringes redundant. The design also makes it easy to perform measurements at low temperatures, as leakage is prevented by the adjustable O-rings of the driving pistons.

This study was financially supported by grants to U.C. from the Swedish National Board for Technical Development (732-88-04392) and the Carl Tryggers Stiftelse för Vetenskaplig Forskn-

ing. A fellowship to P.-O.F. from the Stiftelsen Bengt Lundqvists Minne is also gratefully acknowledged.

REFERENCES

- 1 R.L. Berger, *Biophys. J.*, (1978) 2.
- 2 B. Tonomura, H. Nakatani, M. Ohnishi, J. Yamaguchi-Ito and K. Hiromi, *Anal. Biochem.*, 84 (1978) 370.
- 3 K. Hiromi, *Methods Biochem. Anal.*, 26 (1977) 137.
- 4 W.L. Hubbell, *Rev. Sci. Instrum.*, 58 (1978) 1879.
- 5 A. Matouschek, J.T. Kellis, Jr., L. Serrano and A.R. Fersht, *Nature (London)*, 340 (1989) 122.

Regression analysis of piezoelectric titration data to estimate system parameters

W.-Z. Wei, L.-H. Nie and S.-Z. Yao

Department of Chemistry and Chemical Engineering, Hunan University, Changsha 410082 (China)

(Received 19th September 1991; revised manuscript received 19th May 1992)

Abstract

A non-linear model connecting the frequency response of the piezoelectric quartz crystal detector in acid–base titration with the added quantity of titrants has been derived in detail. It has been verified theoretically and used for the regression analysis of response curves of acid–base titrations for four acid solutions with different dissociation constants to estimate the original acid concentrations of the solutions to be titrated, dissociation constants of the acid, the equivalent ionic conductivities and the other two crystal response parameters, viz., the response sensitivity for conductivity and the basic frequency when the conductance contribution of the reacting substances equals zero. The experiments and computations indicate that the technique possesses good estimation precision and accuracy.

Keywords: Piezoelectric sensors; Titrimetry; Regression analysis

Conductimetric and high-frequency (oscillometric) titrations, which are based on the change in conductance of a reaction system at the end-point, have become established [1]. However, their sensitivity is relatively low and their accuracy is affected by the presence of non-reacting electrolytes. Recently, the use of piezoelectric crystal detectors for titrations has seen wide interest [2–4], since the detectors have many advantages, high sensitivity, simple instrument and small size. The usual technique to determine the end-point of conductimetric titrations is graphic. Since only a small amount of information of response curves is used, the precision strongly relies on the experience of the analysts and other experimental conditions and the system properties. For example, when the dissociation constant of a system is not too large or too small, end-point determina-

tion is very difficult with the graphic technique. On the other hand, regression analysis makes full use of the entire response curve information so that a more accurate estimation of the initial concentrations can be achieved and other parameters reflecting the system and the detector properties can be estimated simultaneously.

The purpose of this work was to derive a theoretical frequency response model of the piezoelectric crystal detector for acid–base titration based on the balance principle of acid–base systems and to test the model theoretically. Then the model was used to estimate unknown parameters for acid–base titration systems.

THEORY

For an acid (HA) in an aqueous system, when a strong base BOH is used to titrate the acid, and if it is assumed that the strong base is dissociated completely in the solution during the titration,

Correspondence to: S.-Z. Yao, Department of Chemistry and Chemical Engineering, Hunan University, Changsha 410082 (China).

the substances in the solution which do not react during the titration are not considered, there are four basic balances in the solution: the balance of positive and negative charges:

$$[\text{H}^+] + [\text{B}^+] = [\text{OH}^-] + [\text{A}^-] \quad (1)$$

the mass balance:

$$[\text{HA}] = C^* - [\text{A}^-] \quad (2)$$

the acid dissociation balance:

$$K_a = [\text{A}^-][\text{H}^+]/[\text{HA}] \quad (3)$$

and the water dissociation balance:

$$K_w = [\text{H}^+][\text{OH}^-] \quad (4)$$

where C^* is the original concentration of HA, $[\]$ the balance concentration of reacting substances during the entire titration, K_a the dissociation constant of HA, and K_w the dissociation constant of water. Combining the above four equations, we obtain

$$[\text{H}^+]^3 + ([\text{B}^+] + K_a)[\text{H}^+]^2 - (K_w + C^*K_a - K_a[\text{B}^+])[\text{H}^+] - K_aK_w = 0 \quad (5)$$

$$[\text{OH}^-] = K_w/[\text{H}^+] \quad (6)$$

and

$$[\text{A}^-] = K_aC^*/([\text{H}^+] + K_a) \quad (7)$$

During the titration, once the parameters K_a , K_w and C^* are known, the added quantity of b^* is independent and hence the concentrations of other substances depend on it and can be computed from the above equations. Thus Eqns. 5–7 can be used as the fundamental model for any sensor titration (when the pH electrode is used to detect the concentration of H^+ in solutions, the parameter model connecting pH with the quantity of BOH added can be established). For the piezoelectric crystal detector, its frequency response to the conductance of a solution is linear under certain range and certain experimental conditions for which this relation exists [5].

$$\Delta f = s \Delta k$$

where Δf is the frequency shift of a crystal in an electrolyte solution with respect to its frequency

in water, Δk , the increase in quantity of the specific conductance and s , the sensitivity of the crystal for the specific conductance which is a constant and independent of the type of electrolyte. The frequency response of the piezoelectric crystal before or during the titration can be expressed as

$$f = s\{I_{\text{B}^+}[\text{B}^+] + I_{\text{OH}^-}[\text{OH}^-] + I_{\text{A}^-}[\text{A}^-] + I_{\text{H}^+}[\text{H}^+]\} + f_0 \quad (8)$$

where f_0 is the fundamental frequency of the crystal when the conductance contribution of the reacting substances is zero and I represents the equivalent ionic conductivity. From Eqns. 5–8 a theoretical model connecting the frequency response of a piezoelectric crystal detector with the added quantity of titrant can be built. It is a non-linear model with four model parameters, i.e., K_a , C^* , s and f_0 , if the equivalent ionic conductivities of all the reacting ions are known. When the equivalent ionic conductivities of some ions are not available, they can be regarded as the parameters to be estimated.

To estimate the model parameters, the error function of the squared residuals is used

$$E = \sum_{i=1}^n (f_i - \hat{f}_i)^2 \quad (9)$$

where n is the number of observed data, f_i and \hat{f}_i are observed and computed frequencies, respectively. The model parameters can be estimated by minimizing the error function. Because there is a closed form for regression, the Marquardt method [6] is suitable. For the multi-parameter problem in this paper, once the partial derivatives of f with respect to all parameters have been derived, the linear Taylor's expansion of f can be substituted for f , and if the initial values of the parameters to be estimated, b_1^0 (K_a^0), b_2^0 (C^{*0}), b_3^0 (s^0), b_4^0 (f_0^0), are given, Eqn. 9 becomes

$$E = \sum_{i=1}^n \left[f_i - \left(f_{i0} + \frac{\partial f_{i0}}{\partial b_1} \Delta 1 + \frac{\partial f_{i0}}{\partial b_2} \Delta 2 + \frac{\partial f_{i0}}{\partial b_3} \Delta 3 + \frac{\partial f_{i0}}{\partial b_4} \Delta 4 \right) \right]^2$$

By the minimax principle, the following linear equations are obtained

$$\begin{cases} (a_{11} + d) \Delta 1 + a_{12} \Delta 2 + a_{13} \Delta 3 + a_{14} \Delta 4 = a_{1f} \\ a_{21} \Delta 1 + (a_{22} + d) \Delta 2 + a_{23} \Delta 3 + a_{24} \Delta 4 = a_{2f} \\ a_{31} \Delta 1 + a_{32} \Delta 2 + (a_{33} + d) \Delta 3 + a_{34} \Delta 4 = a_{3f} \\ a_{41} \Delta 1 + a_{42} \Delta 2 + a_{43} \Delta 3 + (a_{44} + d) \Delta 4 = a_{4f} \end{cases}$$

where

$$a_{kj} = \sum_{i=1}^n \frac{\partial f_{i0}}{\partial b_k} \frac{\partial f_{i0}}{\partial b_j} \text{ for } k, j = 1, \dots, 4$$

$$a_{kf} = \sum_{i=1}^n \frac{\partial f_{i0}}{\partial b_k} (f_i - f_{i0}) \text{ for } k = 1, \dots, 4$$

and

$$d \geq 0$$

$\Delta 1$ – $\Delta 4$ can be obtained by solving the above linear equations and the decrease of E can be insured through adjustment of d . Then $b_i^{\circ'} = b_i^{\circ} + \Delta i$ is used as the initial values for the next iteration. The process is repeated until the δi ($i = 1, \dots, 4$) values are smaller than the given values, then the iteration is ended.

EXPERIMENTAL

Apparatus and reagents

The detection cell and the complete assembly used have been described previously [3]. A 50- μ l microsyringe was used for titrant addition. Analytical reagent grade chemicals and doubly distilled water were used. An IBM PC/XT was used to treat the experimental data.

Procedure

A 10–20-ml volume of sample solution was transferred into the detection cell. A piezoelectric quartz crystal (AT-cut, 9 MHz) was fully immersed in the liquid and the magnetic stirrer was switched on. The titrant was added and the crystal response frequency (f) was recorded. At the same time the added quantity of the titrant was also recorded. All experiments were carried out in a temperature-controlled water bath at $30 \pm 0.2^\circ\text{C}$.

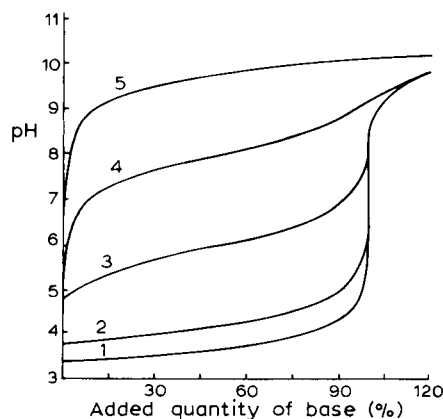


Fig. 1. pH of 0.0004 M acids with different K_a vs. added quantity of strong base according to theoretical model for different K_a . 1, $K_a = 1 \times 10^{-2}$; 2, $K_a = 1 \times 10^{-4}$; 3, $K_a = 1 \times 10^{-6}$; 4, $K_a = 1 \times 10^{-8}$; 5, $K_a = 1 \times 10^{-10}$. $K_w = 1 \times 10^{-14}$.

Regression analysis of the data

All non-linear regression programs were written in BASIC, including the main program which fits the experimental data to the regression model, and three subroutines which compute the function and corresponding derivative values, and solve Eqn. 5 to find its root (about 1×10^{-7}) by Newton's method, respectively. The programs are available from the authors.

The equivalent ionic conductivities were taken from Ref. 7.

RESULTS AND DISCUSSION

Validation of the non-linear regression

For a given set of parameters, the theoretical model can compute the concentrations of the reacting substances at any titration moment, including those before titration, at the end-point and after the end-point. Figures 1 and 2 show the pH of solutions and the concentrations of HA and A^- vs. the quantity of titrant with different K_a added, respectively. It can be seen that correct pH and concentration changes can be achieved with the model. Figure 3 gives the corresponding piezoelectric crystal detector responses for the same set of parameters. The figure shows that the change of K_a makes the response curves

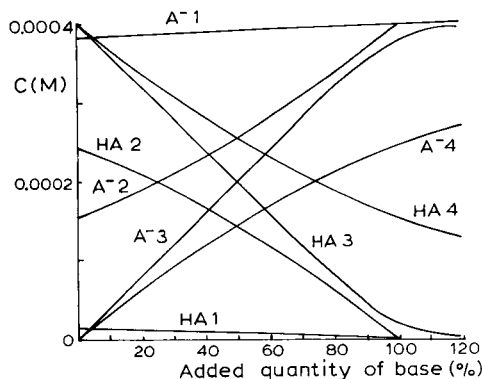


Fig. 2. Concentrations of HA and A^- vs. added quantity of strong base according to theoretical model. 1, $K_a = 1 \times 10^{-2}$; 2, $K_a = 1 \times 10^{-4}$; 3, $K_a = 1 \times 10^{-8}$; 4, $K_a = 1 \times 10^{-10}$. Initial concentration is 0.0004 M; $K_w = 1 \times 10^{-14}$.

change, especially for medium strong and very weak acids, the K_a of which is about 10^{-4} and 10^{-10} , respectively, and hence the technique can estimate K_a for them accurately. This is of great analytical value, since K_a of most of the organic

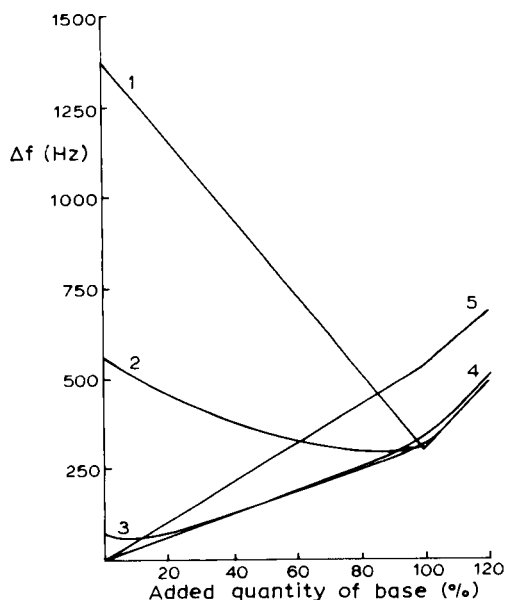


Fig. 3. Synthetic frequency response curves for acids with different K_a . 1, $K_a = 1 \times 10^{-2}$; 2, $K_a = 1 \times 10^{-4}$; 3, $K_a = 1 \times 10^{-6}$; 4, $K_a = 1 \times 10^{-8}$; 5, $K_a = 10^{-10}$. s , 1.023×10^5 Hz Ω m; f_0 , 9 MHz; I_{OH^-} , 0.01968; I_{H^+} , 0.034982; I_{A^-} , 0.00409; I_{B^+} , 0.00501 mho m^2 equiv. $^{-1}$. $K_w = 1 \times 10^{-14}$.

acids are located about the first value. Under the simulated experimental conditions, for strong acids (K_a is larger than 10^{-2}) and some weak acids (K_a is about 10^{-7}), the same percent change of K_a does not obviously influence the detector response and it can be expected that in those cases, the technique cannot give a good estimation of K_a . This fact can be explained theoretically for strong acids. The derivative of f with respect to K_a can be obtained from Eqn. 9

$$\frac{\partial f}{\partial K_a} = s(I_{OH^-} \frac{\partial [OH^-]}{\partial K_a} + I_{H^+} \frac{\partial [H^+]}{\partial K_a} + I_{A^-} \frac{\partial [A^-]}{\partial K_a}) \quad (10)$$

and the partial derivatives of $[OH^-]$, $[H^+]$ and $[A^-]$ with respect to K_a can be derived by Eqns. 5–7.

$$\begin{aligned} \frac{\partial [H^+]}{\partial K_a} &= -\{[H^+]^2 - K_w - [H^+](C^* - [B^+])\} \\ &\quad / \{3[H^+]^2 + 2[H^+](K_a + [B^+]) - K_w \\ &\quad - K_a(C^* - [B^+])\} \end{aligned} \quad (11)$$

$$\frac{\partial [OH^-]}{\partial K_a} = -\frac{\partial [H^+]}{\partial K_a} (K_w / [H^+]^2) \quad (12)$$

and

$$\begin{aligned} \frac{\partial [A^-]}{\partial K_a} &= \{C^* - [A^-] - [A^-] \frac{\partial [H^+]}{\partial K_a}\} \\ &\quad / ([H^+] + K_a) \end{aligned} \quad (13)$$

If C^* is a limited value, which restricts $[H^+]$, and K_a is large enough, i.e., before the end-point $[H^+] \approx C^* - [B^+]$ and after the end-point $[H^+]$ is small, the absolute values of the above derivatives are all small or close to zero, i.e., the change of K_a cannot cause the obvious change of f . For the initial concentration estimation, when K_a is larger than 10^{-9} , an accurate estimation can be obtained; for the very weak acids (K_a is about 10^{-11}), the precision of concentration estimation is lower.

The computations with two different other detector parameters indicate that for any acids the parameters can all be estimated accurately. The computations demonstrate that for $K_a = 10^{-12}$ there is a difference of several tens of hertz from the response of pure water titrated with BOH. Of course, when K_a is far smaller than 10^{-12} , since

the response curves are almost the same as achieved by the titration of water with strong base, they cannot provide any information about the acids to be titrated.

To test the ability of the procedure to estimate parameters, a synthetic frequency response curve vs. the added quantity of titrant according to Eqn. 8 for given parameters was computed, and then a random noise of 1% of the maximum frequency shift, during titration from the beginning to a 20% excess of base, was added to the theoretical data. All the deviation plots were random, indicating a good fit of the theoretical model to the data. The regression results are listed in Table 1.

In all cases, the two parameters s , and f calculated from regression analysis were close to the expected values and the deviations were small. The technique can give an accurate and precise estimation of K_a but for strong acids, estimation of K_a , was poor which is in agreement with that analyzed above. For very weak acids, the concentration estimation was worse than for that for the stronger acids, which can be explained from the computation. Figure 2 shows that for $K_a = 10^{-10}$ the concentration of A^- increases gradually before and after the end-point, and hence the frequency response change about the end-point is not obvious, which influences the precision of the initial concentration estimation.

For non-linear regression, a set of starting values of parameters is needed, it can be seen from Eqn. 8 that the initial guesses of K_a and C^* are more important and s and f_0 are of less importance for rapid and accurate convergence

since the former is non-linear and the latter is linear. The computations indicate that when the initial guesses lie between 2 and 0.5 times the true value for K_a , and 1.4 and 0.001 times the true value for C^* were given, the regression results were the same. For the other two parameters when \pm several times deviations from the true parameters were given the same analysis results can be achieved. Thus, the demand for the initial values is low with this technique.

Validation of non-linear regression with experimental response data

To test whether the response of the piezoelectric crystal detector to the solution conductivity is linear, doubly distilled water was titrated with sodium hydroxide solution. The response curve is given in Fig. 4, which demonstrates that during the titration, the frequency response increases with the increased concentration of the titrant; the relationship between them is more strictly linear from 0 to 1200 Hz for the frequency shift ($R = 0.999$, $n = 3$), and hence in that range the response model can be used to estimate the parameters accurately. Beyond this range the slope of the response curve increases gradually. In this work all of the titration experiments were restricted in the linear range.

Applicability of the non-linear regression approach to the response data of the piezoelectric crystal for titrations of the acids with different original concentrations with the strong base sodium hydroxide were investigated. Table 2 shows the results of regression analysis of data for acetic acid, benzoic acid and hydrochloric

TABLE 1

Regression analysis of synthetic frequency data with random noise

Actual K_a	Estimated $K_a \pm$ S.D.	Actual concentration (mM)	Estimated concentration \pm S.D. (mM)	Actual $s \times 10^{-5}$ (Hz Ω m)	Estimated $s \pm$ S.D. $\times 10^{-5}$ (Hz Ω m)	Actual f (MHz)	Estimated $f \pm$ S.D. MHz \pm Hz)
1×10^{-2}	$0.535 \pm 0.04 \times 10^{-2}$	0.400	0.402 ± 0.001	1.023	1.095 ± 0.038	9	9 ± 47
1×10^{-4}	$0.998 \pm 0.028 \times 10^{-4}$	0.400	0.402 ± 0.001	1.023	1.039 ± 0.022	9	9 ± 4
1×10^{-6}	$1.05 \pm 0.05 \times 10^{-6}$	0.400	0.401 ± 0.002	1.023	1.025 ± 0.020	9	9 ± 1
1×10^{-8}	$1.01 \pm 0.07 \times 10^{-8}$	0.400	0.398 ± 0.004	1.023	1.014 ± 0.026	9	9 ± 2
1×10^{-10}	$1.01 \pm 0.04 \times 10^{-10}$	0.400	0.397 ± 0.011	1.023	1.052 ± 0.031	9	9 ± 1

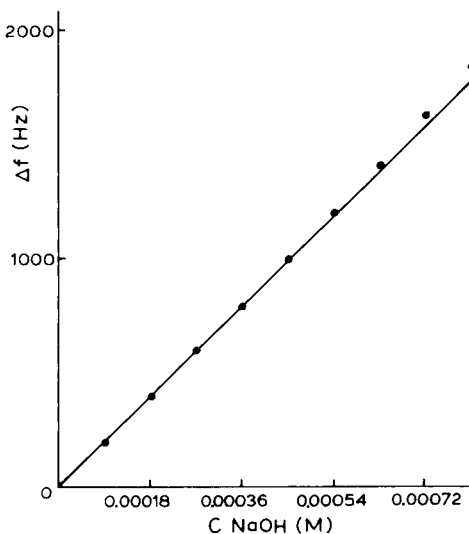


Fig. 4. Response curve of piezoelectric crystal detector for water titrated with sodium hydroxide solution.

acid solutions with different original concentrations. Figures 5 and 6 show the fit and the residual distribution of the 7th sample, which indicates that the theoretical model can fit the true response curve and residual distribution was basi-

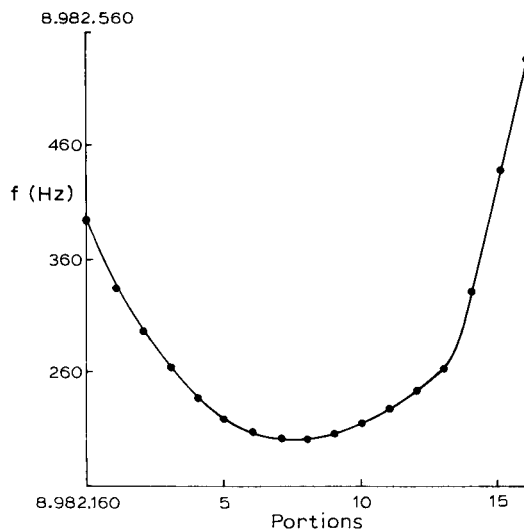


Fig. 5. Response curve of 0.0006 M benzoic acid titrated with sodium hydroxide. Points are experimental data; solid line is computed by non-linear regression procedure. Volume of benzoic acid solution is 10.00 ml and 5 μ l portion of 0.0900 M NaOH is added each time.

cally random, and hence the model reflects the behavior of the titration system correctly and the estimated parameters can be used to describe the

TABLE 2

Regression analysis of response data for acetic acid, benzoic acid and hydrochloric acid

Sample No.	Actual concentration (mM)	Estimated parameters			
		Concentration (mM)	$K_a \times 10^5$	$s \times 10^{-4}$ (Hz Ω m)	f_0 (Hz)
<i>Acetic acid</i>					
1	0.200	0.201	1.88	8.28	8 993 278
2	0.400	0.394	1.85	8.33	8 993 225
3	0.600	0.594	1.73	8.25	8 993 298
4	0.800	0.804	1.91	8.11	8 993 264
<i>Benzoic acid</i> ^a					
5	0.200	0.203	6.50	9.09	8 982 156
6	0.400	0.396	6.66	9.11	8 982 194
7	0.600	0.603	6.59	9.01	8 982 160
8	0.800	0.807	6.53	9.03	8 982 138
<i>Hydrochloric acid</i> ^a					
9	0.0200	0.0201	183 980	9.09	8 982 195
10	0.0400	0.0400	17 900	9.13	8 982 172
11	0.0600	0.0594	2380	9.12	8 982 202
12	0.0800	0.0805	97 980	9.05	8 982 141

^a The same piezoelectric crystal detector was used.

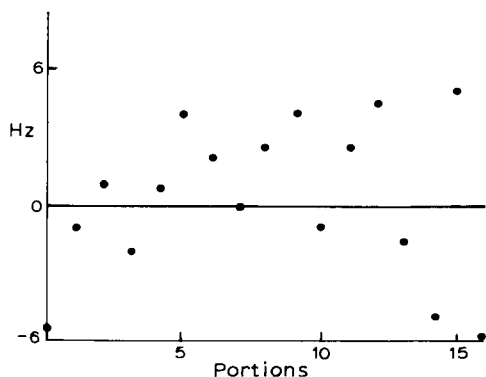


Fig. 6. Residual plot from regression analysis of the data in Fig. 5.

system behavior during titration. From the results listed in Table 2, it can be seen that for different original concentrations the estimated K_a of acetic acid and benzoic acid have been estimated with high precision. When four solutions with different original concentrations were used for the two acid systems, the estimation standard deviations of the estimated K_a were 0.079×10^{-5} for acetic acid and 0.071×10^{-5} for benzoic acid, respectively. The estimated K_a for them were 1.84 and 6.57×10^{-5} respectively, which were slightly higher than those reported in Ref. 8, probably because of differing measurement conditions.

Usefulness and applications

The technique introduced in this paper can be utilized as a sensitive and accurate method to estimate dissociation constants for weaker acids. The results listed in Table 2 indicate that the precision of the estimation of K_a for hydrochloric acid is very low, which is not surprising and

does not damage the estimation of the other parameters. The estimation of the initial concentration of hydrochloric acid is good. Furthermore, the technique can accurately estimate the original concentrations of weak acids (K_a is about 10^{-5}) with acid–base titration data from piezoelectric crystal detectors; a determination which is very difficult with the common graphic method, since there is no obvious planar range before the endpoint for the weak acid, as shown in Fig. 5. The maximum deviations of the estimated concentrations were -1.50% for acetic acid and $+1.50\%$ for benzoic acid respectively. When the three acid systems were used for the estimation of the other two detector parameters, almost the same estimation for s can be achieved and a slightly different f_0 are obtained for the same piezoelectric crystal under the same experimental conditions.

This technique can also be used to estimate equivalent conductivities of some reacting ions with a slightly modified program, when K_a of the acid is already known. For this purpose, phenol solutions with different initial concentrations were titrated with sodium hydroxide solution to estimate the equivalent conductivity of phenol cation, the initial concentrations of the titrated solutions, the response sensitivity and the basic frequency without the reacting substances of the detector. The regression results listed in Table 3 show that the equivalent ionic conductivity can be obtained with high precision for the titration system and the values of s are approximately the same as for samples 8–12 and the estimation of f_0 was close to those for samples 8–12, since the same detector was used. However, the estimation of the initial concentration was worse than those of other

TABLE 3

Regression analysis of the response data for phenol

Sample No.	Actual concentration (mM)	Estimated parameters			
		Concentration (mM)	$I \times 10^3$ (mho m ² equiv. ⁻¹)	$s \times 10^{-4}$ (Hz Ω m)	f_0 (Hz)
1	0.400	0.385	3.35	9.06	8 982 207
2	0.500	0.470	3.31	9.02	8 982 240
3	0.600	0.619	3.42	9.11	8 982 164
4	0.800	0.823	3.47	9.05	8 982 135

acid systems. The regression results indicate that the detector response sensitivity of some piezoelectric crystals under some experimental condition is basically stable and it is approximately constant in a wider conductance range, and hence the parameter is of use for a wider practical application and the study of the electrochemical properties of the piezoelectric crystal.

Conclusion

Non-linear regression analysis of piezoelectric crystal response data for acid–base titration provides a quick and accurate method to estimate system parameters, which can determine the titration end-point, estimate the acid dissociation constant, the equivalent ionic conductivity and two crystal parameters, which are of much theoretical value for research into the behavior of crystals in solutions. Only several minutes were needed to perform the entire regression in a microcomputer, and hence it is of practical use. On the other hand, the method to establish the theoretical model is of wide significance for more

complex balance systems, though it was only used to build the model of acid–base titration systems.

This work was supported by the Natural Science Foundation and SEC Doctorate Foundation of China.

REFERENCES

- 1 E. Pungor, *Oscillometry and Conductometry*, Pergamon, Oxford, 1965.
- 2 S.-Z. Yao, Z.-H. Mo and L.-H. Nie, *Anal. Chim. Acta*, 229 (1990) 205.
- 3 S.-Z. Yao, Z.-H. Mo and L.-H. Nie, *Anal. Chim. Acta*, 230 (1990) 51.
- 4 Z.-H. Mo, S.-Z. Yao and L.-H. Nie, *Sci. China (Ser. B)*, 34 (1991) 1.
- 5 S.-Z. Yao and T.-A. Zhou, *Anal. Chim. Acta*, 212 (1988) 61.
- 6 D.W. Marquardt, *J. Soc. Indust. Appl. Math.*, 11 (1963) 413.
- 7 J.A. Dean (Ed.), *Lange's Handbook of Chemistry*, 13th edn., McGraw-Hill, 1985, New York, p. 6–34.
- 8 R.C. Weast (Ed.), *CRC Handbook of Chemistry and Physics*, 63rd edn. CRC Press, Boca Raton, FL, 1982, p. D-171, D-173.

Thermoanalytical studies of water on aluminum oxides with different porosities

P. Staszczuk

Department of Physical Chemistry, Faculty of Chemistry, M. Curie-Skłodowska University, 20031 Lublin (Poland)

M. Jaroniec and R.K. Gilpin

Department of Chemistry, Kent State University, Kent, OH 44242 (USA)

(Received 11th May 1992)

Abstract

The thermal desorption of water from five aluminum oxide samples with different porosities and specific surface areas was studied under dynamic and quasi-isothermal conditions. The thermogravimetric (TG) curves obtained show multi-step weight losses associated with the initial evaporation of excess water, the removal of the water retained in small pores and the desorption of physisorbed and chemisorbed water from active surface sites with different energies. Further, it appears that the weight losses at the inflection points of the TG curves can be correlated with the surface free energies and porosities of the samples studied.

Keywords: Thermometric methods; Alumina; Waters

The adsorption properties of the γ -form of aluminum oxide (Al_2O_3) have been studied most frequently. It has been suggested that the γ -form consists of an outer surface of charged oxygen atoms (O^{2-}) and an inner layer of charged aluminum (Al^{3+}) and oxygen (O^{2-}) atoms [1,2]. Only about 75% of the total number of aluminum sites are occupied, while the remaining sites exist as surface defects.

Various forms of aluminum oxide have been found to possess differing numbers of OH groups and adsorbed water molecules depending on their thermal history. At relatively low temperatures and in the presence of water vapor a monolayer of hydroxyl groups can be formed. Dehydration at lower temperatures causes the condensation of neighboring OH groups, but only about 66% of

these groups can be removed without affecting the material's structure. Remaining groups in combination with neighboring oxygen and aluminum atoms form the differing types of active sites [2].

The four most common active sites of aluminum oxide are Al^{3+} (acidic sites), O^{2-} (basic sites), OH groups (basic sites) and proton defects (electron acceptors). As noted above, the surface properties of Al_2O_3 depend on its thermal history [2]. The addition of water to the surface of dehydrated Al_2O_3 results in the formation of a chemisorbed layer, in which each water molecule is bonded to two surface oxygen atoms. Most of the surface water is removed at 300°C and the remaining water molecules react with the surface to form the OH groups. Further heating of Al_2O_3 under vacuum results in the gradual loss of these groups. At 400°C there are about six OH groups per nm^2 of surface. All of the hydroxyl groups are

Correspondence to: M. Jaroniec, Department of Chemistry, Kent State University, Kent, OH 44242 (USA).

removed from the surface between 800 and 1000°C and above 1000°C the α -Al₂O₃ form is obtained which has a specific surface area of only about 1 m² g⁻¹ and is inactive.

The types and distribution of active sites and their distribution on the Al₂O₃ surface determine the adsorbate–adsorbent interactions and, consequently, the thickness, structure and properties of adsorbed films. The physico-chemical properties of these films depend also on the chemical nature of the adsorbates, which can differ significantly, e.g., *n*-alkanes and water. The structure of the surface layer of Al₂O₃ consists of regularly distributed strong and weak adsorption sites. The linear molecules interact along rows of active sites and are adsorbed more strongly than non-linear molecules. The Al³⁺ atoms are the strongest adsorption sites, especially for easily polarizable molecules. Adsorbates with acidic functionalities are localized strongly on the basic active sites. The surface hydroxyl groups seem to be less active adsorption sites compared with either the Al³⁺ or O²⁻ sites.

Data derived from adsorption studies are important in understanding processes such as adhesion, catalysis and other related surface phenomena. The surface free energy of a solid material, e.g., aluminum oxide and silica gel, changes varying surface structure. The amount of chemisorbed water controls, to a certain extent, the types of active sites, which play a dominating role in the chromatographic and sorption separations [2,3]. In order to control the separation and catalytic processes, and to optimize the surface (e.g., adhesive and hydrophobic/hydrophilic) properties of

solid materials, it is necessary to determine their surface free energies and estimate possible contributions of non-specific and specific interactions in forming the liquid surface films. This task is not easy because of existing difficulties in the theoretical interpretation of experiments involving solid materials, such as aluminum oxides, with strong surface and structural heterogeneities.

In this work, the physico-chemical properties of five aluminum oxide samples were characterized thermogravimetrically. The dispersion and polar components of the surface free energy were estimated from adsorption data for *n*-octane and water on the Al₂O₃ samples. Additionally, the thicknesses of the adsorbed water layers were estimated and the values obtained correlated with the surface free energies of the individual samples.

EXPERIMENTAL

Five porous Al₂O₃ samples, which contained both mesopores and macropores, were obtained from the Aluminum Company of America (ALCOA Center, PA). Their specific surface areas and porosities were calculated from low-temperature nitrogen adsorption isotherms measured using a Sorptomatic 1800 automated apparatus (Carlo Erba, Milan). The results obtained and with the estimated fraction of pores with widths below 100 Å and their average widths are summarized in Table 1. The specific surface areas of the five materials studied ranged from 185 to 400

TABLE 1

Specific surface areas and porosities of the Al₂O₃ samples studied

Sample code	Specific surface area, <i>S</i> (m ² g ⁻¹)	Total porosity <i>V</i> (cm ³ g ⁻¹)	Fraction of pores with widths < 100 Å	Average width of pores < 100 Å
M-9	185	0.50	0.65	70
M-13	305	0.46	0.80	40
M-19	345	0.82	0.45	40
M-30	390	0.72	0.56	30
M-39	400	0.49	0.70	30

$\text{m}^2 \text{g}^{-1}$ with corresponding total porosities varying from 0.46 to $0.82 \text{ cm}^3 \text{g}^{-1}$. Although samples M-19 and M-30 had the highest total porosity, about 50% of it was from pores with widths that significantly exceeded 100 Å.

The thermal desorption curves were collected on a Q-1500D derivatograph (MOM, Hungary) thermogravimetric analyzer [4,5]. Weight loss experiments were carried out under both dynamic and quasi-isothermal conditions in order to characterize the various processes involved in the removal of water from the Al_2O_3 samples. In addition, the quantities of *n*-octane and water that could be adsorbed from the gas phase at 20°C were measured.

The dynamic thermal measurements were carried out as described previously [6]. Each of the Al_2O_3 samples was first immersed in doubly distilled water and then about 1.5 g of it were placed in the platinum sample pan of the thermogravimetric analyzer. Thermal analysis curves were collected between 20 and 250°C using a constant heating rate of $1.25^\circ\text{C min}^{-1}$. In carrying out these measurements the following data were recorded: the thermogravimetric (TG) changes, the differential thermogravimetric (DTG) changes, the differential thermal analysis (DTA) changes and temperature (*T*) vs. time profiles.

Quasi-isothermal measurements were also carried out as reported previously using a specially designed platinum crucible which could create quasi-isobaric conditions [6,7]. The samples were treated similarly to those used in the dynamic measurements. About 1.5 g of the wetted Al_2O_3 sample were placed in the instrument and both TG and DTG curves recorded [4,5]. The DTG measurements were used to monitor and to adjust continuously the heating rate in order to maintain quasi-isothermal conditions. This was done as follows. Between different thermodesorption processes heating was carried out at a moderately high constant rate (i.e. maximum rate of 6°C min^{-1}) until the onset of a monoenergetic process was observed. At this point the heating rate was automatically switched to and maintained at a much lower rate until the end of the monoenergetic process. Then it was reset to the higher heating rate. The mass loss measurements

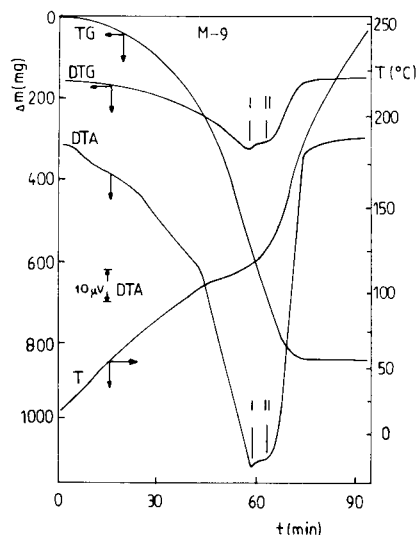


Fig. 1. Thermogravimetric curves measured under dynamic conditions. Sample, M-9.

under quasi-isothermal conditions were carried out at temperatures which ranged from 0 to 250°C.

The measurements of sorption of *n*-octane and water were carried out at 20°C using a modified Q-1500D derivatograph instrument. A detailed description of the methods used is given elsewhere [8–10].

RESULTS AND DISCUSSION

Dynamic measurements of the thermal desorption of water from the Al_2O_3 samples studied are presented in Figs. 1–5. These curves are representative of the TG, DTG, DTA and *T* profiles obtained. In all instances there were at least two endothermic peaks on the DTA curves. However, the shapes of these curves were significantly different between samples and they suggest that the energetic states of surface-bound water molecules were different.

The inflection point temperatures in the DTA and DTG curves and the corresponding weight losses are summarized in Table 2. These data were used to calculate the thickness of water on the surface (i.e., the number of adsorbed monolayers, *n*, given in Table 2) assuming uniform

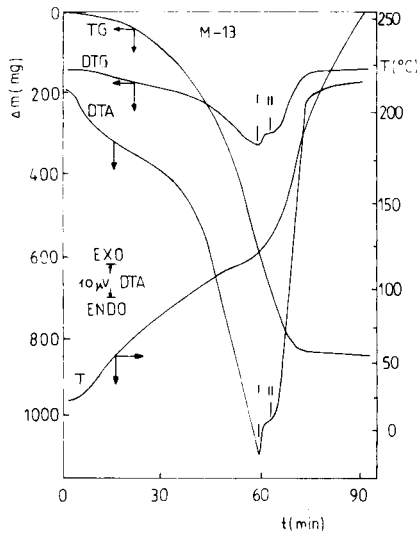


Fig. 2. As Fig. 1; sample, M-13.

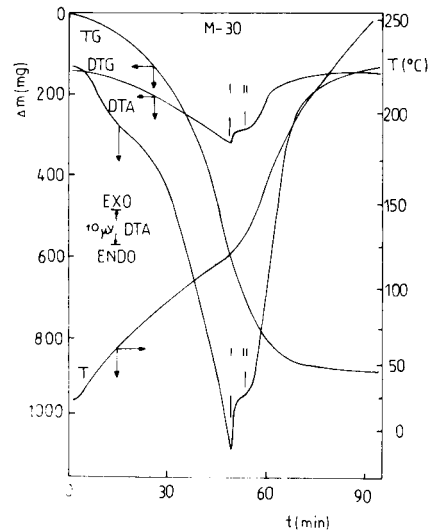


Fig. 4. As Fig. 1; sample, M-30.

coverage and that a molecule of water occupies 7.06 \AA^2 . Also given in Table 2 are the upper thermodesorption temperatures, the total amounts of desorbed water and the remaining mass of Al_2O_3 . It follows that the parameters characterizing the DTG and DTA curves also change from sample to sample.

A comparison of the data in Tables 1 and 2 reveals that there is a direct correlation between

the total porosity of a sample and the amounts of water remaining at the temperature of the first peak. Also, the amount of water remaining on a given sample at the temperature of the second peak increases with increasing total porosity. A detailed interpretation of these results is difficult because the samples studied not only possess different porosities, but they also have different surface properties. For example, the surfaces of

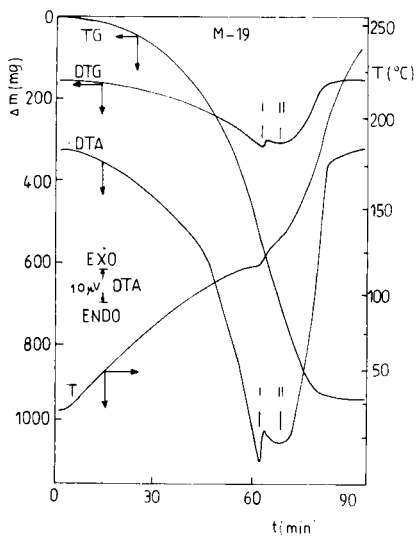


Fig. 3. As Fig. 1; sample, M-19.

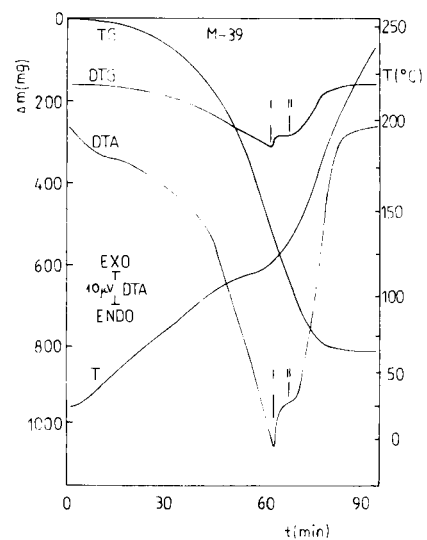


Fig. 5. As Fig. 1; sample, M-39.

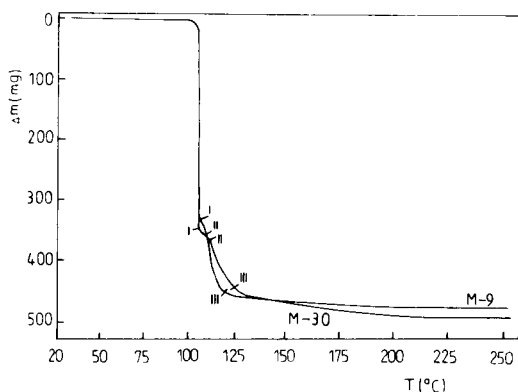


Fig. 6. TG curves measured under quasi-isothermal conditions. Samples, M-9 and M-30.

samples M-9 and M-30 contained a relatively high number of acid sites, whereas the surfaces of samples M-13 and M-39 are slightly basic. Also, the surface and energetic heterogeneities of these samples differ significantly.

Figures 6 and 7 present the thermodesorption TG curves that were measured under quasi-isothermal conditions. Each of the TG curves contains three inflection points, which are associated with different energetic states of water molecules on the Al_2O_3 samples. Table 3 summarizes parameters that characterize these inflection points.

A comparison of the data that were obtained under dynamic conditions with those obtained under quasi-isothermal conditions shows that the temperatures of a process measured quasi-isothermally are lower than those observed dynamically. These differences are consistent with differences in the heating profiles used (i.e., a continuous increase in temperature vs. a fixed tempera-

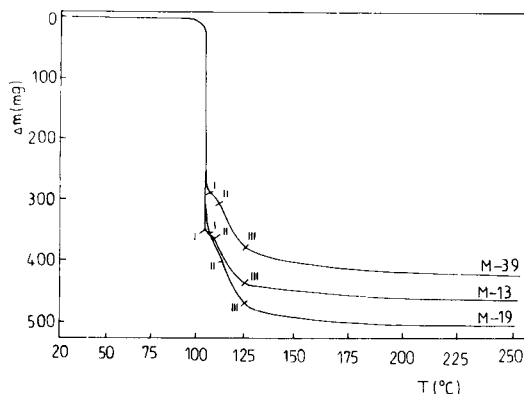


Fig. 7. As Fig. 6; samples, M-13, M-19 and M-39.

ture during the measurement of a weight loss process). Although both types of TG measurements provide analogous information about the thermodesorption of water from the Al_2O_3 surfaces, the quasi-isothermal method shows higher-resolution than the dynamic method and the characteristic points on the TG curve are more distinct.

The thermodesorption curves measured under quasi-isothermal conditions can be interpreted as follows. The first stage of the weight loss process is associated with evaporation of water, which has properties of the bulk water. The next stages below 250°C are associated with the loss of water from macro- and mesopores and with thermodesorption of water adsorbed on the Al_2O_3 surface. Water that is contained inside the small pores and adsorbed on the surface has different properties than the bulk water. This type of water is

TABLE 2

Characterization parameters for the loss of water from the Al_2O_3 samples when measured under dynamic conditions

Sample	Final temperature of desorption process (°C)	Sample weight after thermodesorption process (mg)	Total amount of desorbed water mmol g ⁻¹ n		Peak I		Peak II			
					Temperature (°C)	Amount of water on sample		Temperature (°C)	Amount of water on sample	
						mmol g ⁻¹	n		mmol g ⁻¹	n
M-9	220	616	76.1	17.6	116	24.9	5.77	122	14.8	3.42
M-13	230	620	75.2	10.5	120	20.8	2.89	133	12.2	1.69
M-19	226	498	104.0	12.8	114	42.8	5.28	124	27.7	3.41
M-30	250	662	74.52	8.1	113	17.1	1.86	127	17.1	1.86
M-39	235	662	67.8	7.2	118	23.5	2.5	133	14.1	1.5

influenced by the adsorption forces generated by the pore walls. Also, the active sites present on the surface strongly influence the structure of the surface water, which is usually significantly different from the structure of bulk water [11,12]. While the second inflection point on each quasi-isothermal TG curve can be associated with the porosity (cf., Fig. 8), the third inflection point correlates with the amount of the surface water, which depends on the types of active sites (i.e., surface and energetic heterogeneity) and their surface concentration. Desorption of water molecules from the first and second adsorbed layers takes place at higher activation energies and thus occurs at higher relative temperatures. At the end of this process, the chemisorbed water desorbs, requiring a significantly higher temperature in order to dehydrate the Al_2O_3 surface.

The quasi-isothermal TG curves shown in Figs. 6 and 7 support the three-phase model which has been suggested to describe the loss of water from porous solids [11,12]. The three types of water are the surface water (one or two adsorbed layers thick), the water contained inside the small pores and the excess of water which wets the solid.

As mentioned under Experimental, the modified thermogravimetric analyzer [8–10] was used to measure the adsorption at 20°C of polar (water) and non-polar (*n*-octane) vapors on the Al_2O_3 samples. The resulting isotherms are type II according to the BET classification and suggest formation of multilayer surface films. The *n*-octane and water adsorption isotherms were integrated in order to calculate the surface film pressure π . This integration was done according to the following equation [13–16]:

$$\pi_i = (RT/S) \int_0^p a_i(p) d \ln p = \gamma_s - \gamma_{si} \quad (1)$$

where a_i denotes the amount of the *i*th vapor adsorbed at the equilibrium pressure p and the absolute temperature T , S is the specific surface area of the solid studied, γ_s is the surface free energy of the pure adsorbent, γ_{si} is the surface free energy of the adsorbent covered with the film of the liquid *i* (i.e., either water or *n*-octane), π_i is the film pressure for the *i*th liquid and R is the universal gas constant.

The calculated values of the film pressure π_i depend on the adsorbed amount a_i . Formation of an adsorbed film on a solid surface decreases the surface free energy of the solid up to the value of the surface tension of the liquid adsorbate. Depending on the type of adsorbent and wetting liquid and on the types of molecular interactions existing at the liquid–solid interface, a liquid film is formed on the solid surface having thickness related to the work required for the spreading, immersional or adhesional wetting processes.

In this study, the inflection points (i.e., the dependence of π_i on a_i) can be related to different types of wetting of the samples studied as follows.

(i) Spreading wetting, $\pi_{s,i}$, is the process which occurs as a drop of liquid disperses itself over a solid [15,17–19]. The value of the film pressure which is related to this type of wetting $\pi_{s,i}$ can be expressed in terms of the surface free energies of the pure solid and liquid [15,16,19]:

$$\pi_{s,i} = 2(\gamma_s^d \gamma_i^d)^{1/2} + 2(\gamma_s^n \gamma_i^n)^{1/2} - 2\gamma_i \quad (2)$$

where

$$\gamma_s = \gamma_s^d + \gamma_s^n \quad (3)$$

and

$$\gamma_i = \gamma_i^d + \gamma_i^n \quad (4)$$

where γ_i is the surface free energy of the *i*th pure liquid, γ_i^d and γ_i^n are the dispersion and non-dispersion (polar) components, respectively,

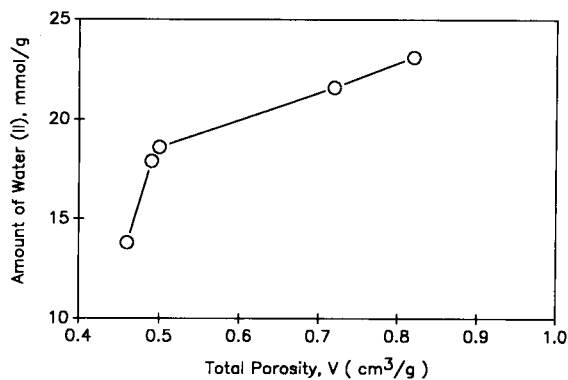


Fig. 8. Dependence between the amount of water at the second inflection point on the TG curves (cf., Table 3) and the total porosity (cf., Table 1) of the samples studied.

TABLE 3
 Characterization parameters for the loss of water from the Al_2O_3 samples when measured under quasi-isothermal conditions

Sample	Final temperature of desorption process (°C)	Sample weight after thermo-desorption process (mg)	Total amount of desorbed water mmol g^{-1}	Inflection I		Inflection II		Inflection III				
				Temperature (°C)	Amount of water on sample mmol g^{-1}	Temperature (°C)	Amount of water on sample mmol g^{-1}	Temperature (°C)	Amount of water on sample mmol g^{-1}			
M-9	215	340	78.4	103	23.5	5.45	106	18.6	4.77	115	4.56	1.06
M-13	225	322	80.8	103	20.0	2.79	107	13.8	1.92	122	4.4	0.61
M-19	180	289	99.2	101	34.6	4.26	106	23.1	2.84	120	6.15	0.76
M-30	225	340	81.7	103	24.2	2.63	108	21.6	2.34	123	8.49	0.92
M-39	250	367	64.8	106	20.9	2.23	113	17.9	1.9	126	6.66	0.71

of the surface free energy γ_i and γ_s^d and γ_s^n are the dispersion and non-dispersion (polar) components, respectively, of γ_s .

(ii) Immersional wetting, $\pi_{1,i}$, is the process which occurs as a solid is covered with a liquid [16–19]. For this wetting, $\pi_{1,i}$ is expressed as follows:

$$\pi_{1,i} = 2(\gamma_s^d \gamma_i^d)^{1/2} + 2(\gamma_s^n \gamma_i^n)^{1/2} - \gamma_i \quad (5)$$

(iii) Adhesional wetting, $\pi_{A,i}$, is the process which occurs as a joint interface is formed between two phases [16–19]. The film pressure is given by

$$\pi_{A,i} = 2(\gamma_s^d \gamma_i^d)^{1/2} + 2(\gamma_s^n \gamma_i^n)^{1/2} \quad (6)$$

The surface free energy of pure octane is $\gamma_0 = 21.8 \text{ mJ m}^{-2}$ at 20°C and the polar component of γ_0^n is assumed to be zero, i.e., $\gamma_0^n = 0$ and $\gamma_0 = \gamma_0^d$ [20]. For pure water, the surface free energy (surface tension) is $\gamma_w = 72.8 \text{ mJ m}^{-2}$ at 20°C and the polar component is calculated by assuming that $\gamma_0^d = \gamma_w^d$. Hence the polar component of γ_w is equal to $\gamma_w^n = \gamma_w - \gamma_0^d = 51 \text{ mJ m}^{-2}$. Identifying the successive inflection points on the π_i vs. a_i plots (obtained from the water and n -octane adsorption isotherms) as $\pi_{S,i}$, $\pi_{1,i}$ and $\pi_{A,i}$, and taking into account the dispersion and polar components of the surface free energies of pure water and n -octane, Eqns. 2, 5 and 6 can be used to evaluate the average values of the dispersion γ_s^d and polar γ_s^n components of the surface free energy of the Al_2O_3 samples studied.

Table 4 contains the values of γ_s^d and γ_s^n for the five Al_2O_3 samples. The values of γ_s decrease in the order $\text{M-9} < \text{M-30} < \text{M-39} < \text{M-19} < \text{M-13}$. The same sequence is observed for the values of γ_s^n . The order observed is related to the

TABLE 4

Dispersion (γ_s^d) and polar (γ_s^n) components of the surface free energy for the Al_2O_3 samples studied

Sample	γ_s^d (mJ m^{-2})	γ_s^n (mJ m^{-2})	γ_s (mJ m^{-2})
M-9	111	155	266
M-13	67	122	189
M-19	62	134	196
M-30	71	140	211
M-39	75	125	200

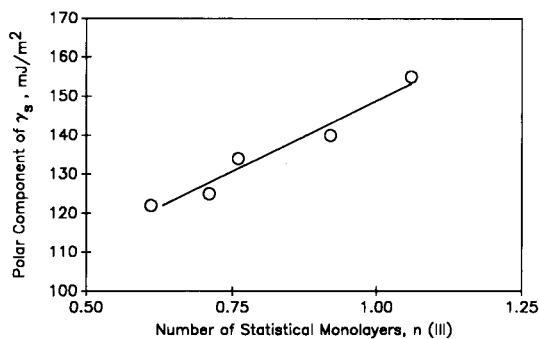


Fig. 9. Dependence between the polar component of the surface free energy (cf., Table 4) and the number of statistical monolayers at the third inflection point on the TG curves (Table 3).

acidity of the samples; the samples which were most acidic were M-9 and M-30, whereas the others were slightly basic [21]. In addition, the values of γ_s^n given in Table 4 correlate with the number of statistical monolayers, n , estimated at the third inflection point (cf., Table 3). Figure 9 shows that n increases linearly with increasing γ_s^n (i.e., an increase in the polar component of the surface free energy causes an increase in the amount of water bound to the Al_2O_3 surface). It is also worth noting that values of γ_s , γ_s^d and γ_s^n presented in Table 4 are analogous to those obtained for an Al_2O_3 sample from POCh (Gliwice, Poland): $\gamma_s^d = 50 \text{ mJ m}^{-2}$, $\gamma_s^n = 146 \text{ mJ m}^{-2}$ and $\gamma_s = 196 \text{ mJ m}^{-2}$ [20]. For four of the samples studied, the values of γ_s are about $200 \text{ mJ m}^{-2} \pm 5\%$.

Conclusions

These thermogravimetric studies suggest that water retained by porous Al_2O_3 may be described in term of a multi-domain structural model. The three types of water are strongly bound surface water, water inside small pores, which is modified structurally by the potential field generated by the pore walls, and excess water which is not influenced by the presence of the solid material. Additionally, the amounts of water at the third inflection point on the TG curves measured under quasi-isothermal conditions correlate with the polar component of the surface free energy of Al_2O_3 . Likewise, a rela-

tionship between the amount of water at the second inflection point on the TG curves and the total porosity was observed.

The authors thank the Research Laboratory of the Aluminum Company of America (ALCOA Center, PA) for donating samples of aluminum oxide.

REFERENCES

- 1 J.B. Peri, *J. Phys. Chem.* 69 (1965) 211, 220; 64 (1960) 1526.
- 2 J. Oscik, *Adsorption*, Horwood, Chichester, 1982.
- 3 Z. Suprynowicz, J. Rayss and A. Patrykiewicz, *Chromatographia*, 11 (1978) 742.
- 4 J. Paulik, F. Paulik and M. Arnold, *Hung. Sci. Instrum.*, 59 (1985) 57.
- 5 B. Wunderlich, *Thermal Analysis*, Academic, New York, 1990, p. 381.
- 6 P. Staszczuk, *J. Thermal Anal.*, 29 (1984) 217.
- 7 P. Staszczuk, A. Dobrowolski and M. Jaroniec, *Langmuir*, 8 (1992) 229.
- 8 P. Staszczuk, *J. Thermal Anal.*, 30 (1985) 1115.
- 9 P. Staszczuk, *J. Thermal Anal.*, 31 (1986) 911.
- 10 P. Staszczuk, *J. Thermal Anal.*, 31 (1986) 1055.
- 11 W. Drost-Hansen, *Chem. Phys. Lett.*, 2 (1968) 647.
- 12 W. Drost-Hansen, *Ind. Eng. Chem.*, 61 (1969) 10.
- 13 A.W. Adamson, *Physical Chemistry of Surfaces*, Wiley, New York, 1990, p. 384.
- 14 P. Staszczuk, *Mater. Chem. Phys.*, 12 (1985) 111.
- 15 P. Staszczuk, B. Janczuk and E. Chibowski, *Mater. Chem. Phys.*, 12 (1985) 469.
- 16 P. Staszczuk, *Mater. Chem. Phys.*, 14 (1986) 279.
- 17 P. Staszczuk, *Chromatographia*, 20 (1985) 724.
- 18 F.M. Fowkes, *J. Phys. Chem.*, 67 (1963) 2538.
- 19 F.M. Fowkes, *J. Adhesion*, 4 (1972) 155.
- 20 P. Staszczuk, Thesis, M.C.S. University, Lublin, 1987.
- 21 Research Laboratory, ALCOA Center, PA, personal communication.

Dr. Lutgarde Buydens wins ELSEVIER CHEMOMETRICS AWARD

At the recently held Fifth International Conference on Chemometrics in Analytical Chemistry, Montreal, Quebec, Canada, July 14-17, 1992, the first Elsevier Chemometrics Award was presented to Dr. Lutgarde Buydens of the Catholic University of Nijmegen, The Netherlands. The selection, based on submitted nominations, was made by a committee consisting of Dr. Olav Kvalheim of the University of Bergen, Professor Thomas Clerc of the Universität Bern, and Professor Philip Hopke of Clarkson University (Chairman). Dr. Buydens' accomplishments in the field can be found in the areas of expert system applications, pattern recognition, and structure-activity relationships. The Elsevier Award has been established to stimulate careers of younger scientists who have made valuable contributions to the field of chemometrics and includes a scroll and an honorarium of US\$ 2000.

The Sprouse Collection of Infrared Spectra

Book IV: Common Solvents - Condensed Phase, Vapor Phase and Mass Spectra

edited by **Diana L. Hansen**

This book consists of infrared (vapor and condensed phase) and mass spectra of nearly all of the solvents in common use today. It is the newest addition to the unique series which constitutes the **Sprouse Collection of Infrared Spectra**.

1990 xxvii + 779 pages

Price: US\$ 295.00 / Dfl. 520.00

ISBN 0-444-98717-7

Peak Table Search Library Software
for Book IV: US\$ 150.00 / Dfl. 270.00
ISBN 0-444-98714-2



Elsevier Science Publishers

P.O. Box 211, 1000 AE Amsterdam, The Netherlands
P.O. Box 882, Madison Square Station, New York, NY 10159, USA

This comprehensive book covers all important separation methods

Chromatography Today

by C.F. Poole and S.K. Poole, Wayne State University, Detroit, MI, USA

Chromatography Today provides an extensive coverage of all important chromatographic methods in a single text. Gas, liquid, thin layer and supercritical fluid chromatographic and capillary electrophoretic methods are handled with an emphasis on the contemporary practice.

Particular attention is given to the optimization of these techniques. Method selection then becomes a more logical process.

As an integral part of the total analytical technique, sample preparation methods as well as preparative scale separations are treated fully. The most common hyphenated techniques used for sample identification are also discussed.

Scope and level of **Chromatography Today** make the book suitable for:

- graduate level students as a textbook in separation science;
- professional institutes offering short courses in chromatography;
- chromatographers who may use the book to refresh their knowledge in the field.

Chromatography Today offers:

- a comprehensive collation of all relevant equations, physical constants and

general information used by chromatographers;

- extensive bibliography of recent literature to facilitate the location of specific items or areas of interest.

Chromatography Today is illustrated with over 200 figures, 110 tables and contains more than 3,330 references to contemporary literature.

Contents:

1. Fundamental Relationships of Chromatography.
 2. The Column in Gas Chromatography.
 3. Instrumental Aspects of Gas Chromatography.
 4. The Column in Liquid Chromatography.
 5. Instrumental Aspects of High Pressure Liquid Chromatography.
 6. Supercritical Fluid Chromatography.
 7. Thin-Layer Chromatography.
 8. Sample Preparation for Chromatographic Analysis.
 9. Hyphenated Methods for Identification after Chromatographic Separation.
- Subject Index.

1991 x + 1026 pages

Price: US \$ 147.50 / Dfl. 295.00

ISBN 0-444-88492-0

Paperback:

Price: US \$ 75.00 / Dfl. 150.00

ISBN 0-444-89161-7



Elsevier Science Publishers

P.O. Box 211, 1000 AE Amsterdam, The Netherlands

P.O. Box 882, Madison Square Station, New York, NY 10159, USA

Introduction to Chemical Process Instrumentation

by I. Nagy, Technical University of Budapest, Budapest, Hungary

Process instrumentation and control are integral parts of modern computerised chemical and biochemical plants. This book covers all aspects of instrumentation and control and reviews the most recent advances in the field.

The first part of the book comprises a brief summary of the fundamentals of metrology, process control theory and design methods of process instrumentation, with a view to help in the logical design of an instrumented process flowsheet. In the second part the evaluation and design of unit operation control schemes are presented with many illustrative instrumentation diagrams, from simple tasks to complex systems. The third part of the book provides practical information on the applied hardware, software and know-how. Aspects and problems of plantwide control, special safety requirements of chemical and biotechnological plants, information management and the economy of automation and control are also discussed.

The instrumentation and control of processes in the chemical industry requires close cooperation between chemists and engineers in the chemical, mechanical, control and instrumentation fields, as well as computer hardware and software experts. This book is intended to promote such teamwork by presenting

a comprehensive description of chemical process control in a way that it may be understood by each team member. The book should prove invaluable to those involved in the development and design of modern process plants and can also be used as textbook or aid for special courses.

Contents:

Part I. Fundamentals. 1. Information and Measurement. 2. Fundamentals of Process Control. 3. Principles of Process Instrumentation Design.

Part II. Automatic Control of Unit Operations and Processes.

4. Hydro-mechanical Unit Operations. 5. Instrumentation of Thermal Unit Operations. 6. Instrumentation of Mass Transfer Unit Operations. 7. Control of Chemical Reactors. 8. Control of Unit Processes.

Part III. Process Plant

Instrumentation. 9. Process Control Hardware Elements. 10. Computer Control. 11. Instrumentation and Management of Chemical Plants. 12. Economic Effects of Instrumentation. Appendix. Subject Index.

1992 xx + 448 pages

Price: US \$ 177.00 / Dfl. 345.00

ISBN 0-444-98712-6

Co-edition with Akadémiai Kiadó and distributed in the East European countries, North Korea, Cuba, Socialist Republic of Vietnam and Mongolia by KULTURA, P.O. Box 149, Budapest, Hungary



Elsevier Science Publishers

P.O. Box 211, 1000 AE Amsterdam, The Netherlands

P.O. Box 882, Madison Square Station, New York, NY 10159, USA

BIOSENSORS

by *F. Scheller and F. Schubert, Zentralinstitut für Molekularbiologie,
Akademie der Wissenschaften, Berlin-Buch, Germany*

Biosensors combine the unique properties of biological systems to selectively recognize and convert molecules with the benefits of physicochemical sensor technology, such as high sensitivity, simplicity of operation and mass production, and modern electronics. Consequently, their development is closely related to progress in two branches of high technology - biotechnology and microelectronics.

This book not only presents the state-of-the-art of biosensor research and development to the specialist, but also introduces the layman to the fundamentals of the subject. The relevant features of physicochemical transducer elements as well as biochemical recognition molecules (enzymes, antibodies, receptors) are outlined. Biochemical and biotechnological aspects of biomolecule immobilization and the interplay of biochemical reactions and mass transfer processes are comprehensively treated with regard to their impact on successful sensor design. Examples of immobilization methods are described in detail. The employment of coupled enzyme reactions, higher integrated biocatalytic systems (cell organelles, microbes, tissue sections) and immunocomponents in biosensors is covered extensively. Optical, thermometric, piezoelectric and particularly electrochemical biosensors for more than 100 analytes are presented, including immunosensors. The relative merits and limits of biosensors are discussed using several examples of their application in clinical chemistry, bio-

process control and environmental monitoring. Finally, the application of biosensors in medicine, biotechnology, food industry and environmental control is discussed, including commercialization and problems to be addressed in future research.

Contents: 1. Introduction. 2. Physicochemical, Biochemical and Technological Fundamentals of Biosensors. Biosensors as Functional Analogs of Chemoreceptors. Structure and Function of Transducers. Biochemical Fundamentals. Immobilization of the Receptor Component in Biosensors. Mathematical Modeling of Amperometric Enzyme Electrodes. 3. Metabolism Sensors. Monoenzyme Sensors. Biosensors Using Coupled Enzyme Reactions. Biosensors Using Higher Integrated Biocatalysts. 4. Affinity Biosensors. Affinity Sensors Using Low-Molecular Weight Ligands. Affinity Sensors Based on Proteins and Enzymes. Immunosensors. Biosensors Using Intact Biological Receptors. 5. Application of Biosensors. General Aspects. Biosensors for Clinical Chemistry. Continuous Patient Monitoring and Implantable Sensors. Food Analysis, Bioprocess Control and Environmental Monitoring. 6. Perspectives - Combination of Biotechnology and Microelectronics in Biosensors. List of Abbreviations and Symbols. References. Subject Index.

1992 x + 360 pages

Price: US \$ 161.50 / Dfl. 315.00

ISBN 0-444-98783-5



Elsevier Science Publishers

P.O. Box 211, 1000 AE Amsterdam, The Netherlands

P.O. Box 882, Madison Square Station, New York, NY 10159, USA

PUBLICATION SCHEDULE FOR 1993

	S'92	O'92	N'92	D'92	J	F
Analytica Chimica Acta	267/1 267/2	268/1 268/2	269/1 269/2	270/1 270/2	271/1 271/2	272/1 272/2
Vibrational Spectroscopy		4/1				4/2

INFORMATION FOR AUTHORS

Manuscripts. The language of the journal is English. English linguistic improvement is provided as part of the normal editorial processing. Authors should submit three copies of the manuscript in clear double-spaced typing on one side of the paper only. *Vibrational Spectroscopy* also accepts papers in English only.

Abstract. All papers and reviews begin with an Abstract (50–250 words) which should comprise a factual account of the contents of the paper, with emphasis on new information.

Figures. Figures should be prepared in black waterproof drawing ink on drawing or tracing paper of the same size as that on which the manuscript is typed. One original (or sharp glossy print) and two photostat (or other) copies are required. Attention should be given to line thickness, lettering (which should be kept to a minimum) and spacing on axes of graphs, to ensure suitability for reduction in size on printing. Axes of a graph should be clearly labelled, along the axes, outside the graph itself. All figures should be numbered with Arabic numerals, and require descriptive legends which should be typed on a separate sheet of paper. Simple straight-line graphs are not acceptable, because they can readily be described in the text by means of an equation or a sentence. Claims of linearity should be supported by regression data that include slope, intercept, standard deviations of the slope and intercept, standard error and the number of data points; correlation coefficients are optional. Photographs should be glossy prints and be as rich in contrast as possible; colour photographs cannot be accepted. Line diagrams are generally preferred to photographs of equipment.

Computer outputs for reproduction as figures must be good quality on blank paper, and should preferably be submitted as glossy prints.

Nomenclature, abbreviations and symbols. In general, the recommendations of the International Union of Pure and Applied Chemistry (IUPAC) should be followed, and attention should be given to the recommendations of the Analytical Chemistry Division in the journal *Pure and Applied Chemistry* (see also *IUPAC Compendium of Analytical Nomenclature, Definitive Rules, 1987*).

References. The references should be collected at the end of the paper, numbered in the order of their appearance in the text (not alphabetically) and typed on a separate sheet.

Reprints. Fifty reprints will be supplied free of charge. Additional reprints (minimum 100) can be ordered. An order form containing price quotations will be sent to the authors together with the proofs of their article.

Papers dealing with vibrational spectroscopy should be sent to: Dr J.G. Grasselli, 150 Greentree Road, Chagrin Falls, OH 44022, U.S.A. Telefax: (+ 1-216) 2473360 (Americas, Canada, Australia and New Zealand) or Dr J.H. van der Maas, Department of Analytical Molecule Spectrometry, Faculty of Chemistry, University of Utrecht, P.O. Box 80083, 3508 TB Utrecht, The Netherlands. Telefax: (+ 31-30) 518219 (all other countries).

© 1992, ELSEVIER SCIENCE PUBLISHERS B.V. All rights reserved.

0003-2670/92/\$05.00

No part of this publication may be reproduced, stored in a retrieval system or transmitted in any form or by any means, electronic, mechanical, photocopying, recording or otherwise, without the prior written permission of the publisher, Elsevier Science Publishers B.V., Copyright and Permissions Dept., P.O. Box 521, 1000 AM Amsterdam, The Netherlands.

Upon acceptance of an article by the journal, the author(s) will be asked to transfer copyright of the article to the publisher. The transfer will ensure the widest possible dissemination of information.

Special regulations for readers in the U.S.A.—This journal has been registered with the Copyright Clearance Center, Inc. Consent is given for copying of articles for personal or internal use, or for the personal use of specific clients. This consent is given on the condition that the copier pays through the Center the per-copy fee for copying beyond that permitted by Sections 107 or 108 of the U.S. Copyright Law. The per-copy fee is stated in the code-line at the bottom of the first page of each article. The appropriate fee, together with a copy of the first page of the article, should be forwarded to the Copyright Clearance Center, Inc., 27 Congress Street, Salem, MA 01970, U.S.A. If no code-line appears, broad consent to copy has not been given and permission to copy must be obtained directly from the author(s). All articles published prior to 1980 may be copied for a per-copy fee of US \$2.25, also payable through the Center. This consent does not extend to other kinds of copying, such as for general distribution, resale, advertising and promotion purposes, or for creating new collective works. Special written permission must be obtained from the publisher for such copying.

No responsibility is assumed by the publisher for any injury and/or damage to persons or property as a matter of products liability, negligence or otherwise, or from any use or operation of any methods, products, instructions or ideas contained in the material herein.

Although all advertising material is expected to conform to ethical (medical) standards, inclusion in this publication does not constitute a guarantee or endorsement of the quality or value of such product or of the claims made of it by its manufacturer.

This issue is printed on acid-free paper.

PRINTED IN THE NETHERLANDS

COMPREHENSIVE ANALYTICAL CHEMISTRY

edited by G. Svehla, formerly edited by C.L. Wilson and D.W. Wilson

Volume XXIX Chemiluminescence Immunoassay

by I. Weeks

This is the first work to present the topic as a subject in its own right. In order to provide a complete picture of the subject, overviews are presented of the individual areas of chemiluminescence and immunoassay with particular emphasis on the requirements for interfacing chemiluminescent and immunochemical reactions.

1992 xvi + 294 pages
Price: US \$ 151.50 / Dfl. 295.00
Subscription price:
US \$ 136.00 / Dfl. 265.00
ISBN 0-444-89035-1

Volume XXVIII Analysis of Substances in the Gaseous Phase

by E. Smolková-Keulemansová
and L. Feltl

The present volume provides a comprehensive description of the state-of-the-art and of future possibilities in the analysis of gaseous substances. In the individual chapters the following themes have been discussed; the theoretical basis for the methods, a description of the instrumentation and the steps necessary in actual analyses and an outline of the principal areas in which each method can be employed.

1991 xiv + 480 pages
Price: US \$ 228.50 / Dfl. 400.00
Subscription price:
US \$ 205.50 / Dfl. 360.00
ISBN 0-444-89122-6

Volume XXVII Analytical Voltammetry

edited by M.R. Smyth and
J.G. Vos

The aim of this volume is to review the state-of-the-art in analytical voltammetry with

regard to theory and instrumentation, and show how these relate to the analysis of inorganic, organometallic, organic and biological molecules.

1992 xxvi + 578 pages
Price: US \$ 283.00 / Dfl. 495.00
Subscription price:
US \$ 254.00 / Dfl. 445.00
ISBN 0-444-88938-8

Volume XXVI Radionuclide X-Ray Fluorescence Analysis with Environmental Application

by J. Tölgýessy, E. Havránek
and E. Dejmková

This work discusses the use of radionuclide XRFA for solving analytical problems of the environment and information is presented concerning the current state of research and use of radionuclide XRFA in this significant area.

1990 282 pages
Price: US \$ 134.50 / Dfl. 235.00
Subscription price:
US \$ 120.00 / Dfl. 210.00
ISBN 0-444-98837-8

*Distributed in the East European Countries,
China, Cuba, Mongolia, North Korea and
Vietnam by SLOVART*

*"...a valuable addition to the
well-known series..."*

*This book deserves to be
recommended to analytical
chemists inexperienced in
environmental problems and also
to environmental scientists
planning to apply XRFA to solve*

*their problems, as it gives readily
available information."*

Analytica Chimica Acta

Volume XII E Thermal Analysis

edited by W.W. Wendtlandt

Part E: Pulse Method of Measuring Basic Thermophysical Parameters

by L'. Kubicár

This book provides a systematic analysis of sources of scatter in experimental data, and describes experimental apparatus for measuring specific heats, thermal diffusivities and thermal conductivities in the temperature range 80-1300 K. Information is given on the measurement of thermophysical parameters of selected materials. The work also lists the most important results published so far on the use of the pulse method.

1990 370 pages
Price: US \$ 165.50 / Dfl. 290.00
Subscription price:
US \$ 151.50 / Dfl. 265.00
ISBN 0-444-98851-3

ORDER INFORMATION

For USA and Canada
**ELSEVIER SCIENCE
PUBLISHERS**
Judy Weislogel
P.O. Box 945
Madison Square Station,
New York, NY 10160-0757
Tel: (212) 989 5800
Fax: (212) 633 3880

In all other countries
**ELSEVIER SCIENCE
PUBLISHERS**
P.O. Box 211
1000 AE Amsterdam
The Netherlands
Tel: (+31-20) 5803 753
Fax: (+31-20) 5803 705
US\$ prices are valid only for the USA &
Canada and are subject to exchange fluctu-
ations; in all other countries the Dutch
guilder price (Dfl.), is definitive. Books are
sent postfree if prepaid.



ELSEVIER
SCIENCE PUBLISHERS